US Coast Guard 47 ft Boats

US	47	Coast Guard		Planing	Hull	Series																							
Model	Lpx	Lwl	Bpx	Dep	βχ	βτχ	Centroid	Lcg aft of Centroid	Lcg from Transom	Lcg/Lwl	Lcg/Lpx	Centerline angle	Ap	Twisted angle	Lpx/Bpx	Ap/Vol	Lpx/Ap	Lpx/Vol	Cv	Vcg/Lpx	Shaft Angle	Lce Transom	
5628	10,400 ft	10,000 ft	3,085 ft	297,760 Lb	20,00	16,61	42,80	-6,18	3,808 ft	0,3808	0,3662	0,00	25,880 ft^2	3,39	3,37	9,119	4,179	6,173	0,158	--------	12,00	0,000	ft
	3,170 m	3,048 m	0,940 m	135,064 kg					1,161 m				2,4043 m^2									0,0000	m
	10,400 ft	10,000 ft	3,085 ft	375,690 Lb	20,00	16,61	42,80	-6,29	3,797 ft	0,3797	0,3651	0,00	25,880 ft^2	3,39	3,37	7,809	4,179	5,713	0,200	--------	12,00	0,000	ft
	3,170 m	3,048 m	0,940 m	170,413 kg					1,157 m				2,4043 m^2									0,0000	m
	10,400 ft	10,000 ft	3,085 ft	483,690 Lb	20,00	16,61	42,80	-6,26	3,800 ft	0,3800	0,3654	0,00	25,880 ft^2	3,39	3,37	6,599	4,179	5,252	0,257	--------	12,00	0,000	ft
	3,170 m	3,048 m	0,940 m	219,402 kg					1,158 m				2,4043 m^2									0,0000	m
	10,400 ft	10,000 ft	3,085 ft	510,160 Lb	20,00	16,61	42,80	-6,26	3,800 ft	0,3800	0,3654	0,00	25,880 ft^2	3,39	3,37	6,368	4,179	5,159	0,271	--------	12,00	0,000	ft
	3,170 m	3,048 m	0,940 m	231,409 kg					1,158 m				2,4043 m^2									0,0000	m
	10,400 ft	10,000 ft	3,085 ft	679,940 Lb	20,00	16,61	42,80	-6,36	3,790 ft	0,3790	0,3644	0,00	25,880 ft^2	3,39	3,37	5,258	4,179	4,688	0,362	--------	12,00	0,000	ft
	3,170 m	3,048 m	0,940 m	308,421 kg					1,155 m				2,4043 m^2									0,0000	m
	10,400 ft	10,000 ft	3,085 ft	297,760 Lb	20,00	16,61	42,80	-2,30	4,212 ft	0,4212	0,4050	0,00	25,880 ft^2	3,39	3,37	9,119	4,179	6,173	0,158	--------	12,00	0,000	ft
	3,170 m	3,048 m	0,940 m	135,064 kg					1,284 m				2,4043 m^2									0,0000	m
	10,400 ft	10,000 ft	3,085 ft	375,690 Lb	20,00	16,61	42,80	-2,38	4,204 ft	0,4204	0,4042	0,00	25,880 ft^2	3,39	3,37	7,809	4,179	5,713	0,200	--------	12,00	0,000	ft
	3,170 m	3,048 m	0,940 m	170,413 kg					1,281 m				2,4043 m^2									0,0000	m
	10,400 ft	10,000 ft	3,085 ft	484,190 Lb	20,00	16,61	42,80	-2,41	4,201 ft	0,4201	0,4039	0,00	25,880 ft^2	3,39	3,37	6,594	4,179	5,250	0,258	--------	12,00	0,000	ft
	3,170 m	3,048 m	0,940 m	219,629 kg					1,280 m				2,4043 m^2									0,0000	m
5629	10,400 ft	10,000 ft	3,085 ft	298,280 Lb	20,00	16,61	42,80	-6,27	3,799 ft	0,3799	0,3653	0,00	20,970 ft^2	3,39	3,37	7,380	5,158	6,170	0,159	--------	12,00	0,000	ft
	3,170 m	3,048 m	0,940 m	135,300 kg					1,158 m				1,9482 m^2									0,0000	m
	10,400 ft	10,000 ft	3,085 ft	375,850 Lb	20,00	16,61	42,80	-6,28	3,798 ft	0,3798	0,3652	0,00	20,970 ft^2	3,39	3,37	6,326	5,158	5,712	0,200	--------	12,00	0,000	ft
	3,170 m	3,048 m	0,940 m	170,486 kg					1,158 m				1,9482 m^2									0,0000	m
	10,400 ft	10,000 ft	3,085 ft	484,180 Lb	20,00	16,61	42,80	-6,26	3,800 ft	0,3800	0,3654	0,00	20,970 ft^2	3,39	3,37	5,343	5,158	5,250	0,258	--------	12,00	0,000	ft
	3,170 m	3,048 m	0,940 m	219,624 kg					1,158 m				1,9482 m^2									0,0000	m
	10,400 ft	10,000 ft	3,085 ft	298,240 Lb	20,00	16,61	42,80	-2,43	4,198 ft	0,4198	0,4037	0,00	20,970 ft^2	3,39	3,37	7,381	5,158	6,170	0,159	--------	12,00	0,000	ft
	3,170 m	3,048 m	0,940 m	135,282 kg					1,280 m				1,9482 m^2									0,0000	m
	10,400 ft	10,000 ft	3,085 ft	376,160 Lb	20,00	16,61	42,80	-2,39	4,203 ft	0,4203	0,4041	0,00	20,970 ft^2	3,39	3,37	6,323	5,158	5,711	0,200	--------	12,00	0,000	ft
	3,170 m	3,048 m	0,940 m	170,626 kg					1,281 m				1,9482 m^2									0,0000	m
	10,400 ft	10,000 ft	3,085 ft	484,180 Lb	20,00	16,61	42,80	-2,36	4,206 ft	0,4206	0,4044	0,00	20,970 ft^2	3,39	3,37	5,343	5,158	5,250	0,258	--------	12,00	0,000	ft
	3,170 m	3,048 m	0,940 m	219,624 kg					1,282 m				1,9482 m^2									0,0000	m
5630	10,400 ft	10,000 ft	3,085 ft	297,770 Lb	20,00	16,61	42,80	-6,23	3,803 ft	0,3803	0,3657	0,00	18,760 ft^2	3,39	3,37	6,610	5,765	6,173	0,158	--------	12,00	0,000	ft
	3,170 m	3,048 m	0,940 m	135,068 kg					1,159 m				1,7429 m^2									0,0000	m
	10,400 ft	10,000 ft	3,085 ft	375,460 Lb	20,00	16,61	42,80	-6,25	3,801 ft	0,3801	0,3655	0,00	18,760 ft^2	3,39	3,37	5,663	5,765	5,714	0,200	--------	12,00	0,000	ft
	3,170 m	3,048 m	0,940 m	170,309 kg					1,159 m				1,7429 m^2									0,0000	m
	10,400 ft	10,000 ft	3,085 ft	483,780 Lb	20,00	16,61	42,80	-6,25	3,801 ft	0,3801	0,3655	0,00	18,760 ft^2	3,39	3,37	4,783	5,765	5,251	0,257	--------	12,00	0,000	ft
	3,170 m	3,048 m	0,940 m	219,443 kg					1,159 m				1,7429 m^2									0,0000	m
	10,400 ft	10,000 ft	3,085 ft	297,770 Lb	20,00	16,61	42,80	-2,42	4,200 ft	0,4200	0,4038	0,00	18,760 ft^2	3,39	3,37	6,610	5,765	6,173	0,158	--------	12,00	0,000	ft
	3,170 m	3,048 m	0,940 m	135,068 kg					1,280 m				1,7429 m^2									0,0000	m
	10,400 ft	10,000 ft	3,085 ft	375,460 Lb	20,00	16,61	42,80	-2,40	4,202 ft	0,4202	0,4040	0,00	18,760 ft^2	3,39	3,37	5,663	5,765	5,714	0,200	--------	12,00	0,000	ft
	3,170 m	3,048 m	0,940 m	170,309 kg					1,281 m				1,7429 m^2									0,0000	m
	10,400 ft	10,000 ft	3,085 ft	483,780 Lb	20,00	16,61	42,80	-2,42	4,200 ft	0,4200	0,4038	0,00	18,760 ft^2	3,39	3,37	4,783	5,765	5,251	0,257	--------	12,00	0,000	ft
	3,170 m	3,048 m	0,940 m	219,443 kg					1,280 m				1,7429 m^2									0,0000	m
5631	10,400 ft	10,000 ft	3,085 ft	298,920 Lb	23,00	20,00	42,80	-6,25	3,801 ft	0,3801	0,3655	0,00	18,760 ft^2	3,00	3,37	6,593	5,765	6,165	0,159	--------	12,00	0,000	ft
	3,170 m	3,048 m	0,940 m	135,590 kg					1,159 m				1,7429 m^2									0,0000	m
	10,400 ft	10,000 ft	3,085 ft	375,340 Lb	23,00	20,00	42,80	-6,25	3,801 ft	0,3801	0,3655	0,00	18,760 ft^2	3,00	3,37	5,664	5,765	5,715	0,200	--------	12,00	0,000	ft
	3,170 m	3,048 m	0,940 m	170,254 kg					1,159 m				1,7429 m^2									0,0000	m
	10,400 ft	10,000 ft	3,085 ft	483,590 Lb	23,00	20,00	42,80	-6,26	3,800 ft	0,3800	0,3654	0,00	18,760 ft^2	3,00	3,37	4,784	5,765	5,252	0,257	--------	12,00	0,000	ft
	3,170 m	3,048 m	0,940 m	219,356 kg					1,158 m				1,7429 m^2									0,0000	m
	10,400 ft	10,000 ft	3,085 ft	298,880 Lb	23,00	20,00	42,80	-2,42	4,200 ft	0,4200	0,4038	0,00	18,760 ft^2	3,00	3,37	6,593	5,765	6,166	0,159	--------	12,00	0,000	ft
	3,170 m	3,048 m	0,940 m	135,572 kg					1,280 m				1,7429 m^2									0,0000	m
	10,400 ft	10,000 ft	3,085 ft	375,270 Lb	23,00	20,00	42,80	-2,42	4,200 ft	0,4200	0,4038	0,00	18,760 ft^2	3,00	3,37	5,665	5,765	5,715	0,200	--------	12,00	0,000	ft
	3,170 m	3,048 m	0,940 m	170,222 kg					1,280 m				1,7429 m^2									0,0000	m
	10,400 ft	10,000 ft	3,085 ft	483,590 Lb	23,00	20,00	42,80	-2,41	4,201 ft	0,4201	0,4039	0,00	18,760 ft^2	3,00	3,37	4,784	5,765	5,252	0,257	--------	12,00	0,000	ft
	3,170 m	3,048 m	0,940 m	219,356 kg					1,280 m				1,7429 m^2									0,0000	m

REPORTS

Report No. CG-D-06-95

Free Running Model Turning Tests of the U.S. Coast Guard 47 FT Motor Life Boat

Edward M. Lewandowski

Davidson Laboratory
Stevens Institute of Technology
711 Hudson Street
Hoboken, NJ 07030

FINAL REPORT
FEBRUARY 1995

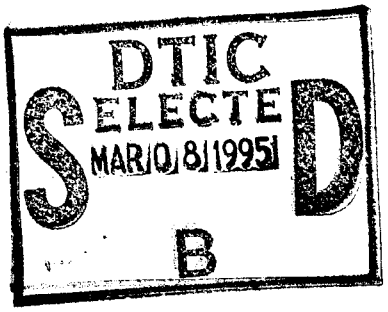

Prepared for:

U.S. Coast Guard
Research and Development Center
1082 Shennecossett Road
Groton, CT 06340-6096

and

U.S. Department Of Transportation
United States Coast Guard
Office of Engineering, Logistics, and Development
Washington, DC 20593-0001

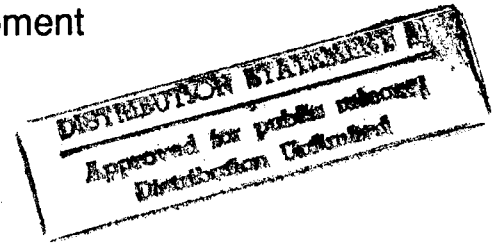

NOTICE

This document is disseminated under the sponsorship of the Department of Transportation in the interest of information exchange. The United States Government assumes no liability for its contents or use thereof.

The United States Government does not endorse products or manufacturers. Trade or manufacturers' names appear herein solely because they are considered essential to the object of this report.

The contents of this report reflect the views of the Coast Guard Research & Development Center. This report does not constitute a standard, specification, or regulation.

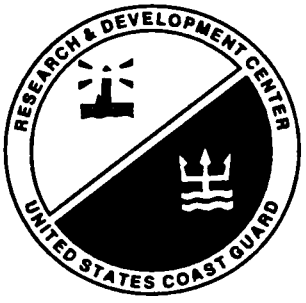

W. E. Colburn, Jr.
Technical Director, Acting
United States Coast Guard
Research & Development Center
1082 Shennecossett Road
Groton, CT 06340-6096

Technical Report Documentation Page

1. Report No.	2. Government Accession No.	3. Recipient's Catalog No.
CG-D-06-95		

4. Title and Subtitle	5. Report Date
Free Running Model Turning Tests of the U.S. Coast Guard 47 FT Motor Life Boat	February 1995
	6. Performing Organization Code
7. Author(s)	8. Performing Organization Report No.
Edward M. Lewandowski	R&DC 20/93
9. Performing Organization Name and Address	10. Work Unit No. (TRAIS)
Davidson Laboratory Stevens Institute of Technology 711 Hudson Street Hoboken, NJ 07030	11. Contract or Grant No. DTCG23-92-D-E01032
	13. Type of Report and Period Covered Final Report
12. Sponsoring Agency Name and Address	14. Sponsoring Agency Code
U.S. Coast Guard Research and Development Center 1082 Shennecossett Road Groton, Connecticut 06340-6096 Department of Transportation U.S. Coast Guard Office of Engineering, Logistics, and Development Washington, D.C. 20593-0001	

15. Supplementary Notes

Coast Guard R&D Center COTR: James A. White, 203-441-2734.

16. Abstract

Free running, radio-controlled, turning tests were performed on a 1/9 scale, self-propelled model of the USCG 47 FT Motor Life Boat (MLB) in order to study the roll characteristics of the boat in turn. Preliminary captive model tests were first carried out on a straight course in a towing tank to calibrate throttle settings and to check rudder effectiveness. Underwater photographs were taken. Little or no ventilation was observed on the rudders.

Free running turning tests were then conducted in a maneuvering basin. The model was outfitted with running lights and a visual roll angle display. Overhead photographs were taken and analyzed to obtain trajectory coordinates, and the roll angle, drift angle and heading of the boat as a function of time. Tests were run at scaled speeds corresponding to 10 and 27 knots, rudder angles of 20 and 30 degrees and scaled rudder rates of 5 and 10 degrees per second. Significant differences were measured between the turning parameters at 10 knots and 27 knots. Less significant differences were measured at the two different rudder rates. All results are presented in both tabular and graphical form.

17. Key Words		18. Distribution Statement
Motor Life Boat Turning Roll	Maneuvering Stability Planing Boats	Document is available to the U.S. public through the National Technical Information Service, Springfield, Virginia 22161

19. Security Classif. (of this report)	20. SECURITY CLASSIF. (of this page)	21. No. of Pages	22. Price
UNCLASSIFIED	UNCLASSIFIED		

Form DOT F 1700.7 (8/72) Reproduction of form and completed page is authorized

METRIC CONVERSION FACTORS

Approximate Conversions to Metric Measures

Symbol	When You Know	Multiply By	To Find	Symbol
		LENGTH		
in	inches	* 2.5	centimeters	cm
ft	feet	30	centimeters	cm
yd	yards	0.9	meters	m
mi	miles	1.6	kilometers	km
		AREA		
in^2	square inches	6.5	square centimeters	cm^2
ft^2	square feet	0.09	square meters	m^2
yd^2	square yards	0.8	square meters	m^2
mi^2	square miles	2.6	square kilometers	km^2
	acres	0.4	hectares	ha
		MASS (WEIGHT)		
oz	ounces	28	grams	g
lb	pounds	0.45	kilograms	kg
	short tons (2000 lb)	0.9	tonnes	t
		VOLUME		
tsp	teaspoons	5	milliliters	ml
tbsp	tablespoons	15	milliliters	ml
fl oz	fluid ounces	30	milliliters	ml
c	cups	0.24	liters	l
pt	pints	0.47	liters	l
qt	quarts	0.95	liters	l
gal	gallons	3.8	liters	l
ft^3	cubic feet	0.03	cubic meters	m^3
yd^3	cubic yards	0.76	cubic meters	m^3
		TEMPERATURE (EXACT)		
°F	Fahrenheit temperature	5/9 (after subtracting 32)	Celsius temperature	°C

*1 in = 2.54 (exactly).

Approximate Conversions from Metric Measures

Symbol	When You Know	Multiply By	To Find	Symbol
		LENGTH		
mm	millimeters	0.04	inches	in
cm	centimeters	0.4	inches	in
m	meters	3.3	feet	ft
m	meters	1.1	yards	yd
km	kilometers	0.6	miles	mi
		AREA		
cm^2	square centimeters	0.16	square inches	in^2
m^2	square meters	1.2	square yards	yd^2
km^2	square kilometers	0.4	square miles	mi^2
ha	hectares (10,000 m^2)	2.5	acres	
		MASS (WEIGHT)		
g	grams	0.035	ounces	oz
kg	kilograms	2.2	pounds	lb
t	tonnes (1000 kg)	1.1	short tons	
		VOLUME		
ml	milliliters	0.03	fluid ounces	fl oz
l	liters	0.125	cups	c
l	liters	2.1	pints	pt
l	liters	1.06	quarts	qt
l	liters	0.26	gallons	gal
m^3	cubic meters	35	cubic feet	ft^3
m^3	cubic meters	1.3	cubic yards	yd^3
		TEMPERATURE (EXACT)		
°C	Celsius temperature	9/5 (then add 32)	Fahrenheit temperature	°F

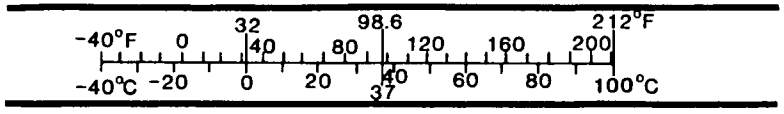

TABLE OF CONTENTS

INTRODUCTION

The initial configuration of the prototype 47 ft Motor Life Boat experienced large transient roll angles while in the initial phase of high-speed, large rudder angle turns. The transient was of short duration, and has been characterized as a "snap roll" phenomenon. To demonstrate that such phenomena can be accurately reproduced using a 5 ft model, a self-propelled, radio-controlled model of this craft was designed, built and tested. Preliminary captive tests were conducted in the High Speed Test Facility at the Davidson Laboratory in March and April, 1993. Free running model tests were conducted in the Maneuvering and Seakeeping Basin at Davidson Lab in April and May, 1993. Most of the free-running tests and some of the captive tests were witnessed by Mr. James White of the US Coast Guard. A portion of the free-running test program was witnessed by Mr. Daniel Bagnell of Band, Lavis and Associates, and by Mr. Walter Lincoln of the US Coast Guard.

MODEL

A model of the 47 ft MLB was fabricated from wood according to USCG Drawing 47 MLB-801-001 C, to a scale of 1/9.032. The scale was chosen in order to make use of stock propellers (Davidson Laboratory #80, Diameter = 0.258 ft). Rudders were fabricated from Lexan according to USCG Drawing 47 MLB-562-010. Brass shaft struts and barrels were fabricated according to USCG Drawing 47 MLB-161-010 B. Mylar strips were placed long the upper chine of the model from bow to stern, extending 1/32 in. (model-scale) below the chine, to provide a sharp edge. The model is shown on Figure 1, which also gives principal dimensions.

A preliminary powering study indicated that an electric motor would not be a satisfactory propulsor because of weight considerations. Thus, an internal combustion motor (O.S. Engines model FS-91, rated at 1.6 BHP @ 11,000 rpm) was chosen. A gearbox was designed and built for the two counterrotating shafts, with a 2:1 reduction. Therefore, both propellers always rotated at the same RPM. The model was outfitted with a Davidson Laboratory receiver and servos to control the throttle and choke (which was used to cut the engine).

A small electric motor was used to drive the rudders through a gear assembly. A circuit was designed to run the motor at two preset adjustable speeds, which were set to 5 and 10 deg/sec full-scale at the rudder stocks. A series of cams were installed on the shaft of the rudder motor, with detents corresponding to rudder angles of 20 and 30 degrees. Microswitches were used in conjunction with the cams to stop the rudders at the desired angle. After the preliminary captive tests, in which large roll angles were observed, the model sides were extended upward to an approximately uniform height of 5 in. model-scale above the afterbody deck.

Ballasting

For setting the CG of the model, pegs were temporarily fastened to the hull of the model. The pegs were attached at the specified full-scale CG, and protruded approximately 1.5 in. from the hull. The pegs were shimmed so that they were perpendicular to the longitudinal centerplane of the model. The model was then placed between two metal blocks, with the pegs resting on the blocks, so that it was free to pivot through 360 degrees. Ballast weights and moveable equipment were then shifted within the model until the CG was at the pivot point. It was noted that this method seemed to be extremely precise, as an applied moment of as little as .005 ft-lb (corresponding to a CG change of roughly 0.0001 ft model scale) caused the model to rotate.

Yaw gyradius was checked by use of the bifilar pendulum method. The model was suspended horizontally using two long steel cables, attached to the model at equal distances ahead of and aft of the CG. Small amplitude yaw oscillations about the CG were then set up and the period measured with a stopwatch. The period of yaw oscillation is related to yaw gyradius as follows:

$$T=\frac{2\pi k\sqrt{L/g}}{a}$$

where T is the period, k is the yaw gyradius; L is the length of the steel cables, and 2a is the distance between the cables. Preliminary tests indicated that the yaw gyradius was too large; the motor was then moved back and electronic equipment moved up to achieve the lowest possible value (see Table 1). The virtual roll moment of inertia was determined from the results of a roll decay test. The virtual roll inertia is related to the roll period as follows:

$$T = 2\pi\sqrt{\frac{I_{xx}'}{W \cdot GM}}$$

where I_{xx}' is the virtual roll inertia, W is the displacement, and GM is the metacentric height. The roll period was measured with a high degree of precision using a recording oscilloscope connected to the output of the gyroscope which was mounted in the model (the gyro is described in the next section).

An inclining test was conducted prior to the captive straight-course tests. Results are shown on Figure 2. The inertial properties of the model, and corresponding target values, are listed in Table 1. All quantities are within specified limits except for yaw gyradius, which was 3.4% high. A small fuel tank (weight = 0.45 lb full) was used, placed as close as possible to the CG of the model to minimize any possible effect of fuel consumption on inertial properties.

APPARATUS AND INSTRUMENTATION

Captive straight-course tests were carried out in the High Speed Test Basin, which is 313 ft long, 12 ft wide, and 5.5 ft deep. The model was towed free to trim and heave (but fixed in surge, sway and yaw) from a point on the propeller shaft line at the LCG, 0.48 ft aft of Station 6 and 2.26 ft above the baseline (dimensions will be given in full-scale unless otherwise noted). Some of the tests were conducted free to roll; a roll pivot box, instrumented to measure roll angle, was mounted above the pitch pivot box for this purpose. The roll pivot was 5.01 ft (99.4% of KG) above the baseline. The rudders were manually operated during these tests; a large protractor on the port rudder shaft was used to set the angle (the two rudders were geared together, as in the later free-running tests). A drag balance, located between the pivot box assembly and the free-to-heave mast, was used to measure net resistance. A tachometer fixed to the port propeller shaft forward of the gearbox was used to monitor engine speed.

All signals were monitored during the test using an oscillograph chart recorder. Figure 3 is a photograph of the model in the rudder effectiveness test rig. A Futaba 4 channel AM radio transmitter/receiver set was used to control the speed (throttle), choke (engine cutoff) and (in the free-running tests) rudder motion. For throttle control, the joystick on the transmitter was replaced by a 10-turn potentiometer, permitting more precise speed settings. For the free-running tests, the pivot boxes were removed and replaced by a gyroscope. To provide power for the gyro (24 volts

DC), two 12-volt battery packs were installed. The analog output of the gyro is a voltage which is linearly proportional to roll angle (0 to 60 deg). An on-board Motorola 6811 8-bit single chip microprocessor was used to digitize the voltage, multiply by a calibration factor, and send the output to a large 3-digit LED display, strobed at 5 Hz with a duration of 1 ms. The first digit of the roll display gave the sign of the roll angle and the second and third digits gave the roll angle to the nearest degree.

The model was also outfitted with running lights at the bow and stern (red light at the bow; green at the stern) which were on continuously during the tests and pulsed at high intensity in synchronization with the roll angle display; the LCG is located at the upper transverse bar of the 10's digit of the roll display. A third LED (yellow) was located on a small "tiller" on the rudder motor, to be used as an indicator of rudder action. The on-board instrumentation is shown on Figure 4. Locations of the running lights are also given on Figure 4. The fully equipped free-running model is shown at rest on Figure 5a and running at 27 knots on Figure 5b. Tests were conducted in the Maneuvering and Seakeeping Basin at Davidson Laboratory, which is 75 ft square with a water depth of 4.5 ft. The room was darkened by covering the windows with aluminum foil. Overhead photographs were taken using two Hasselblad EL cameras with Distagon 40 mm lenses; the aperture setting was f4. The cameras were located 16 ft above the water surface, above the southwest and southeast quadrants of the basin. Figure 6 is a plan view of the basin, showing the camera locations and the platform from which the model was launched. Kodak Vericolor ASA 400 color film was used, which was "pushed" in processing two stops to ASA 1600. The cameras were connected to a common trigger button which was located at tankside near the launch area. The cameras were adaptable to Polaroid film by switching backs; thus preliminary tests could be done using Polaroid film prior to loading the regular film.

TEST PROGRAM AND PROCEDURE

Straight-course Captive Tests

Captive tests were carried out on straight-course to calibrate the model speed vs transmitter throttle setting, to determine the steady state zero yaw rudder effectiveness, and to check for ventilation of the rudder surfaces. For the throttle calibration tests, the model was towed at speeds

of 10 and 27 knots with the motor running. A range of throttle settings (and thus engine RPM's) was run at each speed. In addition, a number of repeat runs was carried out at various throttle settings. The test procedure was first to take zero readings on the drag and RPM transducers with the model floating and at rest, and the motor off. Next, the throttle potentiometer was set to the desired value, and the motor started. Finally, the carriage was towed down the tank at the specified speed (10 or 27 knots). Resistance and RPM readings were acquired in a 50 ft data trap, after the model had reached steady speed and RPM. The running readings less the corresponding zeroes constitute the measured values for each run. An attempt was made to "zero in" on the throttle setting which resulted in a balance of thrust and drag (zero net resistance) and to assess the repeatability of the speed at that setting.

To examine rudder-induced roll behavior on straight course, a series of tests was conducted with the model towed free to roll (in addition to being free to heave and trim). For these tests, the roll locking clamp was removed from the roll pivot box. The test procedure was the same as that described above, with the exception that the rudder angle was set to the desired angle prior to each run, and that zeroes and running readings of roll angle were recorded in addition to drag and RPM; also, underwater running photographs were taken of the stern region of the model to check for ventilation. Tests were conducted at speeds of 10 and 27 knots, at a single throttle setting appropriate for each speed at zero rudder deflection. At 10 knots, tests were conducted at rudder angles of -30, -20, -10, 0, 10, 20, 25 and 30 degrees; positive rudder angles correspond to clockwise rotation about the rudder shaft, looking down. At 27 knots, tests were run at -15, -10, 0 and 10 degrees; higher rudder angles were not run because of the large roll angle (36 degrees) experienced at the rudder angle of -15 degrees which resulted in water above the lower deck edge. Prior to the free-running model tests, some problems were encountered with the model engine, necessitating removal and cleaning of the carburetor.

To check the speed calibration, runs were made straight across the Maneuvering and Seakeeping basin at a range of throttle settings. Overhead Polaroid photographs were taken, and speed determined using a "calibration photo" of an object of known length. These and other preliminary "practice tests" showed that the model tracked straight at zero rudder angle, and that it reached steady speed very quickly (practically instantaneous at 10 knots; within 15 ft of launch from zero speed at 27 knots). Unfortunately one of these calibration tests resulted in a head-on collision of the model with a tank wall at high speed, resulting in a large vertical crack in the model

extending from the deck to just above the upper chine. This was quickly repaired and no subsequent problems (such as leakage) were noted.

For the tests, the model was launched from a platform at the northwest corner of the Maneuvering and Seakeeping Basin. All lights were extinguished except for three fluorescent fixtures along the north edge of the tank; these were found to not adversely affect the quality of the photographs. The throttle was set to the appropriate point, and the motor started. Observers were stationed around the perimeter of the tank to prevent a collision with the walls. After starting the motor, the model was manually held using a handle on the transom while the gyro and flashing display were powered up. The model was then aimed parallel to the west tank wall (it was later found to be more effective to aim at the southwest corner of the basin) and released; the model was given a "push" at the start of the 27 knot runs to aid in reaching speed quickly. The camera shutters were opened manually at launch and held on "time" until the model was stopped due to proximity of a wall, or until a complete turn was negotiated. The motor was cut when it became apparent that the model would otherwise strike a tank wall, however at 10 knots and at some conditions at 27 knots, a full turn could be made.

Free-running tests were conducted at speeds of 10 and 27 knots, rudder angles of -20 and -30 degrees, and at rudder rates of 5 and 10 degrees/second. Rudder action was initiated at various points in the tank in an attempt to capture all phases of the turns on at least one of the two cameras. In the first test session, twelve rolls of 12-exposure film were shot during these tests, of which 90 photographs were found to contain sufficient information for processing. Color 8 x 8 inch prints of these 90 negatives were made. All negatives were marked with film roll and shot number immediately after processing.

Preliminary analysis of the prints indicated that the approach phase of the trajectory was not visible on any photograph for three of the four conditions at 27 knots. Thus, additional tests were conducted in which the model was launched from the west end of the tank, parallel to the south wall, so that the approach phase would be recorded by the southwest camera. Twelve runs were made, consuming an additional two rolls of film (one per camera). Twenty-two additional 8 x 8 prints were made from the negatives.

RESULTS

Results of the throttle calibration tests are given in Table 2, which lists run number, nominal boat speed in knots, actual model speed (fps), potentiometer setting, shaft speed (model RPM), and net resistance (lb, model). The results of runs 1-173 have not been included in the table as they were conducted with a motor which overheated and had to be replaced (with an identical model, which seemed to perform better). Net resistance is plotted as a function of propeller RPM on Figures 7 and 8, and as a function of throttle setting on Figures 9 and 10, for speeds of 10 and 27 knots, respectively. The throttle potentiometer units are arbitrary, with a setting of 12.60 corresponding to closed and 16.90 corresponding to wide open.

Results of the rudder effectiveness test are given in Tables 3.1 and 3.2, for speeds of 10 and 27 knots, respectively. The tables list run number, rudder angle, roll angle, model speed (fps), propeller RPM (model), and net resistance (model lb). Roll angle is plotted against rudder angle on Figures 11 and 12 for speeds of 10 and 27 knots, respectively. Underwater photographs revealed no evidence of ventilation except possibly at a speed of 10 knots and a rudder angle of 30 degrees, where a few isolated air bubbles could be seen on the low pressure side of the port rudder. A set of the underwater photographs has been delivered to Mr. White of the Coast Guard at his request.

Results of the free-running model tests, from analysis of the overhead photographs, are presented in Tables 4-7 for the approach speed of 10 knots and in Tables 8-11 for the approach speed of 27 knots. The tables list time in seconds; x and y coordinates of the CG in feet; and heading, roll and drift angles in degrees; these quantities are defined on Figure 13. Steady-state turning qualities are tabulated in Table 12, which lists advance, transfer, and tactical diameter in feet for each test condition. Steady-state turning parameters are defined on Figure 14. The tabulated quantities were determined by the method described under Analysis below.

Trajectories at 10 knots are shown on Figures 15 and 16, and time histories of heading, roll and drift angles are plotted in Figures 17 - 21. Trajectories for the approach speed of 27 knots are shown on Figures 22 and 23, and the corresponding time histories of heading, roll and drift appear on Figures 24 - 27. Figures 24a - 27a show an expansion of the first eight seconds of the maneuvers depicted in the corresponding Figures 24 - 27. Figures 24a - 27a also show the rudder angle; the rudder angles are shown negative (they are positive according to the sign convention defined above). The time of rudder execution was taken to be at 0 seconds on these figures; the actual instant of rudder execution is not precisely known as discussed below.

ANALYSIS

Analysis of the overhead photographs to determine the trajectories of the 47 ft MLB was carried out in four basic steps, as described below:

1. Assemble photographs

The first step in the analysis was to sort the photographs by condition (speed, rudder angle, rudder rate). As the camera field was limited to a 20 ft x 20 ft area, a complete turn could not be photographed on a single negative. Photographs covering various phases of the turns were obtained by launching from several locations in the tank and throwing the rudder at different times as described under Test Procedure above. Thus as many as 30 photographs were obtained for each condition. The photographs were carefully examined to find those which best showed the various portions of the trajectories. These prints were then joined together to form the complete trajectory. The photographs were joined by visually matching the curvature of the trajectories of the bow and stern lights, and by matching the roll angles as indicated by the display. As few as three photographs were required to obtain a complete picture of a turn at low speed, whereas many as 7 were assembled for a high-speed case (with a considerable amount of "overlap").

2. Measurement

A large transparent grid was prepared for measurement of the coordinates of the model from the photographs. The grid had 0.05 in. graduations permitting measurements to the nearest 0.025 in. The x (advance) axis of the grid was aligned with the trajectory of the model CG in the approach (straight line) portion of the turn. The origin was chosen to coincide with the model CG one time step (0.2 sec model-scale) before any apparent deviation (in heading, drift or transfer) from the initial straight trajectory. The rudder indicator light (yellow LED) was not useful for determining the rudder position because the yellow trace did not show well on the photographs, and because roll motion caused an apparent displacement of this light because it was not in the same horizontal plane as the bow and stern lights. Thus it was not possible to determine the time of rudder execution. However it is expected that the coordinate system described above will permit a valid comparison among the conditions examined.

Using the grid, the coordinates of the model CG, indicated by the forward transverse bar of the roll LED display, were recorded. Coordinates were recorded at each pulse (0.2 sec) for the high-speed runs, and at every other pulse for the low speed runs. Next, a transparent protractor was used with the grid to measure the heading angle between the longitudinal axis of the boat and the initial course (x-direction); the protractor permitted measurement to the nearest 0.5 degree.

Finally, the drift angle was measured at each time step (alternate time steps at low speed). To do this, the local radius of curvature was found by fitting a circle to the trajectory of the CG in the vicinity of the point of interest, using a transparent circle template. The angle between a normal to the radial line passing through the CG, at the CG, and the longitudinal axis of the model determines the drift angle, as shown on Figure 13. The roll angle was simply read (to the nearest degree) from the LED display.

3. Determination of Scale

The scale of the photographs was determined by measuring the distance between the bow and stern lights using a digital caliper. It was determined that the scale was not constant on each photograph, presumably due to distortion produced by the lens. After some investigation it was found that the photographic image became consistently smaller as the model progressed from right to left across the field of view, typically ranging from 2.0 in. at the lower right corner of a print to 2.15 in. at the upper left corner. To correct for this distortion, the length of the first and last image used on each photograph was recorded. Then, a scale factor for each time step was computed assuming a linear variation across the photograph. The scale factors were used to compute new x and y coordinates at each time step. No corrections were applied to the drift and heading measurements, which were not expected to be significantly affected by distortion.

4. Final adjustments

Further analysis of the corrected trajectory data showed that in the photographs obtained in the second test session, showing the approach phase of the turns, the model was not up to speed when the turns were initiated. This affects the measured advance but has little effect on other quantities since transfer, heading, drift and roll were all small in this phase of the turn. Unfortunately it was not feasible to conduct additional tests when this deficiency was discovered. Thus a further

correction was applied as described in Appendix A. It is emphasized that this second correction most strongly affects the x-coordinates in the trajectories and thus has little influence on key parameters such as transfer and tactical diameter.

At an approach speed of 27 knots and a rudder deflection of 30 degrees, the tactical diameter could not be determined directly from the photographs because of insufficient length of the trajectory. In this case the tactical diameter was estimated by assuming a steady speed and rate of heading change from the end of the measured trajectory.

DISCUSSION

Captive Straight Course Tests

The salient feature of the results of the throttle calibration tests was the amount of scatter in the RPM obtained for a given transmitter setting. It was thought that inconsistent fuel flow was partially responsible; two types of fuel pumps were tried, as well as raising the fuel tank, all with little effect. It was noticed, however, that after a warm up period, the behavior was much more consistent than in the initial runs during any test period.

After some preliminary tests, two steel flywheels were fabricated and attached to the front of the motor to improve low RPM performance and to help the motor to come to a more gradual halt when stopped. Prior to installation of the flywheels, the engine stopped so abruptly that a propeller shaft coupling broke; also it could not be run at the low RPM's required for 10 knots. The flywheels greatly improved the performance of the engine.

The free-to-roll tests conducted at 10 knots showed a nearly linear variation of roll angle with rudder deflection in the range of rudder angles from -30 to +20 degrees. Some loss of rudder effectiveness is apparent at +25 and +30 degrees; the reason for the asymmetry (no loss of effectiveness at -30 degrees) is unknown.

As the model came up to speed for the first free to roll run at 27 knots with nonzero rudder angle (+10 degrees was run), the roll angle of the model very rapidly reached its final value of -27 degrees; the model deck was then dangerously close to the water surface on the port side. This happened too quickly for the drive operator (the author) to stop the carriage; fortunately the equilibrium roll angle was not large enough to swamp the model, and there was little (if any) roll

overshoot. For subsequent runs, a mylar sheet, extending 3 1/2 inches above the model deck, was fastened to the model. A roll angle of 36.26 degrees was measured at a rudder deflection of -15 degrees; higher rudder angles were not attempted.

It is noted that in a turn, the angle of attack of the rudders is reduced by the drift angle and angular velocity of the craft; thus such large roll angles at moderate rudder deflections are not expected. The absence of roll overshoot in the straight-course tests is probably related to the test procedure: the model was brought up to speed with the rudders deflected, resulting in a relatively gradual buildup of rudder force.

Free-Running Tests

One of the most striking results of the free-running tests is the large difference in turning diameter at the two test speeds. Figures 28 and 29 show a comparison of the trajectories at rudder angles of 30 and 20 degrees, respectively. This is quite different from the performance of displacement ships, for which tactical diameter is virtually independent of approach speed. At the approach speed of 10 knots and a rudder angle of 30 degrees the turning diameter of the 47 ft MLB is just under 4 boat lengths, which is slightly inferior to what one would expect of a typical displacement ship (reference 2). The corresponding diameter at an approach speed of 27 knots is about 8.7 boat lengths.

The reason that the turning diameter of a displacement ship is nearly independent of approach speed is that both the required centripetal force and the hydrodynamic forces and moments on the ship are proportional to the square of the ship's velocity. This is apparently not the case for planing craft. In addition, the roll motion of the 47 ft MLB at 27 knots is significant, whereas the roll motion of displacement ships in turns is often neglected. Thus maneuvering standards applicable to displacement ships, which do not consider speed or roll effects, would appear to be inappropriate for planing craft.

At the higher speed of 27 knots, a "snap-roll" phenomenon was indeed observed, in which the boat would initially roll into the turn to as much as 34 degrees, and then abruptly return to a lower roll angle of about 18 degrees; the turning diameter would become much wider at this point. After several seconds at the lower roll angle, there was a tendency for the roll to increase again; subsequent readings as high as 28 degrees were noted. In the initial transient, a large plume of

water was noticed, emanating from the outboard propeller; it is possible that this propeller and the outboard rudder are losing effectiveness at the large roll angles, due to the proximity of the free surface, inducing the observed "flattening out" of the turn. Such a tendency was not observed in the straight-course tests; however the combination of turning and drift may bring the propellers closer to the surface than was the case on straight-course.

The effect of rudder rate on roll angle at high speed is shown on Figures 30 and 31 for rudder angles of 20 and 30 degrees, respectively. It an be seen that at the higher rate, the roll angle reaches a peak sooner (as expected) and that the peak is somewhat larger at the high rate. The oscillatory behavior mentioned above is evident here. The period of oscillation appears to be about 8 seconds which is larger than the natural roll period at zero speed, which was 3.05 seconds.

The time histories of the heading and roll of the craft on Figures 24 and 25 show that the rate of change of heading (turning rate) in the high speed turns increased in the initial phase of the turn until the time at which the maximum roll angle was reached, after which the turning rate steadied at a lower value (shallower slope on the figures). This is consistent with the observed "flattening out" of the turns mentioned above.

On six different runs, at 27 knots at a 20 degree rudder angle, the model was observed to turn through 90 degrees and then to rather abruptly stop turning, continuing in a straight line toward the tank wall. This happened five times at the slow rudder rate and once at the fast rudder rate. Photographs indicate that the drift angle and yaw rate approached zero, but that the roll angle held at about 20 degrees as the model approached straight-course. Subsequent equipment checks revealed no apparent problems. A satisfactory explanation for this phenomenon has yet to be found.

CONCLUDING REMARKS

This test program has successfully demonstrated that the "snap roll" phenomenon observed on the prototype 47 ft MLB could be duplicated at model scale; thus, the results of model studies can be applied with confidence to the investigation of such phenomena. It is strongly recommended that captive stability tests of the 47 ft MLB be carried out, and that the results be analyzed to provide further insight into the behavior of the craft. The present data can serve as a valuable check on the results of simulations which could be developed on the basis of the captive data; the simulator could then be applied to quickly assess the effects of simple geometry changes such as addition of skegs or changes in rudder geometry.

Comparisons of the present data to the turning performance of displacement ships indicate important differences: The roll behavior of planing craft can not be neglected, and the turning diameter at a particular rudder angle depends on speed, for example. It would thus appear that maneuvering standards which have been proposed for displacement ships should not be applied to planing craft.

REFERENCES

1. Mandel, P., "Ship Maneuvering and Control", chapter VIII in Principles of Naval Architecture, SNAME, 1967.

2. Barr, R.A., Miller, E.R., Ankudinov, V. and Lee, F.C. "Technical Basis for Maneuvering Standards", U.S. Coast Guard Report CG-M-8-81, December 1981.

TABLE 1 INERTIAL PROPERTIES

PROPERTY	TEST VALUE	TARGET VALUE
Displacement, lb	41,983a 41,972b	41,985* ± 840
LCG, ft aft of amidships	4.84	4.84 ± 0.10
VCG, ft above baseline	5.04	5.04
Virtual Roll Radius of Gyration, ft	5.77	5.75 ± 0.115
Yaw Gyradius, ft	11.10	10.73 ± 0.21
GM, ft	4.40	4.42 ± 0.09

Notes:

a Straight-course tests (basin temperature 71 deg F)
b Free-running tests (basin temperature 69 deg F)
* Seawater at 59 deg F assumed

TABLE 2 RESULTS OF SPEED CALIBRATION TESTS

Run no	Speed knots	Speed (model) fps	Pot. setting	Propeller RPM (model)	Net resistance lb (model)
174	27	15.12	14.20	4469	-0.77
175	27	15.17	14.20	4075	3.95
176	27	15.17	14.20	4103	3.50
177	27	15.17	14.20	4385	0.29
178	27	15.15	14.20	4377	0.51
179	27	15.17	14.20	4351	0.82
180	27	15.13	14.20	4344	0.90
181	27	15.17	14.20	4380	0.51
182	27	15.19	14.20	4374	0.63
183	27	15.15	14.20	4344	1.01
184	27	15.17	14.30	4454	-0.32
185	27	15.19	14.30	4448	-0.16
186	27	15.17	14.30	4443	-0.15
187	27	15.15	14.28	4451	-0.28
188	27	15.17	14.28	4453	-0.34
189	27	15.19	14.25	4449	-0.36
190	27	15.21	14.25	4459	-0.46
191	27	15.19	14.20	4385	0.38
192	27	15.15	14.22	4405	0.19
193	27	15.13	14.22	4417	-0.06
194	27	15.17	14.22	4418	0.02
195	27	15.13	14.22	4394	0.21
196	27	15.15	14.22	4404	0.17
197	27	15.13	14.22	4397	0.19
198	27	15.15	14.24	4410	0.06
199	27	15.17	14.24	4390	0.37
200	27	15.17	14.24	4396	0.17
201	27	15.19	14.24	4413	0.11
202	27	15.15	14.26	4424	-0.02
203	27	15.17	14.26	4420	0.03
204	27	15.21	14.26	4952	-0.34
205	27	15.17	14.26	4437	-0.10
206	10	5.60	13.40	2016	1.54
207	10	5.63	13.60	2514	-1.54
208	10	5.62	13.50	2430	-0.90
209	10	5.61	13.46	2168	0.90
210	10	5.61	13.48	2166	0.95
211	10	5.62	13.48	2232	0.42
212	10	5.61	13.48	2075	1.32
213	10	5.61	13.50	2290	0.13
214	10	5.62	13.50	2348	-0.29
215	10	5.62	13.50	2319	-0.18
216	10	5.62	13.50	2293	0.12
217	10	5.62	13.50	2334	-0.11
218	10	5.62	13.50	2403	-0.55

TABLE 3.1 RESULTS OF RUDDER EFFECTIVENESS TESTS
Speed: 10 knots

Run no	Rudder angle deg	Roll angle deg	Model speed fps	Prop RPM (model)	Net resistance lb (model)
85	0	-0.04	5.61	2188	-0.07
86	10	-2.73	5.61	2193	0.38
87	20	-6.11	5.59	2205	1.10
89	25	-6.56	5.59	2181	1.72
88	30	-5.26	5.58	2113	2.68
90	-10	2.85	5.60	2232	-0.44
91	-20	6.32	5.58	2213	0.70
92	-30	8.47	5.58	2225	2.04

TABLE 3.2 RESULTS OF RUDDER EFFECTIVENESS TESTS
Speed: 27 knots

Run no	Rudder angle deg	Roll angle deg	Model speed fps	Prop RPM (model)	Net resistance lb (model)
98	0	-1.50	15.15	4307	-0.60
100	0	-1.46	15.12	4251	0.31
101	10	-27.03	15.13	4248	2.30
102	-10	17.41	15.12	4341	-0.22
110	-10	17.61	15.15	4252	1.10
103	-15	36.26	15.12	4411	2.19

TABLE 4 Full-scale trajectory measured from overhead photographs.
Approach speed: 10 knots Rudder angle: 20 deg
Rudder rate: 10 deg/sec

Time sec	x ft	y ft	Heading angle deg	Roll angle deg	Drift angle deg
.0	.0	.0	-2.0	-2.0	.0
1.2	21.9	-.9	-6.0	-2.0	-2.0
2.4	43.8	-2.8	-10.5	-2.0	-3.0
3.6	64.3	-6.3	-16.0	-3.0	-4.5
4.8	84.2	-11.0	-23.5	-4.0	-6.5
6.0	102.4	-18.0	-32.0	-2.0	-7.0
7.2	119.1	-26.6	-39.5	-2.0	-8.5
8.4	134.4	-37.1	-47.5	-2.0	-9.0
9.6	148.1	-49.0	-54.5	-2.0	-10.0
10.8	159.9	-62.6	-62.5	-1.0	-9.5
12.0	169.5	-77.2	-70.0	-1.0	-9.0
13.2	177.3	-93.3	-78.0	-1.0	-9.5
14.4	182.9	-109.4	-85.0	-1.0	-10.0
15.6	186.3	-126.8	-92.0	-1.0	-9.5
16.8	187.5	-144.3	-99.5	-1.0	-9.5
18.0	186.3	-161.9	-106.5	-1.0	-9.5
19.2	182.2	-178.6	-113.5	-1.0	-8.5
20.4	176.8	-194.7	-121.0	-1.0	-8.5
21.6	169.1	-210.5	-127.5	-2.0	-8.0
22.8	159.1	-225.8	-136.0	-3.0	-9.5
24.0	146.2	-240.4	-144.0	-2.0	-8.5
25.2	131.5	-252.8	-151.5	-2.0	-8.5
26.4	115.4	-262.9	-159.0	-2.0	-8.0
27.6	97.9	-270.9	-167.0	-2.0	-8.0
28.9	79.8	-276.0	-175.5	-2.0	-8.0
30.1	61.1	-278.8	-184.0	-2.0	-8.5
31.3	42.4	-279.0	-192.5	-1.0	-9.0

TABLE 5 Full-scale trajectory measured from overhead photographs.
Approach speed: 10 knots Rudder angle: 20 deg
Rudder rate: 5 deg/sec

Time sec	x ft	y ft	Heading angle deg	Roll angle deg	Drift angle deg
.0	.0	.0	.0	.0	.0
1.2	22.6	.0	-.5	-1.0	-.5
2.4	44.5	-.2	-4.5	-1.0	-.5
3.6	65.9	-1.5	-9.5	-2.0	-3.0
4.8	86.5	-4.1	-15.0	-2.0	-5.0
6.0	106.5	-8.4	-21.0	-2.0	-6.5
7.2	125.4	-14.3	-28.5	-2.0	-8.0
8.4	142.9	-22.0	-36.5	-2.0	-8.0
9.6	158.5	-31.3	-44.0	-2.0	-8.0
10.8	172.3	-42.3	-51.0	-2.0	-8.0
12.0	185.1	-55.6	-59.0	-2.0	-9.0
13.2	196.0	-70.5	-67.5	-2.0	-9.0
14.4	204.3	-87.2	-75.0	-2.0	-8.5
15.6	209.7	-104.3	-83.0	-2.0	-8.0
16.8	214.8	-123.2	-91.0	-2.0	-8.5
18.0	216.0	-142.0	-98.5	-2.0	-8.0
19.2	214.6	-160.7	-106.0	-2.0	-8.0
20.4	210.2	-178.6	-112.5	-2.0	-8.0
21.6	204.1	-195.9	-120.0	-2.0	-7.0
22.8	195.7	-212.4	-128.0	-2.0	-7.0
24.0	184.9	-228.8	-136.5	-2.0	-8.0
25.2	172.3	-242.0	-145.0	-2.0	-8.0
26.4	157.4	-254.4	-153.0	-2.0	-8.5
27.6	141.3	-263.7	-160.5	-2.0	-8.5
28.9	123.8	-271.2	-168.5	-2.0	-8.5
30.1	105.4	-278.3	-178.0	-2.0	-9.5
31.3	86.9	-280.9	-185.0	-2.0	-11.0
32.5	68.7	-281.4	-193.0	-2.0	-11.0
33.7	50.6	-279.5	-200.5	-2.0	-10.5
34.9	33.5	-275.1	-208.5	-2.0	-10.0
36.1	16.6	-268.6	-216.0	-2.0	-11.0
37.3	1.0	-259.9	-223.0	-2.0	-10.0
38.5	-12.6	-249.7	-231.0	-2.0	-10.0
39.7	-25.2	-237.3	-238.0	-2.0	-10.0

TABLE 6 Full-scale trajectory measured from overhead photographs.
Approach speed: 10 knots Rudder angle: 30 deg
Rudder rate: 10 deg/sec

Time sec	x ft	y ft	Heading angle deg	Roll angle deg	Drift angle deg
.0	.0	.0	.0	.0	1.0
1.2	22.7	-.5	.0	-1.0	.0
2.4	45.2	-1.0	-4.0	-4.0	-2.0
3.6	67.4	-1.9	-11.5	-5.0	-6.5
4.8	87.9	-5.0	-21.5	-6.0	-11.0
6.0	107.2	-10.4	-33.5	-5.0	-11.0
7.2	124.0	-18.3	-43.0	-4.0	-11.5
8.4	138.6	-29.2	-54.0	-4.0	-10.0
9.6	148.2	-39.7	-66.0	-3.0	-10.0
10.8	158.1	-56.3	-77.5	-3.0	-11.0
12.0	163.9	-72.9	-89.5	-3.0	-11.0
13.2	166.1	-90.2	-100.0	-3.0	-12.0
14.4	165.4	-107.4	-110.5	-3.0	-12.5
15.6	161.6	-124.4	-121.0	-2.0	-13.0
16.8	154.9	-140.5	-132.5	-2.0	-13.0
18.0	145.3	-154.6	-143.5	-3.0	-13.5
19.2	133.1	-167.1	-154.0	-2.0	-13.5
20.4	118.8	-176.2	-165.0	-2.0	-13.5
21.6	102.9	-183.2	-176.0	-3.0	-14.0
22.8	86.5	-187.1	-187.5	-2.0	-14.5
24.0	69.6	-187.8	-197.5	-2.0	-13.0
25.2	52.7	-185.1	-208.0	-2.0	-14.0
26.4	37.1	-179.3	-218.0	-3.0	-14.0
27.6	22.3	-170.5	-230.0	-3.0	-13.5
28.9	9.7	-159.9	-240.5	-3.0	-13.0
30.1	-1.4	-145.3	-251.5	-5.0	-13.0
31.3	-9.0	-129.3	-262.5	-3.0	-13.0
32.5	-13.5	-112.3	-273.0	-3.0	-13.0
33.7	-14.6	-93.8	-284.5	-5.0	-13.0
34.9	-12.0	-74.7	-296.0	-5.0	-13.0
36.1	-4.2	-58.1	-309.0	-5.0	-13.0
37.3	4.0	-41.5	-321.5	-6.0	-13.0
38.5	18.0	-28.1	-334.5	-5.0	-13.0
39.7	33.9	-17.9	-345.0	-4.0	-13.0
40.9	51.5	-11.0	-356.0	-4.0	-13.0
42.1	69.8	-7.4	-368.5	-4.0	-13.0
43.3	88.6	-7.6	-380.5	-3.0	-13.0
44.5	106.6	-11.0	-391.0	-2.0	-13.0
45.7	119.7	-16.4	-399.0	-3.0	-13.0

TABLE 7 Full-scale trajectory measured from overhead photographs.
Approach speed: 10 knots Rudder angle: 30 deg
Rudder rate: 5 deg/sec

Time sec	x ft	y ft	Heading angle deg	Roll angle deg	Drift angle deg
.0	.0	.0	.0	.0	1.0
1.2	22.7	.0	-1.0	-2.0	.0
2.4	44.4	-.5	-4.0	-2.0	-1.5
3.6	66.1	-1.7	-8.5	-3.0	-2.5
4.8	86.9	-4.7	-15.0	-3.0	-5.5
6.0	107.0	-9.0	-22.0	-4.0	-7.0
7.2	126.3	-16.1	-31.5	-5.0	-10.0
8.4	143.5	-24.8	-42.0	-5.0	-10.0
9.6	158.7	-36.5	-53.5	-5.0	-11.0
10.8	171.0	-48.3	-64.0	-3.0	-12.5
12.0	181.0	-63.6	-75.0	-3.0	-11.5
13.2	188.4	-80.2	-86.0	-3.0	-13.0
14.4	192.0	-97.7	-96.5	-3.0	-13.0
15.6	192.5	-114.6	-106.0	-2.0	-13.5
16.8	189.6	-133.9	-118.5	-3.0	-13.0
18.0	182.9	-150.3	-129.5	-2.0	-13.0
19.2	173.3	-165.6	-141.0	-2.0	-13.0
20.4	160.2	-178.6	-151.0	-3.0	-11.0
21.6	145.8	-189.5	-162.0	-3.0	-12.0
22.8	129.5	-197.8	-172.5	-3.0	-13.0
24.0	112.1	-202.2	-182.5	-3.0	-13.0
25.2	94.4	-202.9	-195.0	-3.0	-13.0
26.4	76.9	-201.1	-207.5	-3.0	-13.0
27.6	60.4	-194.7	-220.0	-3.0	-12.0
28.9	44.9	-185.4	-231.0	-2.0	-12.5
30.1	32.1	-173.3	-242.0	-3.0	-12.0
31.3	21.9	-158.9	-252.5	-3.0	-12.5
32.5	14.3	-142.6	-263.0	-3.0	-13.0
33.7	9.4	-125.5	-274.0	-3.0	-13.0
34.9	9.0	-107.6	-285.5	-3.0	-13.0
36.1	11.3	-90.2	-298.0	-3.0	-13.0
37.3	15.9	-75.0	-309.0	-4.0	-13.0
38.5	24.8	-59.4	-320.0	-5.0	-13.0
39.7	37.1	-45.9	-332.0	-4.0	-13.0
40.9	51.6	-35.4	-343.5	-3.0	-13.5
42.1	67.9	-27.9	-355.0	-3.0	-14.0
43.3	84.6	-24.2	-364.0	-4.0	-12.5
44.5	103.2	-23.3	-375.0	-5.0	-12.5
45.7	121.8	-25.9	-386.5	-5.0	-12.0
46.9	138.7	-31.9	-397.5	-3.0	-12.0
48.1	154.7	-41.6	-409.0	-3.0	-12.0
49.3	168.2	-53.9	-418.0	-3.0	-12.0

TABLE 8 Full-scale trajectory measured from overhead photographs.
Approach speed: 27 knots Rudder angle: 20 deg
Rudder rate: 10 deg/sec

Time sec	x ft	y ft	Heading angle deg	Roll angle deg	Drift angle deg
.0	.0	.0	.0	-1.0	.0
.6	27.4	-.3	.0	-1.0	.0
1.2	55.0	-.6	-1.0	.0	.0
1.8	82.2	-1.5	-2.5	-2.0	.0
2.4	109.2	-2.3	-5.5	-7.0	-2.0
3.0	135.9	-4.2	-9.5	-12.0	-3.5
3.6	162.0	-7.3	-14.0	-18.0	-6.0
4.2	187.4	-12.0	-20.0	-23.0	-5.0
4.8	212.5	-19.5	-27.0	-29.0	-7.5
5.4	235.1	-28.5	-34.5	-30.0	-9.0
6.0	256.1	-40.4	-41.5	-27.0	-8.0
6.6	274.7	-54.7	-52.5	-25.0	-11.0
7.2	291.3	-72.0	-61.0	-23.0	-11.0
7.8	304.4	-90.9	-69.0	-19.0	-12.0
8.4	315.5	-110.7	-76.5	-18.0	-11.0
9.0	323.6	-132.5	-83.0	-18.0	-10.0
9.6	329.1	-154.5	-89.0	-20.0	-10.0
10.2	332.0	-177.1	-95.5	-22.0	-10.0
10.8	332.9	-200.4	-101.5	-23.0	-9.5
11.4	330.2	-223.4	-109.0	-23.0	-9.5
12.0	325.1	-245.6	-115.0	-25.0	-9.0
12.6	317.2	-267.6	-121.5	-25.0	-10.0
13.2	306.9	-290.4	-128.5	-27.0	-11.0
13.8	293.9	-313.9	-136.5	-28.0	-11.5
14.4	277.3	-332.8	-144.0	-27.0	-11.5
15.0	261.3	-348.6	-152.0	-27.0	-11.5
15.6	242.2	-361.9	-161.0	-25.0	-12.0
16.2	220.0	-373.3	-170.0	-23.0	-12.0
16.8	196.8	-383.1	-175.5	-25.0	-11.5
17.4	173.6	-387.5	-183.0	-25.0	-12.0
18.0	150.0	-388.4	-190.5	-26.0	-11.5
18.6	126.8	-387.5	-197.5	-26.0	-11.5

TABLE 9 Full-scale trajectory measured from overhead photographs.
Approach speed: 27 knots Rudder angle: 20 deg
Rudder rate: 5 deg/sec

Time sec	x ft	y ft	Heading angle deg	Roll angle deg	Drift angle deg
.0	.0	.0	.0	1.0	.0
.6	27.5	.0	.0	.0	.0
1.2	55.1	-.3	-1.5	-1.0	-1.0
1.8	82.5	-.8	-3.0	-3.0	-1.0
2.4	109.9	-2.4	-5.0	-6.0	-2.0
3.0	137.1	-3.6	-7.0	-7.0	-3.0
3.6	163.7	-6.4	-10.0	-10.0	-4.0
4.2	190.1	-9.4	-14.0	-12.0	-5.0
4.8	216.0	-14.4	-18.5	-15.0	-6.5
5.4	241.2	-20.5	-22.5	-17.0	-6.0
6.0	265.8	-30.0	-27.0	-21.0	-7.0
6.6	289.7	-39.2	-32.5	-24.0	-9.0
7.2	312.4	-50.8	-39.5	-27.0	-10.0
7.8	333.3	-64.8	-47.0	-28.0	-10.0
8.4	351.6	-80.9	-54.0	-29.0	-9.0
9.0	367.6	-99.1	-61.0	-28.0	-9.5
9.6	380.9	-118.5	-68.5	-27.0	-9.0
10.2	391.2	-139.0	-72.0	-24.0	-9.5
10.8	398.9	-160.1	-83.5	-23.0	-9.5
11.4	404.8	-182.7	-90.0	-20.0	-9.5
12.0	405.9	-206.5	-97.0	-18.0	-9.5
12.6	405.0	-230.1	-103.5	-18.0	-10.0
13.2	403.1	-254.5	-110.0	-19.0	-10.5
13.8	397.7	-278.3	-115.5	-21.0	-8.0
14.4	387.5	-300.7	-122.0	-24.0	-8.5
15.0	376.2	-322.3	-128.5	-26.0	-9.5
15.6	363.6	-342.7	-135.5	-27.0	-10.0
16.2	348.5	-360.6	-142.0	-27.0	-10.0
16.8	332.4	-376.9	-150.5	-27.0	-10.0
17.4	312.6	-390.8	-157.5	-27.0	-10.0
18.0	292.2	-401.8	-165.5	-24.0	-10.0
18.6	270.9	-409.8	-174.0	-23.0	-10.0
19.2	248.9	-414.8	-180.5	-20.0	-10.0
19.8	226.2	-416.1	-187.5	-19.0	-10.0
20.4	202.8	-417.2	-193.5	-20.0	-10.0
21.0	180.8	-414.1	-199.5	-18.0	-9.0

TABLE 10 Full-scale trajectory measured from overhead photographs.
Approach speed: 27 knots Rudder angle: 30 deg
Rudder rate: 10 deg/sec

Time sec	x ft	y ft	Heading angle deg	Roll angle deg	Drift angle deg
.0	.0	.0	.0	-1.0	.0
.6	27.4	.0	.0	-1.0	-.5
1.2	54.5	.8	.0	-3.0	-.5
1.8	81.0	-.2	-2.5	-6.0	-.5
2.4	106.7	-.8	-5.5	-9.0	-1.5
3.0	131.6	-2.5	-8.5	-14.0	-3.0
3.6	155.3	-4.8	-14.0	-19.0	-6.0
4.2	178.0	-8.7	-20.5	-24.0	-8.5
4.8	199.4	-14.2	-28.5	-28.0	-11.0
5.4	219.4	-21.5	-38.5	-33.0	-13.5
6.0	237.8	-30.2	-46.5	-30.0	-13.0
6.6	254.2	-42.2	-54.0	-24.0	-11.0
7.2	268.0	-60.2	-59.0	-20.0	-8.0
7.8	280.7	-78.2	-64.5	-19.0	-8.0
8.4	292.0	-96.1	-69.0	-19.0	-9.0
9.0	301.8	-115.0	-75.0	-20.0	-9.0
9.6	309.6	-133.9	-84.0	-22.0	-9.0
10.2	314.2	-156.7	-87.5	-25.0	-8.0
10.8	316.5	-177.0	-91.0	-27.0	-7.0
11.4	317.7	-199.1	-95.0	-26.0	-7.0
12.0	317.0	-220.6	-100.0	-26.0	-6.5
12.6	314.1	-242.1	-108.5	-25.0	-8.0
13.2	308.5	-263.8	-117.5	-24.0	-9.0
13.8	299.9	-284.1	-122.0	-23.0	-7.5
14.4	289.2	-303.5	-128.5	-21.0	-8.0
15.0	277.5	-322.6	-133.0	-20.0	-7.0
15.6	264.0	-339.2	-138.0	-19.0	-8.0
16.2	249.4	-355.1	-144.5	-20.0	-7.0

TABLE 11 Full-scale trajectory measured from overhead photographs.
Approach speed: 27 knots Rudder angle: 30 deg
Rudder rate: 5 deg/sec

Time sec	x ft	y ft	Heading angle deg	Roll angle deg	Drift angle deg
.0	.0	.0	1.0	-1.0	.0
.6	27.4	.0	.0	-1.0	.5
1.2	54.8	-.3	-1.5	-3.0	.5
1.8	82.0	-.9	-2.5	-5.0	.0
2.4	108.9	-2.1	-5.0	-7.0	-1.0
3.0	135.6	-4.0	-8.0	-9.0	-2.5
3.6	161.7	-6.9	-11.0	-10.0	-3.5
4.2	187.4	-11.4	-14.5	-14.0	-4.0
4.8	212.2	-16.7	-19.0	-16.0	-5.0
5.4	236.4	-23.3	-24.5	-18.0	-6.5
6.0	259.0	-32.5	-31.0	-21.0	-7.5
6.6	281.4	-43.6	-38.5	-25.0	-10.0
7.2	302.2	-56.6	-46.5	-30.0	-11.5
7.8	320.7	-71.6	-51.0	-28.0	-8.5
8.4	337.3	-89.1	-54.5	-27.0	-6.0
9.0	351.8	-107.3	-59.5	-28.0	-4.5
9.6	364.7	-126.8	-62.5	-28.0	-5.0
10.2	375.9	-146.2	-67.0	-27.0	-5.0
10.8	385.9	-166.6	-72.0	-26.0	-5.0
11.4	394.4	-188.6	-76.5	-24.0	-6.0
12.0	401.0	-210.4	-81.5	-23.0	-5.5
12.6	405.0	-232.8	-85.5	-24.0	-5.0
13.2	407.9	-255.1	-90.0	-24.0	-5.0
13.8	409.0	-277.4	-95.0	-25.0	-5.0
14.4	408.6	-299.6	-99.0	-24.0	-6.0
15.0	406.3	-321.4	-104.5	-24.0	-6.0

TABLE 12 Full-Scale Turning Parameters

Approach speed, kt	Rudder angle deg	Rudder rate deg/sec	Advance ft	Transfer ft	Tactical diameter ft
10	20	5	214	221	279
10	20	10	185	122	278
10	30	5	190	87	201
10	30	10	164	74	185
27	20	5	405	183	414
27	20	10	330	158	386
27	30	5	408	255	501*
27	30	10	316	171	408*

*Estimated

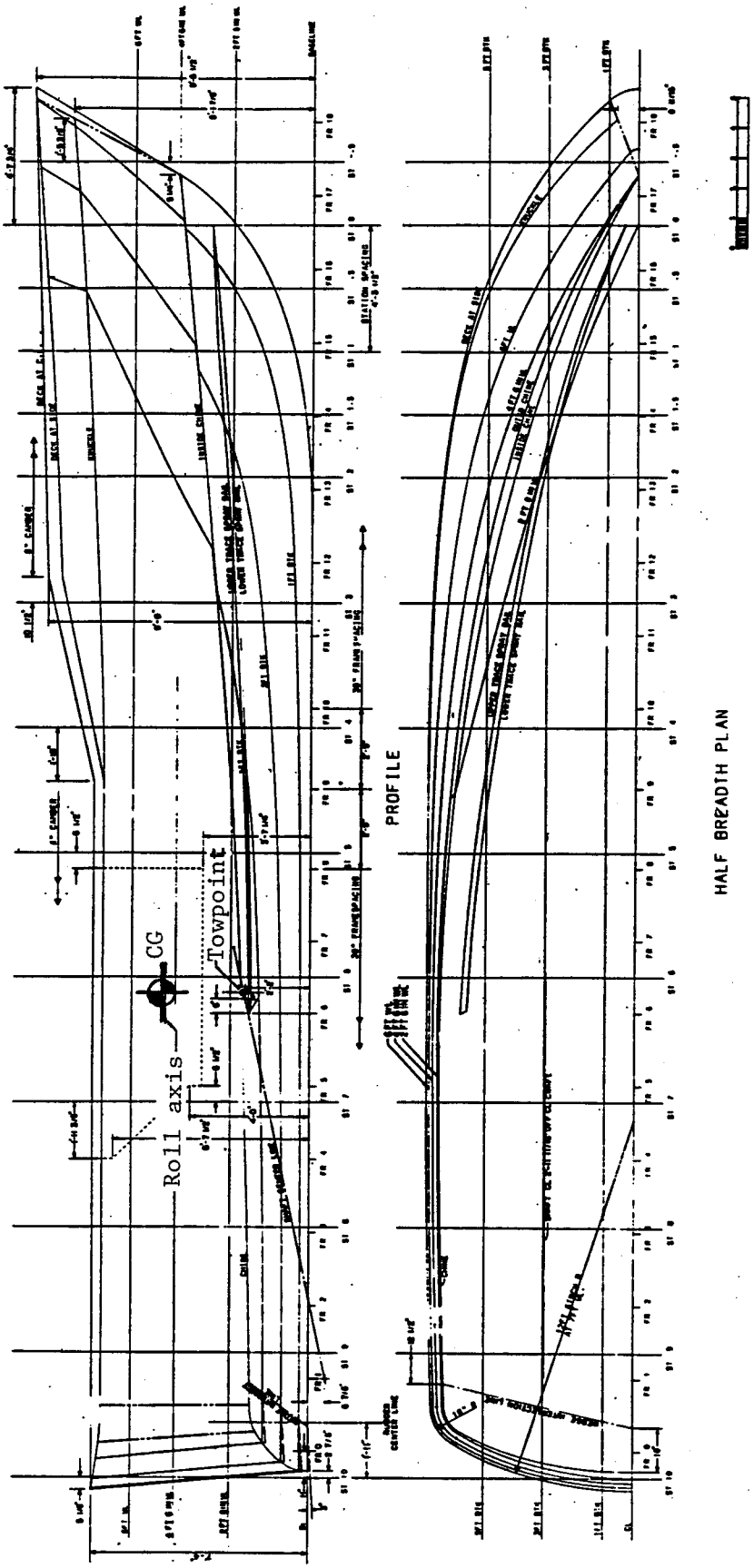

PARTICULARS

Length overall	47.3 ft
Length between perpendiculars	42.9 ft
Max. beam at chine	14.0 ft
Displacement	41,985 lb
LCG, aft of amidships	4.84 ft
VCG, above baseline	5.04 ft
Propeller diameter	2.33 ft
Model scale ratio	9.032

FIGURE 1 Lines and particulars of the USCG 47 ft Motor Life Boat

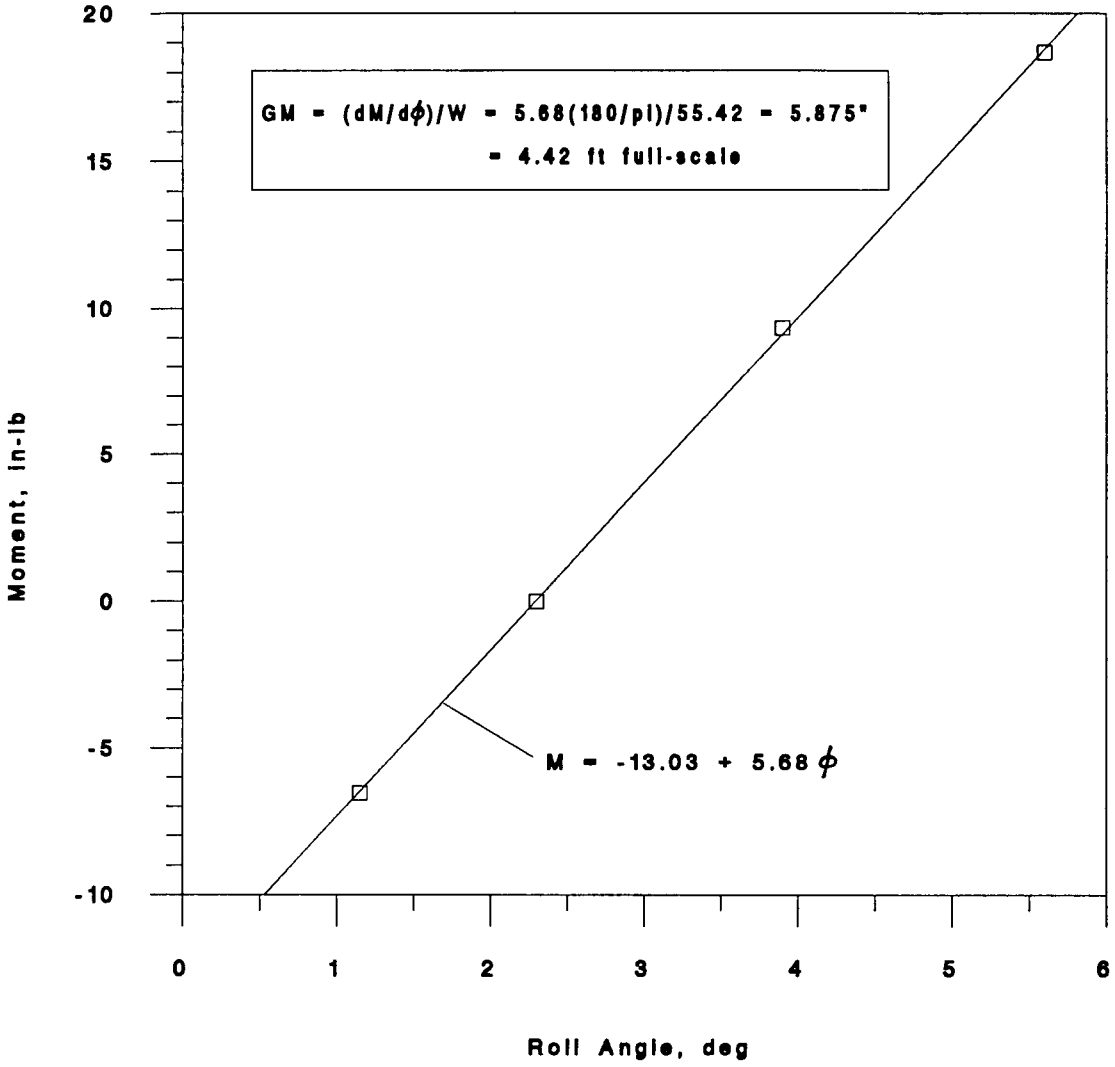

Figure 2 Inclining Experiment

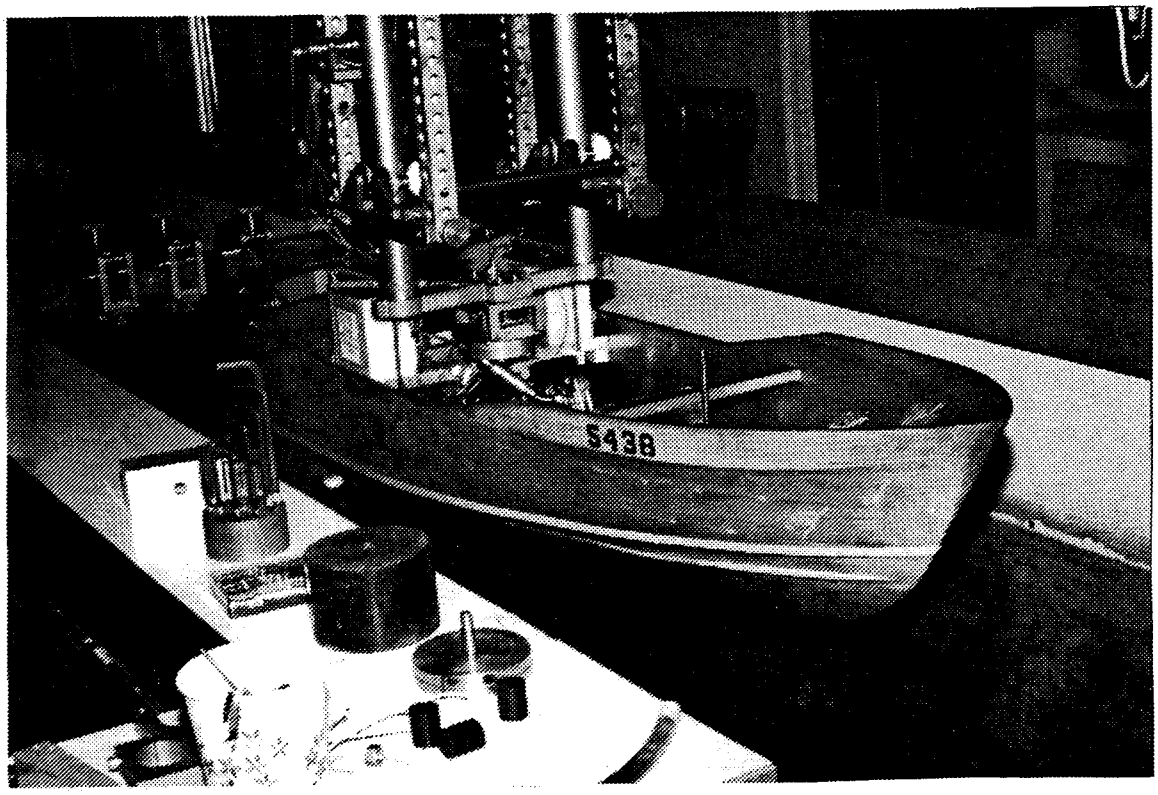

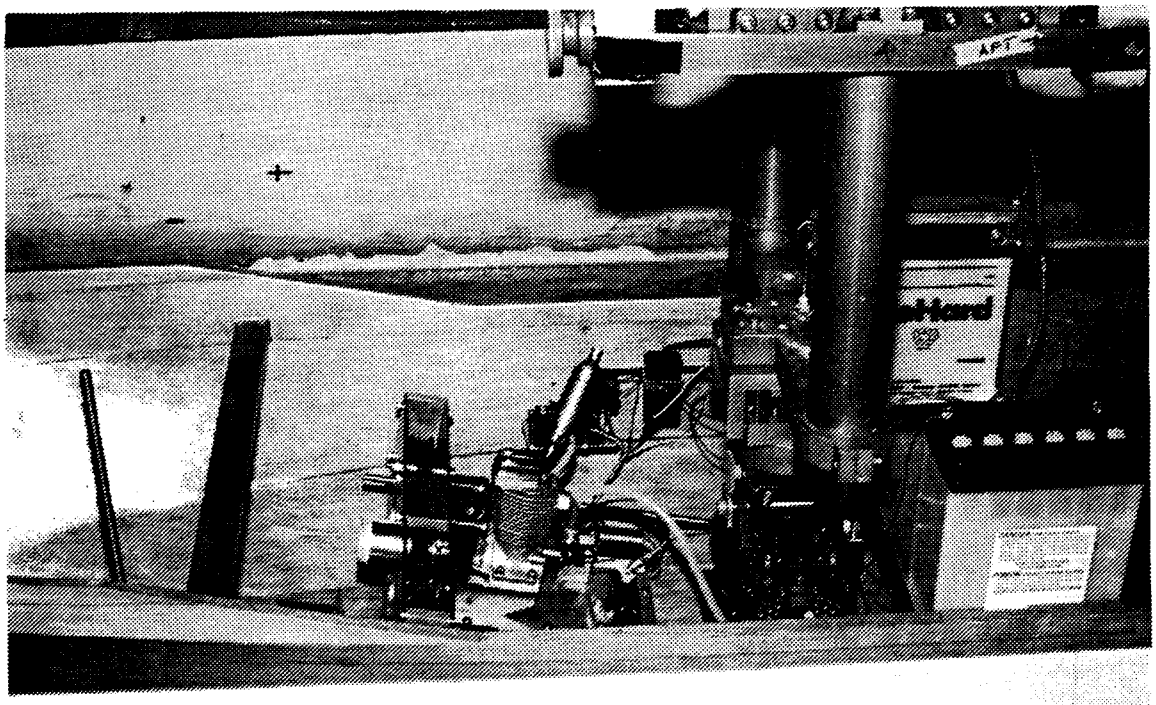

FIGURE 3 Rudder Effectiveness Test Rig

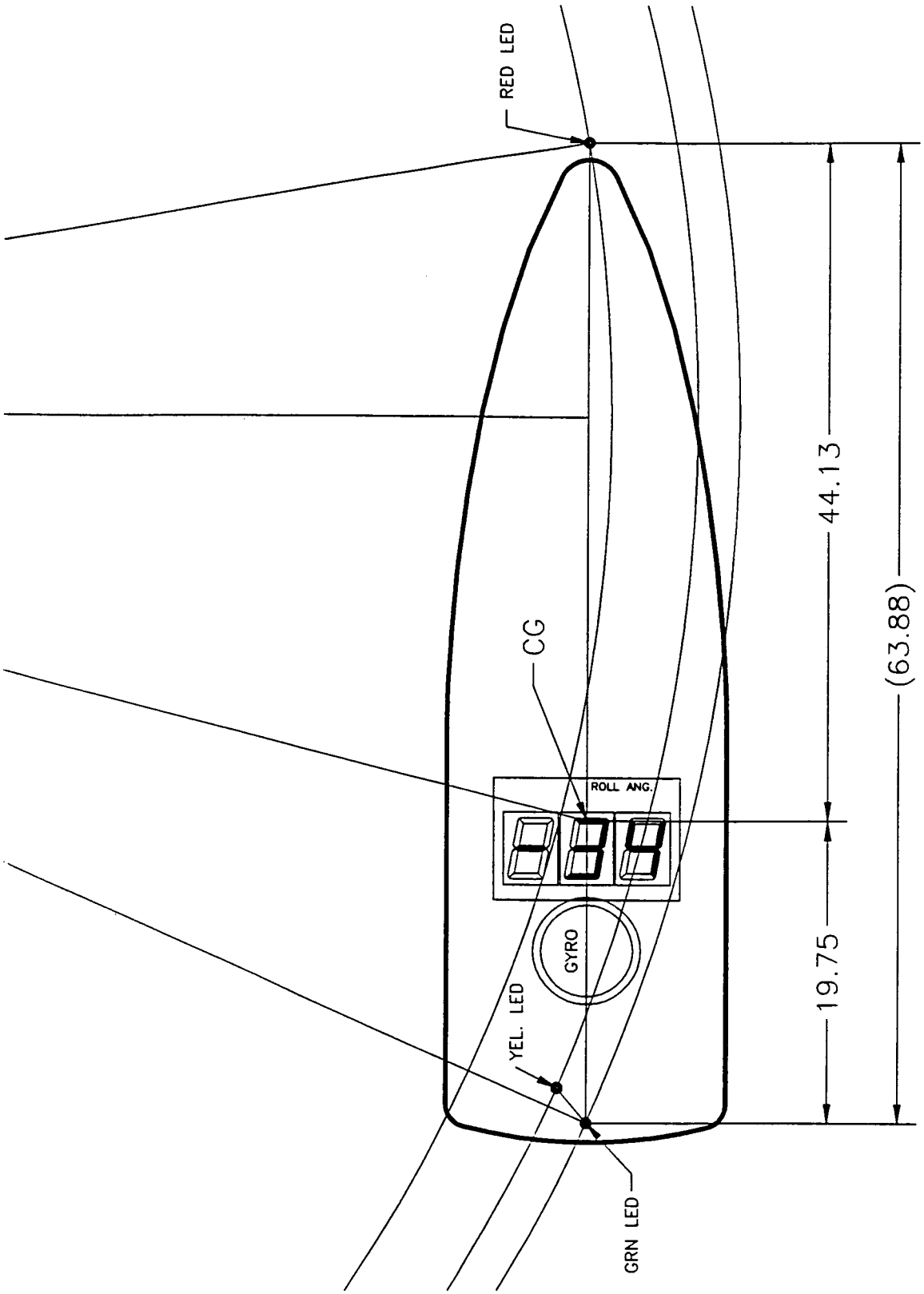

FIGURE 4 INSTRUMENTATION FOR FREE-RUNNING MODEL TESTS. LIGHT LOCATIONS IN INCHES (MODEL)

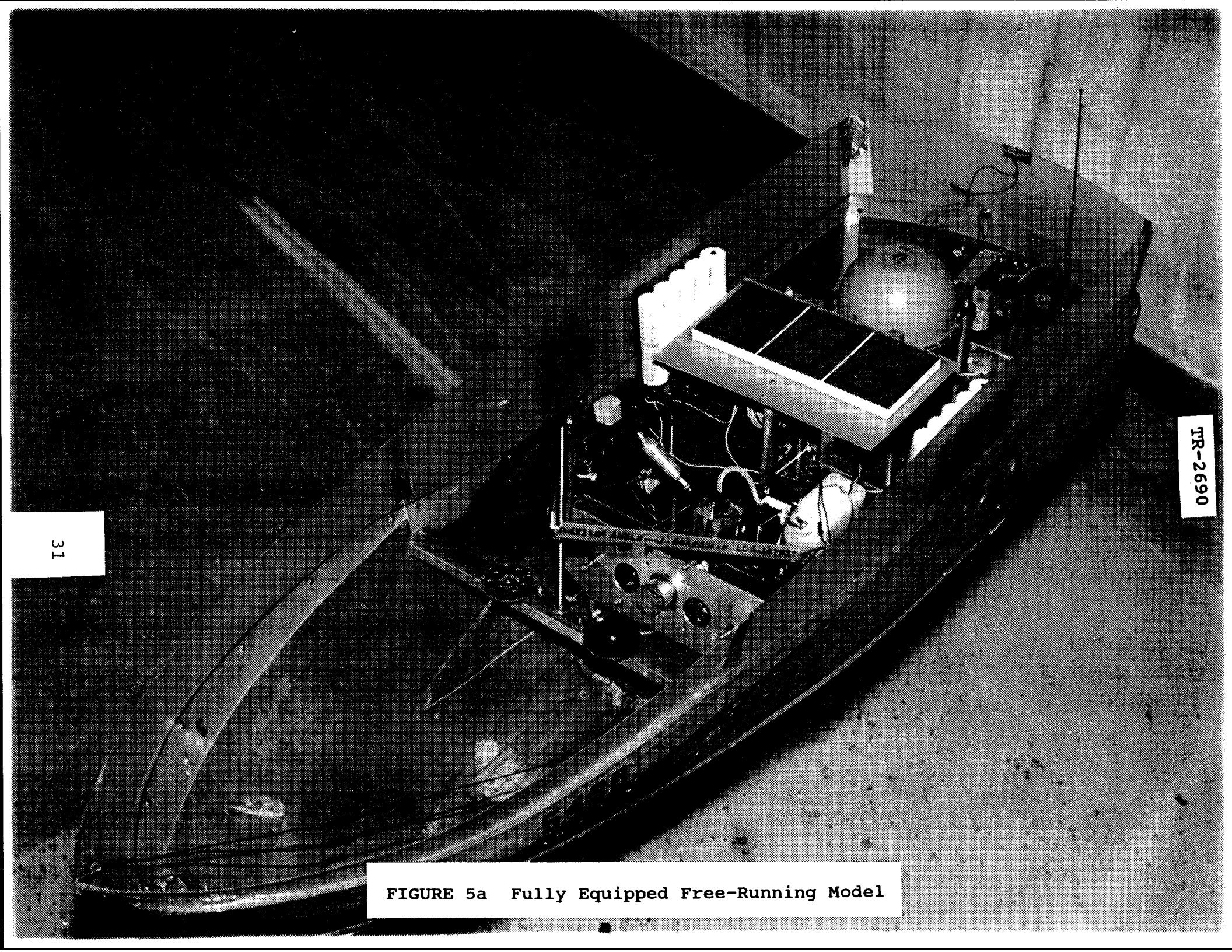

FIGURE 5a Fully Equipped Free-Running Model

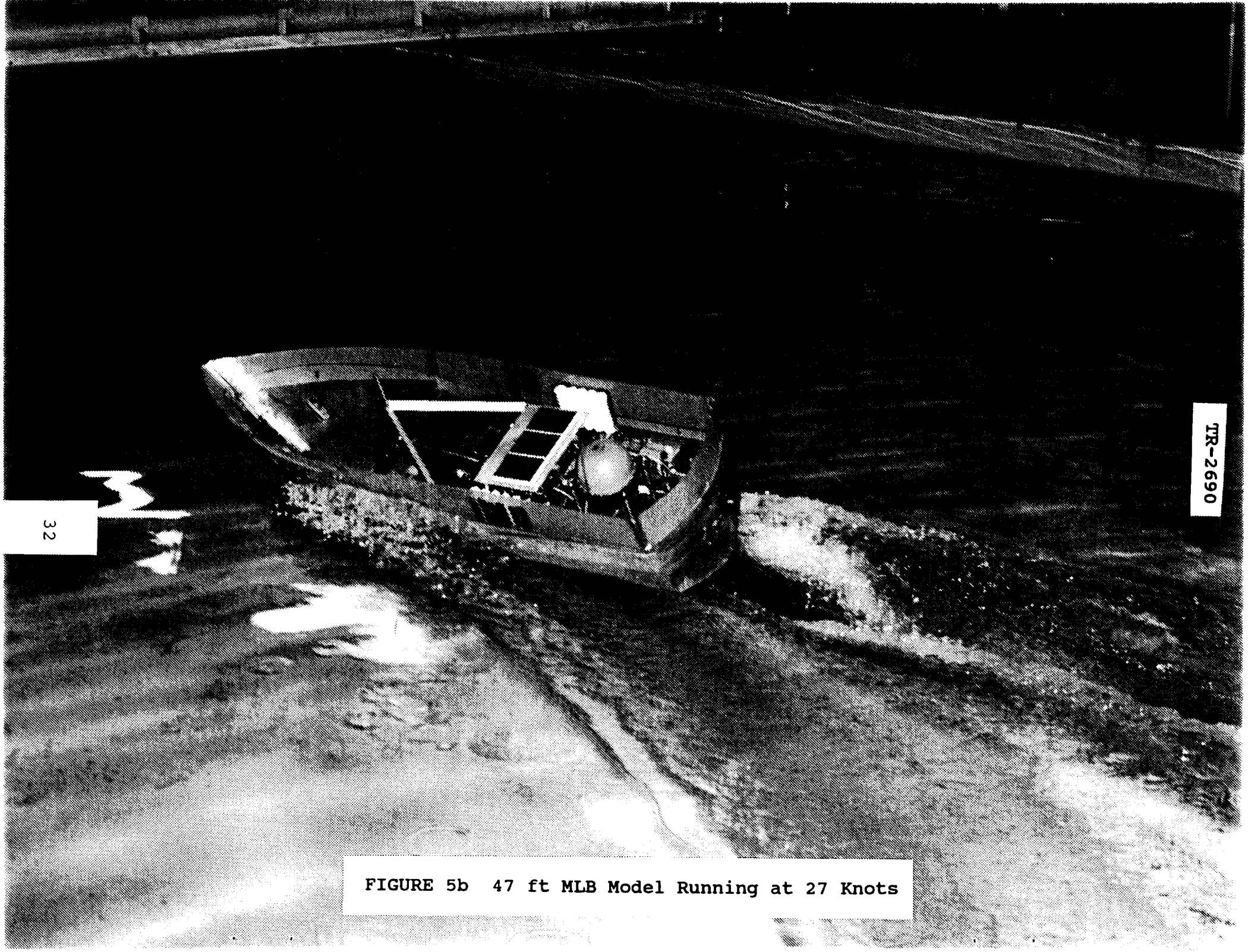

FIGURE 5b 47 ft MLB Model Running at 27 Knots

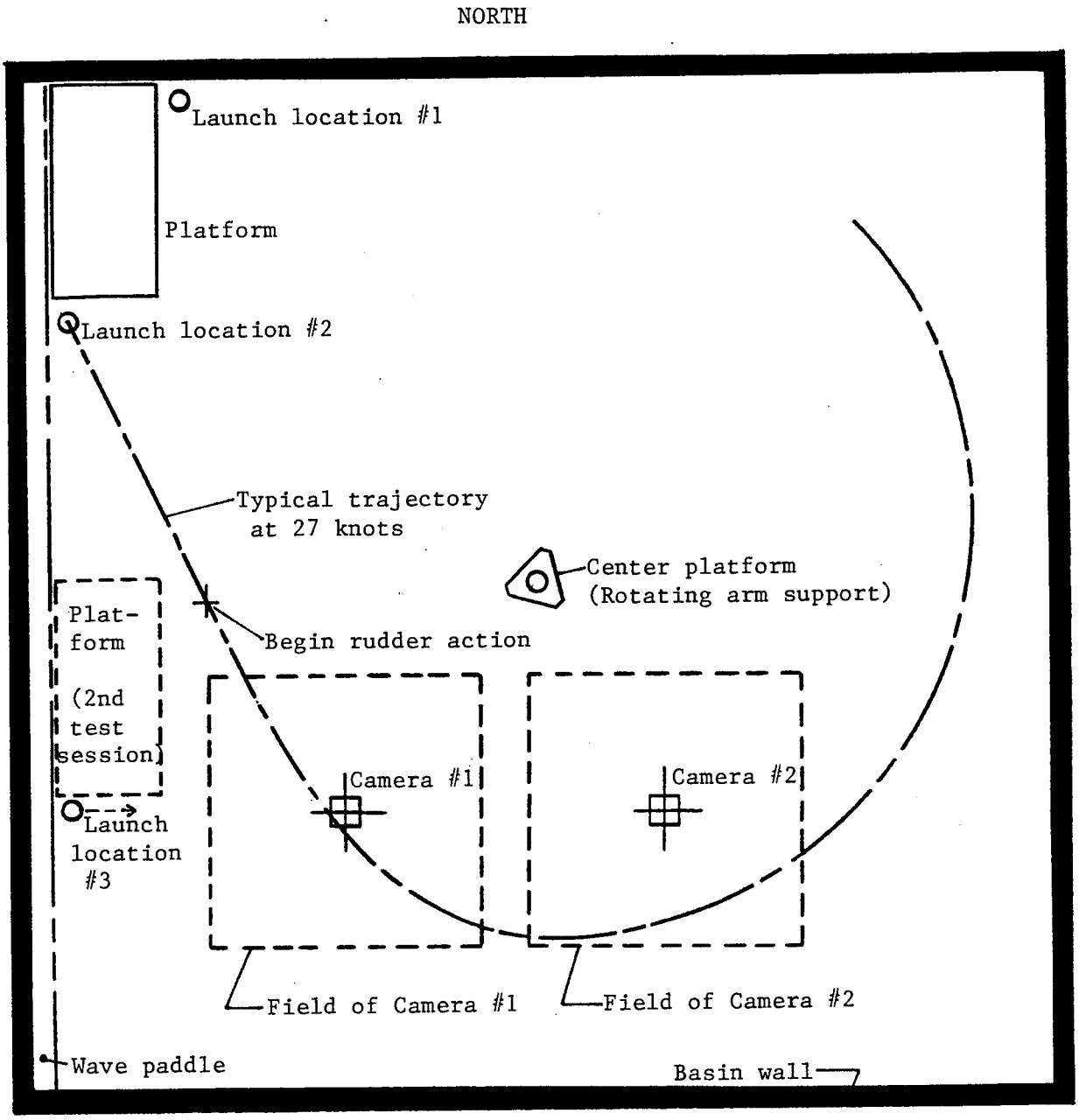

FIGURE 6 Plan View of Maneuvering Basin showing Platform and Camera Locations and a Typical High-Speed Trajectory

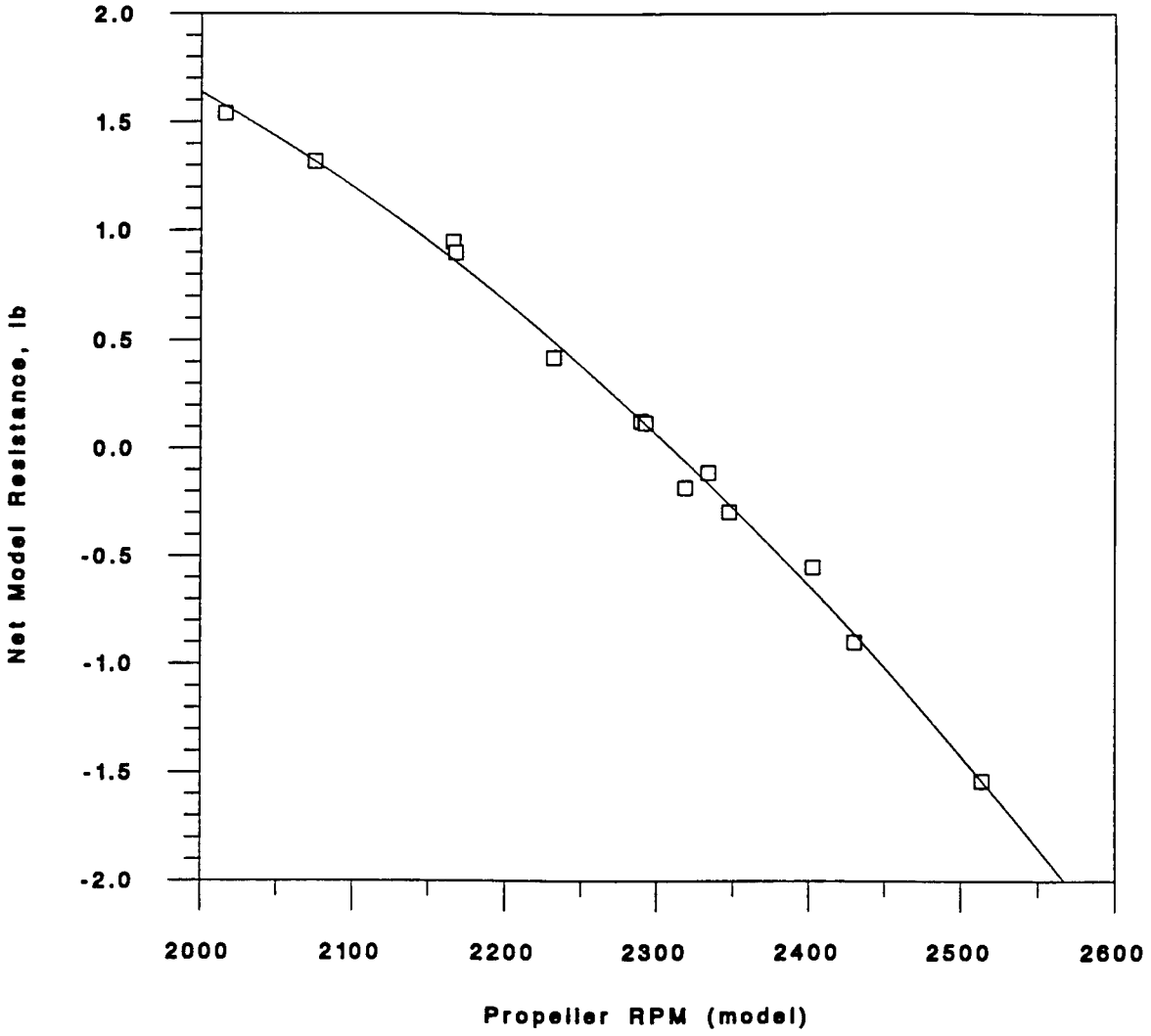

Figure 7 Net Resistance vs Propeller Speed
Speed: 10 knots

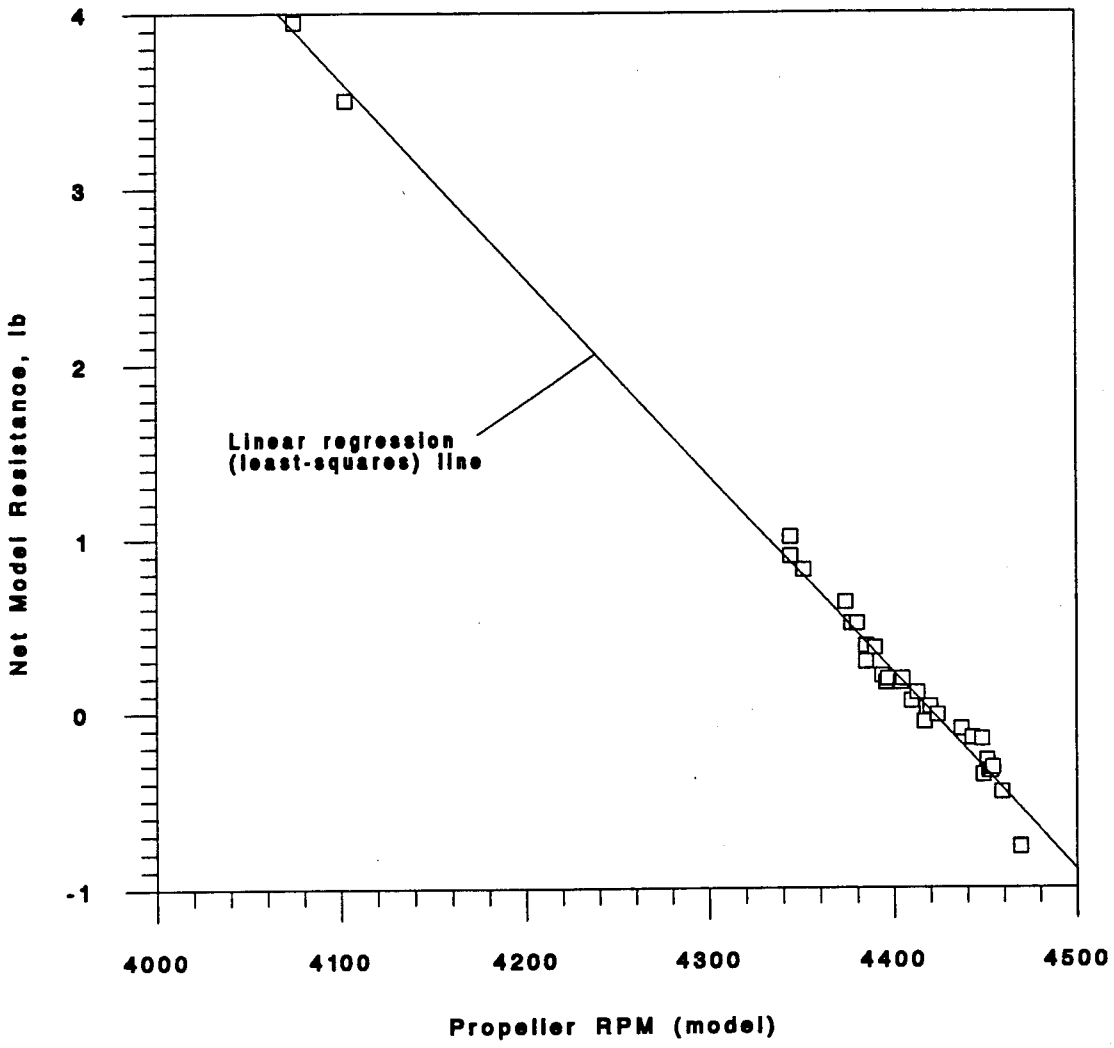

Figure 8 Net Resistance vs Propeller Speed
Speed: 27 knots

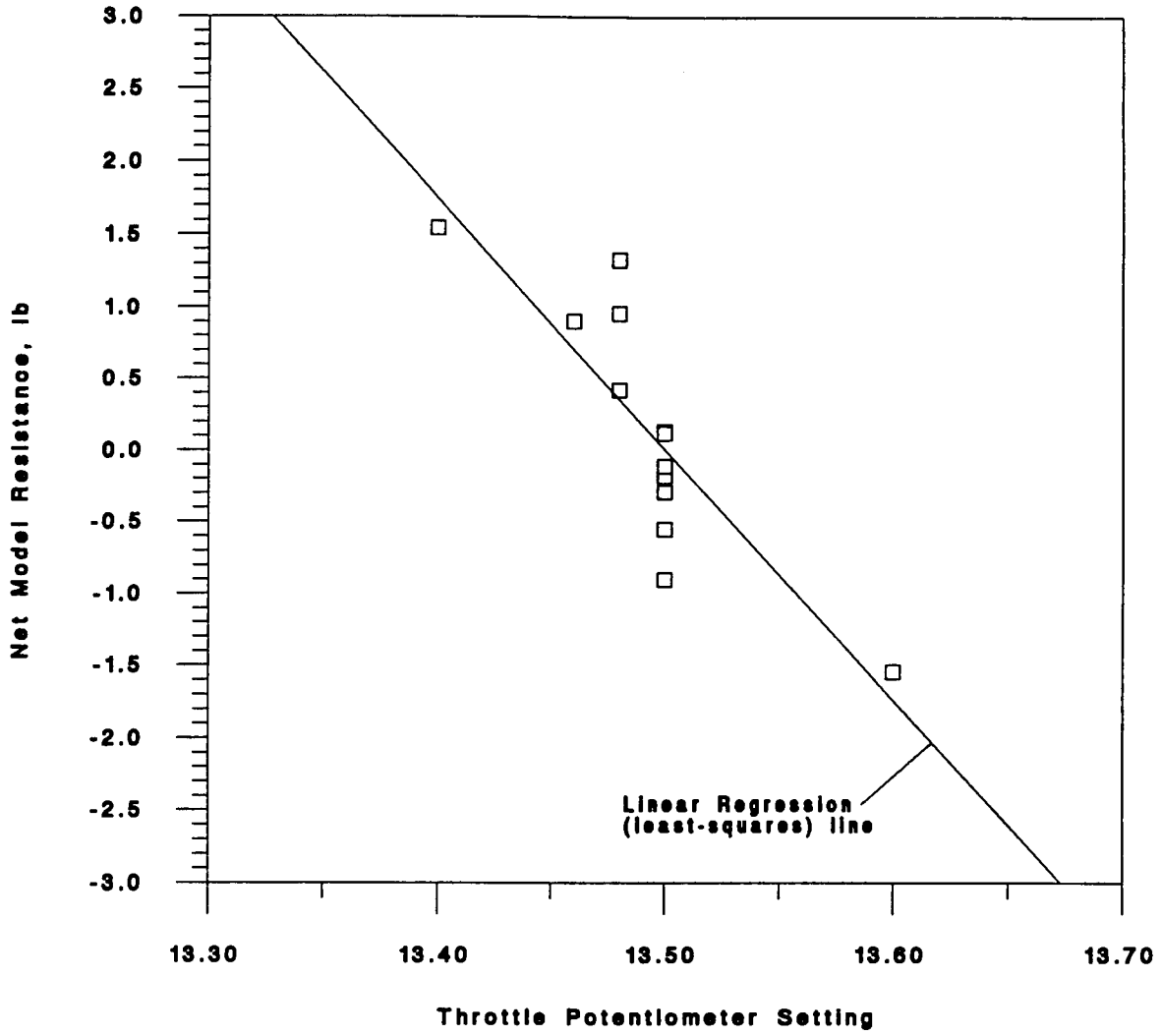

Figure 9 Net Resistance vs Throttle Setting
Speed: 10 knots

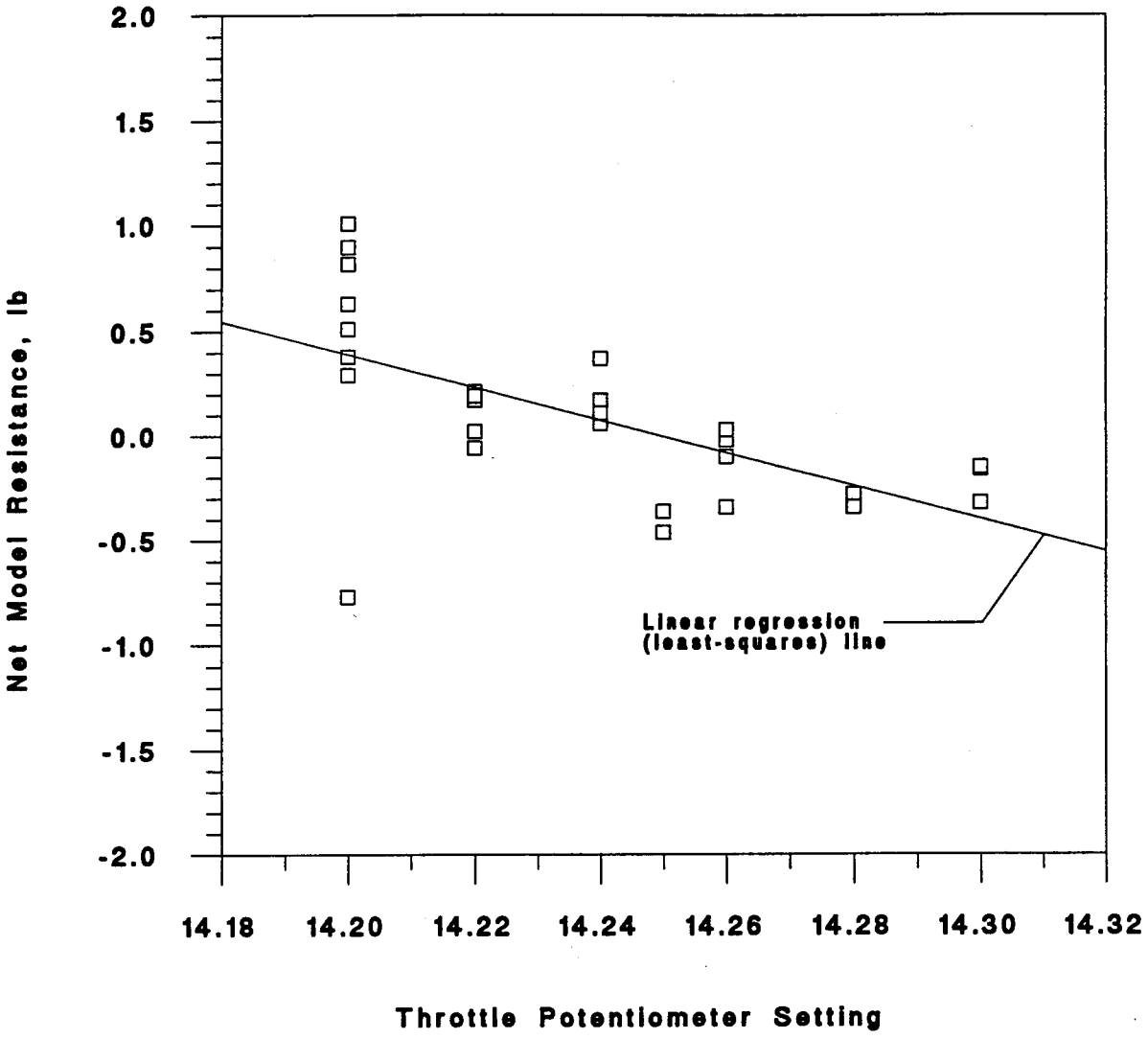

Figure 10 Net Resistance vs Throttle Setting
Speed: 27 knots

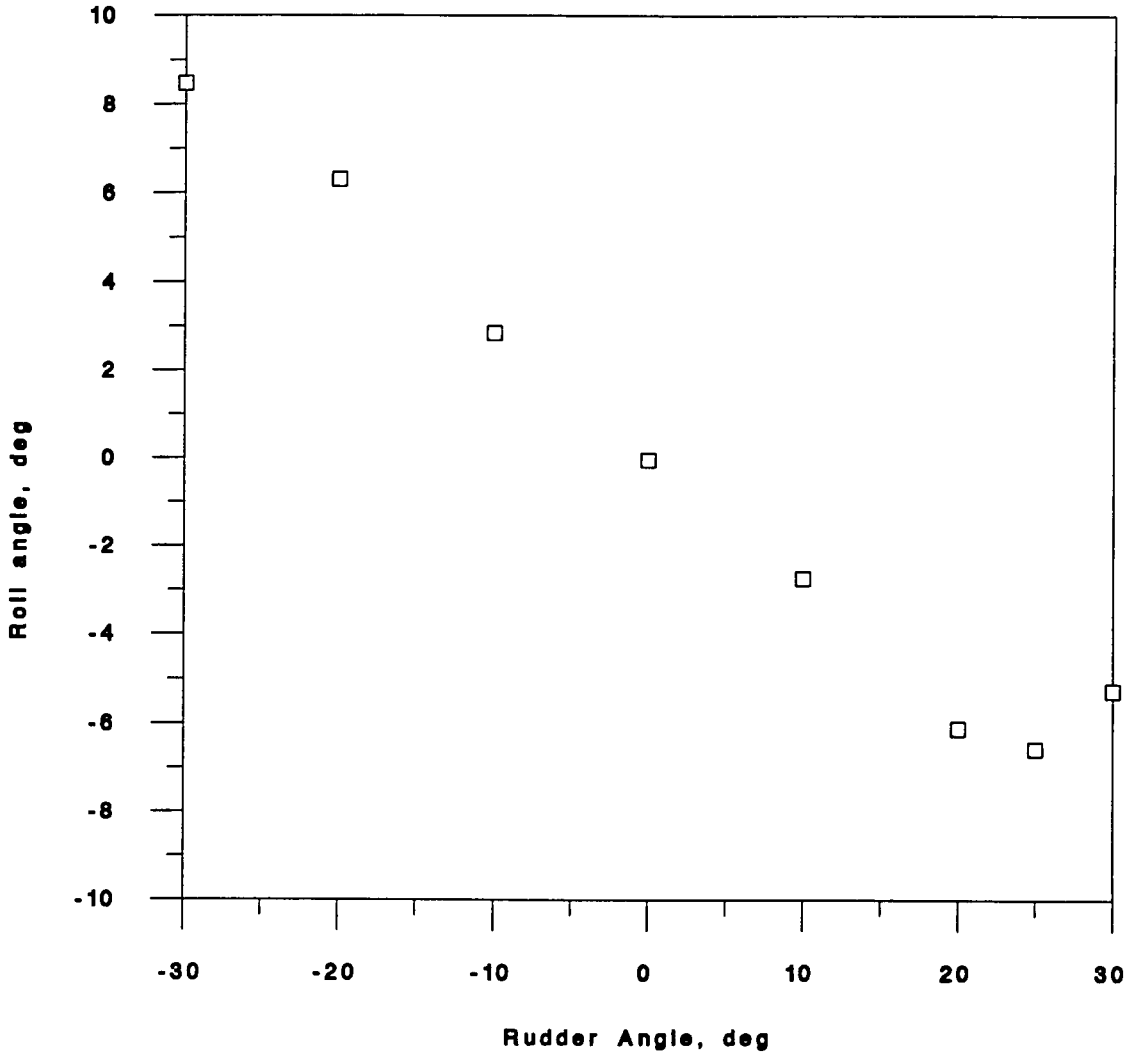

Figure 11 Roll angle vs Rudder Deflection on Straight-Course; Speed = 10 knots

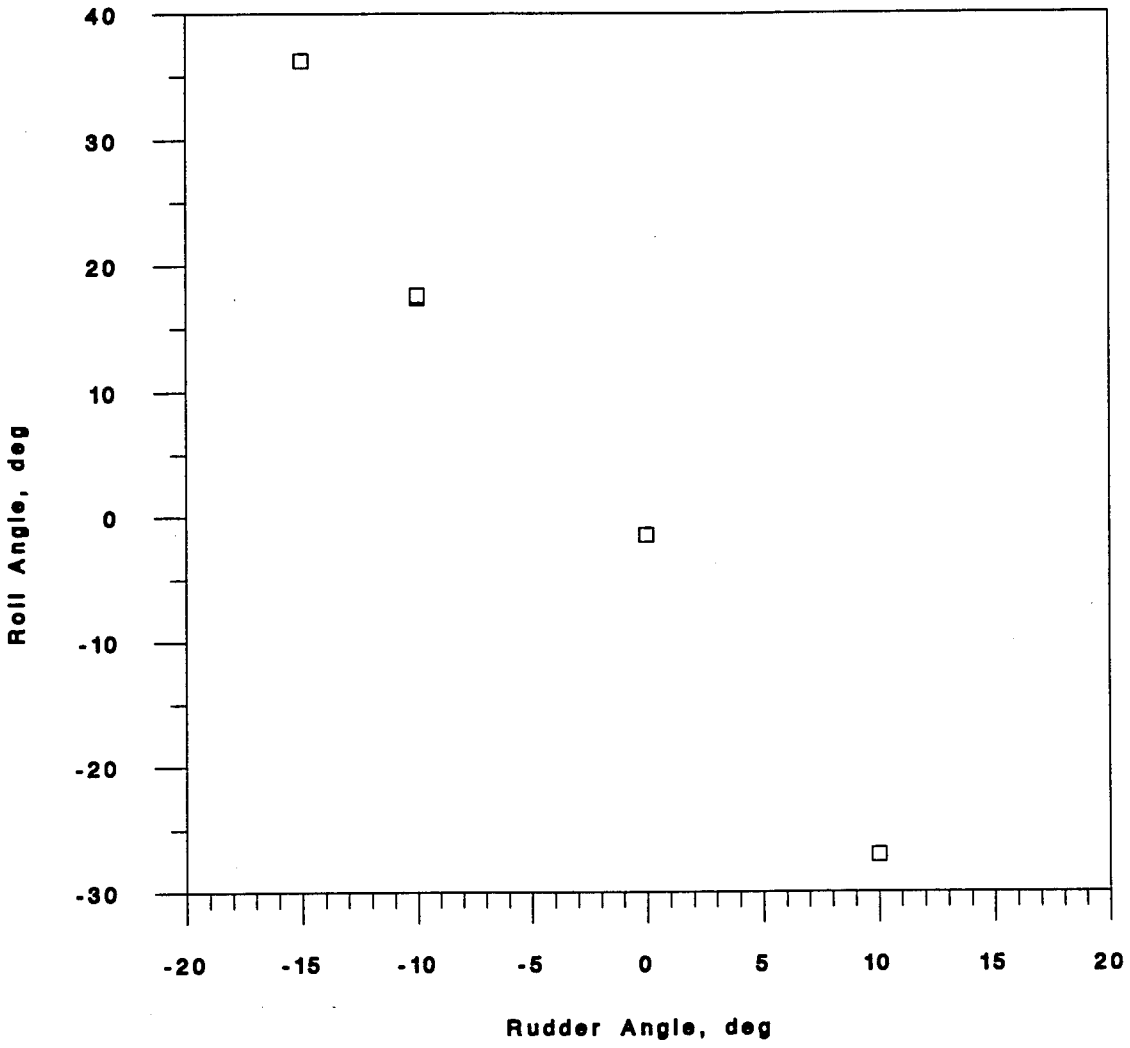

Figure 12 Roll Angle vs Rudder Deflection on Straight Course; Speed = 27 knots

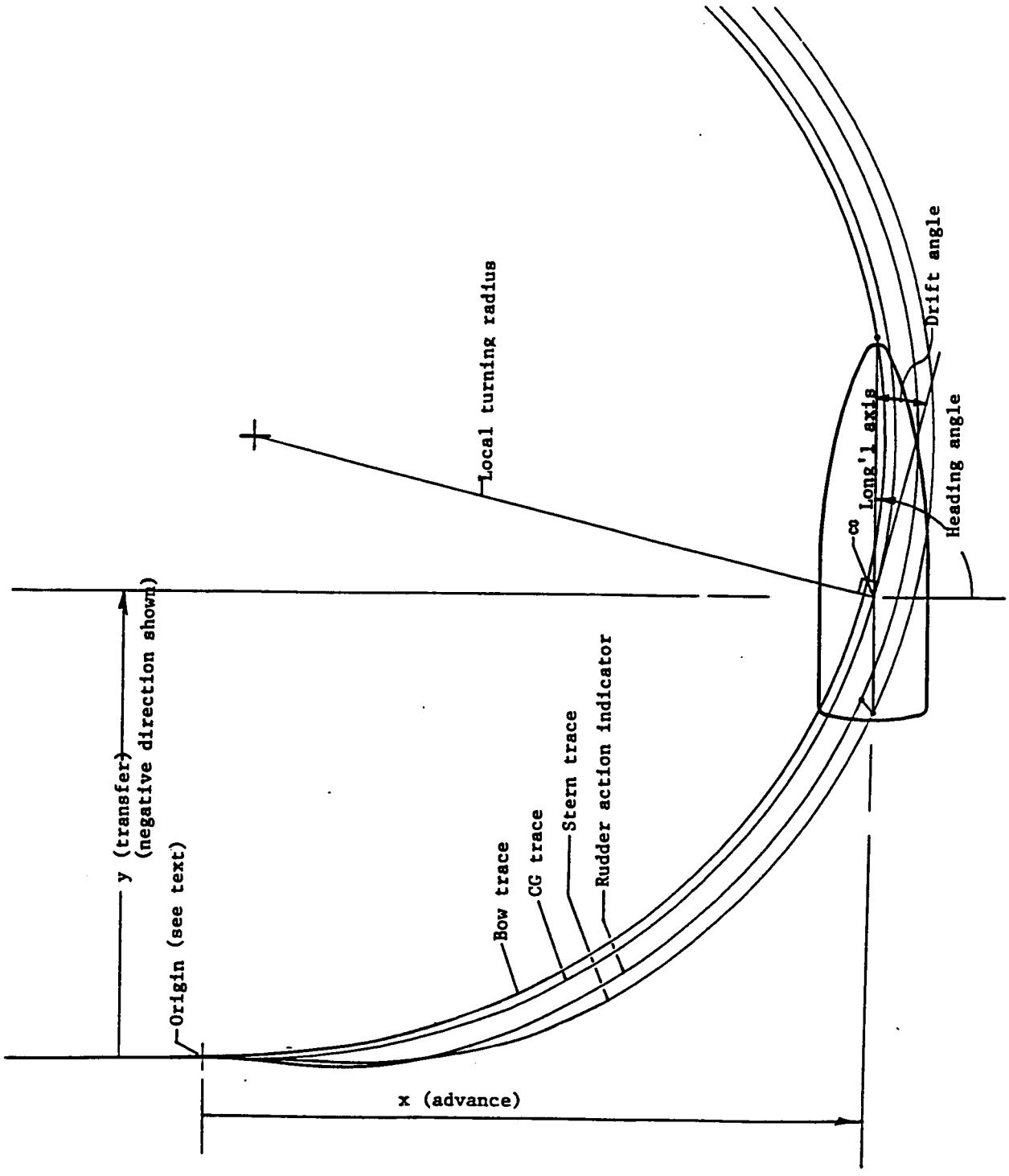

FIGURE 13 Definition of turning parameters and coordinate system

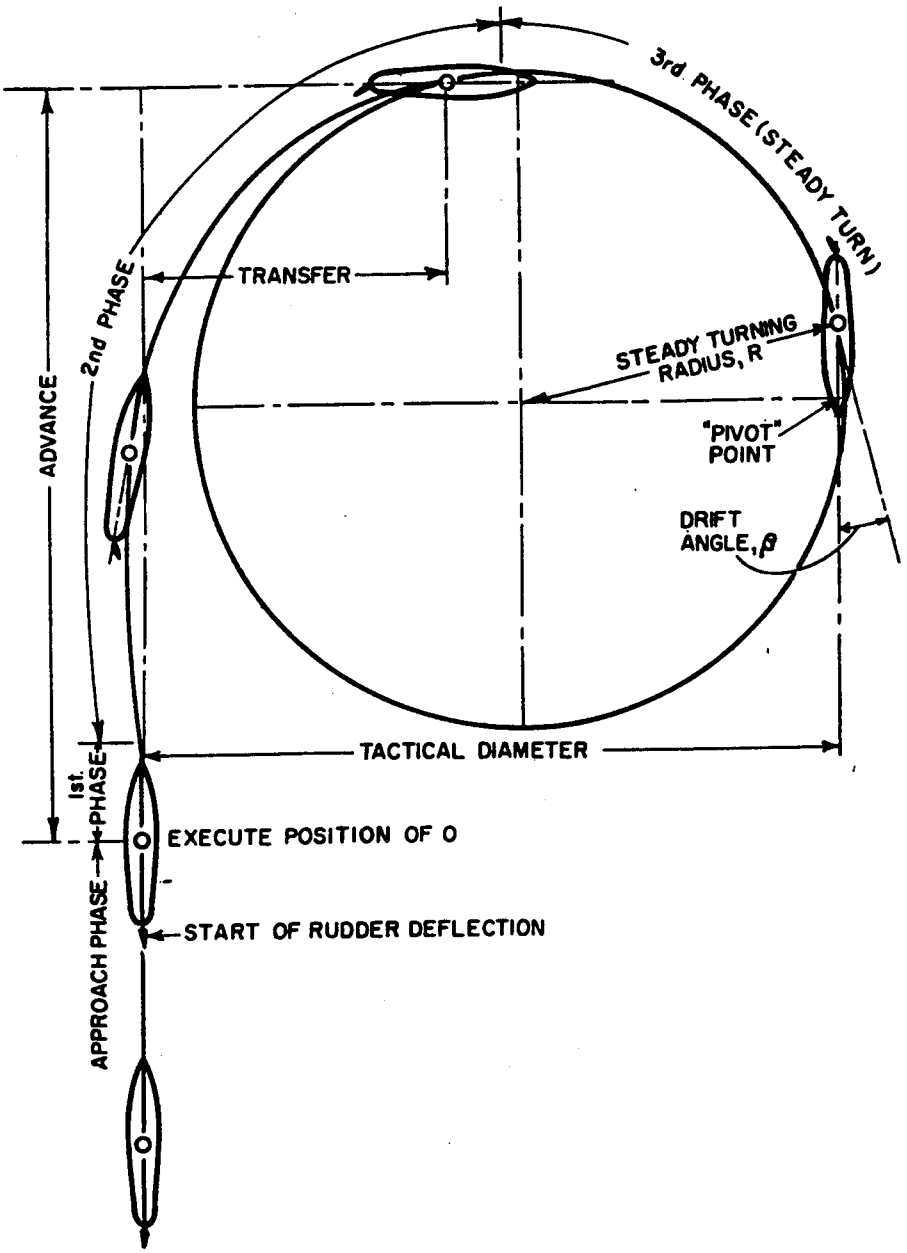

FIGURE 14 Definition of Turning Parameters (from Ref. 1)

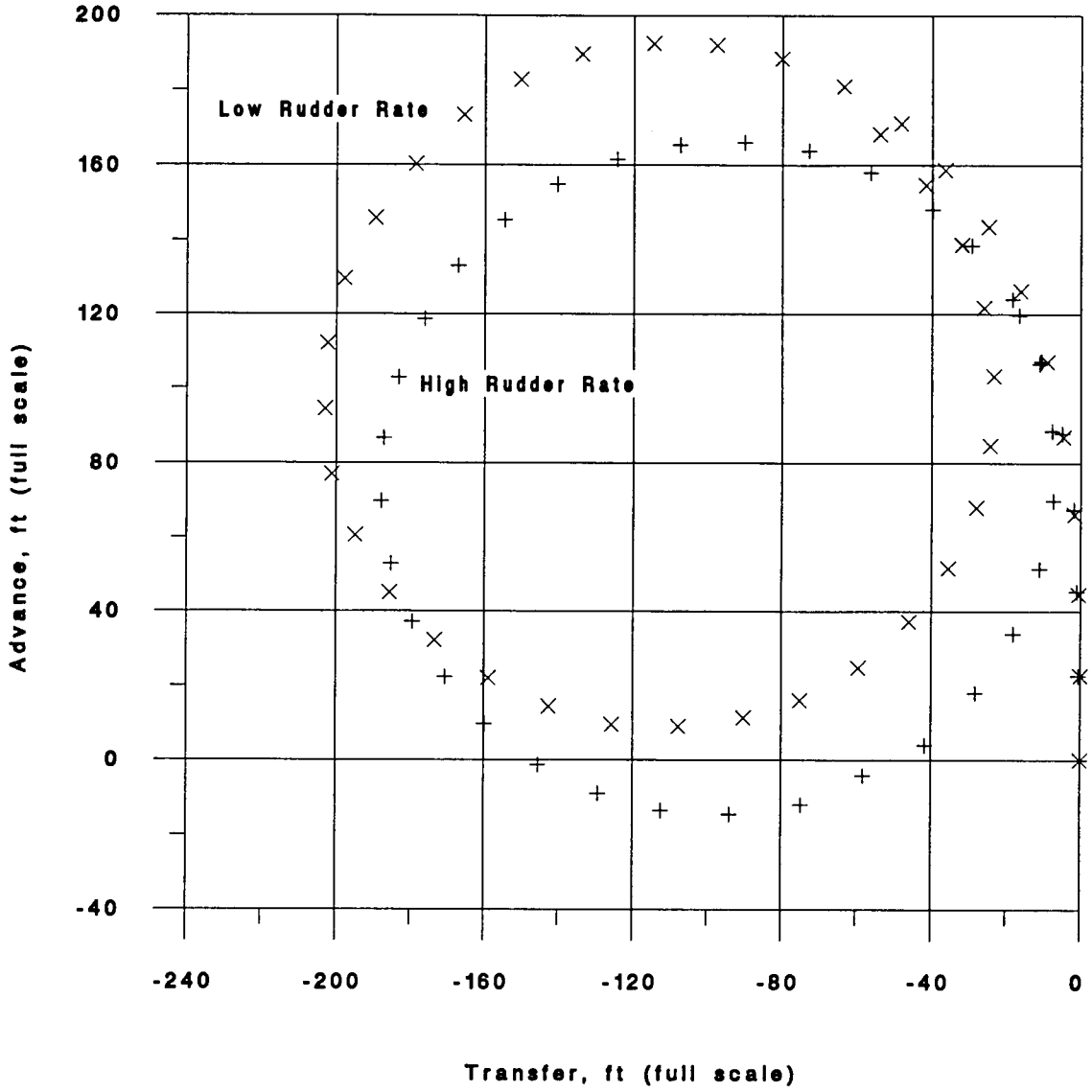

FIGURE 15 Turning Trajectory of 47 ft MLB
Approach: 10 kt Rudder: 30 deg

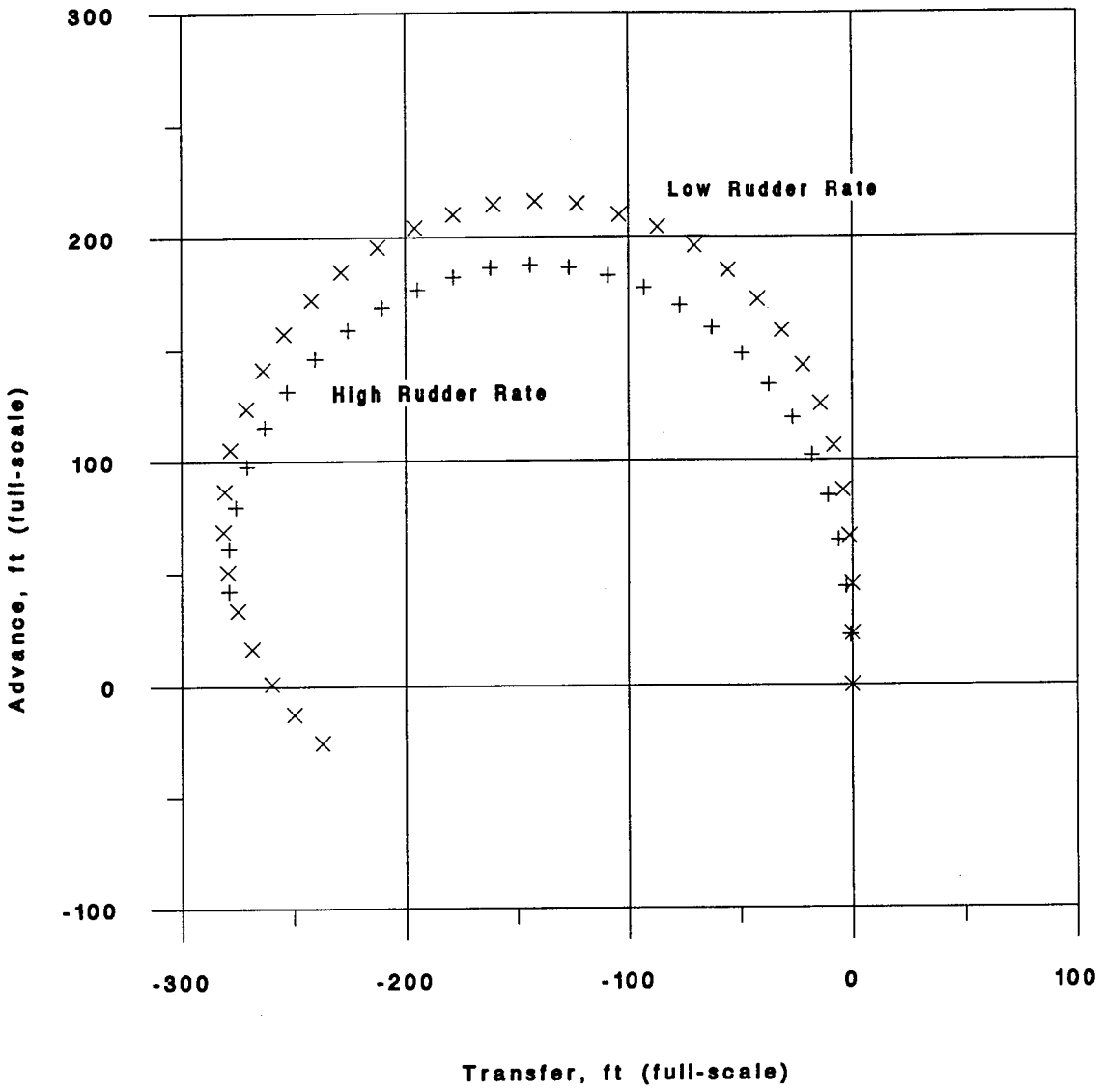

FIGURE 16 Turning Trajectory of 47 ft MLB
Approach: 10 kt Rudder: 20 deg

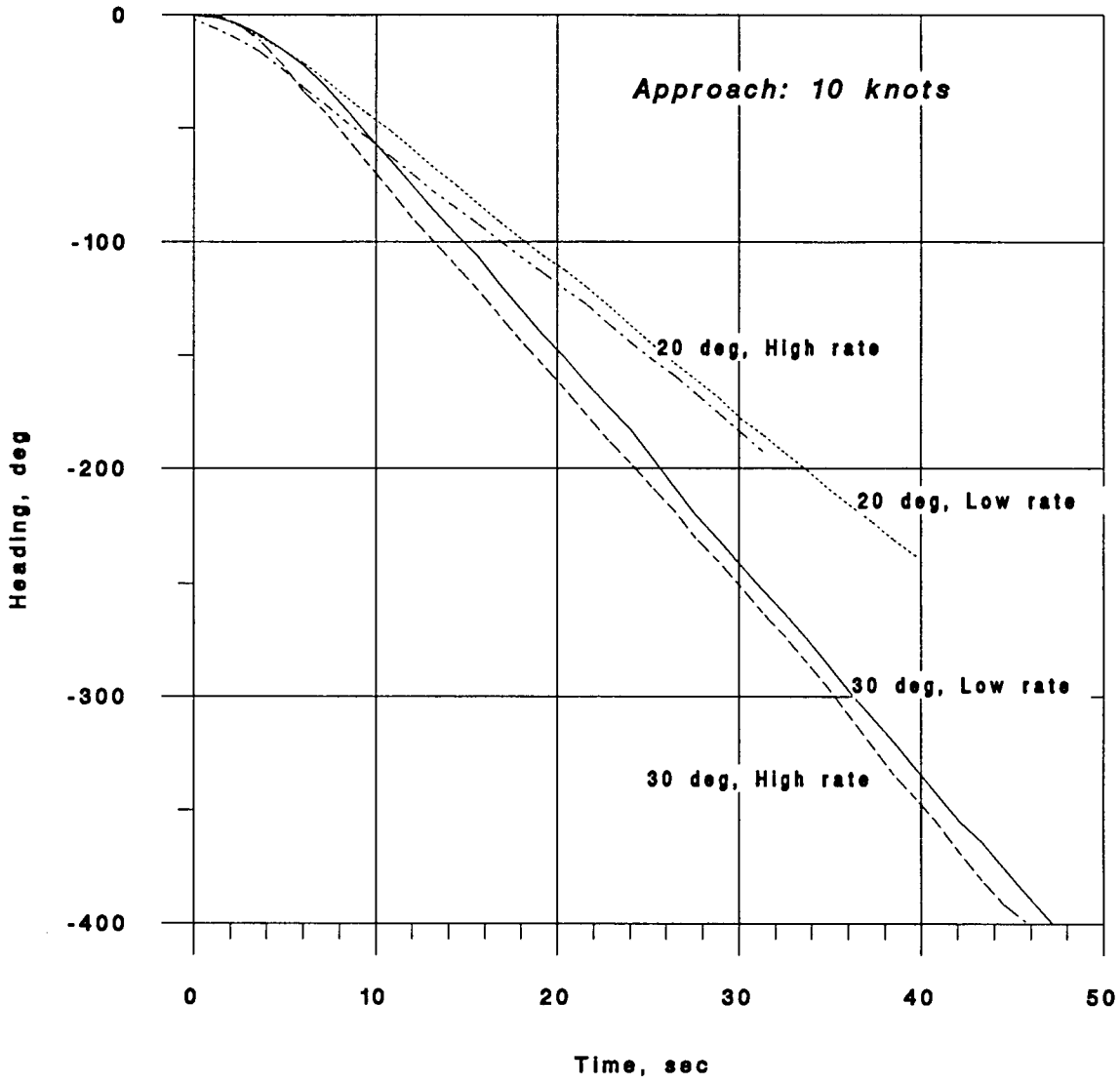

FIGURE 17 Time history of heading in low speed turns. Full scale units.

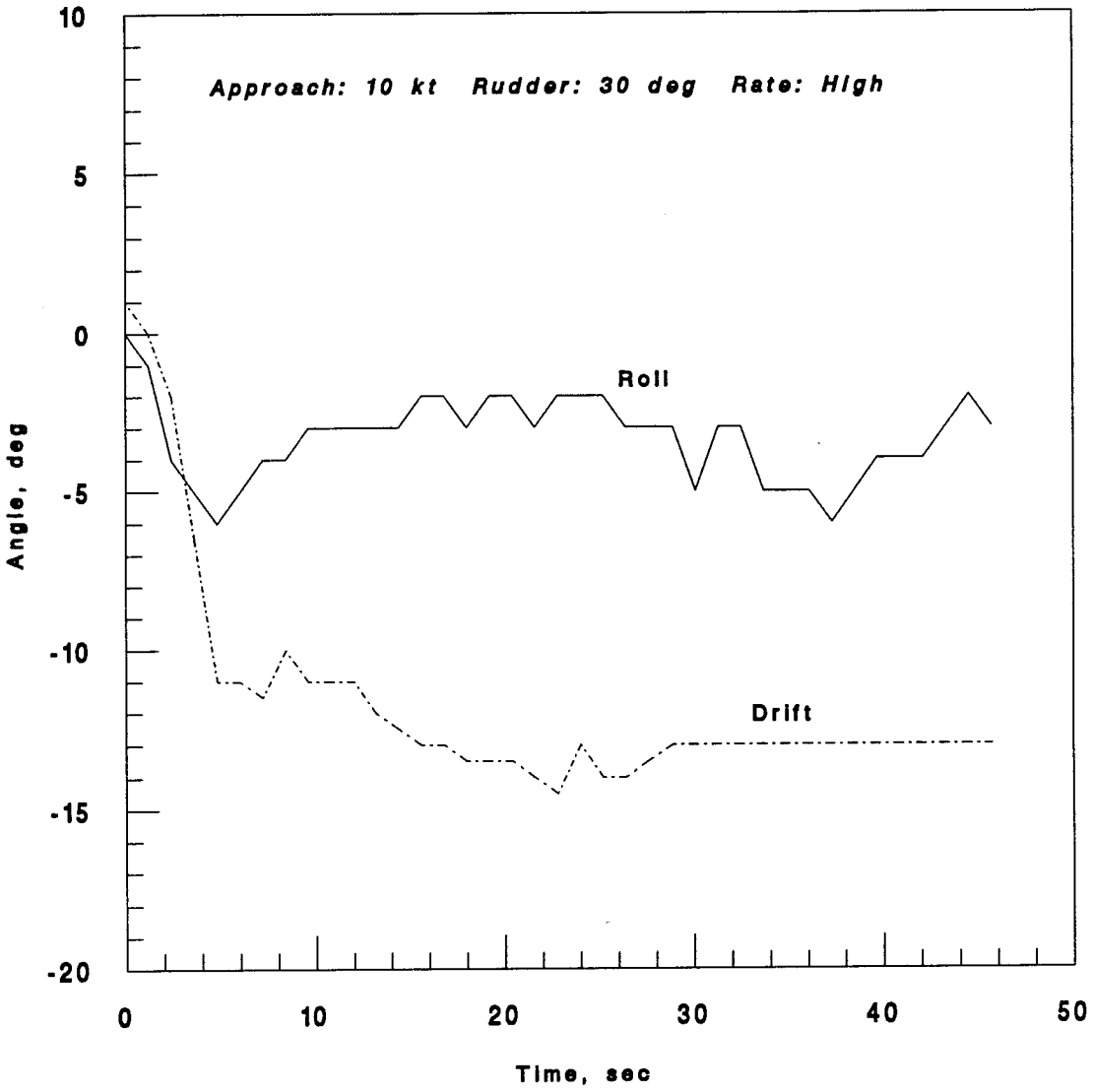

FIGURE 18 Time history of roll and drift angles in a turn. Full scale units.

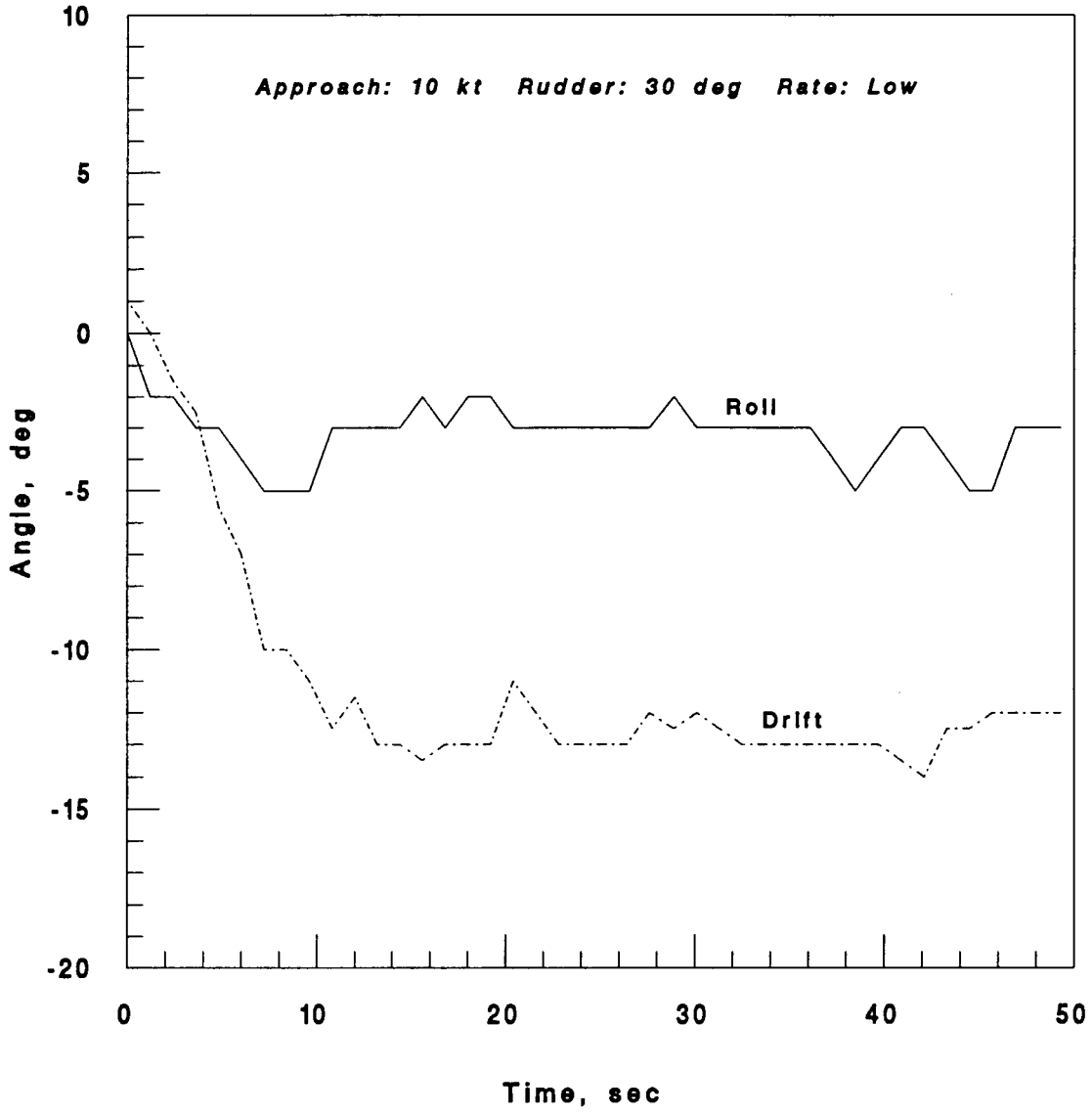

FIGURE 19 Time history of roll and drift angles in a turn. Full scale units.

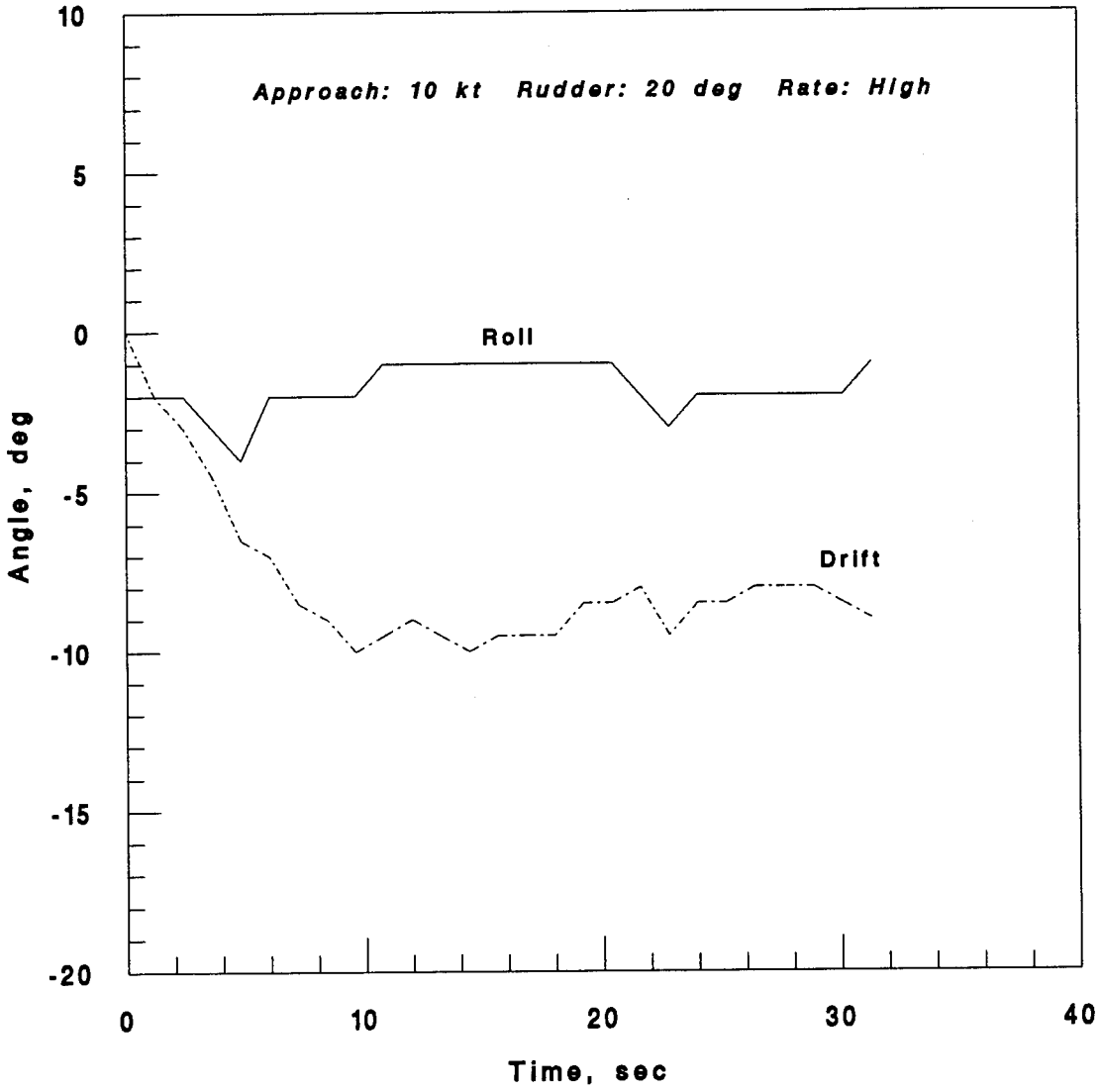

FIGURE 20 Time history of roll and drift angles in a turn. Full scale units.

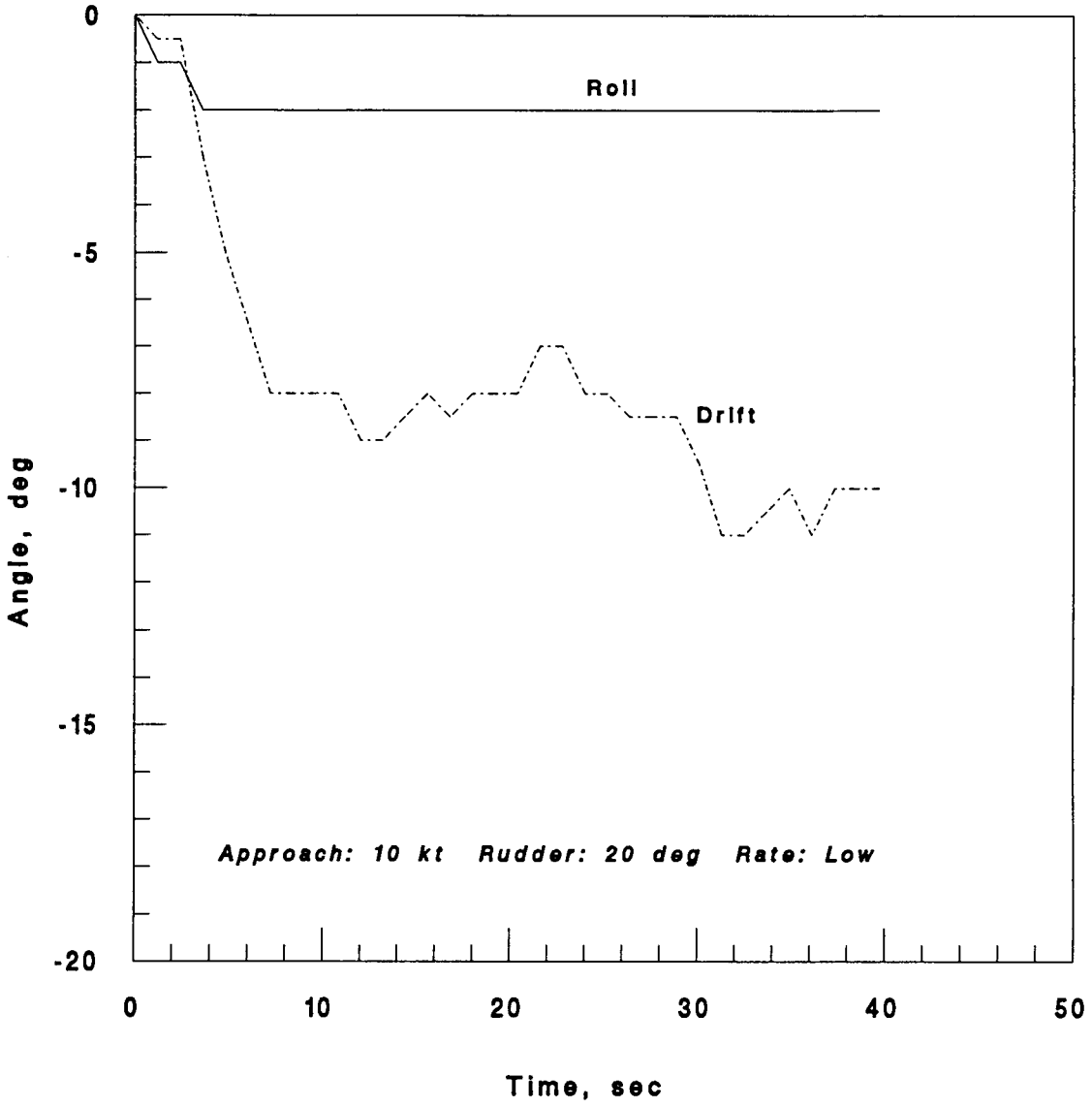

FIGURE 21 Time history of roll and drift angles in a steady turn. Full scale units.

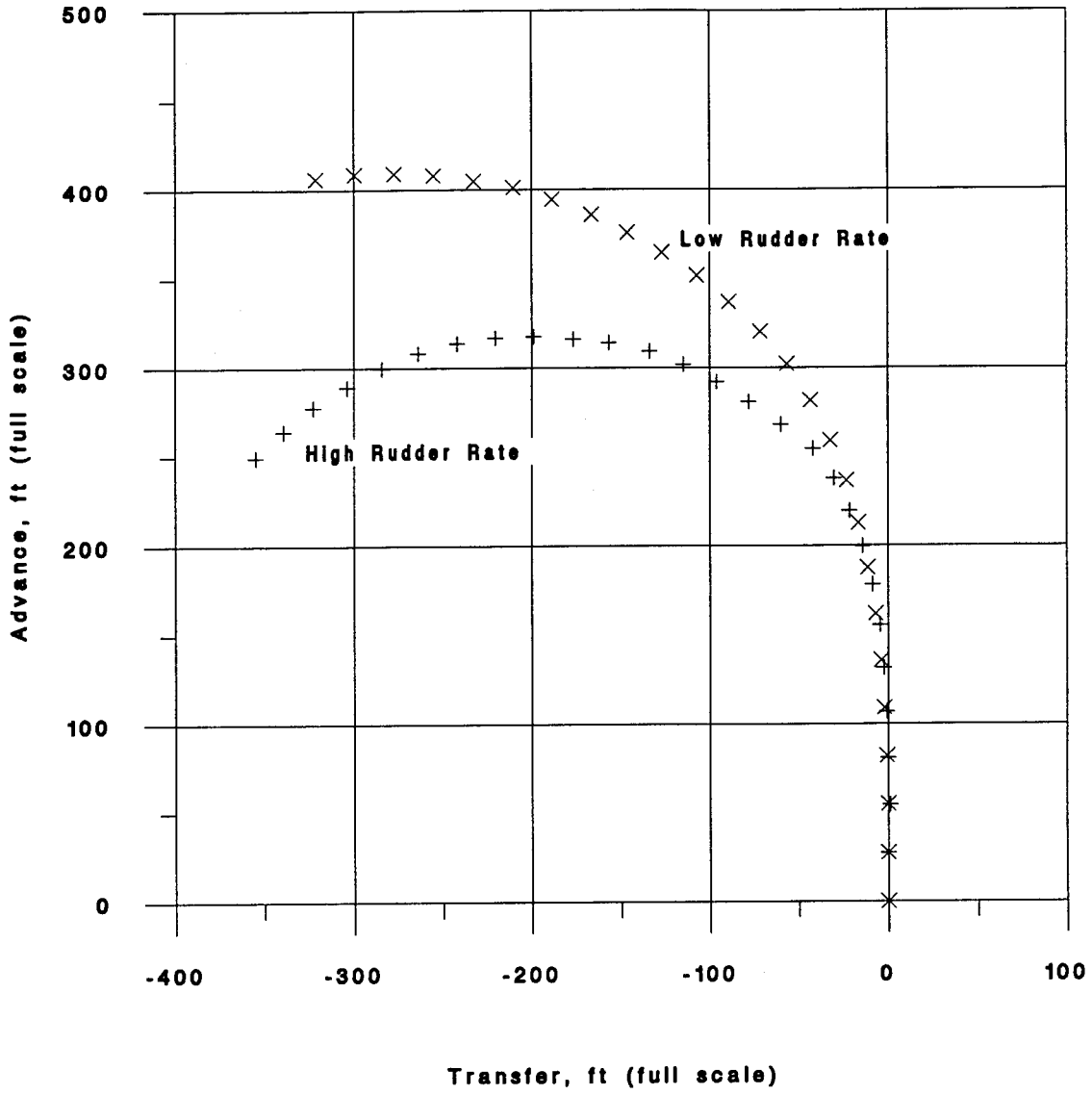

FIGURE 22 Turning Trajectory of 47 ft MLB
Approach:27 kt Rudder: 30 deg

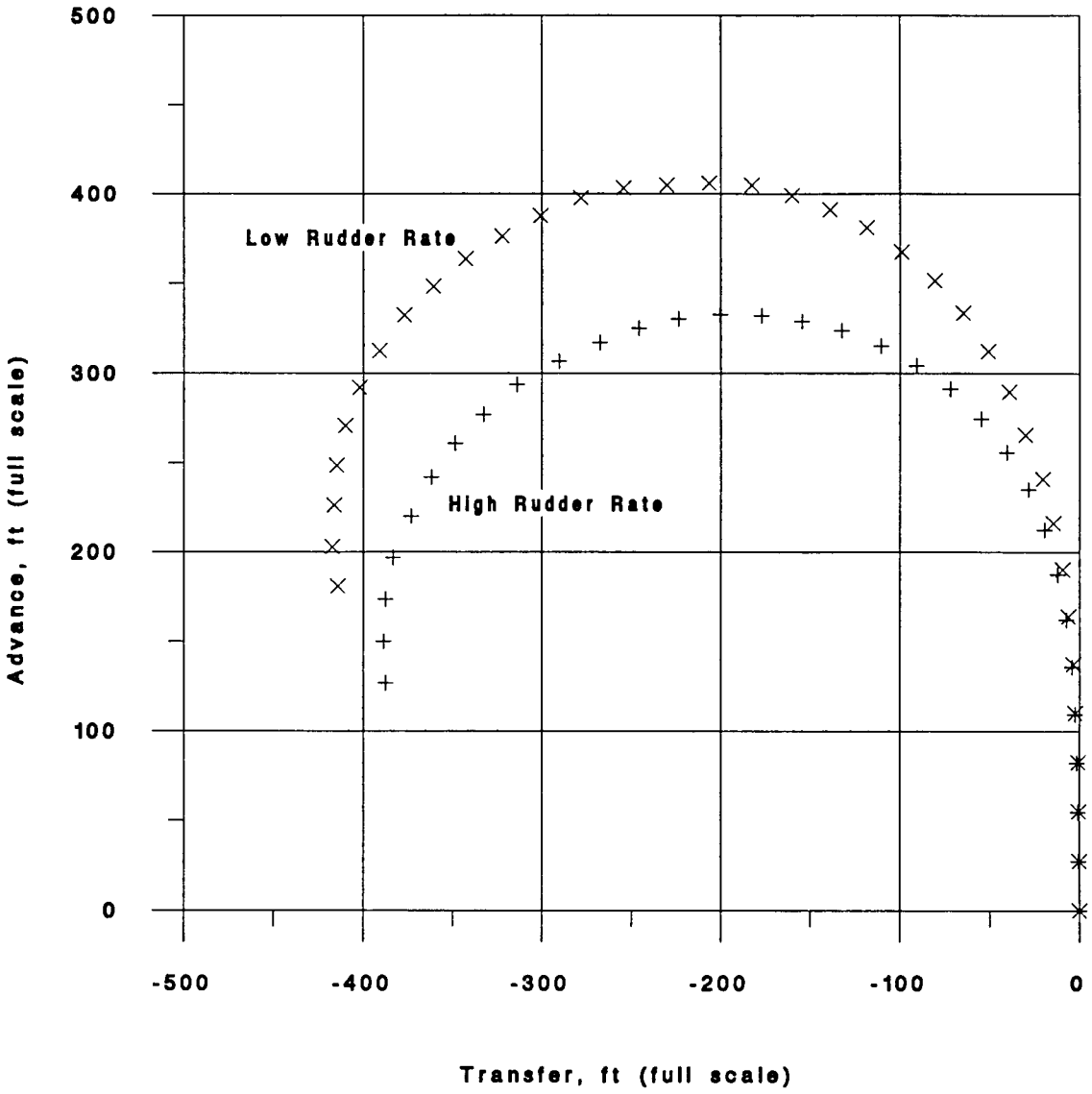

FIGURE 23 Turning Trajectory of 47 ft MLB
Approach: 27 kt Rudder: 20 deg

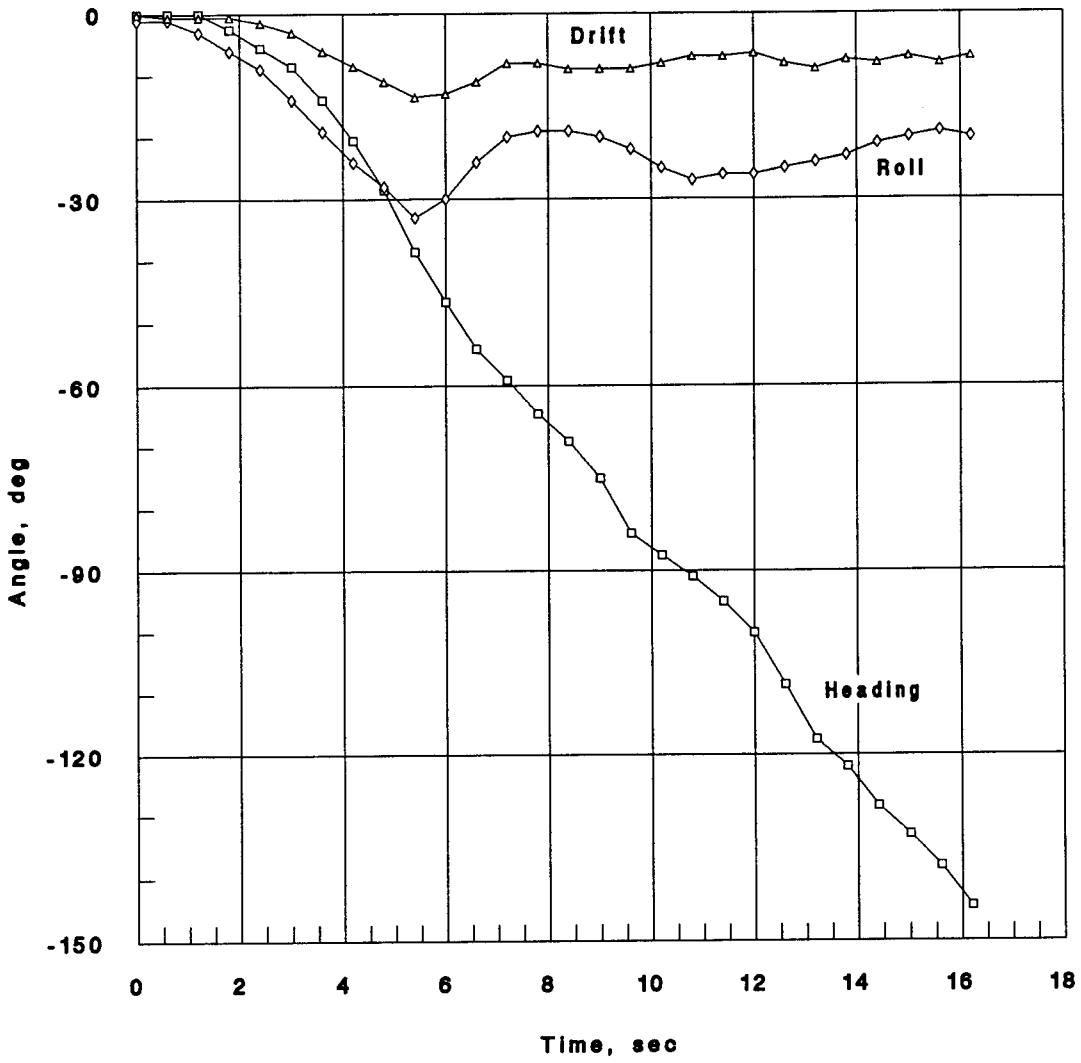

Approach: 27 kt Rudder: 30 deg Rate: High

FIGURE 24 Time histories of roll, drift and heading angles in a high speed turn. Full-scale units.

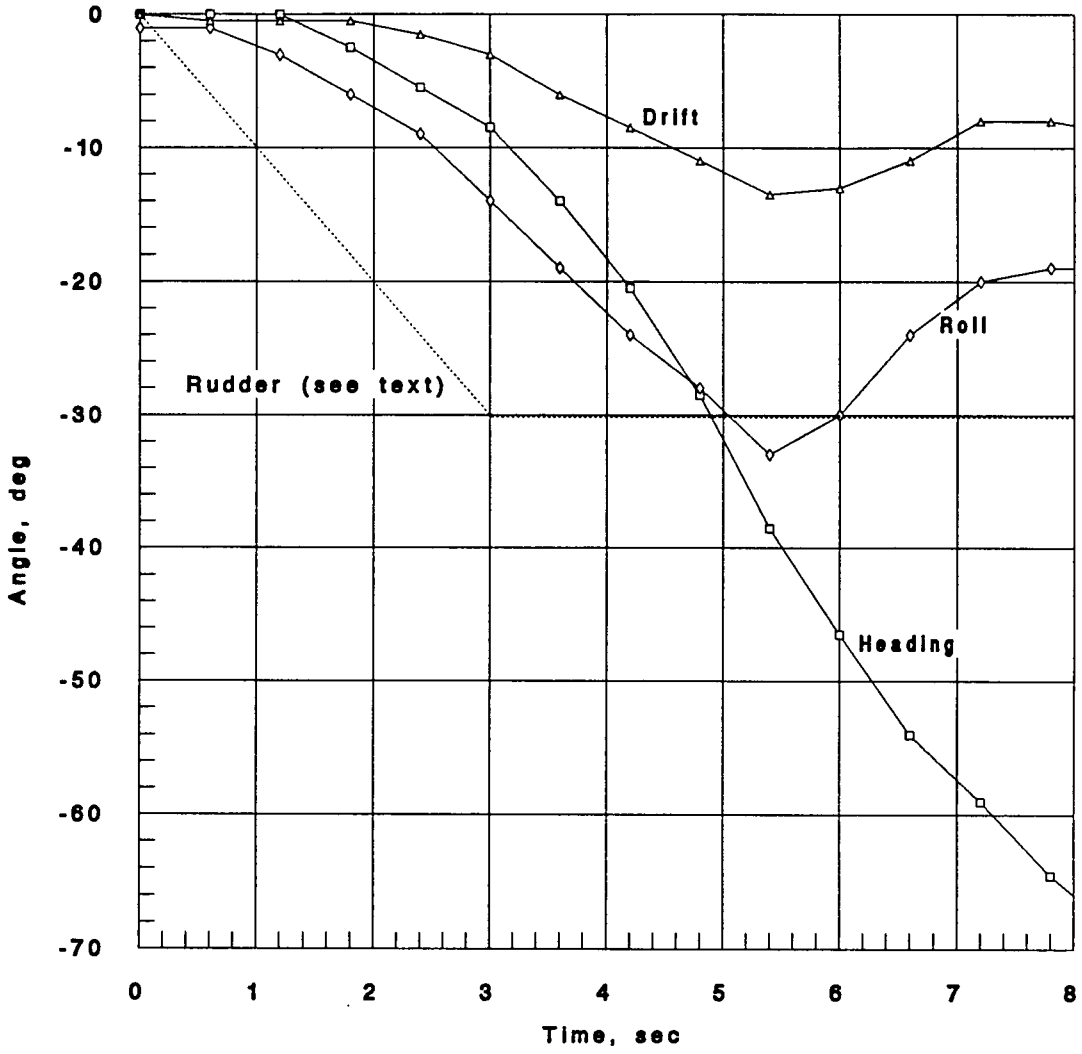

Approach: 27 kt Rudder: 30 deg Rate: High

FIGURE 24a Time histories of roll, drift and heading angles in the early portion of a high speed turn. Full-scale units.

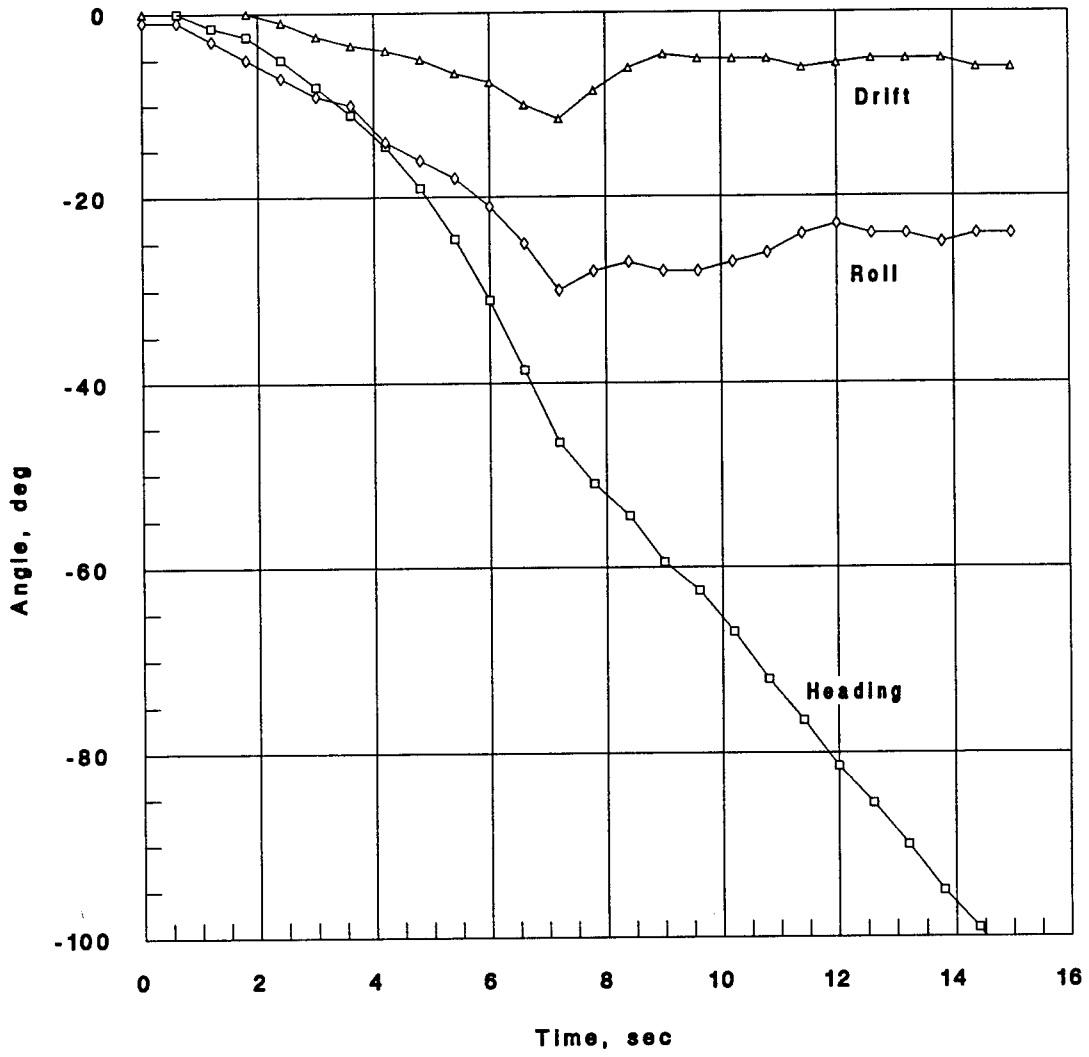

Approach: 27 kt Rudder: 30 deg Rate: Low

FIGURE 25 Time history of roll, drift and heading angles in a high speed turn. Full-scale units.

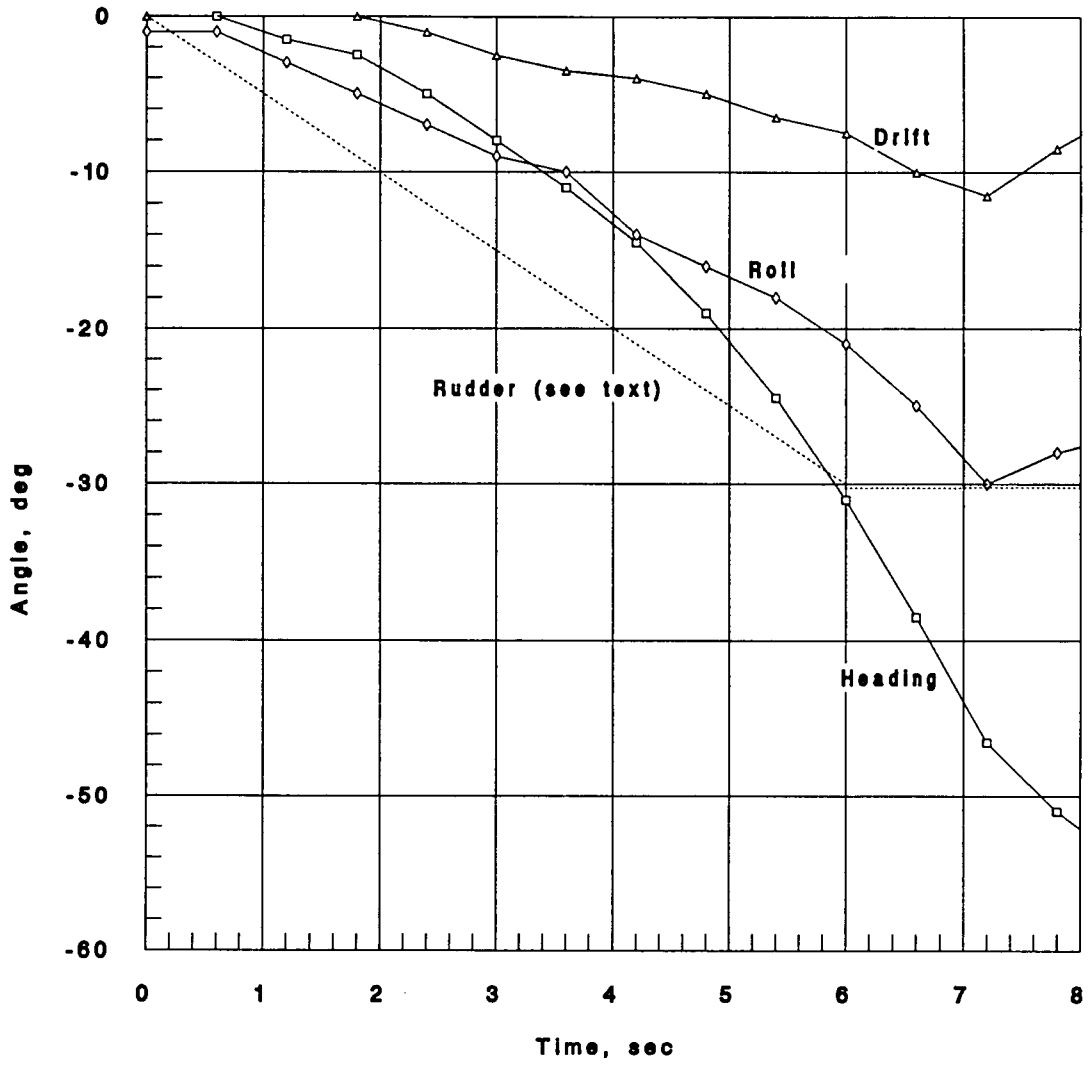

Approach: 27 kt Rudder: 30 deg Rate: Low

FIGURE 25a Time history of roll, drift and heading angles in the early portion of a high speed turn. Full-scale units.

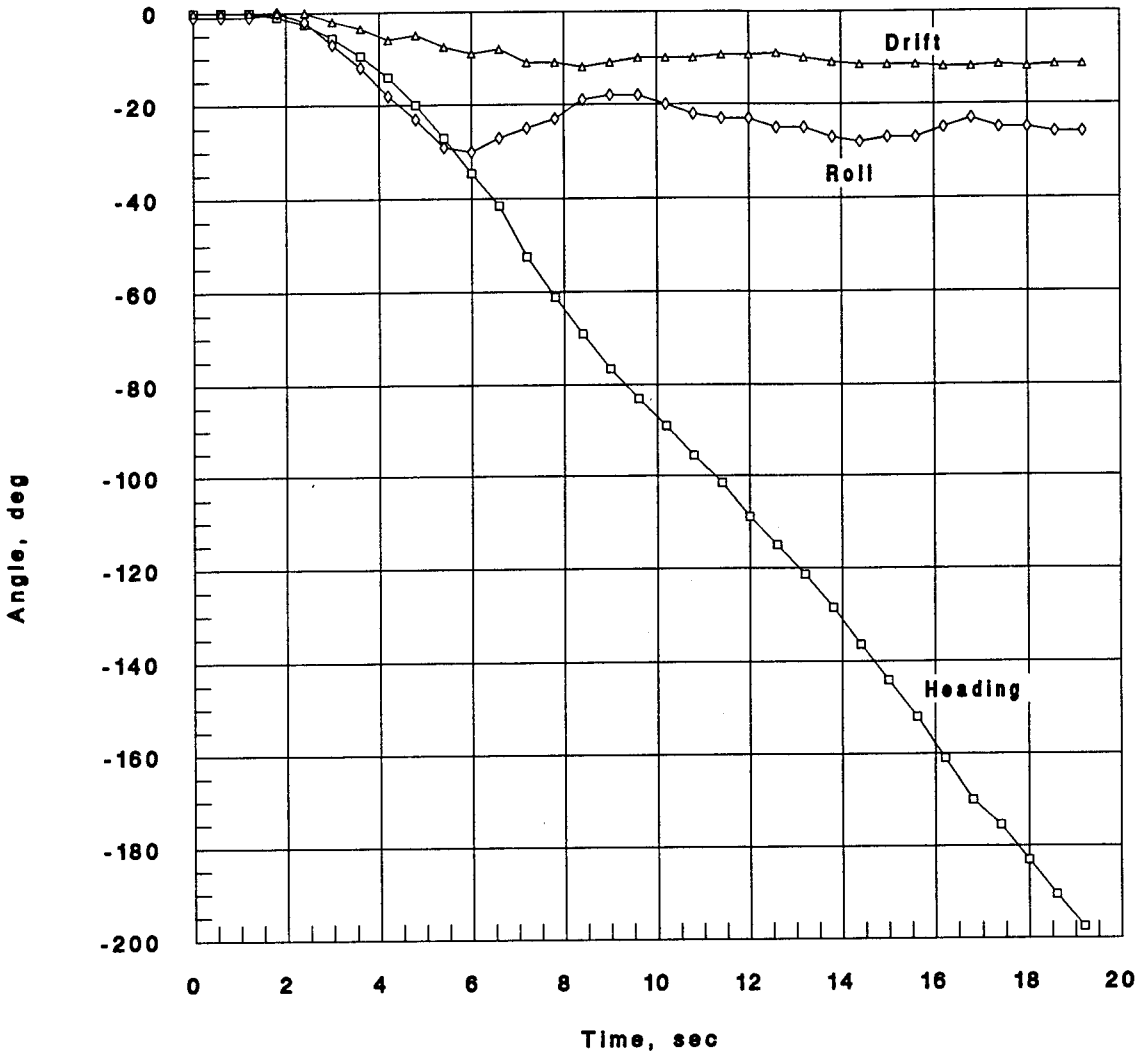

Approach: 27 kt Rudder: 20 deg Rate: High

FIGURE 26 Time history of roll, drift and heading angles in a high speed turn (Full-scale units)

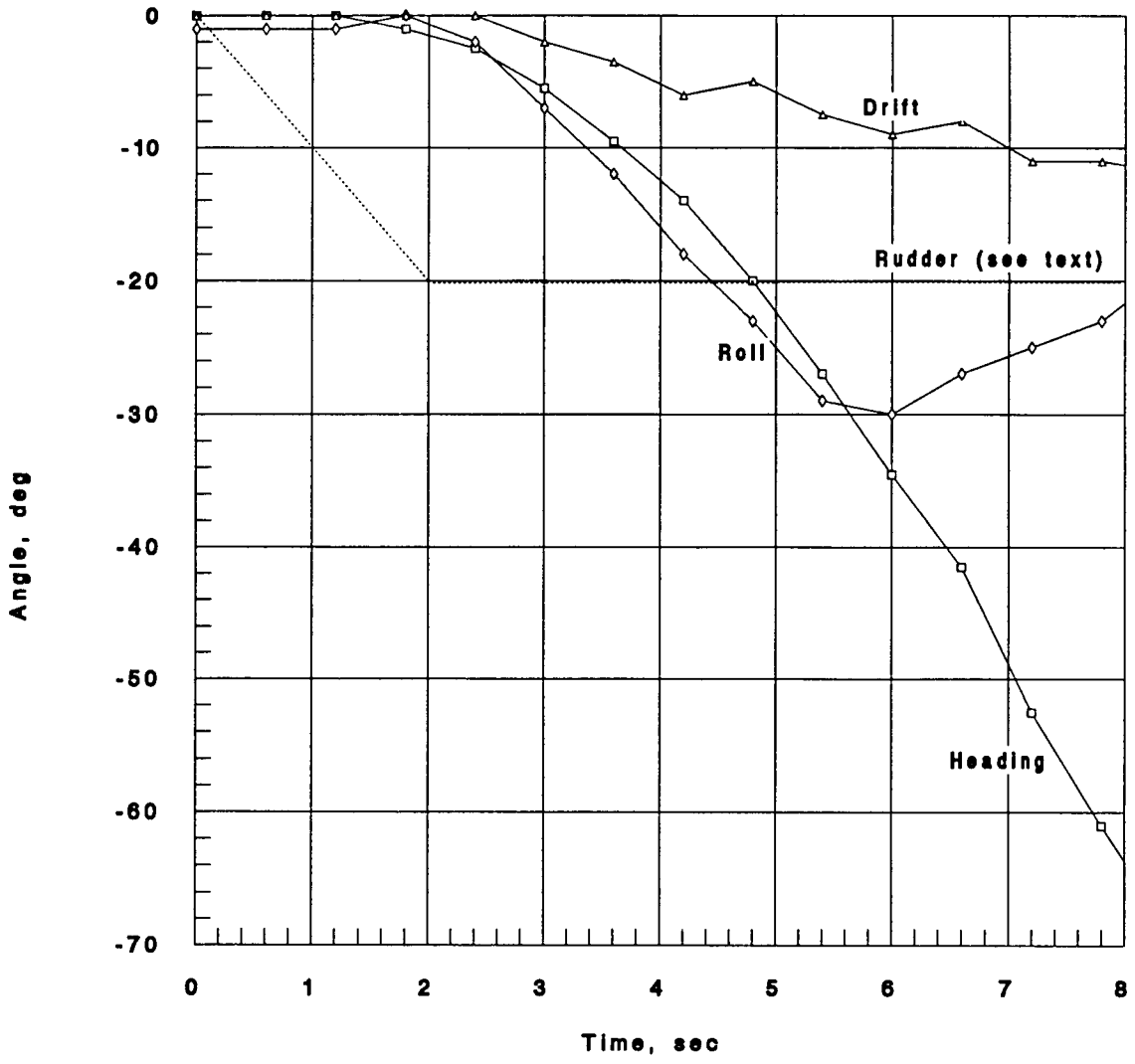

Approach: 27 kt Rudder: 20 deg Rate: High

FIGURE 26a Time history of roll, drift and heading angles in the initial portion of a high speed turn (Full-scale units)

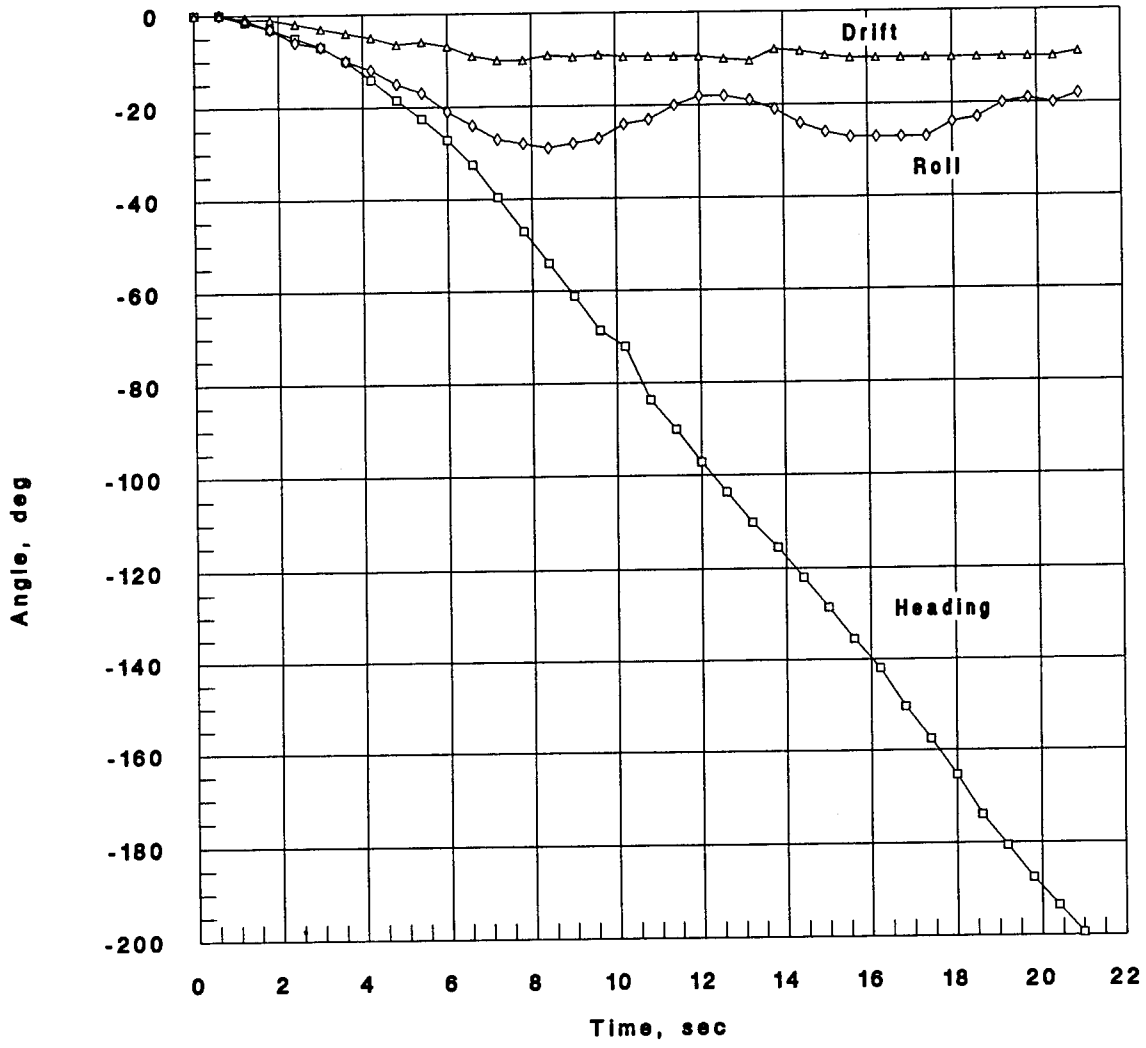

Approach: 27 kt Rudder: 20 deg Rate: Low

FIGURE 27 Time history of roll, drift and heading angles in a high speed turn. Full-scale units.

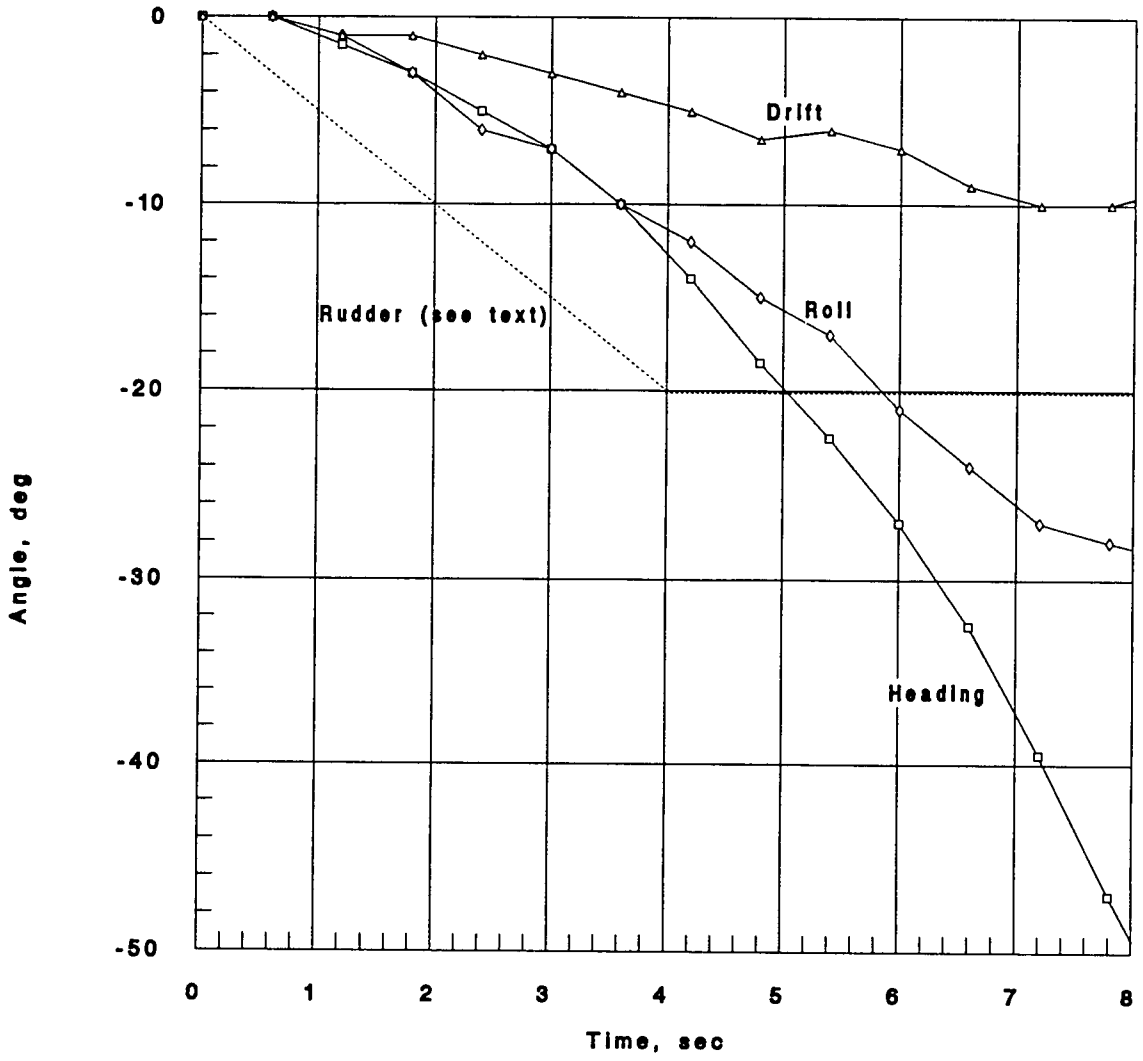

Approach: 27 kt Rudder: 20 deg Rate: Low

FIGURE 27a Time history of roll, drift and heading angles in initial portion of a high speed turn. Full-scale units.

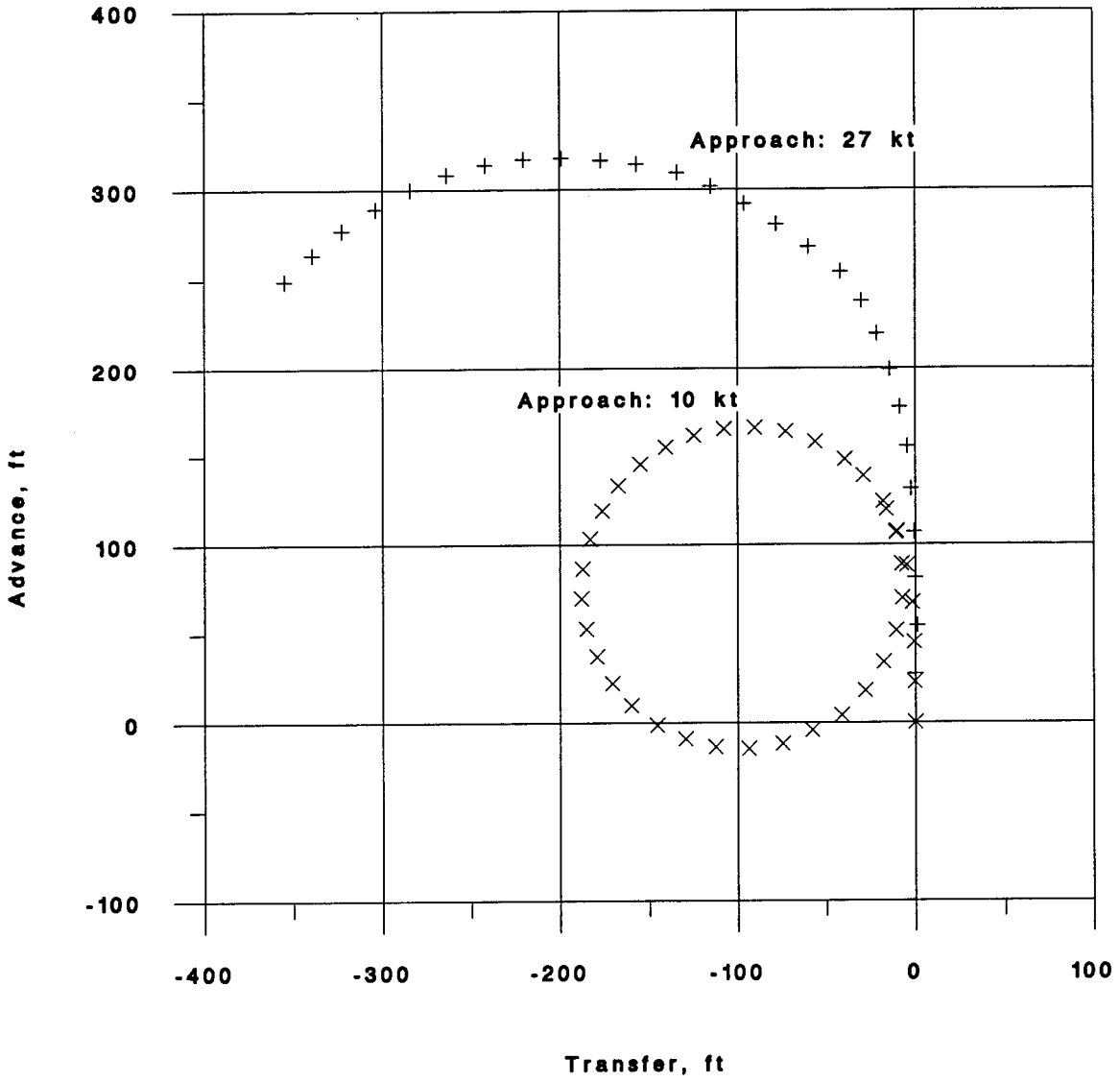

FIGURE 28 Effect of Approach Speed on Turning Trajectory; Rudder: 30 deg; Rate: High Full-scale units.

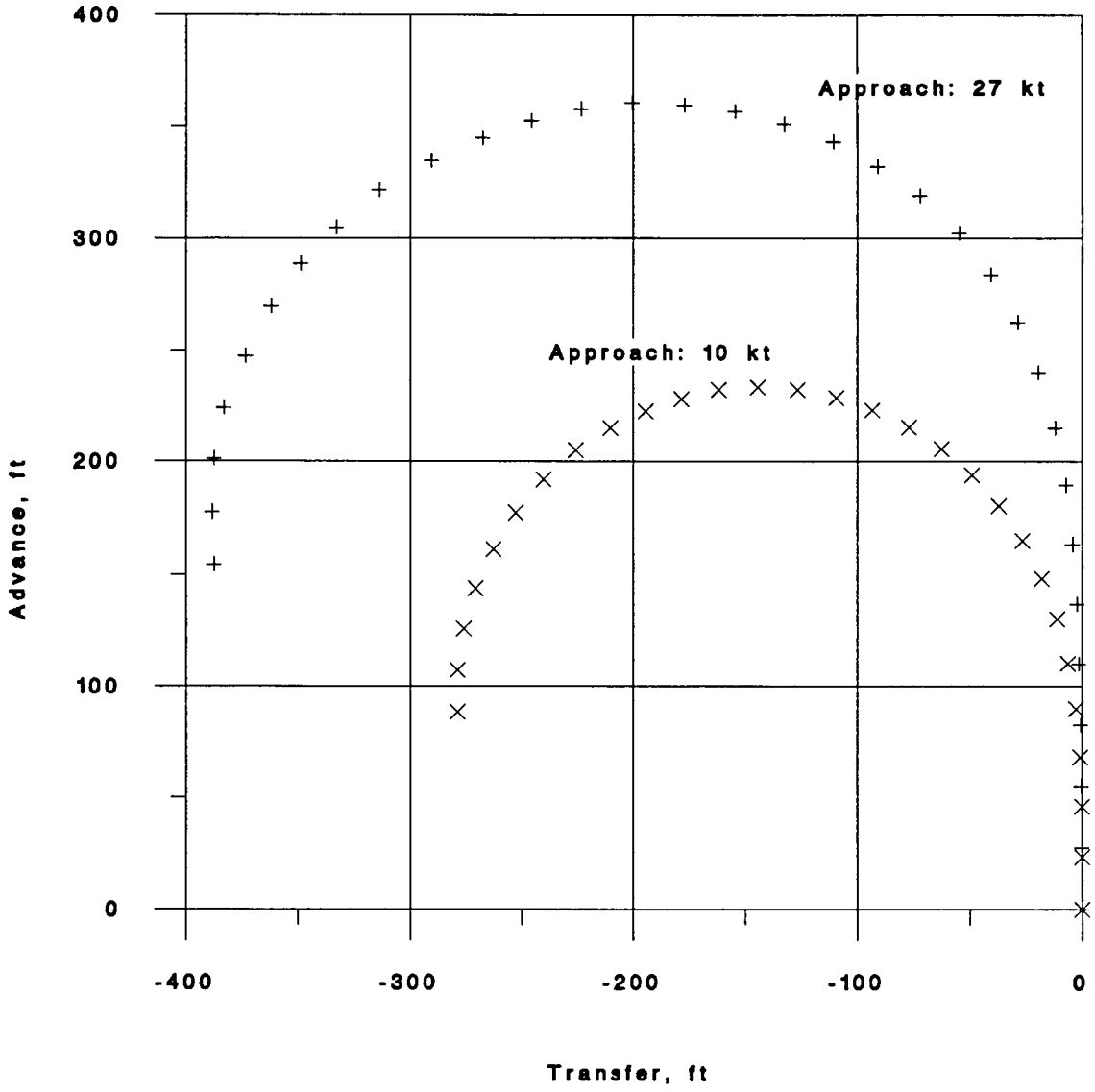

FIGURE 29 Effect of Approach Speed on Turning Trajectory; Rudder: 20 deg; Rate: High Full-scale units.

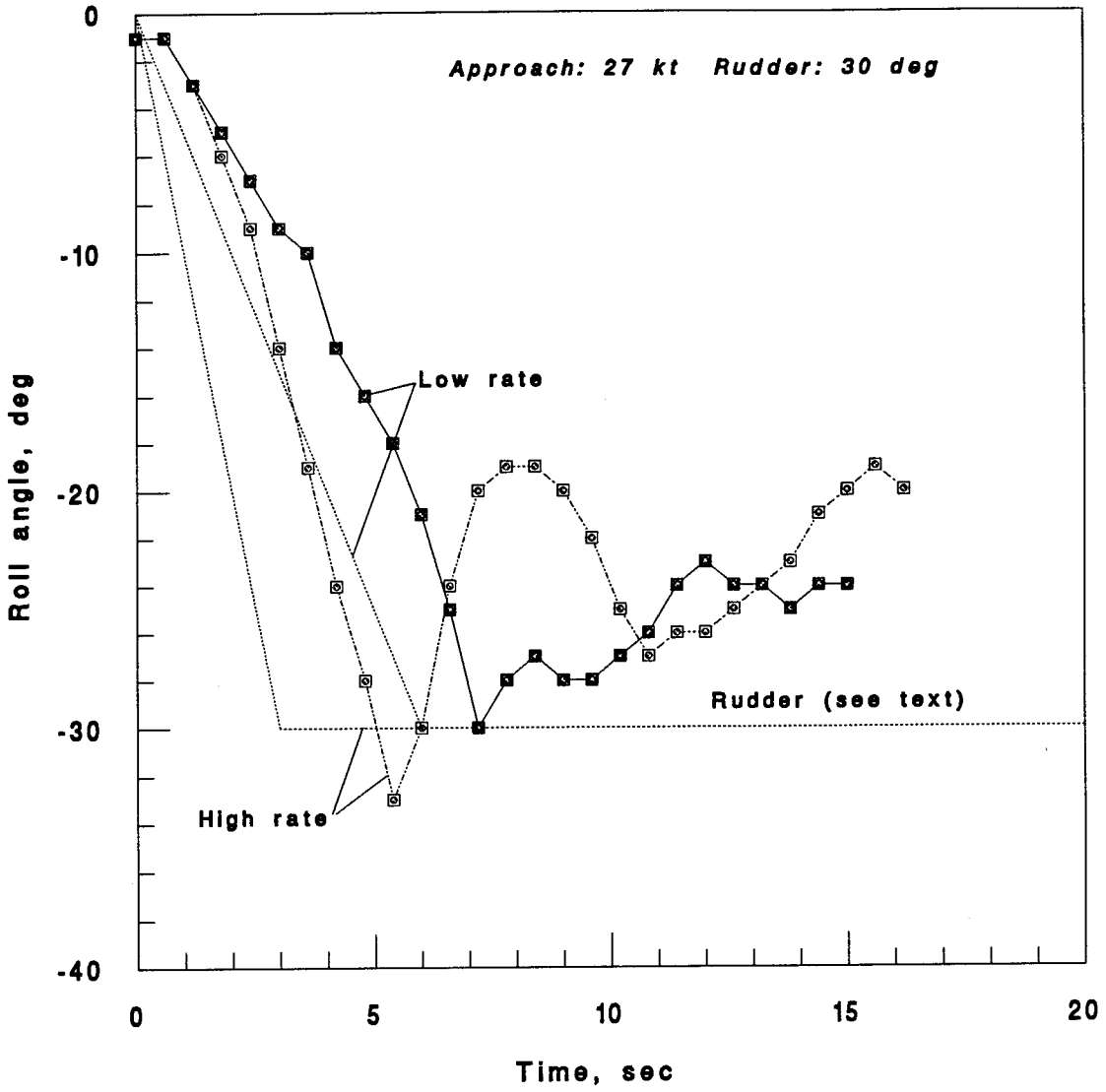

FIGURE 30 Effect of rudder rate on rolling in a turn. Full scale units.

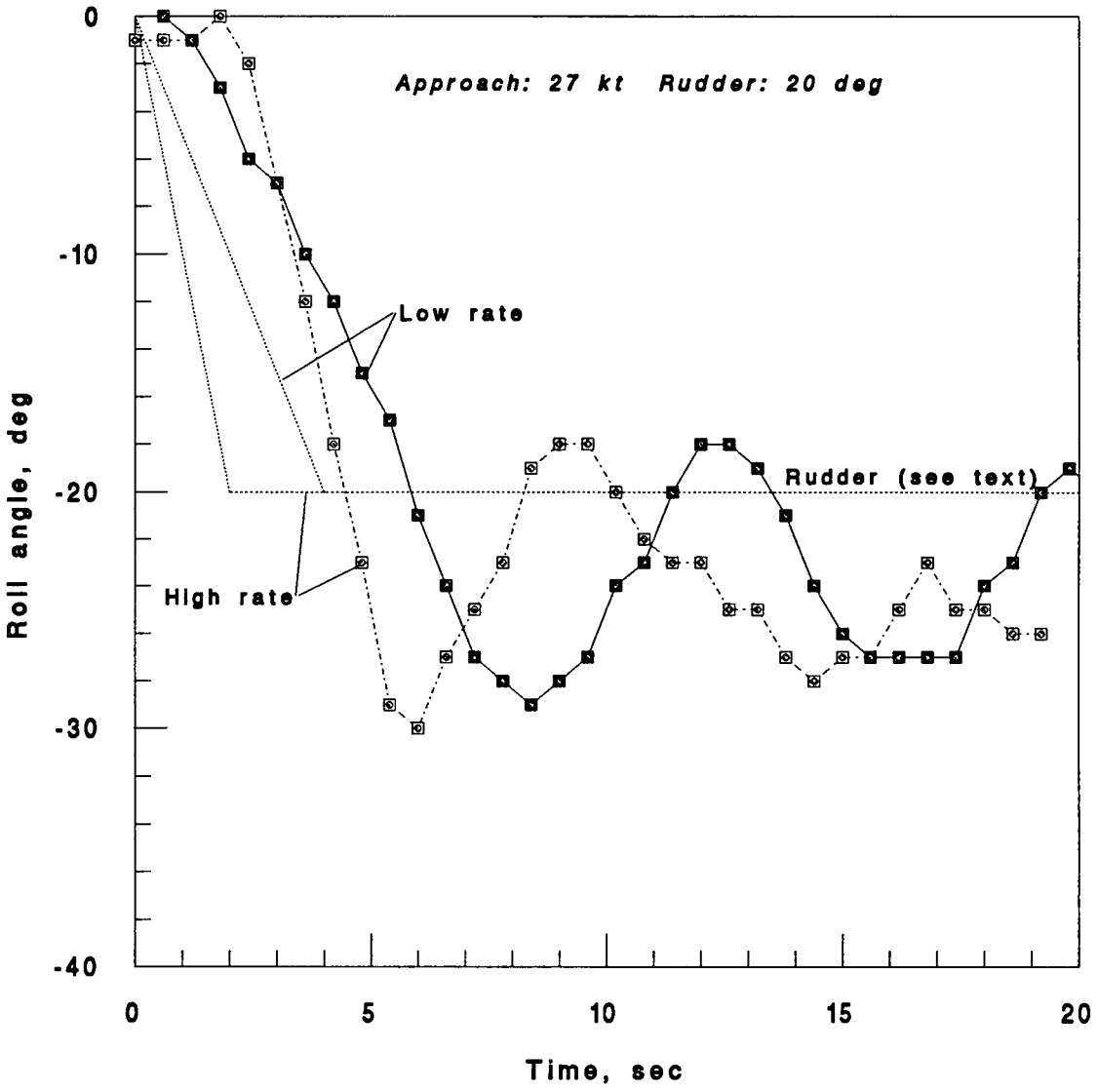

FIGURE 31 Effect of rudder rate on rolling in a turn
Full scale units.

APPENDIX A

INITIAL VELOCITY CORRECTIONS

Analysis of the trajectories from the photographs, after correction for lens distortion as described in the text, showed that in some of the photographs of the approach phase of the high-speed turns, the model was not up to speed at the initiation of the turn. This problem was restricted to the photographs obtained in the second free-running model test session; in the first session, more space was available for acceleration. Thus, only the initial points of the measured high-speed trajectories were affected (subsequent points being from previous runs which were initiated at the proper speed); fortunately, the drift, roll, heading and transfer were all small in this phase of the turns. A simple correction was applied to the trajectories as described below.

First, the x and y components of velocity were estimated from the measured trajectories as follows:

$$u = dx/dt = [x(t) - x(t-dt)]/dt$$

$$v = dy/dt = [y(t) - y(t-dt)]/dt$$

where dt is the time interval between LED pulses (0.2 sec model-scale). The velocity components were next plotted against time. Then, the curve of u(t) was extrapolated back from the points which were determined from the first set of photographs, to the proper initial velocity of 27 knots, using the shape of the measured curve as a guide (a smooth variation of u with time was assumed). The "corrected" u velocity component was then read from the extrapolated curve; the v-component was multiplied by the ratio of the corrected to the measured u-components. The trajectory was then recomputed using the new velocity components.

Figure A1 shows the original and corrected velocity components in a typical case. It can be seen that there are also some discontinuities in the velocity curves where two photographs were joined; these were also smoothed in the correction process as shown. Figure A2 shows the measured

and corrected trajectories in this case.

As mentioned in the text, the measured trajectories at an approach speed of 27 knots and a rudder deflection of 30 degrees ended before the heading changed 180 degrees. To estimate the tactical diameter in these cases, the trajectories were extrapolated by assuming that a constant speed and rate of change of heading had been reached at the end of the measured trajectories. The results are shown on Figures A3 and A4.

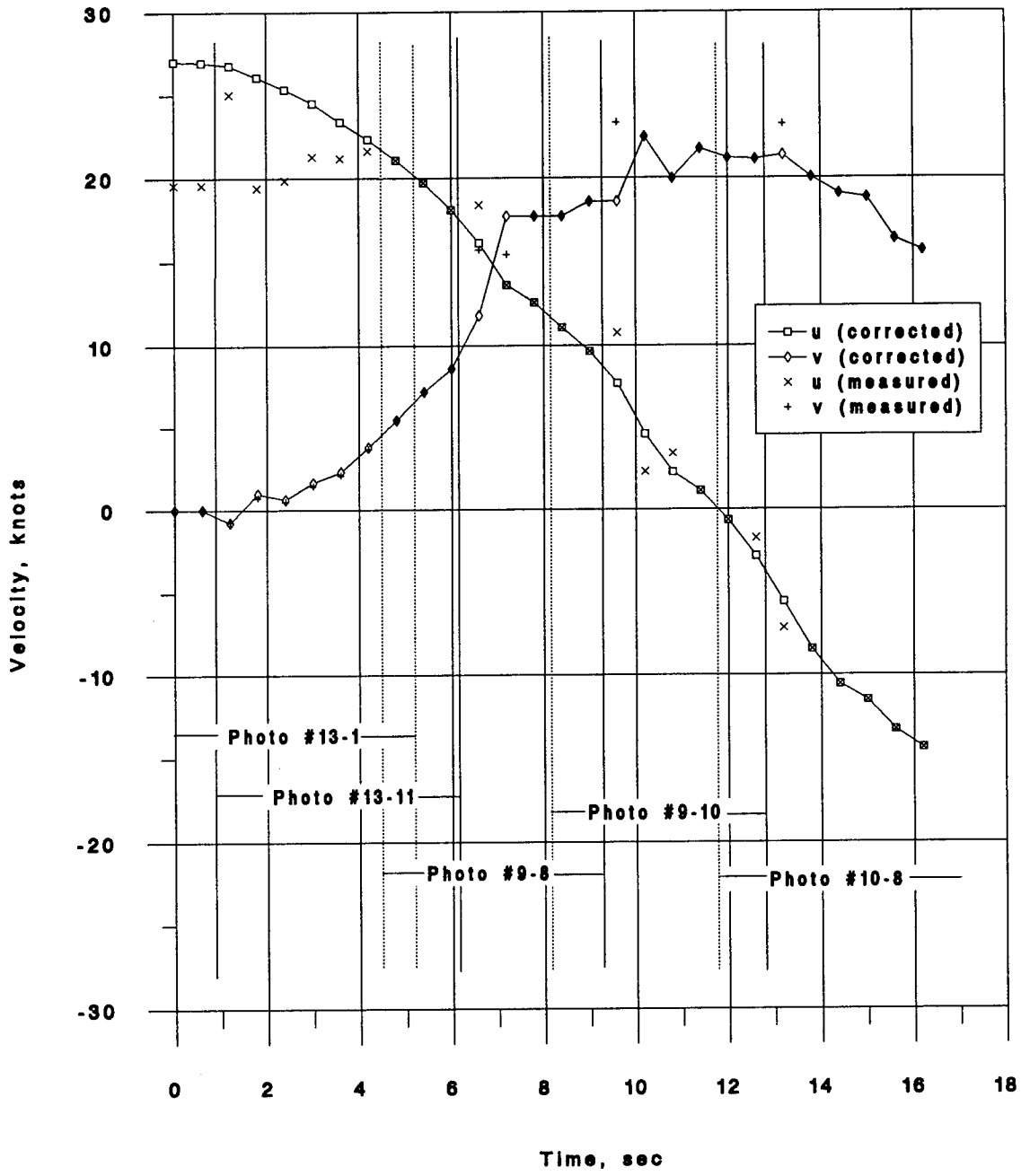

Figure A1 Comparison of measured and corrected velocity components. Approach: 27 kt; Rudder: 30 deg; Rudder rate: High

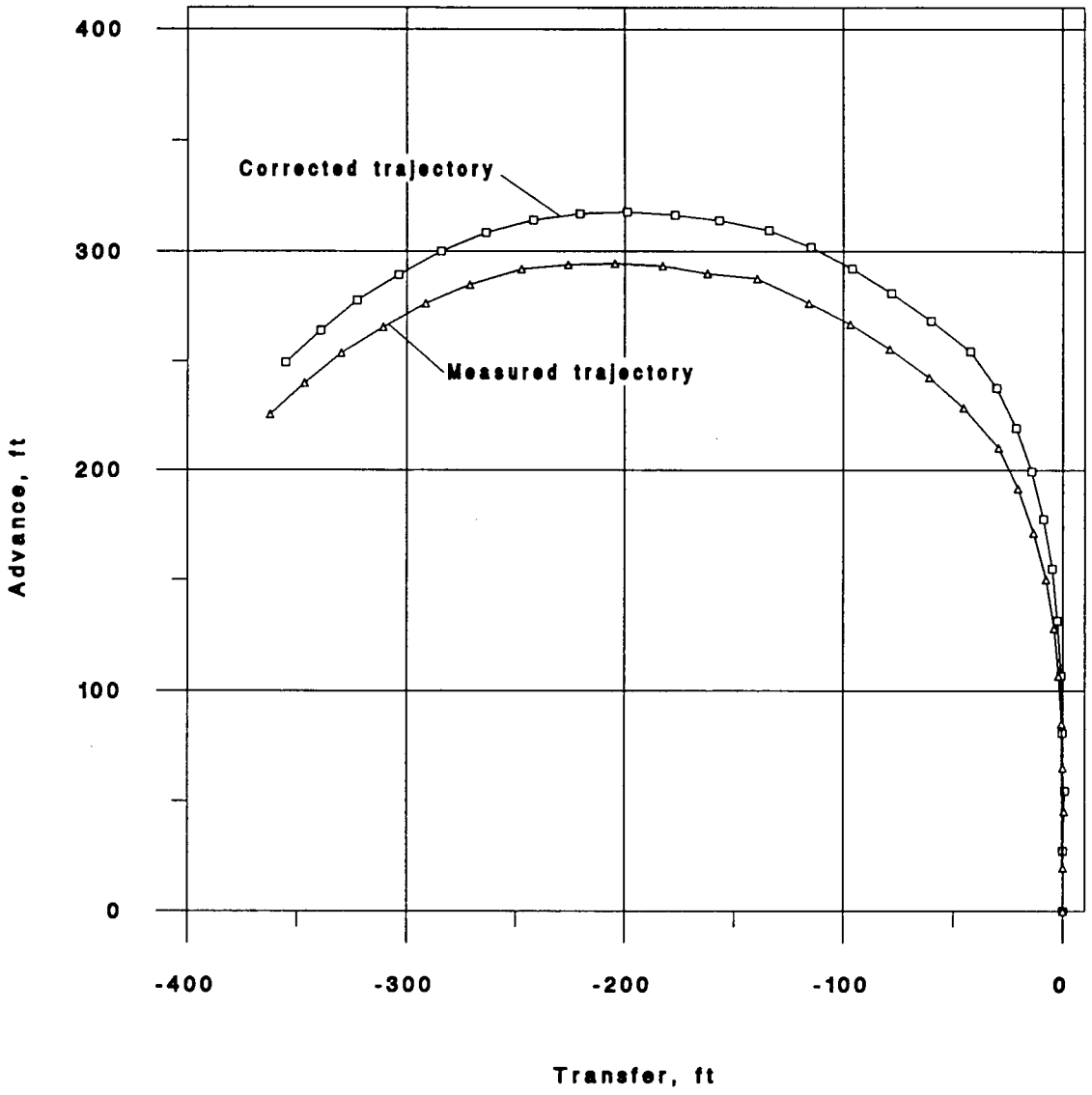

Figure A2 Effect of velocity correction on trajectory. Approach: 27 kt; Rudder: 30 deg; Rudder rate: High

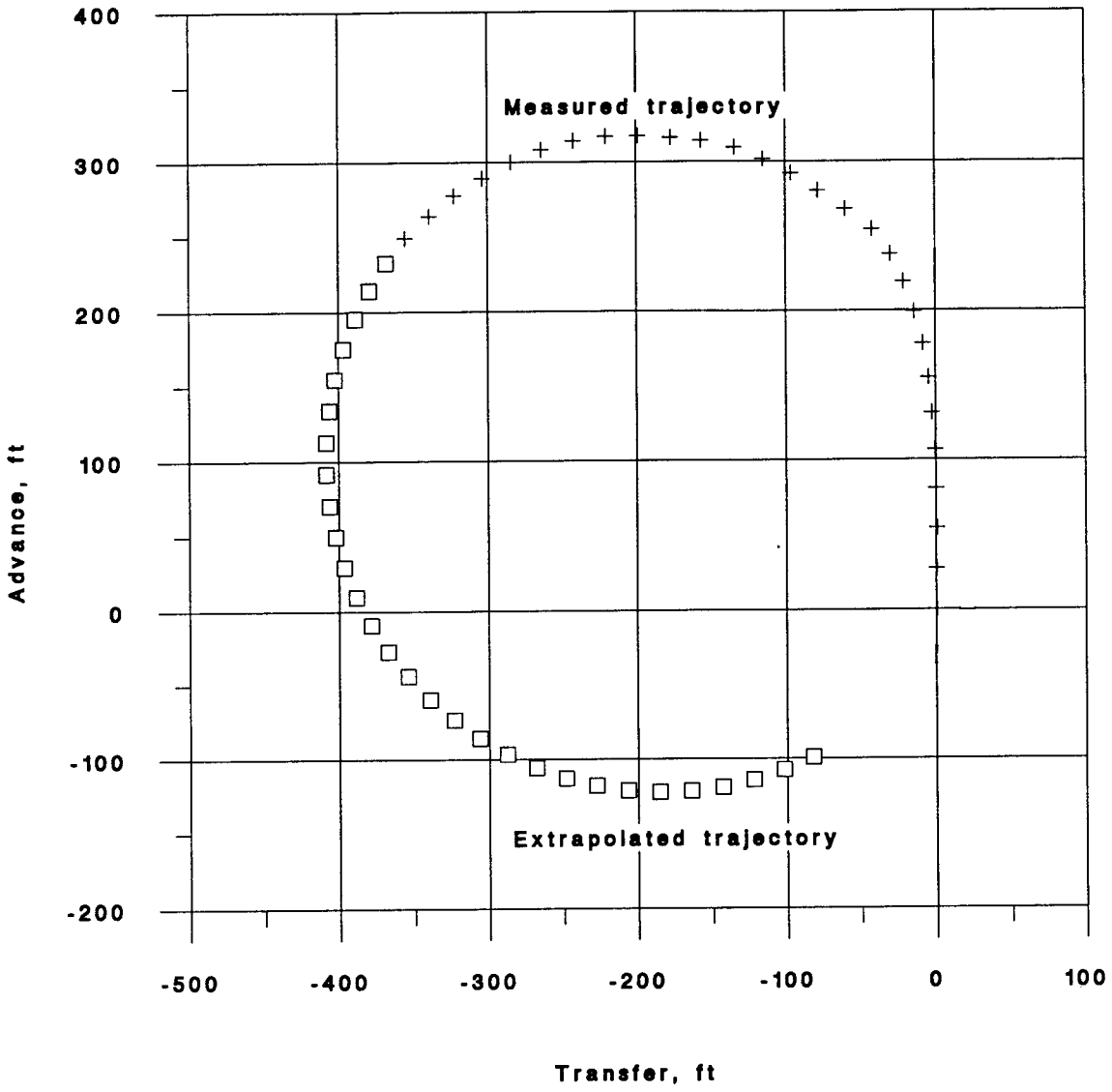

Approach: 27 kt Rudder: 30 deg Rate: High

FIGURE A3 Extrapolated trajectory

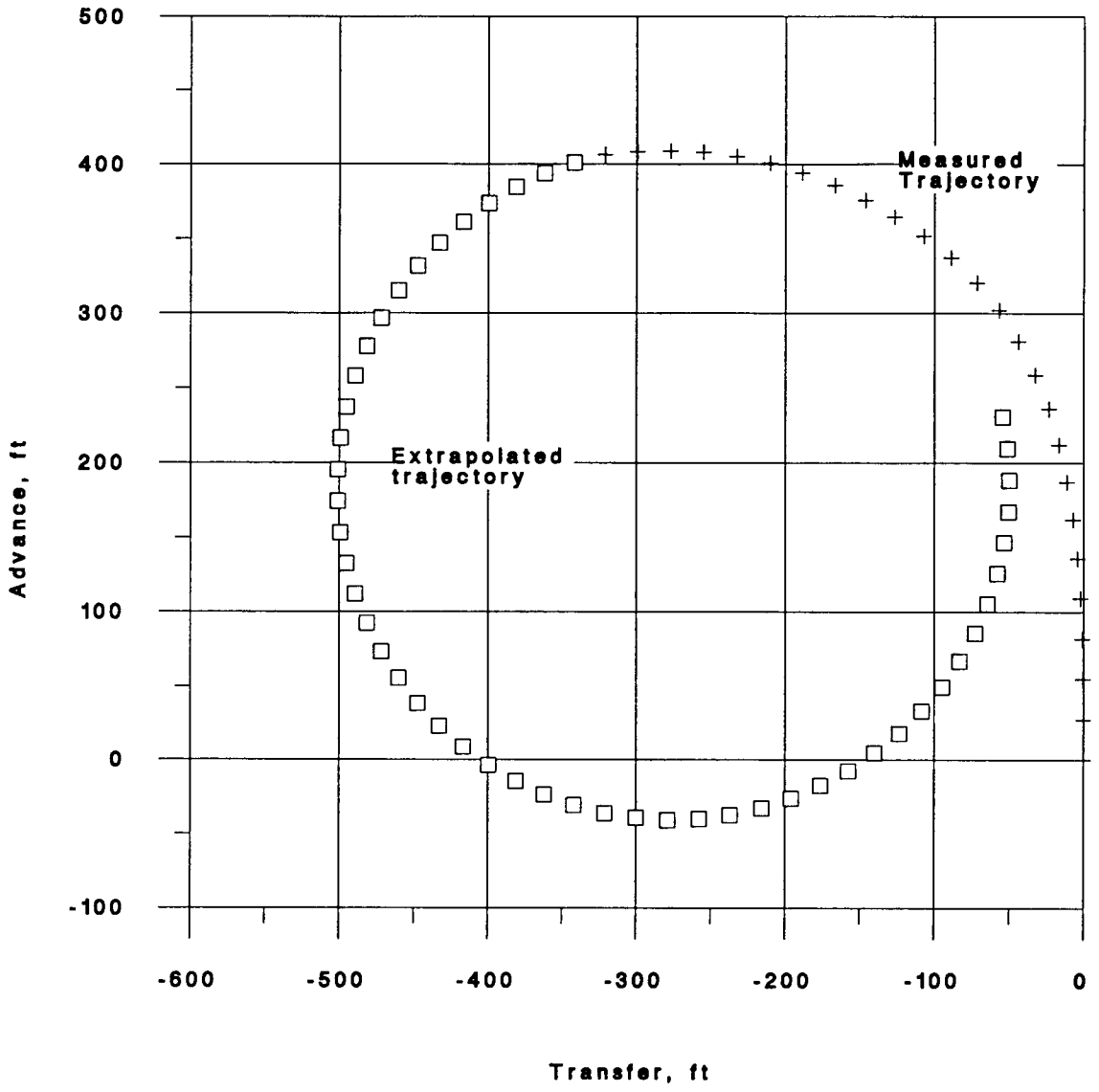

Approach: 27 kt Rudder: 30 deg Rate: Low

FIGURE A4 Extrapolated trajectory

A USCG Systematic Series of High Speed Planing Hulls

Dina H. Kowalyshyn (AM), and Bryson Metcalf (V)

ABSTRACT

This experimental program was designed to explore the possibility of adapting the US Coast Guard 47 ft MLB hull form to longer vessels of higher speed. The series, including the 47 ft MLB geometry, became four models with varying length-to-beam ratios (3.24, 4.0, 4.47) and one variant with transom deadrise angle, β, increased from 16.6 to 20 degrees. A matrix of speeds and displacements typical of small patrol boats was tested in calm water and the resulting data are presented.

KEY WORDS: Model test; resistance; calm water; high speed; planing; length – to –beam ratio; deadrise angle.

INTRODUCTION

The US Coast Guard's mission has expanded since the September 11th terrorist attacks on our country. Under the Department of Homeland Security (DHS) stronger focus on high speed and port security is changing the specifications for future Coast Guard platforms. The most prominent specification change for new acquisitions is a maximum speed requirement of 40 knots. There are presently no standard boats with a top speed of 30 knots in this length range. The USCG fleet of small patrol boats has the following length-to-beam ratios and top speeds: the 47 ft Motor Lifeboat (MLB) has a L/B of 3.24 and was designed as a 25 knot boat, the 87 ft WPB has an L/B of 4.3 and a top speed of 25 knots, and the 110 ft WPB has an L/B of 4.8 and a top speed of 29.5 knots. This project's goal was to create a database for evaluation of proposed replacement boats. Starting from the MLB the variants focused on L/B, because of the obvious differences between the MLB and the WPB's, and deadrise angle for the commonly known seakeeping benefits. Three variations of the parent 47 ft MLB hull form were constructed. Model resistance experiments were performed in the towing tank at the Naval Surface Warfare Center, Carderock Division (NSWCCD).

NOMENCLATURE

The notation herein conforms to the International Towing Tank Conference (ITTC) Symbols and Terminology List – 2002.

Ap	Projected planing bottom area, ft^2
C_A	Correlation Allowance
C_B	Block Coefficient
C_F	Frictional Resistance Coefficient
C_P	Prismatic Coefficient
C_R	Residuary Resistance Coefficient
C_T	Total Resistance Coefficient
LCG	Longitudinal Center of Gravity
L_K	Wetted Keel Length
L_C	Wetted Chine Length
β	Deadrise angle, degrees
Δ	Displacement, lbs
∇	Displaced volume, ft^3
F_∇	Volume Froude number $V/\sqrt{g\nabla^{1/3}}$
G	Acceleration due to gravity, ft/sec^2
L/B	Length-to- Beam ratio
R_T	Total resistance, lbs
RN	Reynolds's Number
S	Wetted surface of model underway

HULL FORM DEVELOPMENT

The USCG 47 ft MLB is not a traditional deep vee planing hull because of its mission as a lifeboat. The design trade-offs made to produce good self-righting characteristics and good low speed seakeeping for operations in short crested waves produced a hull with more waterplane area (beam) and fuller forward sections than are typical of high speed planing boats. The deep-vee and hard chine were chosen to prevent broaching by resisting yaw and provide stability by lowering the center of buoyancy. The deadrise was then varied continually along the length, decreasing aft of midships to produce a flatter planing area, while gaining the benefit of large deadrise angles in the forward sections. The stern is rounded and flared in keeping with traditional lifeboats. The hull buoyancy is balanced bow to stern and the fullness in the bow is not so large as to cause pounding at high speeds. The body plan of the 47 ft MLB is included in Appendix A as an illustration of the basic form. Appendix A also has body plans of the parent model and the three other model forms and a table of hull characteristics.

The four scale models were developed from the 47 ft MLB lines by removing the stern wedge and transom curvature and extending the buttocks and waterlines aft to create a flat transom located at the aft perpendicular. This modified hull was then used as the parent for the three series variants, and was designated number 5628 by NSWCCD. It has an L/B of 3.24. The first variant represents a direct scaling of the y and z-axes (breath and depth reduced) to maintain the parent deadrise angle and increase L/B to 4.0. This model was designated 5629. The second variant further decreased the depth and beam to the

minimum beam corresponding to the limits of intact stability while maintaining the deadrise angle. Direct scaling of y and z-axes resulted in an L/B of 4.47. This model was designated 5630. The third variant is a modification of Variant #2 in which the hull below the chine is stretched in the z-direction to obtain a transom deadrise of 20 degrees by increasing hull draft while maintaining the Variant #2 hull shape above and including the chine. Each station's shape below the chine was scaled independently to achieve a smooth hull form connecting the chine to the flat keel. This model was designated 5631. Basic model hull form particulars can be found in Table 1, with more details in Appendix A. Note that the drafts listed correspond to the scaled design waterline of the 47 ft MLB and do not correspond to the exact model test displacements. Figure 1 is a plot showing the variation in deadrise angle by stations of these models to help illustrate the warping of the hull and the change for hull variant 3.

Table 1: Model Particulars

Model No.	Parent 5628	Variant 1 5629	Variant 2 5630	Variant 3 5631
LBP ft(m)	10 (3.05)	10 (3.05)	10 (3.05)	10 (3.05)
Beam ft(m)	3.09(0.94)	2.5(0.76)	2.24(0.68)	2.24(0.68)
Draft* ft(m)	0.61(0.18)	0.49(0.15)	0.44(0.14)	0.51(0.16)
L/B	3.24	4.0	4.47	4.47
B/T	5.08	5.08	5.08	4.39
β, deg.	16.61	16.61	16.61	20.0
∇, $ft^3(m^3)$	8.05(0.23)	5.29(0.15)	4.24(0.12)	4.88(0.14)

*Drafts are scaled from the MLB design waterline

The only appendages on these models during the tests were simple spray rails. The spray rails were of constant isosceles-triangle cross section shape that was scaled from the 47 ft MLB. The modeled spray rails were approximately 40 inches long with triangle legs of 5/8 inch. They were attached to the hulls beginning at station 0, as scaled from the 47 ft MLB.

The ballast conditions for the test series were provided as model displacement and LCG by the U.S. Coast Guard Engineering Logistics Center, Boat Engineering Branch. These test conditions were developed from examination of existing patrol boat type vessels and calculating different geometric ratios such as the ratio of the projected planing area to the displaced volume, $Ap/\nabla^{2/3}$, and the slenderness ratio $L/\nabla^{1/3}$. The most likely vessel sizes of interest to the Coast Guard in the near future are 45 ft(14m) to 140 ft(43m). Speed restrictions in the towing basin caused the testing to focus around an 80 foot waterline length boat, and the different form ratios were used as a check of reasonableness for a planing hull. Figure 2 shows data for eight existing patrol boats plotted with our models showing the overlap of weights for length of vessel. Because there were no specific requirements at the time of testing an effort was made to bracket what was thought to be a reasonable range of weights for the lengths, for future use. The model test displacements and LCG positions are shown in Table 2.

EXPERIMENTAL PROCEDURES AND DATA REDUCTION

All the resistance experiments reported herein were conducted on Carriage 3 in the high-speed basin at NSWCCD, which has a cross sectional area of 21 feet wide by 12 feet deep. During these experiments the models were free to pitch, heave, and roll, but were restrained in surge, sway and yaw. Measurements taken for each test run were x-force, y-force, sinkage at the CG and aft, and model speed. Also for each run, the wetted length of the hull was visually observed and recorded to use in determining the wetted area per run for data reduction. All models were tested at speeds corresponding to a range from 10 – 55 knots, full scale.

The longitudinal position of the tow point was located at the desired LCG's, 38 and 42 percent of the LBP forward of the aft perpendicular. The models were attached through a gimbal to a light heave staff and mounted to the towing carriage. Two two-inch block gauges were used to measure drag (calibrated to ± 200 lbf) and side force (calibrated to ± 20 lbf). Running sinkage which allows the calculation of trim angle was measured with string potentiometers at the LCG and the stern of each model. A "grasshopper" was mounted at approximately station 8 in each model to restrain the model in yaw and provide a limited yaw adjustment capability, while two tethers extended from the bow forward and outward, port and starboard, for safety purposes if the model should yaw excessively and/or break free from the carriage. The tethers were attached with enough slack such that they would not interfere with the model running trim or influence the drag measurements.

Table 2: Test Conditions For All Models

LCG %LBP Fwd AP	Displacement Lbs(Kg)	Volume ft^3(m^3)
38	298 (135.5)	4.78 (0.135)
	375 (170.5)	6.01 (0.17)
	483 (219.5)	7.75 (0.22)
42	298 (135.5)	4.78 (0.135)
	375 (170.5)	6.01 (0.17)
	483 (219.5)	7.75 (0.22)

The tow point heights, listed in Table 3, were determined from the height (above the keel) of the shaft thrust bearing on the full scale MLB. For each variant hull form the height was scaled according to the appropriate z-scale ratio. A mount for the existing two-inch gimbals was designed and built to lower the tow points to the desired levels.

Table 3: Model Tow Point Heights

Model	5628	5629	5630	5631
ABL, mm	155.45	124.97	111.56	128.02

To obtain the proper model ballast conditions, the longitudinal centers of gravity were first determined for the unballasted, rigged models. This was achieved by hanging each model from the 38% LCG position such that it was free to pivot about this transverse axis. Small weights were added to level the model in trim, which allowed the unballasted models' longitudinal center of gravity to be calculated by a simple balancing of moments. Given each of the models unballasted longitudinal centers of gravity, the desired displacement and

center of gravity for each test configuration was obtained through the precise placement of ballast weights.

The models were tested over a range of speeds. Data were collected at 100 Hz in ten-second spots, with two or more data spots taken per speed. Additionally, at each speed, the wave profile on the hull was observed at four (4) locations on the model and recorded. This was documented to determine the wetted surface area underway (S) of the model. These locations pertained to:

A. the keel-water intersection,
B. the foremost location of the intersection between the chine and the spray-sheet,
C. the chine reattachment point (the location where the chine no longer sheds water from the hull above the chine), and
D. the height of the water on station 10 (side of the model at the transom).

Figure 3 shows these points for model 5631 (Variant 3) at 10.87 knots and 375 lbs of displacement at the 38% LCG. The solid line represents a generalized wave profile from the four observed locations on the model. The surface of the model was discretized into thousands of triangular panels in order to determine the wetted surface areas. The colors on Figure 3, represent the fully wetted panels, the non-wetted panels, and the panels in between (split by the generalized wave profile). The underway wetted surface area is then assumed to be the total of the fully wetted panels and ½ of the panels split by the generalized wave profile. This dynamic area is then used, as a function of speed, in the data reduction and analysis whenever surface area is used to non-dimensionalize (see Appendix C for more information). Figure 4 is a photograph of model 5630 during testing.

TEST RESULTS

All of the data collected during these experiments are included in this paper as Appendix B. Model total and residuary resistance coefficients, LCG rise, model trim, measured wetted surface, and observed wetted keel length are tabulated for every test condition. The following discussion of results includes model R_T/Δ, S, LCG Rise, and Trim angle. Additionally, full scale EHP predictions were made for model 5628 to compare with predictions for the parent hull, the 47 ft MLB. The expansion to full scale EHP is required for comparison because the original model test was of an 8 foot model with the rounded transom and stern wedge of the parent hull while these tests were conducted with 10 foot models having flat transoms and no wedge. Discussion of the results will start with a comparison of the historical EHP data to the current test results. Subsequent discussions pertain to the impact, on the hydrodynamic performance, of varying the L/B ratio, transom deadrise angle, displacement, and the longitudinal center of gravity, respectively.

The EHP comparison plots (Figure 5, and 6) were developed from the test data for model 5628 and previously published data in Zseleczky (1988), collected at the United States Naval Academy, Division of Engineering and Weapons. The EHP was calculated identically to the previous experiment using a correlation allowance of zero, the ITTC 1957 friction line and assuming the full scale vessel is operating in smooth, deep salt water with a uniform standard temperature of 59° Fahrenheit (15° Celsius). The differences in geometry, besides the scale ratio of the models, are that model 5628 has a flat transom without a stern wedge. The only appendages on both models as tested were simple spray rails. The current data fits reasonably well with the historical data, bearing in mind that the displacement conditions are not identical. This comparison gives good assurance that the current data are reasonable and further analysis is trustworthy.

The R_T/Δ data is presented two ways, first for all models (varying L/B ratios and deadrise angles) at 375 lbs displacement and an LCG 38% forward of the transom in Figure 7 and then for model 5630 at 38% LCG for all displacements in Figure 8. The inflection point represents the transition region to planing. Each variable can be plotted from the data in Appendix B. Figure 7 shows that increasing the L/B ratio produced lower resistance at high speed. Comparing model 5630 to 5631 in Figure 7 shows that deadrise angle increase for these models results in an increase in resistance at high speeds. And finally, Figure 8 clearly shows the effect of increasing displacement and its relationship with the transition to planing. At speeds higher than the transition inflection point the R_T/Δ is lower for increasing displacement.

All of these data are consistent with classical planing data: (1) for increases in displacement, as well as increases in length-beam ratio, the point of inflection moves to the right, occurring at higher speed, (2) the resistance per pound of displacement increases with more forward LCG location, (3) the resistance per pound of displacement increases with increased deadrise angle, and (4) for increased deadrise angle, the magnitude of change in resistance per pound of displacement is much larger in the high-speed than the low-speed region. All of these observations have been seen and reported by many other researchers.

The dynamic wetted surface areas, S, are presented in Appendix B for each corresponding model at the two LCG locations. Figure 9 is a graphical presentation of the data for the medium displacement condition. We expected that for a particular hull form and LCG location the wetted surface area becomes approximately constant once the hull is fully planing and has reached its equilibrium trim angle. For hulls 5629 and 5630 the constant is achieved at a F_V of 3.6. For hull 5628, the parent hull of the series, and hull 5631, the hull with increased deadrise angles, our data does not extend out far enough for the wetted surface to reach a constant value indicating that they have not reached equilibrium. Appendix C gives more details of the wetted surface measurement procedures. Figure 10 is an example of the LCG rise plotted vs Volume Froude number for all the models at 375 Lbs displacement and 38% LCG location. The initial response, as speed increases from zero, is to sink slightly (displacement mode) before

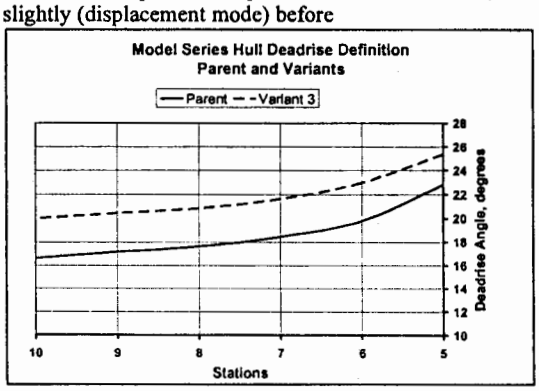

Figure 1: Series Hull Deadrise Angles Aft of Midships

steadily increasing at medium speed prior to leveling out once planing equilibrium is achieved. The figure shows that the magnitude of LCG rise once planing is insensitive to L/B ratio variation, although, it is sensitive to the increased deadrise angle, which slightly increased the amount of rise while on plane. The L/B variation shows the effect on the rate of LCG rise increase, producing a lower planing speed for lower L/B ratios. Trim data is presented in a similar manner to the LCG data in Figure 11. The comparison of these two figures shows a dependence on L/B and deadrise angle on the projected planing area for the location of the peak in trim angle and the magnitude of the equilibrium trim angle when the boat finally levels out. These trends are normal for planing boats.

The presented trim data is the change in model trim from the static condition. The trim angle of the keel relative to the calm water surface can be determined adding the static trim conditions for the models presented in Table B1 of Appendix B.

ANALYSES AND EXPANSION TO A NOTIONAL 80 FOOT PATROL BOAT

One of the primary goals of this project was to expand the base of resistance data available to designers of boats that the USCG would be buying to replace its current fleet. To that end the authors felt it was necessary to place quality value to the results. It is not the aim of this paper to complete a design but rather to present data to be used as a tool in future design efforts. The data was therefore expanded to a notional LWL of 80 feet and a comparison done with the Savitsky method as described by Blount and Fox , (Blount, 1976). For these calculations we used the maximum chine beam and the deadrise angle as measured at the transom. Figure 12 presents a curve of resistance per pound of displacement versus Volumetric Froude Number for model 5631at one displacement and 38% LCG compared to the Savitsky prediction. The curve shows that for most of the operating speed range 5631 has less resistance than a Savitsky prediction and is likely to perform well. When comparing all the models we observe that there are humps in the model data, getting more pronounced with increased displacement, which could be an indication of wave influence on resistance. The added wave drag in Savitsky is significant in the 20 knot range which we are passing through and it could be suggested that the shape differences in the curves can be attributed to this wave drag. These hull forms seem to have less hump drag than Savitsky would predict. Recall that these models have no stern wedge or appendages and it is possible that further refinements could make them more favorable.

A comparison of the predicted trim angle of the 80 footer to the Savitsky calculated trim angle is also presented in Figure 13 as part of the discussion of the differences in resistance predictions. This was presented to show that the results look reasonable and are worthy of future use as preliminary design data. Savitsky consistently predicts larger trim angles which would translate into higher resistance. The "peak" in the curve is in approximately the same speed range, but the Savitsky value is roughly 1 degree higher. The notional patrol boat's trim is only considering the hydrodynamic forces measured during model testing and is not a prediction of the final vessels trim because it does not account for all the possible appendages or deck structures. Data is provided in the appendices for future consideration.

In March of 2006 Dr. Savitsky and his associates at Davidson Laboratory published a paper on the inclusion of whisker spray drag in the prediction of full scale performance. We believe that the data provided in this paper would allow a naval architect in preliminary design to use this method to make accurate full scale predictions. In our project which was completed prior to the papers publication, we selected an approach to wetted area that acknowledged the changing waterline with speed and included the wetted area of the spray sheet. When these data are used for future preliminary design, enough information has been provided to allow for the inclusion of whisker spray drag in full scale predictions.

CONCLUSIONS

The purpose of this project was to generate data for use in evaluating the resistance of planing hulls for the US Coast Guard. The models were developed and tested for a range of displacements that was believed to be typical for military boats of this kind. The speed range examined was expanded to meet the requirements of current Coast Guard specifications for new patrol boats. This is a pre-design exercise and is not tied to any specific hull or specification. All of the data presented and collected are in standard formats which will allow other researchers to use the data as they see fit.

ACKNOWLEDGEMENTS

This project was sponsored by the USCG Engineering Logistics Center's Survey and Design Funds. The authors would like to thank those members of the towing tank staff at Carderock for their efforts in conducting these tests, specifically Lisa Faul, Ellissa Bumiller, and Jonathan Slutsky. There have also been large contributions made by the USCG Engineering Logistics Center's Small Boat Engineering Branch, Tracy Byington for hull form illustrations, and Debu Ghosh and Chris Barry for editorial comments.

The views and opinions expressed are those of the authors and are not to be construed as official policy or reflecting the views of the U S Coast Guard or the Department of Homeland Security.

REFERENCES

Cohen, S. et al, "Design and Construction of the U.S. Coast Guard's 47-ft Self-Righting, Heavy Weather Rescue Craft", SNAME Transactions 1990.

International Towing Tank Conference ITTC Symbols and Terminology List, Version 2002, July 2002.

Metcalf, B et al, "Resistance Tests of a Systematic Series of US Coast Guard Planing Hulls" NSWCCD-50-TR-2005-063, December 2005.

Zseleczky, "Effective Horsepower Model Tests of the U.S. Coast Guard 47 ft Motor Lifeboat (MLB)", Rpt EW-5-88, May 1988.

Radojcic, D., et al, "The Resistance and Trim of Semi-Displacement, Double-Chine, Transom-Stern Hull Series", International Conference on Fast Sea Transportation (FAST), Southampton, 2001.

Blount, D. and Fox, W., "Small-Craft Power Prediction", *Marine Technology*, January 1976 Society of Naval Architects and Marine Engineers, Jersey City, NJ

Savitsky, D et al, "Inclusion of Whisker Spray Drag in Performance Prediction Method For High-Speed Planing Hulls" March 2006, New York Metropolitan Section of the Society of Naval Architects and Marine Engineers, Jersey City, NJ

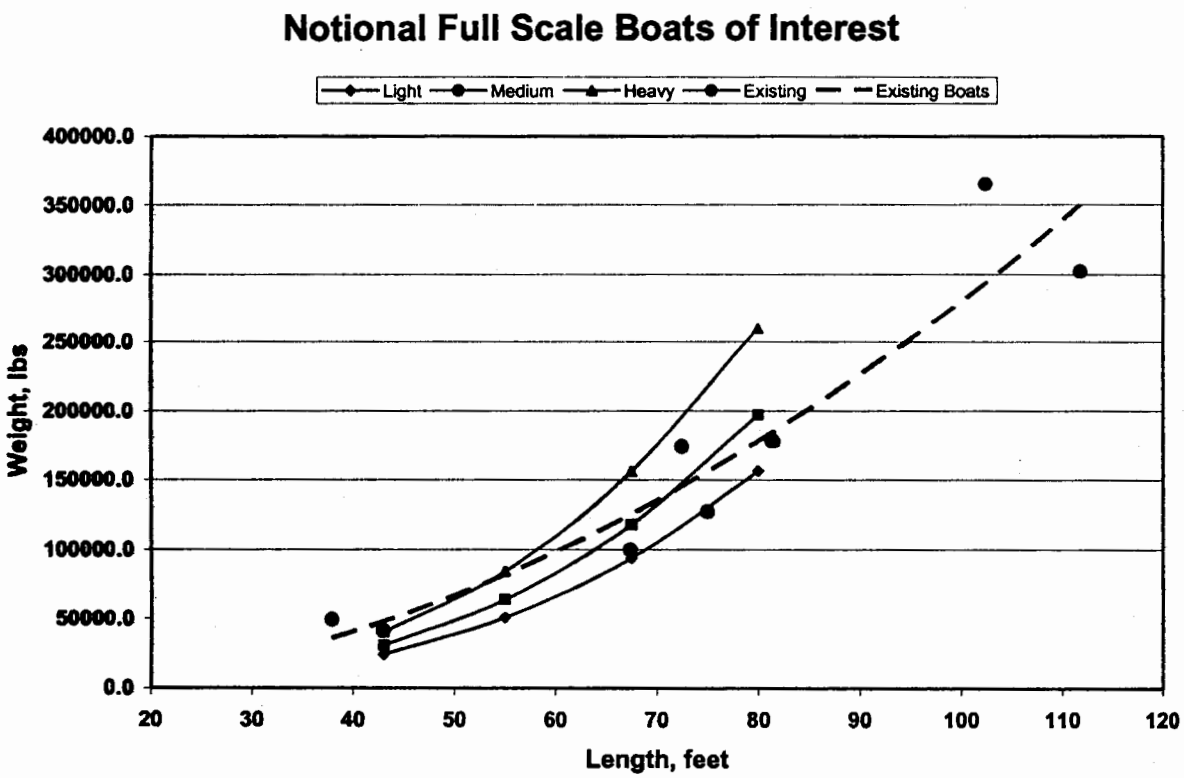

Figure 2: Examples of Notional Boats and Existing Patrol Boats Used In the Determination of Test Conditions

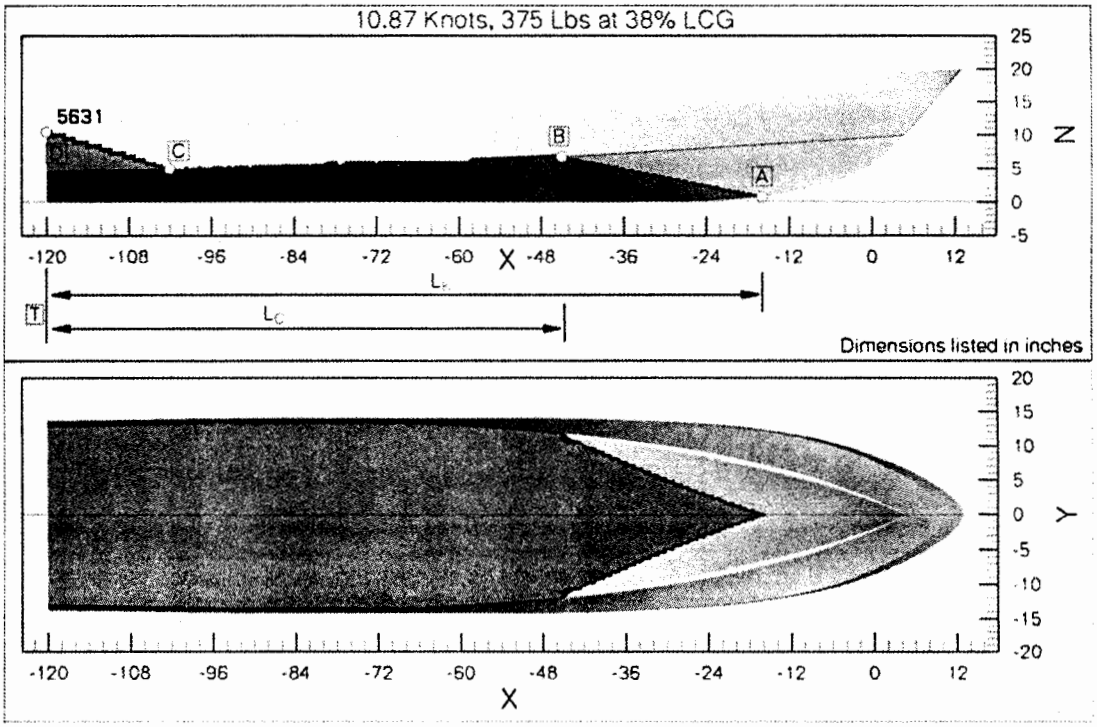

Dark Grey – Fully WET triangular panels (below wave profile A B C D)
Black – Triangular panels partially wet by wave profile along line A B C D
Light Grey – Fully DRY triangular panels (above wave profile A B C D)

Figure 3: Underway Wetted Surface Area of Model 5631

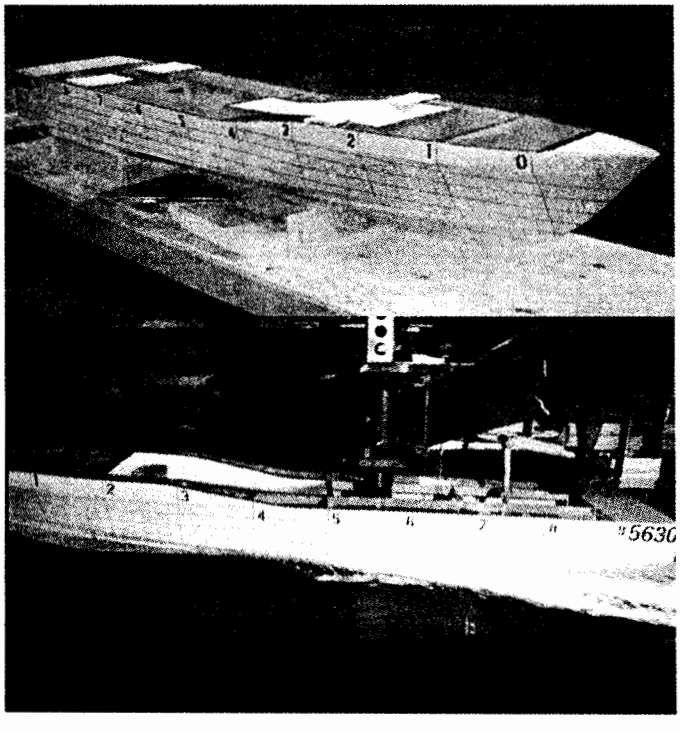

Figure 4: Model 5630 Underway at 298lbs, 43%, 25.47 Knots

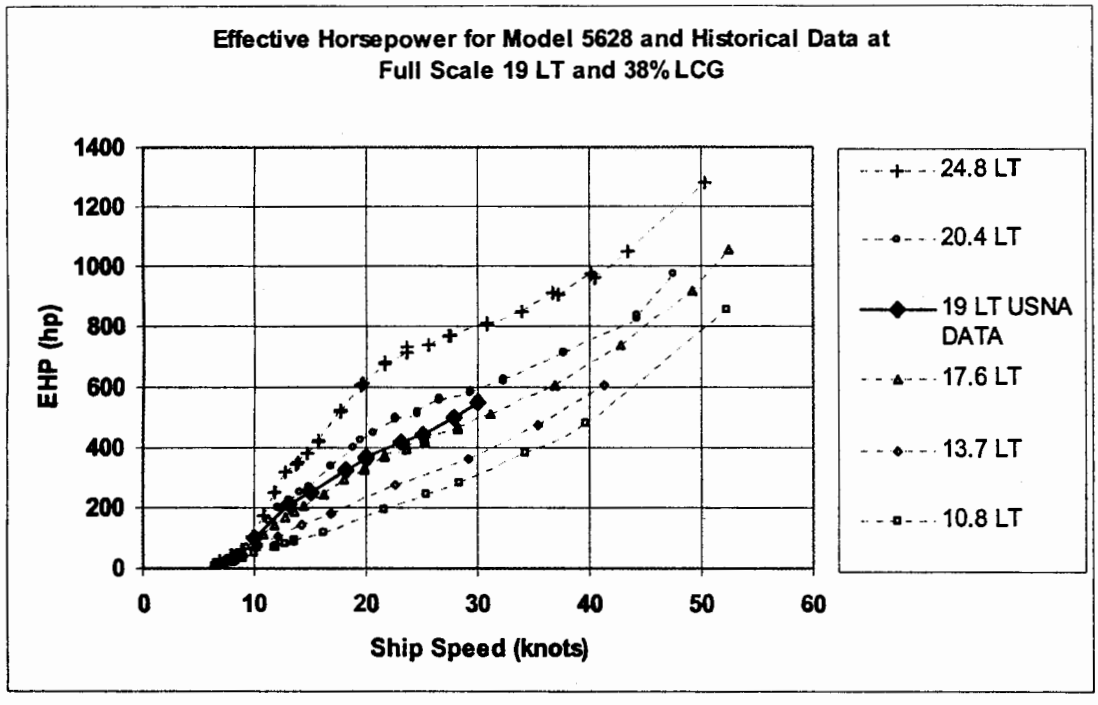

Figure 5: EHP for Full Scale 47 ft MLB at 38% LCG

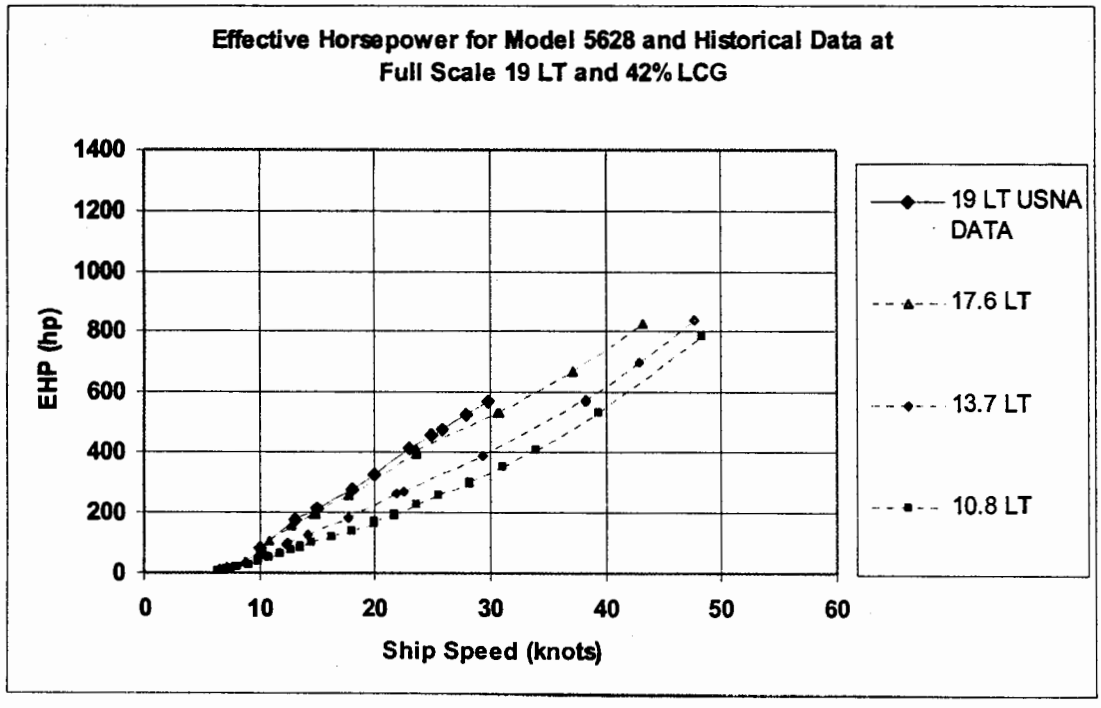

Figure 6: EHP for Full Scale 47 ft MLB at 42% LCG

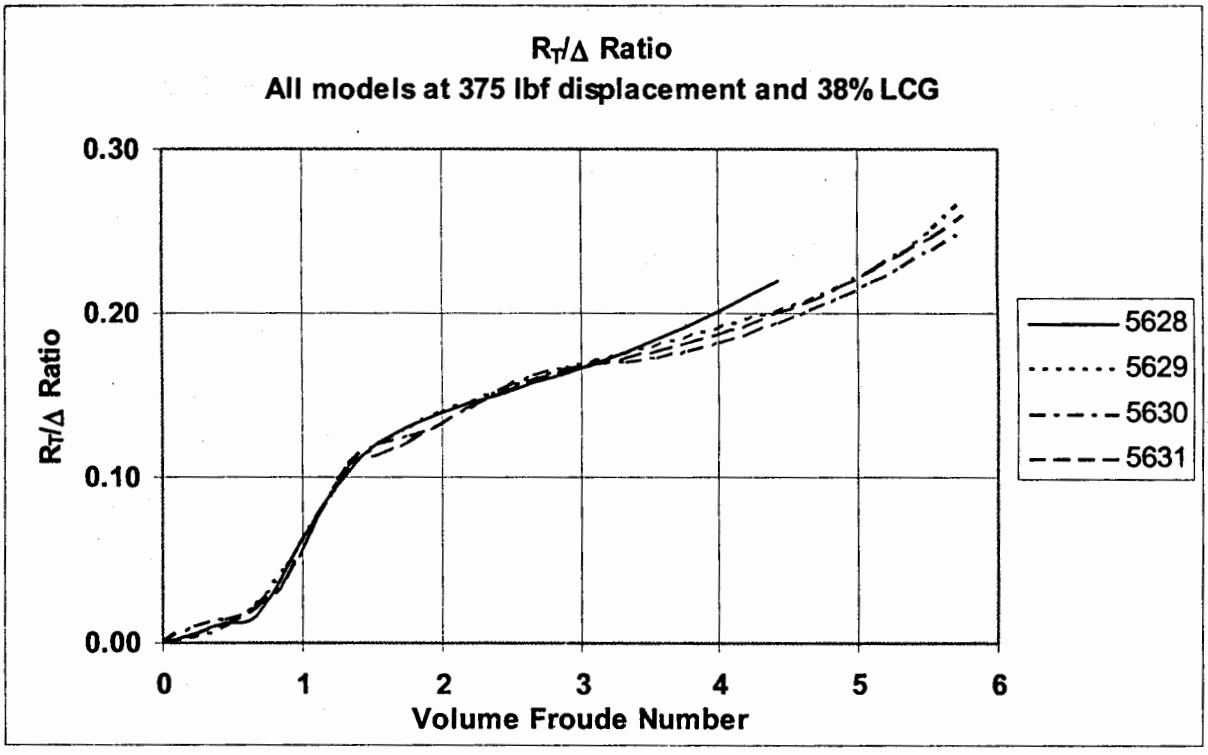

Figure 7: L/B & Deadrise Influence on Resistance at 375Lbs and 38% LCG

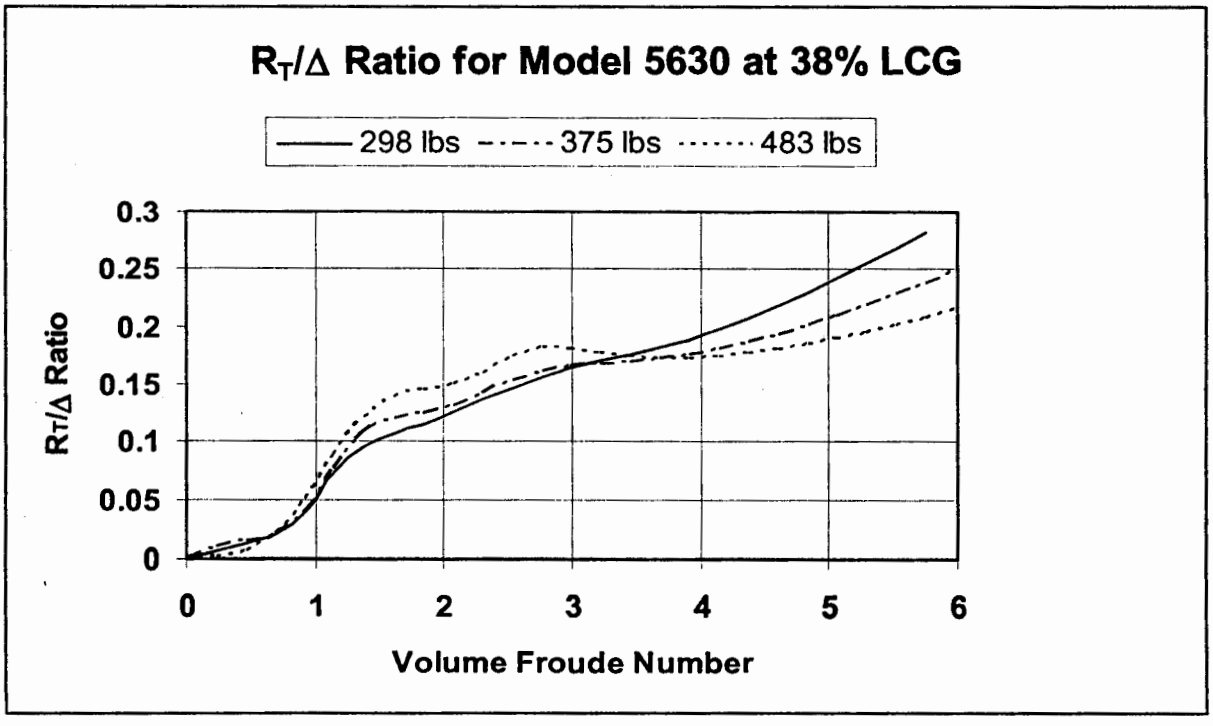

Figure 8: R_T/Δ Ratio For Model 5630 at 38% LCG

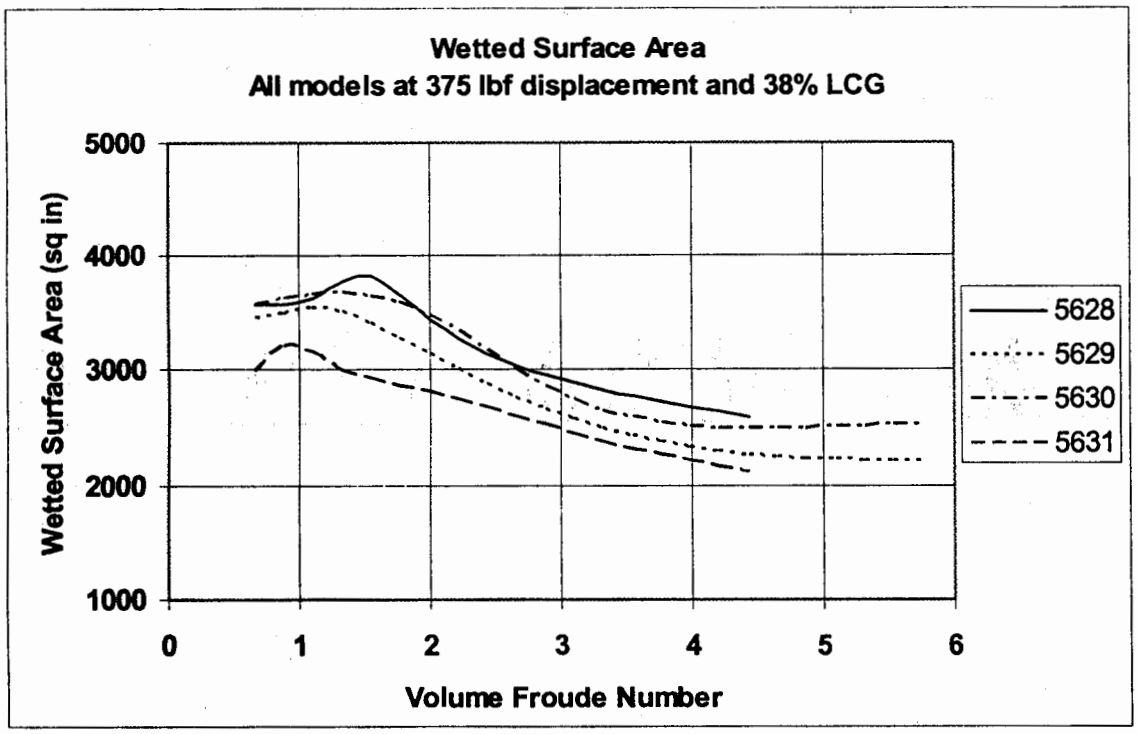

Figure 9: Wetted Surface Area at 375 Lbs and 38% LCG

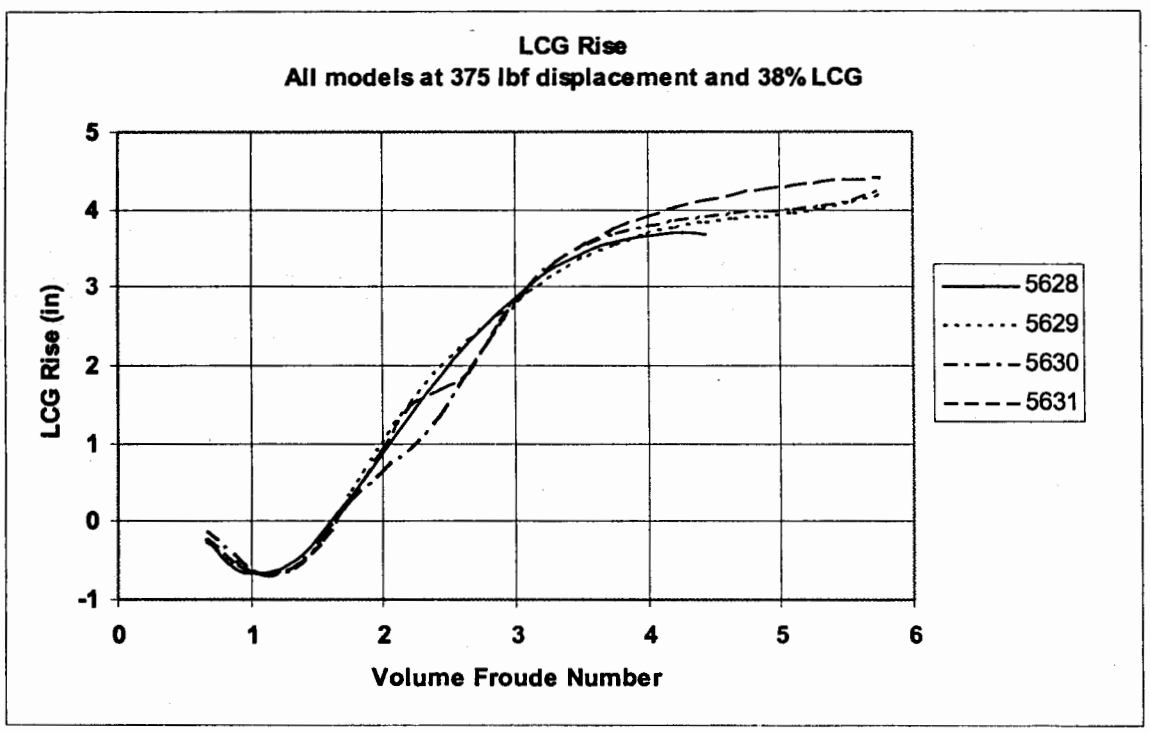

Figure 10: LCG Rise for All Models at 375 Lbs and 38% LCG

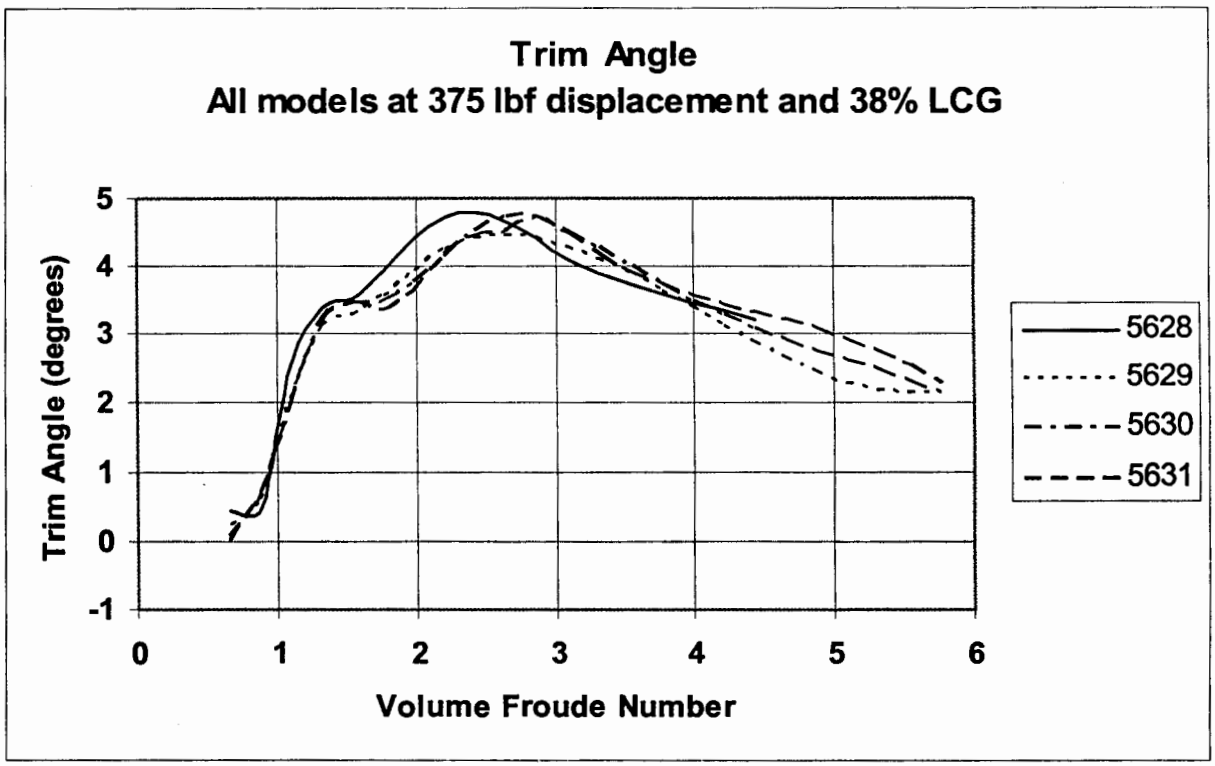

Figure 11: Trim Angle for All Models at 375 Lbs and 38% LCG

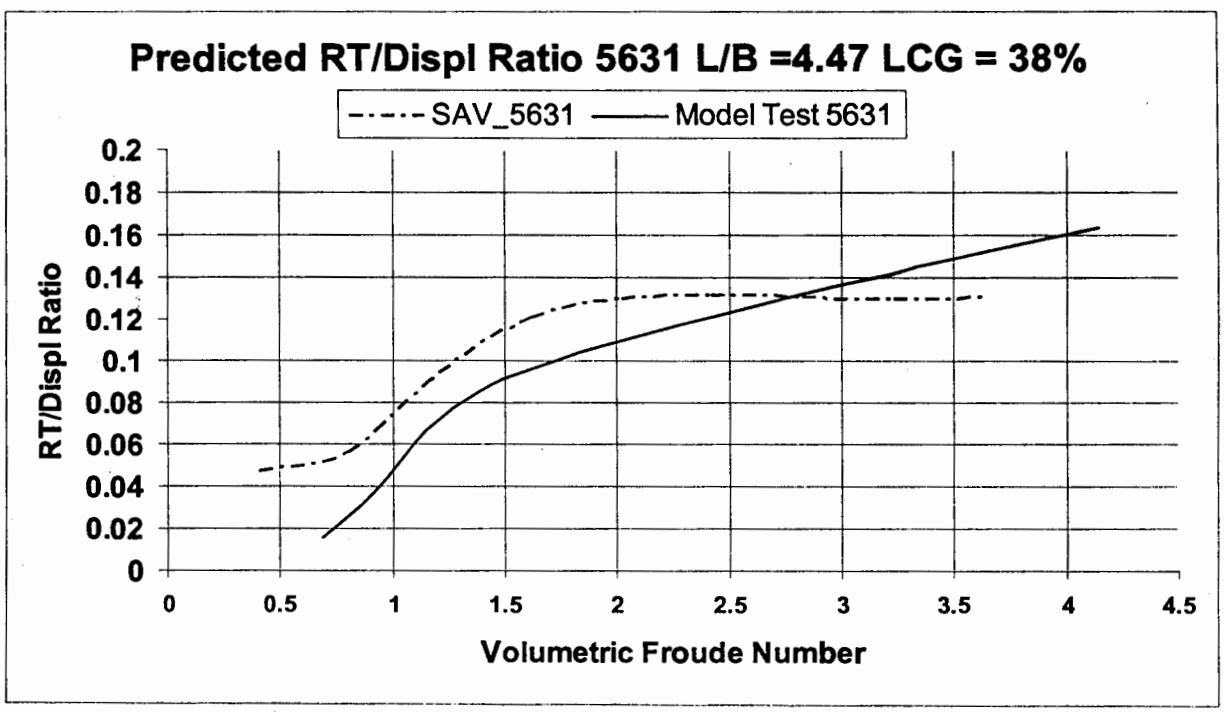

Figure 12: Notional 80 footer of Model 5631 at 156,000 lbs and 38% LCG

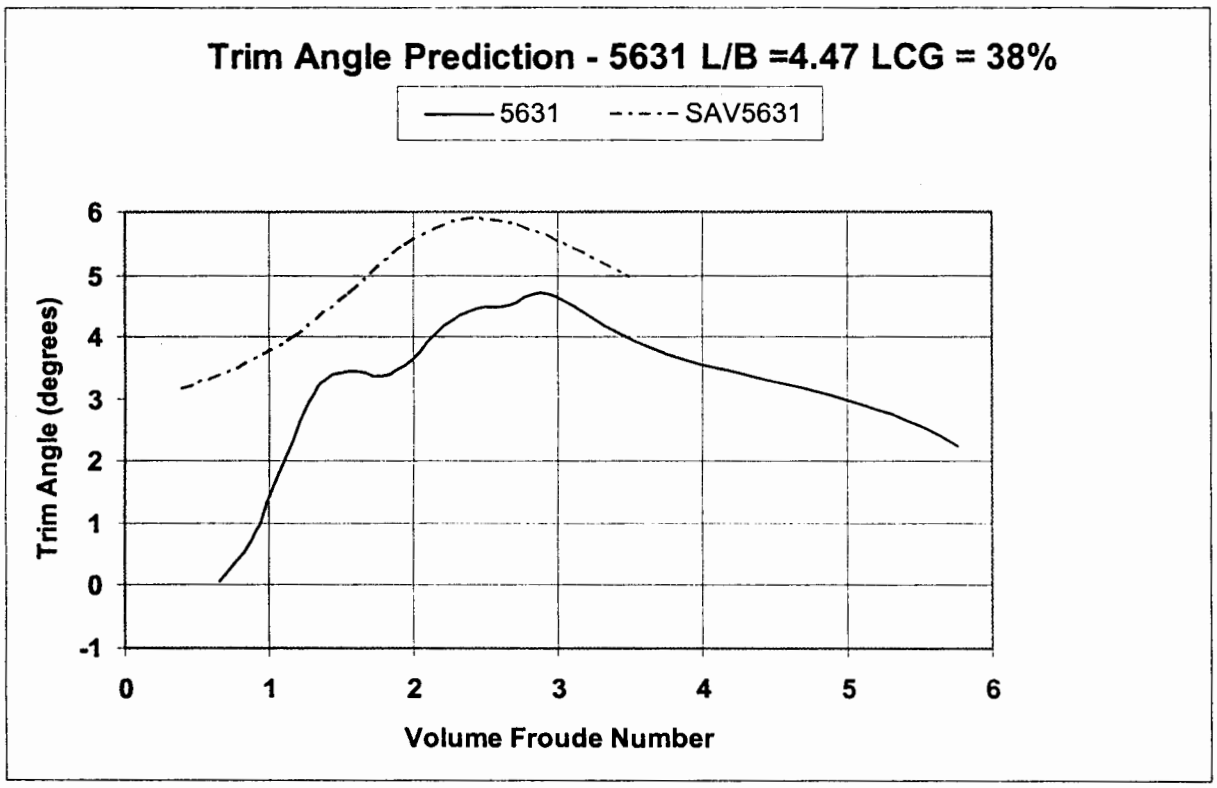

Figure 13: Trim Angle Prediction Comparison between Savitsky and Notional 80 Foot Boat

APPENDIX A PARENT HULL AND MODEL LINES AND HULL CHARACTERISTICS

Figure A1: Body Plan of the USCG 47' MLB – Full Scale
Reference: USCG Drawing Number 47B-MLB_801_1_1_-_C.dwg

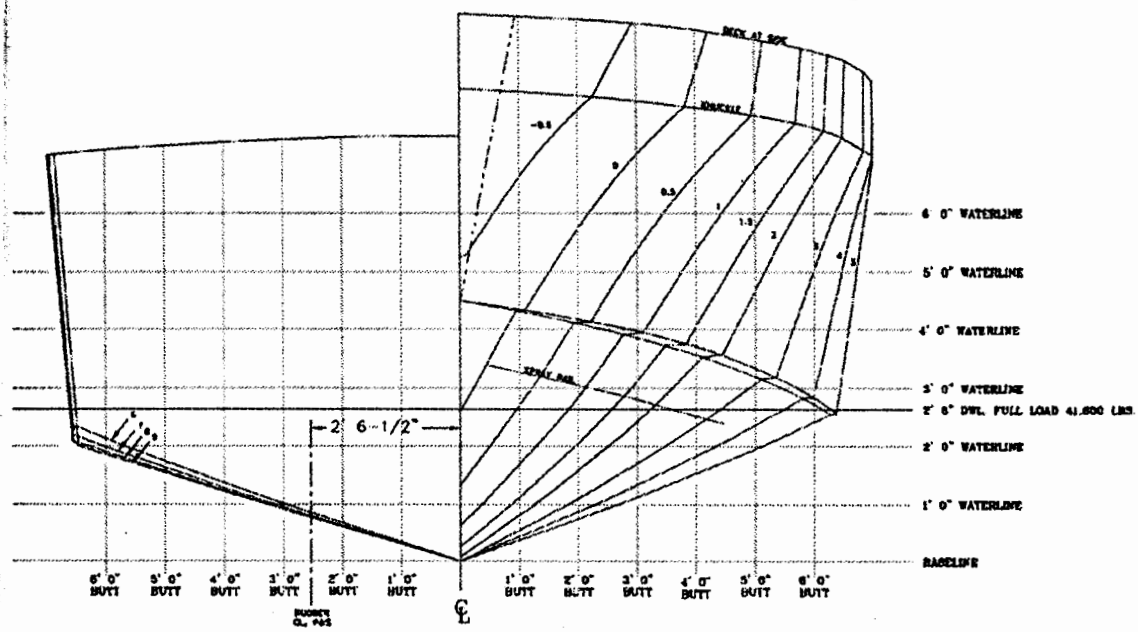

BODY PLAN

Figure A2: Stern Wedge of the USCG 47' MLB – Full Scale
Reference: USCG Drawing Number 47B-MLB_801_1_2_-_C.dwg

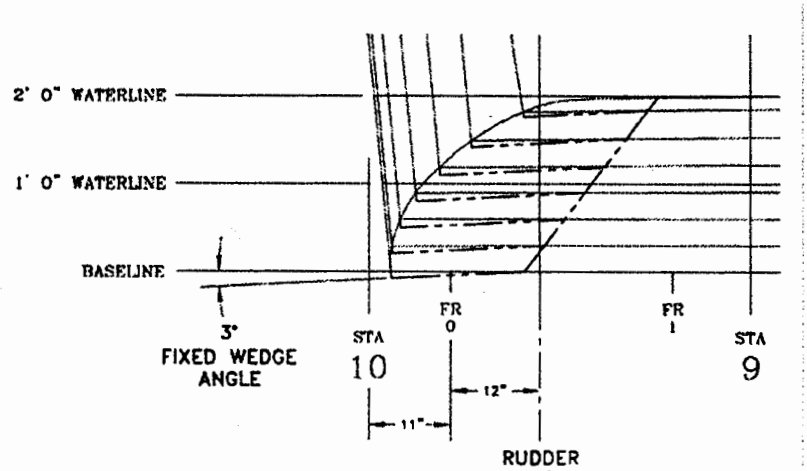

STERN WEDGE

Figure A3: Body Plan of Parent Model 5628

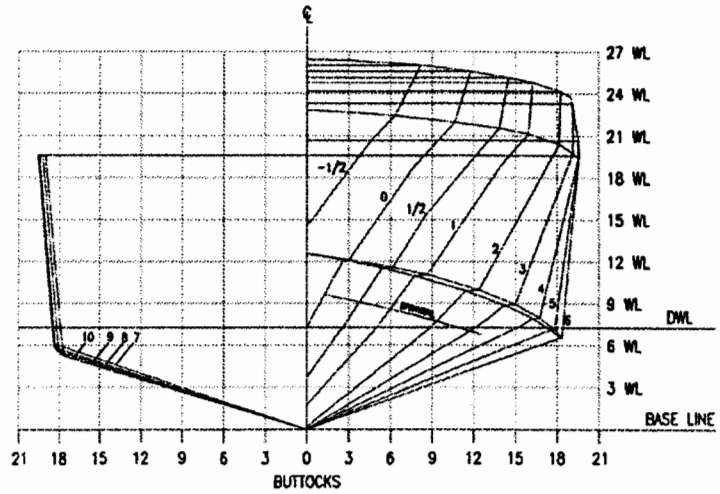

Figure A4: Body Plan of Variant 1 Model 5629

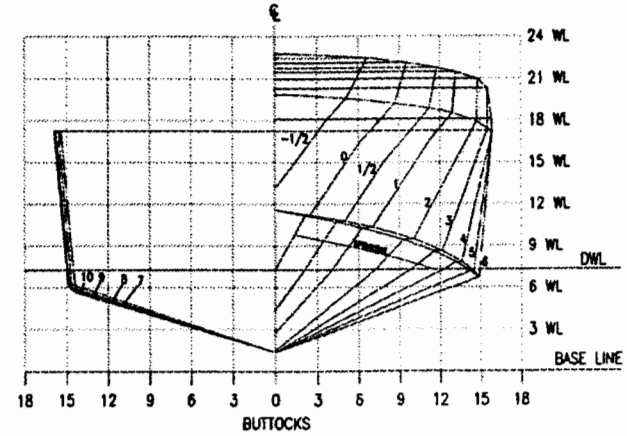

Figure A5: Body Plan of Variant 2 Model 5630

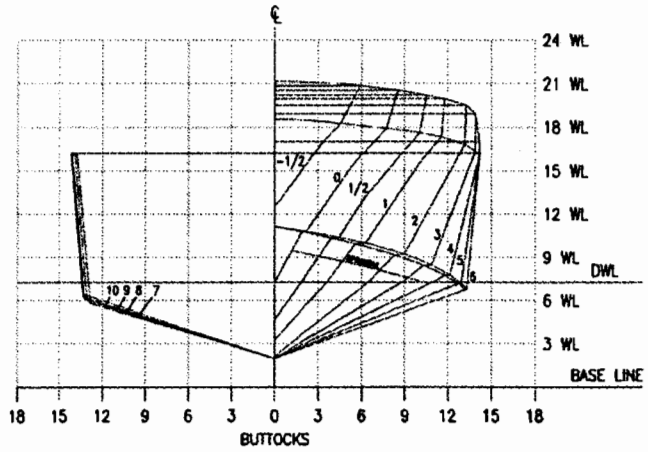

Figure A6: Body Plan of Variant 3 Model 5631

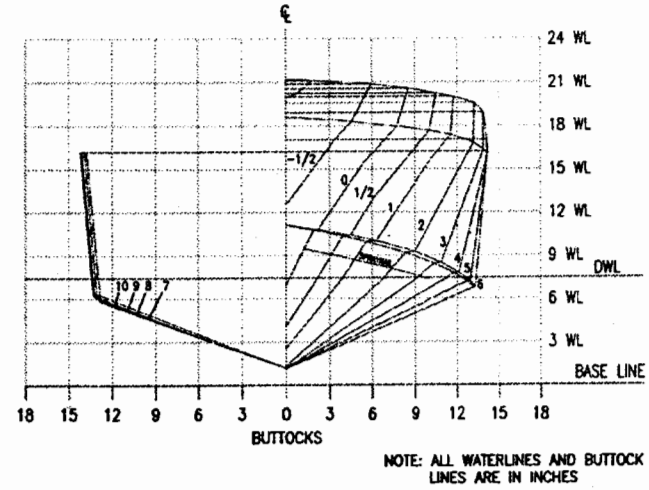

Figure A7: Plan and Profile of Parent Model 5628

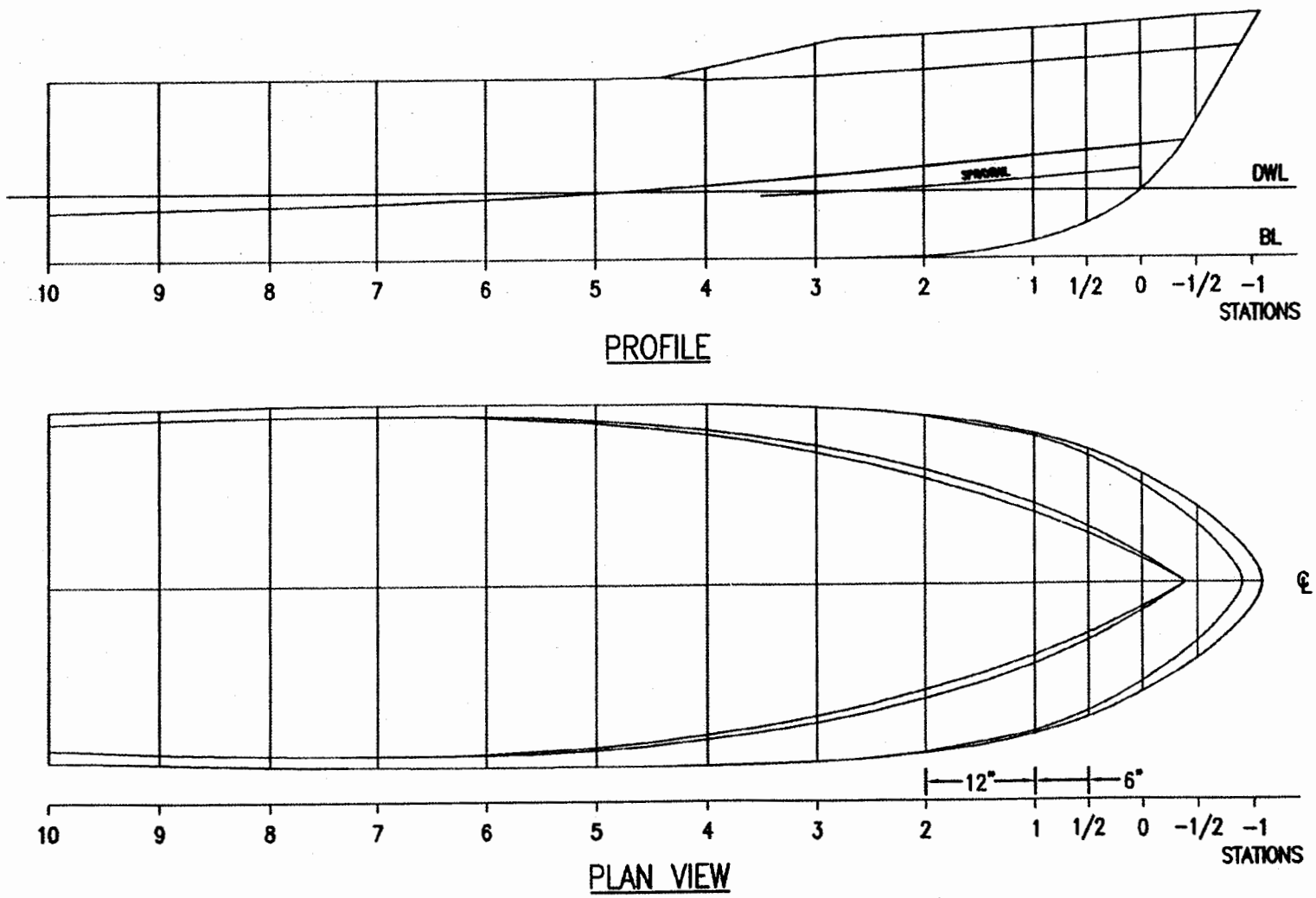

Table A1: Hull Characteristics – feet (meters)

	Parent 5628	Variant 1 5629	Variant 2 5630	Variant 3 5631
Length, OA	10.9(3.32)	10.9	10.9	10.9
Length, WL	10.0(3.05)	10.0	10.0	10.0
Beam, OA	3.258(0.99)	2.643(0.81)	2.364(0.72)	2.364(0.72)
Beam, WL	3.085(0.94)	2.5(0.76)	2.237(0.68)	2.237(0.68)
Draft, nominal	0.607(0.18)	0.492(0.15)	0.440(0.13)	0.511(0.16)
Deadrise, Sta 5	22.81	22.81	22.81	25.35
Deadrise, transom	16.61	16.61	16.61	20.00
Half Entrance Angle	19.5	19.5	19.5	21.0
Volume, cubic ft	8.0(0.23)	5.3(0.15)	4.2(0.12)	4.8(0.14)
Displacement, lbs	513.5	337.663	270.321	310.72
LCB(buoyancy aft sta 0))	6.2(1.9)	6.2(1.9)	6.2(1.9)	6.16(1.88)
LCF(floatation aft sta 0))	5.97(1.82)	5.98(1.82)	5.97(1.82)	5.95(1.81)
C_B	0.428	0.428	0.429	0.423
C_P	0.696	0.696	0.696	0.708
Transom Area, sq ft	4.30(0.4)	2.82(0.26)	2.26(0.21)	2.34((0.22)
Transom Immersion, sq ft	1.16(0.11)	0.76(0.07)	0.61(0.06)	0.68(0.06)

APPENDIX B: MODEL DATA PRESENTATION

Model Total Resistance Coefficient Faired Data - all models at 483 lbs

rho	9.33546E-05	$lb\text{-}s^2/in^4$							
Temp	72	F							
Test #		2	7	24	27	12	15	18	21
Model #		5628	5628	5629	5629	5630	5630	5631	5631
D =		483	483	483	483	483	483	483	483
LCG		0.38	0.42	0.38	0.42	0.38	0.42	0.38	0.42
Vm	Vm	CT	CT	CT	CT	CT	CT	CT	CT
(knots)	in/sec	1000	1000	1000	1000	1000	1000	1000	1000
0	0								
1	20.256								
2	40.512								
3	60.768	10.629	8.380	13.908	13.211	16.568	12.585	14.976	13.096
4	81.024	16.212	14.415	16.568	15.780	21.448	13.974	16.831	16.978
5	101.28	21.378	17.271	21.663	19.828	23.616	17.756	22.630	21.357
6	121.536	19.676	16.690	24.439	21.536	21.968	19.035	25.117	22.762
7	141.792	16.134	14.660	19.953	17.968	18.367	16.255	20.208	18.668
8	162.048	13.534	12.578	16.371	14.780	15.008	12.873	16.508	15.010
9	182.304	11.853	10.912	13.862	12.647	12.797	10.566	14.384	13.024
10	202.56	10.696	9.697	12.096	11.051	11.814	9.220	12.922	11.660
11	222.816	9.792	8.822	11.611	10.116	11.514	8.328	11.943	10.526
12	243.072	9.001	8.148	11.341	9.759	10.922	7.687	11.616	9.739
13	263.328	8.268	7.563	10.355	9.287	9.876	7.545	11.379	9.650
14	283.584	7.578	7.010	9.165	8.535	8.757	7.533	10.448	9.502
15	303.84	6.935	6.478	8.098	7.722	7.754	7.026	9.223	8.586
16	324.096	6.343	5.974	7.216	6.978	6.902	6.304	8.109	7.598
17	344.352	5.806	5.508	6.502	6.339	6.188	5.639	7.191	6.782
18	364.608	5.327	5.086	5.930	5.803	5.594	5.087	6.455	6.127
19	384.864	4.909	4.709	5.472	5.358	5.097	4.638	5.866	5.596
20	405.12	4.555	4.376	5.088	4.989	4.682	4.272	5.395	5.163
21	425.376	4.268	4.084	4.734	4.685	4.334	3.972	5.019	4.809
22	445.632	4.051		4.460	4.435	4.040	3.723	4.720	4.520
23	465.888	3.909		4.258	4.232	3.791	3.515	4.484	4.286
24	486.144	3.846		4.104	4.068	3.580	3.340	4.302	4.102
25	506.4	3.871		3.988	3.940	3.401	3.192	4.167	3.964
26	526.656			3.905	3.844	3.248	3.067	4.073	3.870
27	546.912			3.853	3.777	3.118	2.961	4.018	3.821

28	567.168		3.831			2.871	4.000	3.822

Model Total Resistance Coefficient Faired Data - all models at 375 lbs

rho	9.33546E-05		$lb\text{-}s^2/in^4$	Temp	72	F			
Test #		9	6	23	26	11	14	17	20
Model #		5628	5628	5629	5629	5630	5630	5631	5631
D =	(lbf)	375	375	375	375	375	375	375	375
LCG		0.38	0.42	0.38	0.42	0.38	0.42	0.38	0.42
Vm	Vm	CT	CT	CT	CT	CT	CT	CT	CT
(knots)	in/sec	1000	1000	1000	1000	1000	1000	1000	1000
0	0								
1	20.256								
2	40.512								
3	60.768	9.671	8.540	14.024	10.271	12.662	10.633	14.650	12.308
4	81.024	16.065	11.890	16.298	14.366	13.411	11.425	14.642	13.537
5	101.28	16.993	14.058	17.058	14.609	16.518	13.762	18.667	15.877
6	121.536	15.043	12.831	15.921	14.508	16.068	13.519	19.348	15.485
7	141.792	12.689	10.823	14.016	12.406	13.149	11.511	15.478	12.995
8	162.048	11.076	9.357	12.219	10.498	10.689	9.675	12.951	10.806
9	182.304	9.847	8.371	10.756	9.086	9.172	8.291	11.403	9.303
10	202.56	8.766	7.635	9.594	8.015	8.336	7.203	10.229	8.251
11	222.816	7.833	7.025	8.655	7.203	7.827	6.364	9.219	7.532
12	243.072	7.053	6.491	7.876	6.699	7.333	6.008	8.326	7.120
13	263.328	6.411	6.013	7.214	6.515	6.749	5.900	7.546	6.877
14	283.584	5.885	5.586	6.641	6.259	6.145	5.594	6.879	6.577
15	303.84	5.452	5.209	6.139	5.803	5.594	5.175	6.315	6.170
16	324.096	5.093	4.878	5.694	5.332	5.115	4.761	5.844	5.727
17	344.352	4.795	4.593	5.299	4.920	4.707	4.397	5.453	5.309
18	364.608	4.545	4.349	4.947	4.574	4.358	4.090	5.128	4.940
19	384.864	4.334	4.143	4.636	4.286	4.059	3.835	4.860	4.622
20	405.12	4.155	3.971	4.362	4.047	3.803	3.622	4.639	4.353
21	425.376		3.829	4.125	3.851	3.582	3.443		4.125
22	445.632		3.715	3.925	3.691	3.392	3.291		3.932
23	465.888		3.625	3.761	3.561	3.228	3.161		3.769
24	486.144			3.637	3.457	3.086	3.049		3.632
25	506.4			3.558	3.374	2.963	2.951		3.516
26	526.656			3.532	3.308	2.858	2.866		3.418
27	546.912								
28	567.168								

Model Total Resistance Coefficient Faired Data - all models at 298 lbs

rho	9.33546E-05		lb-s^2/in^4	Temp	72	F			
Test #		8	5	22	25	10	13	16	19
Model #		5628	5628	5629	5629	5630	5630	5631	5631
D =		298	298	298	298	298	298	298	298
LCG		0.38	0.42	0.38	0.42	0.38	0.42	0.38	0.42
Vm	Vm	CT	CT	CT	CT	CT	CT	CT	CT
(knots)	in/sec	1000	1000	1000	1000	1000	1000	1000	1000
0	0.000								
1	20.256								
2	40.512								
3	60.768	8.455	6.803	11.719	8.886	10.621	8.224	10.712	10.544
4	81.024	13.026	9.112	14.610	11.033	11.490	10.340	14.107	10.288
5	101.280	12.418	12.378	16.372	11.562	13.779	10.862	16.083	13.079
6	121.536	10.855	11.537	12.959	10.884	12.154	9.971	14.149	11.420
7	141.792	9.474	9.570	10.648	9.752	9.805	8.803	11.754	10.025
8	162.048	8.362	8.018	9.476	8.566	8.259	7.725	9.874	8.644
9	182.304	7.489	6.967	8.268	7.525	7.294	6.784	8.505	7.587
10	202.560	6.797	6.257	7.299	6.652	6.643	5.973	7.518	6.809
11	222.816	6.237	5.741	6.613	5.955	6.141	5.328	6.804	6.247
12	243.072	5.776	5.334	6.199	5.530	5.694	4.898	6.279	5.844
13	263.328	5.388	4.998	5.892	5.432	5.262	4.618	5.881	5.538
14	283.584	5.058	4.722	5.559	5.269	4.844	4.382	5.558	5.273
15	303.840	4.776	4.494	5.209	4.951	4.465	4.153	5.273	5.017
16	324.096	4.532	4.305	4.879	4.624	4.144	3.933	4.998	4.763
17	344.352	4.321	4.148	4.586	4.336	3.882	3.730	4.723	4.517
18	364.608	4.139	4.015	4.334	4.091	3.671	3.547	4.448	4.288
19	384.864	3.981	3.901	4.121	3.883	3.499	3.383	4.188	4.078
20	405.120	3.846	3.802		3.707	3.354	3.238	3.954	3.889
21	425.376	3.730	3.715		3.559	3.228	3.111	3.762	3.721
22	445.632	3.633	3.639		3.434	3.116	3.001	3.616	3.575
23	465.888	3.553	3.572		3.330	3.013	2.906	3.516	3.450
24	486.144	3.490			3.245	2.916	2.825	3.455	3.347
25	506.400	3.442			3.178	2.825	2.758	3.420	3.272

Model Residuary Resistance Coefficient Faired Data - all models at 483 lbs

Test #		2	7	24	27	12	15	18	21
Model #		5628	5628	5629	5629	5630	5630	5631	5631
D =		483	483	483	483	483	483	483	483
LCG		0.38	0.42	0.38	0.42	0.38	0.42	0.38	0.42
Vm	Vm	CR	CR	CR	CR	CR	CR	CR	CR
(knots)	in/sec	1000	1000	1000	1000	1000	1000	1000	1000
0	0								
1	20.256								
2	40.512								
3	60.768	7.223	4.974	10.502	9.805	13.162	9.179	11.570	9.690
4	81.024	12.980	11.184	13.336	12.548	18.216	10.743	13.600	13.746
5	101.28	18.263	14.166	18.553	16.723	20.510	14.650	19.518	18.252
6	121.536	16.648	13.681	21.407	18.522	18.943	16.028	22.093	19.749
7	141.792	13.176	11.721	16.989	15.025	15.419	13.324	17.255	15.727
8	162.048	10.642	9.695	13.476	11.895	12.118	10.004	13.614	12.129
9	182.304	8.993	8.074	11.018	9.810	9.946	7.749	11.537	10.197
10	202.56	7.850	6.894	9.277	8.251	8.986	6.449	10.105	8.877
11	222.816	6.971	6.050	8.804	7.344	8.701	5.596	9.139	7.764
12	243.072	6.207	5.403	8.551	7.010	8.123	4.963	8.831	6.993
13	263.328	5.501	4.845	7.588	6.558	7.094	4.831	8.617	6.926
14	283.584	4.839	4.321	6.426	5.829	5.997	4.854	7.712	6.802
15	303.84	4.222	3.818	5.389	5.040	5.020	4.377	6.512	5.912
16	324.096	3.655	3.340	4.536	4.323	4.195	3.682	5.421	4.949
17	344.352	3.143	2.898	3.851	3.709	3.508	3.041	4.526	4.159
18	364.608	2.687	2.497	3.306	3.198	2.940	2.510	3.812	3.528
19	384.864	2.291	2.140	2.875	2.775	2.467	2.081	3.244	3.021
20	405.12	1.957	1.825	2.515	2.428	2.074	1.734	2.794	2.611
21	425.376	1.689	1.548	2.183	2.145	1.745	1.450	2.437	2.277
22	445.632	1.490		1.927	1.914	1.470	1.217	2.157	2.007
23	465.888	1.365		1.741	1.728	1.239	1.024	1.940	1.791
24	486.144	1.318		1.602	1.581	1.047	0.864	1.775	1.624
25	506.4	1.358		1.501	1.468	0.887	0.729	1.656	1.501
26	526.656			1.432	1.387	0.755	0.617	1.579	1.421
27	546.912			1.394	1.334	0.646	0.523	1.539	1.385
28	567.168			1.385			0.445	1.535	1.399

Model Residuary Resistance Coefficient Faired Data - all models at 375 lbs

Test #		9	6	23	26	11	14	17	20
Model #		5628	5628	5629	5629	5630	5630	5631	5631
D =	(lbf)	375	375	375	375	375	375	375	375
LCG		0.38	0.42	0.38	0.42	0.38	0.42	0.38	0.42
Vm	Vm	CR	CR	CR	CR	CR	CR	CR	CR
(knots)	in/sec	1000	1000	1000	1000	1000	1000	1000	1000
0	0								
1	20.256								
2	40.512								
3	60.768	6.258	5.134	10.618	6.865	9.256	7.227	11.244	8.902
4	81.024	12.829	8.658	13.065	11.134	10.176	8.193	11.411	10.306
5	101.28	13.873	10.950	13.944	11.503	13.402	10.656	15.554	12.772
6	121.536	12.007	9.815	12.899	11.498	13.044	10.511	16.320	12.476
7	141.792	9.719	7.880	11.067	9.470	10.197	8.576	12.521	10.060
8	162.048	8.163	6.472	9.327	7.621	7.794	6.802	10.055	7.931
9	182.304	6.979	5.533	7.909	6.260	6.321	5.468	8.557	6.481
10	202.56	5.932	4.837	6.780	5.231	5.520	4.421	7.419	5.478
11	222.816	5.023	4.261	5.866	4.456	5.038	3.617	6.433	4.792
12	243.072	4.268	3.756	5.111	3.983	4.565	3.291	5.562	4.406
13	263.328	3.655	3.307	4.473	3.827	4.001	3.209	4.807	4.189
14	283.584	3.160	2.908	3.926	3.596	3.418	2.929	4.167	3.914
15	303.84	2.757	2.557	3.450	3.164	2.889	2.534	3.631	3.531
16	324.096	2.424	2.253	3.032	2.718	2.436	2.143	3.187	3.112
17	344.352	2.151	1.991	2.663	2.333	2.054	1.802	2.822	2.716
18	364.608	1.929	1.769	2.337	2.013	1.731	1.517	2.522	2.368
19	384.864	1.741	1.583	2.050	1.750	1.458	1.282	2.277	2.071
20	405.12	1.575	1.430	1.799	1.534	1.226	1.089	2.077	1.822
21	425.376		1.306	1.583	1.359	1.027	0.929		1.613
22	445.632		1.208	1.403	1.217	0.858	0.795		1.439
23	465.888		1.134	1.258	1.103	0.712	0.683		1.294
24	486.144			1.152	1.014	0.588	0.588		1.174
25	506.4			1.089	0.944	0.482	0.506		1.074
26	526.656			1.079	0.890	0.391	0.436		0.992
27	546.912								
28	567.168								

Model Residuary Resistance Coefficient Faired Data - all models at 298 lbs

Test #		8	5	22	25	10	13	16	19
Model #		5628	5628	5629	5629	5630	5630	5631	5631
D =		298	298	298	298	298	298	298	298
LCG		0.38	0.42	0.38	0.42	0.38	0.42	0.38	0.42
Vm	Vm	CR	CR	CR	CR	CR	CR	CR	CR
(knots)	in/sec	1000	1000	1000	1000	1000	1000	1000	1000
0	0.000								
1	20.256								
2	40.512								
3	60.768	5.044	3.396	8.313	5.470	7.214	4.818	7.306	7.138
4	81.024	9.783	5.880	11.374	7.794	8.256	7.109	10.874	7.056
5	101.280	9.297	9.270	13.255	8.457	10.659	7.756	12.968	9.973
6	121.536	7.826	8.518	9.930	7.874	9.124	6.963	11.120	8.405
7	141.792	6.517	6.621	7.690	6.811	6.849	5.866	8.794	7.087
8	162.048	5.464	5.127	6.578	5.686	5.363	4.849	6.977	5.770
9	182.304	4.634	4.125	5.420	4.697	4.447	3.962	5.661	4.765
10	202.560	3.967	3.457	4.491	3.872	3.835	3.201	4.717	4.029
11	222.816	3.443	2.979	3.841	3.216	3.364	2.592	4.034	3.502
12	243.072	3.014	2.604	3.458	2.824	2.944	2.189	3.535	3.130
13	263.328	2.656	2.299	3.179	2.753	2.535	1.936	3.160	2.852
14	283.584	2.354	2.050	2.872	2.611	2.140	1.726	2.864	2.613
15	303.840	2.096	1.848	2.547	2.314	1.783	1.522	2.606	2.381
16	324.096	1.876	1.683	2.241	2.011	1.483	1.326	2.359	2.151
17	344.352	1.686	1.548	1.971	1.748	1.244	1.144	2.109	1.928
18	364.608	1.524	1.435	1.741	1.527	1.056	0.982	1.860	1.720
19	384.864	1.385	1.340	1.548	1.341	0.906	0.837	1.622	1.530
20	405.120	1.267	1.260		1.187	0.783	0.712	1.410	1.360
21	425.376	1.168	1.191		1.058	0.677	0.603	1.237	1.210
22	445.632	1.086	1.131		0.951	0.583	0.510	1.110	1.080
23	465.888	1.020	1.079		0.865	0.497	0.432	1.028	0.970
24	486.144	0.970			0.797	0.417	0.367	0.984	0.884
25	506.400	0.935			0.745	0.343	0.316	0.964	0.825
26	526.656								0.804
27	546.912								
28	567.168								

Model CG Rise Faired Data – all models at 483 lbs

Test #		2	7	24	27	12	15	18	21
Model #		5628	5628	5629	5629	5630	5630	5631	5631
D =		483	483	483	483	483	483	483	483
LCG		0.38	0.42	0.38	0.42	0.38	0.42	0.38	0.42
Vm	Vm	hCG	hCG	hCG	hCG	hCG	hCG	hCG	hCG
(knots)	in/sec	in	in	in	in	in	in	in	in
0	0								
1	20.256								
2	40.512								
3	60.768	-0.014	-0.131	-0.723	-0.557	-0.299	-0.616	0.152	-0.110
4	81.024	-0.662	-0.641	-0.823	-0.550	-0.552	-0.623	-0.362	-0.627
5	101.28	-0.825	-0.981	-0.920	-0.963	-0.752	-0.791	-0.699	-0.719
6	121.536	-0.582	-0.721	-0.634	-0.436	-0.735	-0.789	-0.648	-0.576
7	141.792	-0.135	-0.248	-0.156	0.006	-0.290	-0.554	-0.210	-0.270
8	162.048	0.450	0.155	0.443	0.507	0.331	-0.128	0.414	0.173
9	182.304	1.159	0.735	1.120	1.099	0.982	0.419	1.080	0.736
10	202.56	1.935	1.397	1.827	1.745	1.656	1.022	1.731	1.391
11	222.816	2.672	2.028	2.510	2.384	2.317	1.627	2.340	2.090
12	243.072	3.275	2.572	3.115	2.963	2.923	2.200	2.892	2.764
13	263.328	3.708	3.015	3.607	3.447	3.444	2.717	3.379	3.348
14	283.584	3.990	3.368	3.974	3.827	3.871	3.166	3.800	3.809
15	303.84	4.166	3.645	4.228	4.113	4.208	3.543	4.156	4.145
16	324.096	4.275	3.864	4.394	4.322	4.466	3.849	4.454	4.380
17	344.352	4.349	4.038	4.501	4.472	4.659	4.090	4.699	4.544
18	364.608	4.406	4.179	4.573	4.579	4.801	4.273	4.899	4.663
19	384.864	4.459	4.294	4.627	4.659	4.903	4.408	5.061	4.758
20	405.12	4.516	4.390	4.677	4.720	4.974	4.505	5.191	4.840
21	425.376	4.580	4.472	4.730	4.771	5.022	4.577	5.295	4.917
22	445.632	4.656		4.790	4.816	5.052	4.632	5.377	4.994
23	465.888	4.745		4.861	4.861	5.069	4.684	5.441	5.072
24	486.144	4.848		4.943	4.907	5.076	4.743	5.490	5.152
25	506.4	4.969		5.036	4.957	5.076	4.820	5.528	5.235
26	526.656			5.140	5.013	5.070	4.923	5.555	5.320
27	546.912			5.254	5.075	5.060	5.063	5.575	5.407
28	567.168			5.378	5.145	5.047	5.248	5.588	5.495

Model CG Rise Faired Data – all models at 375 lbs

Test #		9	6	23	26	11	14	17	20
Model #		5628	5628	5629	5629	5630	5630	5631	5631
D =	(lbf)	375	375	375	375	375	375	375	375
LCG		0.38	0.42	0.38	0.42	0.38	0.42	0.38	0.42
Vm	Vm	hCG	hCG	hCG	hCG	hCG	hCG	hCG	hCG
(knots)	in/sec	in	in	in	in	in	in	in	in
0	0								
1	20.256								
2	40.512								
3	60.768	-0.227	-0.327	-0.268	-0.193	-0.141	-0.403	-0.236	-0.351
4	81.024	-0.608	-0.523	-0.536	-0.644	-0.483	-0.556	-0.564	-0.589
5	101.28	-0.672	-0.701	-0.695	-0.778	-0.689	-0.683	-0.707	-0.698
6	121.536	-0.485	-0.525	-0.601	-0.639	-0.608	-0.716	-0.603	-0.673
7	141.792	-0.122	-0.169	-0.199	-0.313	-0.212	-0.538	-0.251	-0.508
8	162.048	0.347	0.286	0.390	0.127	0.273	-0.066	0.285	-0.208
9	182.304	0.862	0.782	0.994	0.614	0.625	0.544	0.901	0.201
10	202.56	1.380	1.272	1.525	1.097	0.916	0.924	1.466	0.680
11	222.816	1.869	1.727	1.968	1.542	1.344	1.052	1.676	1.183
12	243.072	2.310	2.131	2.339	1.932	1.925	1.385	1.902	1.669
13	263.328	2.691	2.479	2.657	2.266	2.509	1.982	2.548	2.111
14	283.584	3.009	2.772	2.935	2.545	2.979	2.507	2.995	2.494
15	303.84	3.262	3.016	3.177	2.779	3.314	2.851	3.315	2.815
16	324.096	3.453	3.217	3.382	2.976	3.540	3.061	3.557	3.078
17	344.352	3.586	3.382	3.548	3.142	3.688	3.197	3.745	3.290
18	364.608	3.666	3.517	3.673	3.286	3.786	3.295	3.894	3.457
19	384.864	3.696	3.627	3.761	3.412	3.851	3.377	4.014	3.589
20	405.12	3.682	3.717	3.821	3.526	3.897	3.456	4.110	3.691
21	425.376		3.790	3.863	3.630	3.933	3.539	4.188	3.770
22	445.632		3.850	3.900	3.727	3.965	3.630	4.251	3.830
23	465.888		3.899	3.943	3.821	4.001	3.733	4.303	3.876
24	486.144			4.000	3.911	4.049	3.849	4.343	3.910
25	506.4			4.079	4.001	4.122	3.983	4.374	3.935
26	526.656			4.185	4.091	4.252	4.135	4.394	3.952
27	546.912								
28	567.168								

Model CG Rise Faired Data – all models at 298 lbs

Test #		8	5	22	25	10	13	16	19
Model #		5628	5628	5629	5629	5630	5630	5631	5631
D =		298	298	298	298	298	298	298	298
LCG		0.38	0.42	0.38	0.42	0.38	0.42	0.38	0.42
Vm	Vm	hCG	hCG	hCG	hCG	hCG	hCG	hCG	hCG
(knots)	in/sec	in	in	in	in	in	in	in	in
0	0.000								
1	20.256								
2	40.512								
3	60.768	-0.152	-0.113	-0.326	-0.062	-0.164	-0.217	-0.189	-0.284
4	81.024	-0.444	-0.475	-0.428	-0.382	-0.444	-0.502	-0.435	-0.356
5	101.280	-0.599	-0.647	-0.715	-0.642	-0.616	-0.647	-0.702	-0.746
6	121.536	-0.460	-0.553	-0.504	-0.530	-0.484	-0.579	-0.541	-0.583
7	141.792	-0.054	-0.203	-0.102	-0.232	-0.073	-0.299	-0.131	-0.274
8	162.048	0.410	0.193	0.322	0.101	0.195	0.110	0.180	0.079
9	182.304	0.809	0.530	0.727	0.442	0.360	0.536	0.454	0.437
10	202.560	1.182	0.888	1.102	0.779	0.732	0.874	0.785	0.780
11	222.816	1.586	1.275	1.441	1.102	1.249	1.018	1.204	1.099
12	243.072	1.991	1.654	1.746	1.406	1.736	1.192	1.667	1.392
13	263.328	2.330	1.996	2.017	1.689	2.121	1.608	2.090	1.660
14	283.584	2.581	2.289	2.256	1.948	2.409	1.944	2.416	1.903
15	303.840	2.759	2.533	2.467	2.185	2.623	2.188	2.640	2.125
16	324.096	2.890	2.732	2.650	2.398	2.786	2.377	2.790	2.327
17	344.352	2.992	2.892	2.810	2.589	2.914	2.534	2.896	2.512
18	364.608	3.079	3.021	2.947	2.759	3.020	2.668	2.980	2.682
19	384.864	3.158	3.123	3.064	2.909	3.110	2.787	3.056	2.839
20	405.120	3.234	3.205	3.163	3.042	3.189	2.895	3.131	2.984
21	425.376	3.310	3.271	3.246	3.158	3.262	2.995	3.209	3.118
22	445.632	3.389	3.323	3.314	3.259	3.331	3.089	3.294	3.243
23	465.888	3.471	3.364	3.369	3.346	3.397	3.178	3.385	3.359
24	486.144	3.558		3.411	3.422	3.461	3.265	3.485	3.467
25	506.400	3.650		3.443	3.488	3.524	3.349	3.592	3.569
26	526.656								3.664
27	546.912								
28	567.168								

Model Trim Faired Data – all models at 483 lbs

Test #		2	7	24	27	12	15	18	21
Model #		5628	5628	5629	5629	5630	5630	5631	5631
D =		483	483	483	483	483	483	483	483
LCG		0.38	0.42	0.38	0.42	0.38	0.42	0.38	0.42
Vm	Vm	trim	trim	trim	trim	trim	trim	trim	trim
(knots)	in/sec	degrees	degrees	degrees	degrees	degrees	degrees	degrees	degrees
0	0.000								
1	20.256								
2	40.512								
3	60.768	0.327	0.286	0.187	0.110	0.010	-0.529	0.309	0.141
4	81.024	0.593	0.282	0.566	0.566	0.781	0.825	0.833	0.537
5	101.280	2.323	1.838	2.138	1.638	2.168	2.009	2.055	1.937
6	121.536	4.125	3.500	3.978	3.678	3.992	2.865	3.755	3.650
7	141.792	4.209	3.870	4.006	3.827	4.196	3.480	4.130	3.862
8	162.048	4.775	4.138	4.531	4.197	4.365	3.949	4.011	3.718
9	182.304	5.439	4.694	5.011	4.644	4.973	4.336	4.503	4.051
10	202.560	5.700	5.269	5.349	5.048	5.553	4.668	5.179	4.608
11	222.816	5.648	5.617	5.541	5.340	5.899	4.947	5.690	5.161
12	243.072	5.461	5.667	5.590	5.491	5.976	5.167	5.915	5.576
13	263.328	5.214	5.504	5.500	5.502	5.833	5.323	5.869	5.788
14	283.584	4.939	5.265	5.289	5.396	5.550	5.410	5.625	5.793
15	303.840	4.657	5.041	4.986	5.207	5.196	5.429	5.274	5.630
16	324.096	4.384	4.868	4.630	4.968	4.820	5.385	4.884	5.360
17	344.352	4.131	4.745	4.257	4.708	4.452	5.282	4.502	5.039
18	364.608	3.902	4.658	3.892	4.445	4.105	5.132	4.151	4.712
19	384.864	3.697	4.582	3.556	4.193	3.784	4.943	3.839	4.404
20	405.120	3.516	4.468	3.257	3.958	3.490	4.727	3.567	4.130
21	425.376	3.356	3.912	3.002	3.745	3.221	4.496	3.331	3.897
22	445.632	3.213		2.791	3.553	2.973	4.261	3.128	3.703
23	465.888	3.085		2.623	3.382	2.741	4.034	2.951	3.548
24	486.144	2.970		2.496	3.227	2.521	3.828	2.797	3.427
25	506.400	2.865		2.406	3.085	2.307	3.652	2.661	3.335
26	526.656			2.350	2.944	2.091	3.518	2.542	3.271
27	546.912			2.325	2.786	1.865	3.435	2.436	3.228
28	567.168			2.328	2.563		3.413	2.329	3.204

Model Trim Faired Data - all models at 375 lbs

Test #		9	6	23	26	11	14	17	20
Model #		5628	5628	5629	5629	5630	5630	5631	5631
D =	(lbf)	375	375	375	375	375	375	375	375
LCG		0.38	0.42	0.38	0.42	0.38	0.42	0.38	0.42
Vm	Vm	Trim	Trim	Trim	Trim	Trim	Trim	Trim	Trim
(knots)	in/sec	degrees	degrees	degrees	degrees	degrees	degrees	degrees	degrees
0	0								
1	20.256								
2	40.512								
3	60.768	0.444	-0.087	0.230	0.096	0.007	0.069	0.064	0.366
4	81.024	0.475	0.322	0.615	0.370	0.693	0.338	0.723	0.026
5	101.28	2.559	1.705	2.066	1.512	1.958	1.600	1.996	1.848
6	121.536	3.387	2.844	3.125	2.797	3.204	2.881	3.186	2.742
7	141.792	3.529	3.150	3.290	3.132	3.465	2.923	3.450	2.870
8	162.048	3.954	3.504	3.564	3.144	3.476	3.081	3.368	2.988
9	182.304	4.425	3.861	3.932	3.334	3.758	3.510	3.626	3.214
10	202.56	4.741	4.142	4.234	3.662	4.152	3.751	4.190	3.518
11	222.816	4.811	4.322	4.409	4.013	4.513	3.726	4.444	3.846
12	243.072	4.663	4.408	4.461	4.305	4.719	3.924	4.508	4.145
13	263.328	4.400	4.421	4.412	4.498	4.709	4.391	4.727	4.383
14	283.584	4.125	4.381	4.287	4.577	4.529	4.736	4.502	4.543
15	303.84	3.893	4.309	4.107	4.550	4.268	4.837	4.180	4.621
16	324.096	3.715	4.216	3.889	4.438	3.989	4.754	3.912	4.623
17	344.352	3.578	4.113	3.644	4.270	3.725	4.566	3.715	4.562
18	364.608	3.462	4.004	3.382	4.072	3.486	4.327	3.564	4.451
19	384.864	3.350	3.895	3.116	3.871	3.273	4.076	3.439	4.304
20	405.12	3.230	3.785	2.858	3.682	3.083	3.837	3.323	4.133
21	425.376		3.676	2.623	3.517	2.910	3.626	3.204	3.950
22	445.632		3.565	2.422	3.380	2.751	3.453	3.073	3.765
23	465.888		3.447	2.268	3.273	2.599	3.324	2.922	3.584
24	486.144			2.165	3.196	2.449	3.242	2.744	3.415
25	506.4			2.121	3.146	2.296	3.207	2.527	3.262
26	526.656			2.136	3.121	2.137	3.222	2.258	3.126
27	546.912								
28	567.168								

Model Trim Faired Data - all models at 298 lbs

Test #		8	5	22	25	10	13	16	19
Model #		5628	5628	5629	5629	5630	5630	5631	5631
D =		298	298	298	298	298	298	298	298
LCG		0.38	0.42	0.38	0.42	0.38	0.42	0.38	0.42
Vm	Vm	trim	trim	trim	trim	trim	trim	trim	trim
(knots)	in/sec	degrees	degrees	degrees	degrees	degrees	degrees	degrees	degrees
0	0.000								
1	20.256								
2	40.512								
3	60.768	0.316	0.139	0.212	-0.189	0.207	0.208	0.115	0.294
4	81.024	0.590	0.300	0.620	0.648	0.609	0.467	0.642	0.234
5	101.280	2.012	1.594	1.901	1.412	1.785	1.355	1.703	1.511
6	121.536	2.710	2.414	2.585	2.067	2.627	2.319	2.587	2.313
7	141.792	3.036	2.772	2.756	2.503	2.856	2.674	2.793	2.535
8	162.048	3.351	3.059	2.950	2.799	2.950	2.707	2.862	2.708
9	182.304	3.548	3.216	3.165	3.044	2.980	2.746	3.002	2.896
10	202.560	3.659	3.350	3.355	3.250	3.234	2.847	3.211	3.083
11	222.816	3.762	3.490	3.492	3.411	3.584	3.032	3.447	3.256
12	243.072	3.838	3.609	3.563	3.523	3.814	3.538	3.642	3.406
13	263.328	3.829	3.689	3.563	3.587	3.863	3.964	3.726	3.530
14	283.584	3.725	3.726	3.499	3.606	3.774	3.958	3.677	3.627
15	303.840	3.559	3.725	3.381	3.585	3.606	3.860	3.532	3.697
16	324.096	3.370	3.692	3.223	3.534	3.407	3.771	3.341	3.742
17	344.352	3.183	3.637	3.041	3.461	3.205	3.696	3.146	3.763
18	364.608	3.013	3.566	2.853	3.375	3.017	3.627	2.966	3.760
19	384.864	2.868	3.487	2.672	3.284	2.847	3.558	2.809	3.735
20	405.120	2.749	3.401	2.507	3.196	2.696	3.486	2.675	3.687
21	425.376	2.656	3.314	2.365	3.116	2.562	3.408	2.558	3.617
22	445.632	2.589	3.227	2.248	3.048	2.439	3.322	2.451	3.526
23	465.888	2.547	3.141	2.155	2.994	2.324	3.226	2.347	3.413
24	486.144	2.527		2.086	2.955	2.208	3.118	2.236	3.278
25	506.400	2.529		2.035	2.929	2.085	2.997	2.103	3.121
26	526.656								2.939
27	546.912								
28	567.168								

Model Wetted Surface Faired Data - all models at 483 lbs

Test #		2	7	24	27	12	15	18	21
Model #		5628	5628	5629	5629	5630	5630	5631	5631
D =		483	483	483	483	483	483	483	483
LCG		0.38	0.42	0.38	0.42	0.38	0.42	0.38	0.42
Vm	Vm	S	S	S	S	S	S	S	S
(knots)	in/sec	(sq in)	(sq in)	(sq in)	(sq in)	(sq in)	(sq in)	(sq in)	(sq in)
0	0.00								
1	20.26								
2	40.51								
3	60.77	4118.55	4057.01	3742.18	3725.43	3625.52	3790.57	3566.12	3322.98
4	81.02	3964.71	4116.60	3852.69	3810.58	3708.82	3877.48	3513.03	3452.90
5	101.28	3812.07	4172.91	3819.47	3847.87	3789.24	3926.73	3453.17	3516.35
6	121.54	4065.81	4216.41	3539.40	3687.58	3851.52	3918.83	3391.04	3504.60
7	141.79	4248.47	4231.66	3397.23	3553.09	3870.07	3873.33	3330.61	3450.22
8	162.05	4178.52	4198.38	3394.63	3499.55	3812.67	3827.26	3274.10	3381.08
9	182.30	3937.52	4098.85	3448.09	3497.42	3658.13	3805.05	3218.35	3311.93
10	202.56	3641.98	3931.86	3405.18	3480.10	3421.05	3811.91	3142.85	3246.10
11	222.82	3365.54	3721.92	3036.96	3306.74	3153.55	3822.94	2983.57	3168.57
12	243.07	3138.36	3509.38	2656.38	2978.36	2911.98	3727.70	2672.38	3011.05
13	263.33	2964.88	3327.82	2495.45	2725.57	2726.07	3360.01	2364.09	2669.78
14	283.58	2838.72	3191.38	2437.18	2596.74	2597.90	2955.43	2229.25	2386.26
15	303.84	2751.00	3098.16	2408.52	2532.30	2516.17	2792.50	2194.83	2333.96
16	324.10	2693.71	3039.20	2386.41	2494.24	2467.45	2766.33	2185.67	2344.71
17	344.35	2660.19	3004.77	2364.02	2466.81	2440.74	2778.30	2178.13	2351.52
18	364.61	2644.43	2986.94	2339.12	2443.88	2428.21	2795.96	2167.74	2347.77
19	384.86	2640.32	2979.95	2311.41	2423.00	2424.64	2811.15	2154.71	2336.46
20	405.12	2641.04	2979.85	2289.04	2403.19	2426.63	2822.46	2139.98	2320.57
21	425.38	2639.11	2984.06	2286.36	2384.03	2431.98	2830.22	2124.42	2302.12
22	445.63	2626.71		2275.56	2365.35	2439.31	2835.03	2108.65	2282.36
23	465.89	2596.52		2253.79	2347.08	2447.72	2837.52	2093.08	2262.08
24	486.14	2542.77		2229.28	2329.20	2456.63	2838.16	2077.96	2241.77
25	506.40	2462.44		2204.41	2311.70	2465.70	2837.33	2063.44	2221.71
26	526.66			2179.71	2294.58	2474.69	2835.33	2049.62	2202.09
27	546.91			2155.31	2277.83	2483.46	2832.40	2036.53	2183.02
28	567.17			2131.27	2261.46	2491.93	2828.69	2024.18	2164.56

Model Wetted Surface Faired Data - all models at 375 lbs

Test #		9	6	23	26	11	14	17	20
Model #		5628	5628	5629	5629	5630	5630	5631	5631
D =	(lbf)	375	375	375	375	375	375	375	375
LCG		0.38	0.42	0.38	0.42	0.38	0.42	0.38	0.42
Vm	Vm	S	S	S	S	S	S	S	S
(knots)	in/sec	(sq in)	(sq in)	(sq in)	(sq in)	(sq in)	(sq in)	(sq in)	(sq in)
0	0.00								
1	20.26								
2	40.51								
3	60.77	3566.14	3794.44	3447.40	3361.83	3568.54	3663.19	2977.17	3131.30
4	81.02	3556.67	3775.79	3481.18	3192.50	3613.61	3769.80	3198.67	3123.31
5	101.28	3617.18	3857.98	3526.09	3644.17	3644.47	3796.78	3149.57	3333.04
6	121.54	3752.67	3995.74	3495.62	3542.12	3653.61	3747.55	2982.31	3328.94
7	141.79	3807.28	4065.24	3397.58	3458.51	3631.76	3664.19	2909.92	3212.80
8	162.05	3645.67	4000.30	3266.62	3403.01	3570.44	3591.20	2858.12	3162.44
9	182.30	3430.12	3854.76	3127.22	3363.05	3466.32	3559.13	2801.90	3146.00
10	202.56	3259.77	3694.79	2991.95	3329.57	3325.32	3585.15	2736.94	3131.22
11	222.82	3133.14	3549.56	2866.48	3280.28	3163.10	3622.33	2665.46	3071.67
12	243.07	3034.80	3425.23	2753.09	3152.98	3000.00	3455.64	2591.10	2924.59
13	263.33	2954.19	3320.02	2652.45	2917.96	2853.61	3172.71	2516.99	2731.05
14	283.58	2885.24	3230.55	2564.45	2750.53	2733.94	3013.94	2445.33	2581.99
15	303.84	2824.38	3153.64	2488.62	2701.79	2643.31	2940.26	2377.39	2499.70
16	324.10	2769.49	3086.77	2424.27	2692.96	2579.00	2901.32	2313.80	2460.24
17	344.35	2719.22	3027.99	2370.60	2689.05	2536.18	2877.06	2254.75	2441.76
18	364.61	2672.65	2975.80	2326.70	2682.82	2509.76	2859.87	2200.15	2432.63
19	384.86	2629.17	2929.07	2291.62	2673.98	2495.34	2846.56	2149.79	2427.48
20	405.12	2588.32	2886.91	2264.37	2663.53	2489.43	2835.63	2103.35	2423.95
21	425.38		2848.63	2243.93	2652.46	2489.44	2826.30		2420.96
22	445.63		2813.65	2229.31	2641.56	2493.45	2818.10		2418.08
23	465.89		2781.55	2219.50	2631.50	2500.12	2810.75		2415.12
24	486.14			2213.57	2622.81	2508.50	2804.06		2412.03
25	506.40			2210.63	2615.99	2517.92	2797.90		2408.80
26	526.66			2209.87	2611.51	2527.91	2792.17		2405.44
27	546.91								
28	567.17								

Model Wetted Surface Faired Data - all models at 298 lbs

Test #		8	5	22	25	10	13	16	19
Model #		5628	5628	5629	5629	5630	5630	5631	5631
D =		298	298	298	298	298	298	298	298
LCG		0.38	0.42	0.38	0.42	0.38	0.42	0.38	0.42
Vm	Vm	S	S	S	S	S	S	S	S
(knots)	in/sec	(sq in)	(sq in)	(sq in)	(sq in)	(sq in)	(sq in)	(sq in)	(sq in)
0	0.00								
1	20.26								
2	40.51								
3	60.77	3454.13	4370.43	3026.50	3240.00	3410.45	3575.32	2834.30	3257.34
4	81.02	3441.24	3926.30	2968.35	3423.31	3338.67	3666.46	2791.48	3234.68
5	101.28	3644.08	3333.48	2900.06	3558.39	3318.18	3658.28	2791.49	3235.28
6	121.54	3763.91	3309.58	3199.37	3418.49	3403.13	3589.80	2815.73	3208.21
7	141.79	3724.28	3432.13	3242.37	3269.00	3441.37	3508.14	2844.53	3065.69
8	162.05	3605.23	3538.74	3062.22	3193.46	3400.23	3444.15	2860.52	3037.86
9	182.30	3459.67	3590.57	3002.02	3164.20	3309.68	3413.41	2851.30	3015.95
10	202.56	3313.84	3583.65	2956.13	3161.19	3198.44	3415.34	2811.09	2975.39
11	222.82	3179.04	3530.16	2873.96	3159.06	3084.52	3412.28	2741.00	2908.88
12	243.07	3058.96	3447.34	2731.32	3077.00	2977.54	3342.20	2648.12	2818.46
13	263.33	2953.70	3350.31	2584.32	2859.13	2881.88	3221.19	2543.58	2719.22
14	283.58	2861.96	3249.52	2484.34	2712.19	2798.95	3110.86	2439.93	2630.65
15	303.84	2781.99	3151.13	2423.19	2675.05	2728.55	3030.26	2348.56	2563.44
16	324.10	2712.04	3058.25	2381.48	2671.91	2669.78	2973.40	2277.43	2517.19
17	344.35	2650.56	2972.14	2348.26	2673.87	2621.45	2932.16	2229.74	2486.46
18	364.61	2596.23	2893.03	2318.73	2674.45	2582.34	2901.04	2203.62	2465.65
19	384.86	2547.94	2820.63	2290.90	2672.75	2551.31	2876.67	2193.05	2450.73
20	405.12	2504.76	2754.43		2669.03	2527.34	2857.01	2189.61	2439.15
21	425.38	2465.94	2693.82		2663.74	2509.54	2840.76	2184.88	2429.41
22	445.63	2430.87	2638.22		2657.26	2497.16	2827.05	2172.91	2420.65
23	465.89	2399.01	2587.08		2649.87	2489.55	2815.32	2152.23	2412.38
24	486.14	2369.95			2641.80	2486.17	2805.14	2127.04	2404.34
25	506.40	2343.32			2633.22	2486.58	2796.22	2107.19	2396.40
26	526.66								2388.48
27	546.91								
28	567.17								

Wetted Keel Length Faired Data - all models at 483 lbs

Test #		2	7	24	27	12	15	18	21
Model #		5628	5628	5629	5629	5630	5630	5631	5631
D =		483	483	483	483	483	483	483	483
LCG		0.38	0.42	0.38	0.42	0.38	0.42	0.38	0.42
Vm	Vm	keel	keel	keel	keel	keel	keel	keel	keel
(knots)	in/sec	in	in	in	in	in	in	in	in
0	0								
1	20.256								
2	40.512								
3	60.768	120.000	120.000	120.000	120.000	120.000	120.000	120.000	120.000
4	81.024	120.000	120.000	120.000	120.000	120.000	120.000	120.000	120.000
5	101.28	117.820	120.000	118.920	120.000	119.929	120.000	118.645	120.000
6	121.536	115.360	119.634	114.648	118.649	116.088	120.000	116.426	118.710
7	141.792	113.144	117.607	112.065	116.613	115.364	119.574	114.301	117.079
8	162.048	113.148	115.088	112.288	114.653	113.622	118.421	112.397	115.671
9	182.304	107.373	112.132	110.794	112.482	109.219	117.345	110.206	114.810
10	202.56	99.499	108.874	105.125	109.615	103.069	116.563	105.563	113.577
11	222.816	95.236	105.591	98.149	105.809	96.730	115.503	98.754	108.025
12	243.072	92.372	102.742	93.095	101.625	91.371	107.795	94.025	102.577
13	263.328	90.401	100.766	90.408	98.126	87.524	101.758	91.377	99.345
14	283.584	89.069	99.729	89.280	95.886	85.198	102.028	89.678	97.345
15	303.84	88.178	99.280	88.986	94.747	84.091	102.147	88.444	96.182
16	324.096	87.569	98.996	89.119	94.295	83.785	101.877	87.505	95.654
17	344.352	87.131	98.623	89.506	94.190	83.877	101.406	86.786	95.565
18	364.608	86.788	98.080	90.114	94.229	84.061	100.838	86.246	95.723
19	384.864	86.495	97.375	90.939	94.308	84.157	100.226	85.853	95.978
20	405.12	86.223	96.545	91.735	94.378	84.105	99.597	85.582	96.229
21	425.376	85.955	95.628	91.996	94.420	83.951	98.965	85.410	96.420
22	445.632	85.683		91.715	94.426	83.805	98.339	85.320	96.525
23	465.888	85.403		91.290	94.397	83.811	97.722	85.296	96.538
24	486.144	85.111		90.917	94.337	84.105	97.118	85.325	96.462
25	506.4	84.810		90.613	94.247	84.781	96.527	85.396	96.307
26	526.656			90.357	94.134	85.861	95.951	85.500	96.083
27	546.912			90.129	93.999	87.269	95.388	85.630	95.800
28	567.168			89.913	93.847		94.839	85.779	95.467

Wetted Keel Length Faired Data - all models at 375 lbs

Test #		9	6	23	26	11	14	17	20
Model #		5628	5628	5629	5629	5630	5630	5631	5631
D =	(lbf)	375	375	375	375	375	375	375	375
LCG		0.38	0.42	0.38	0.42	0.38	0.42	0.38	0.42
Vm	Vm	wetkeel	wetkeel	wetkeel	wetkeel	wetkeel	wetkeel	wetkeel	wetkeel
(knots)	in/sec	in	in	in	in	in	in	in	in
0	0								
1	20.256								
2	40.512								
3	60.768	118.622	120.000	120.000	120.000	120.000	120.000	120.000	120.000
4	81.024	119.139	120.000	119.747	120.000	119.358	120.000	120.000	120.000
5	101.28	116.895	119.385	118.096	120.000	117.734	120.000	118.353	120.000
6	121.536	113.625	118.212	116.724	119.532	116.302	119.945	115.584	119.866
7	141.792	110.775	116.588	115.203	118.157	114.589	118.431	113.457	118.397
8	162.048	108.400	114.571	113.113	116.690	112.313	117.353	112.015	116.964
9	182.304	105.592	112.279	110.127	115.112	109.359	115.906	110.397	116.086
10	202.56	101.797	109.822	106.253	113.407	105.764	113.953	107.237	116.071
11	222.816	97.573	107.351	102.028	111.566	101.736	111.658	102.585	113.414
12	243.072	94.173	105.100	98.280	109.612	97.676	109.301	98.483	110.064
13	263.328	92.431	103.333	95.566	107.628	94.094	107.134	95.990	107.665
14	283.584	92.008	102.163	93.939	105.807	91.419	105.311	94.733	105.863
15	303.84	91.795	101.459	93.148	104.453	89.818	103.878	94.156	104.468
16	324.096	91.206	100.989	92.892	103.864	89.172	102.808	93.919	103.401
17	344.352	90.976	100.575	92.942	104.087	89.201	102.042	93.852	102.613
18	364.608	91.854	100.135	93.149	104.820	89.606	101.517	93.870	102.061
19	384.864	91.911	99.649	93.427	105.629	90.156	101.172	93.931	101.707
20	405.12	90.062	99.122	93.729	106.213	90.703	100.961	94.013	101.513
21	425.376		98.569	94.029	106.468	91.168	100.845	94.105	101.447
22	445.632		98.002	94.314	106.411	91.517	100.798	94.201	101.482
23	465.888		97.431	94.579	106.104	91.739	100.800	94.297	101.592
24	486.144			94.823	105.609	91.841	100.835	94.392	101.758
25	506.4			95.046	104.976	91.832	100.892	94.484	101.966
26	526.656			95.248	104.245	91.727	100.965	94.573	102.201
27	546.912								
28	567.168								

Wetted Keel Length Faired Data - all models at 298 lbs

Test #		8	5	22	25	10	13	16	19
Model #		5628	5628	5629	5629	5630	5630	5631	5631
D =		298	298	298	298	298	298	298	298
LCG		0.38	0.42	0.38	0.42	0.38	0.42	0.38	0.42
Vm	Vm	wetkeel	wetkeel	wetkeel	wetkeel	wetkeel	wetkeel	wetkeel	wetkeel
(knots)	in/sec	in	in	in	in	in	in	in	in
0	0.000								
1	20.256								
2	40.512								
3	60.768	118.958	119.828	120.000	117.991	119.799	120.000	119.961	120.000
4	81.024	117.810	120.000	119.165	118.407	119.600	120.000	119.677	120.000
5	101.280	116.560	119.370	117.438	120.000	116.911	120.000	118.048	120.000
6	121.536	115.170	117.553	115.275	119.438	115.077	119.741	115.092	118.373
7	141.792	113.568	115.441	113.308	117.075	113.732	118.055	112.962	117.658
8	162.048	111.587	113.322	111.640	115.662	112.199	116.694	111.890	117.143
9	182.304	108.401	111.325	109.742	114.771	110.136	116.062	110.886	116.063
10	202.560	102.927	109.498	107.707	114.088	107.536	116.233	109.116	114.323
11	222.816	100.746	107.849	105.634	113.332	104.593	114.274	106.203	112.190
12	243.072	99.052	106.369	103.619	112.084	101.583	111.266	102.754	110.002
13	263.328	97.606	105.042	101.761	109.884	98.773	109.157	100.001	108.024
14	283.584	96.318	103.851	100.161	107.042	96.371	107.615	98.481	106.402
15	303.840	95.141	102.780	98.900	104.902	94.502	106.379	97.891	105.168
16	324.096	94.050	101.814	98.005	104.001	93.201	105.345	97.778	104.272
17	344.352	93.026	100.939	97.413	103.831	92.420	104.468	97.854	103.620
18	364.608	92.058	100.145	96.932	103.912	92.054	103.726	97.979	103.101
19	384.864	91.137	99.420	96.216	104.037	91.959	103.110	98.093	102.619
20	405.120	90.256	98.758		104.138	91.982	102.614	98.176	102.110
21	425.376	89.410	98.151		104.202	91.992	102.236	98.223	101.556
22	445.632	88.595	97.591		104.230	91.913	101.975	98.237	100.995
23	465.888	87.807	97.075		104.230	91.748	101.833	98.221	100.524
24	486.144	87.043			104.207	91.617	101.811	98.180	100.301
25	506.400	86.302			104.167	91.782	101.914	98.118	100.544
26	526.656								101.530
27	546.912								
28	567.168								

Table B1. Static Model Conditions

Model	Δ [Lbs]	Δ [in^3]	LCG [in]	T_{AP} [in]	T_{FP} [in]	Trim [in]	Trim [deg]	WpArea [in^2]	S [in^2]
5628	298	8252.3	45.60	5.41	5.71	-0.30	-0.145	2950.4	3228.4
	375	10384.6	45.60	6.00	6.56	-0.56	-0.265	3211.0	3558.2
	483	13375.4	45.60	7.00	7.31	-0.31	-0.149	3391.3	3866.7
	560	15507.7	45.60	7.75	7.75	0.00	0.000	3475.0	4052.0
	680	18830.8	45.60	9.00	8.24	0.76	0.361	3564.6	4304.9
	298	8252.3	50.40	4.75	6.74	-1.99	-0.951	2948.4	3250.7
	375	10384.6	50.40	5.35	7.55	-2.20	-1.052	3279.6	3632.4
	483	13375.4	50.40	6.00	8.77	-2.77	-1.321	3497.2	3978.5
5629	298	8252.3	45.60	5.59	5.56	0.04	0.017	2699.6	3021.9
	375	10384.6	45.60	6.40	6.27	0.13	0.060	2820.4	3295.8
	483	13375.4	45.60	7.65	7.30	0.35	0.167	2924.2	3583.3
	298	8252.3	50.40	4.91	6.58	-1.67	-0.798	2777.1	3131.4
	375	10384.6	50.40	6.03	6.81	-0.78	-0.373	2855.3	3334.3
	483	13375.4	50.40	7.03	7.88	-0.85	-0.407	2969.3	3637.5
5630	298	8252.3	45.60	5.75	5.52	0.23	0.111	2515.2	2934.9
	375	10384.6	45.60	6.90	5.89	1.01	0.483	2589.5	3152.8
	483	13375.4	45.60	8.25	6.70	1.55	0.742	2682.3	3455.1
	298	8252.3	50.40	5.00	6.59	-1.59	-0.758	2583.9	3009.5
	375	10384.6	50.40	5.75	7.49	-1.74	-0.830	2674.4	3252.5
	483	13375.4	50.40	7.00	8.41	-1.41	-0.673	2764.1	3556.0
5631	298	8252.3	45.60	6.44	5.48	0.96	0.458	2438.8	2870.2
	375	10384.6	45.60	7.50	6.01	1.49	0.711	2536.6	3108.4
	483	13375.4	45.60	8.75	7.01	1.74	0.833	2644.8	3426.8
	298	8252.3	50.40	5.52	6.83	-1.31	-0.627	2526.0	3964.1
	375	10384.6	50.40	6.21	7.86	-1.65	-0.787	2633.6	3221.9
	483	13375.4	50.40	8.00	8.07	-0.07	-0.033	2691.9	3486.4

APPENDIX C: DEFINITION OF THE VISCOUS FRICTION FORCE AND THE DYNAMIC WETTED SURFACE AREA

Dynamic wetted surface area in the context of this analysis refers to the entire wetted surface area of the hull for each individual speed, displacement, and LCG location. It includes the whisker spray area and the pressure area, defined by Savitsky (2006), and includes the reattached spray area above the chine. The reattached spray area is only present at low to medium speeds when the viscous effect of the fluid flowing over the chine is greater than the inertial forces of the fluid. This area disappears at higher speeds when the fluid flowing over the chine has enough inertia to shed the fluid away from the hull form over the entire wetted length of the chine. The dynamic wetted surface area and the varying size of the reattached spray area is illustrated in Figure C-1.

The dynamic wetted surface area computed herein was chosen and performed to adhere with the time and budget constraints of the present experiment. The methodology involved visually documenting the wave profiles on the hulls to define the intersection between the wetted and non-wetted surfaces. Subsequently, using electronic three dimensional representations of the hull surfaces the area below the visually obtained wave profile was calculated revealing the total dynamic wetted surface area.

During the experiment great care was taken to identify the wave profiles. They were defined by the; wetted keel length (A-T) and chine lengths (B-T), the reattachment point (C) and the reattachment spray area height (D) on the transom corner. These locations are presented in Figure C-1. The four locations were determined visually and documented with close-up video. Visual inspection was made by the investigators for each test run from a plank positioned just above the water along the port side of the model, Figure C-2. Every run was videotaped from the starboard side. The measurements were quantified within 0.25 inches by using the grid markings on the hull. The wetted surface area bound by these locations was calculated using a computer code created at NSWCCD to return the areas of 3D electronic hullforms split by known wave profiles. The code utilizes three-dimensional triangular meshes representative of the model hullform and electronic wave profiles. For this particular test the effective area of a single triangular panel is equivalent to 0.09 in^2 of the model surface. The example is shown in Figure C-3.

The area is bound by the keel, chine, transom, and straight lines between the keel and chine intersections (A-B) and the reattachment point and transom height (C–D). Inspection of the forward edge of the spray sheet supports the common practice of a straight line assumption.

The coefficient of friction presented herein is calculated using the 1957 ITTC friction correlation line and the Reynolds number using the length of the wetted keel as the characteristic length. The viscous force is assumed to be acting in the horizontal plane over the entire wetted area as is the normally, undocumented, approach.

Savitsky (2006) introduces a concept of decomposing the horizontal component of the friction force from the flow velocity on the hull surface of a prismatic planing craft. Certainly in the region of the spray root one can find significant effects although, in general, velocity distributions also exist on other types of craft that have a significant flow velocity variation over the wetted hull surface. However, for all practical purposes, the current method for model tests is established and new correlation allowances would have to be developed for the new methodology presented by Savitsky.

We highly recommend and welcome future efforts to define the actual velocity distribution over the wetted hull surface to more accurately calculate the horizontal component of viscous friction drag. With today's Laser Doppler Velocimetry techniques the definition of the velocity distribution is potentially a practical matter.

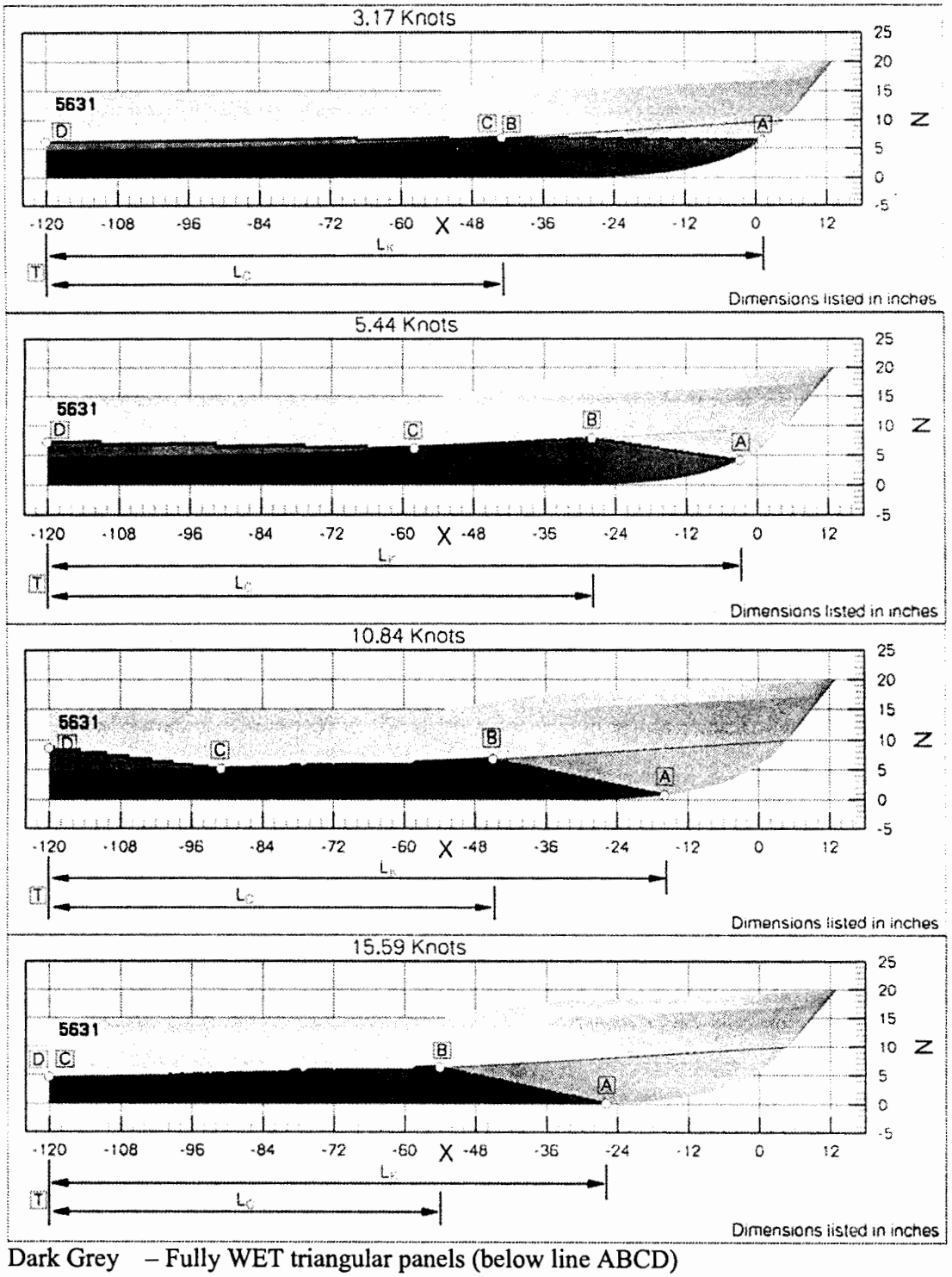

Dark Grey – Fully WET triangular panels (below line ABCD)
Black – Triangular panels split by wave profile (along line ABCD)
Light Grey – Fully DRY triangular panels (above line ABCD)

Figure C-1. Illustration of the Dynamic Wetted Surface Area as a Function of Speed.

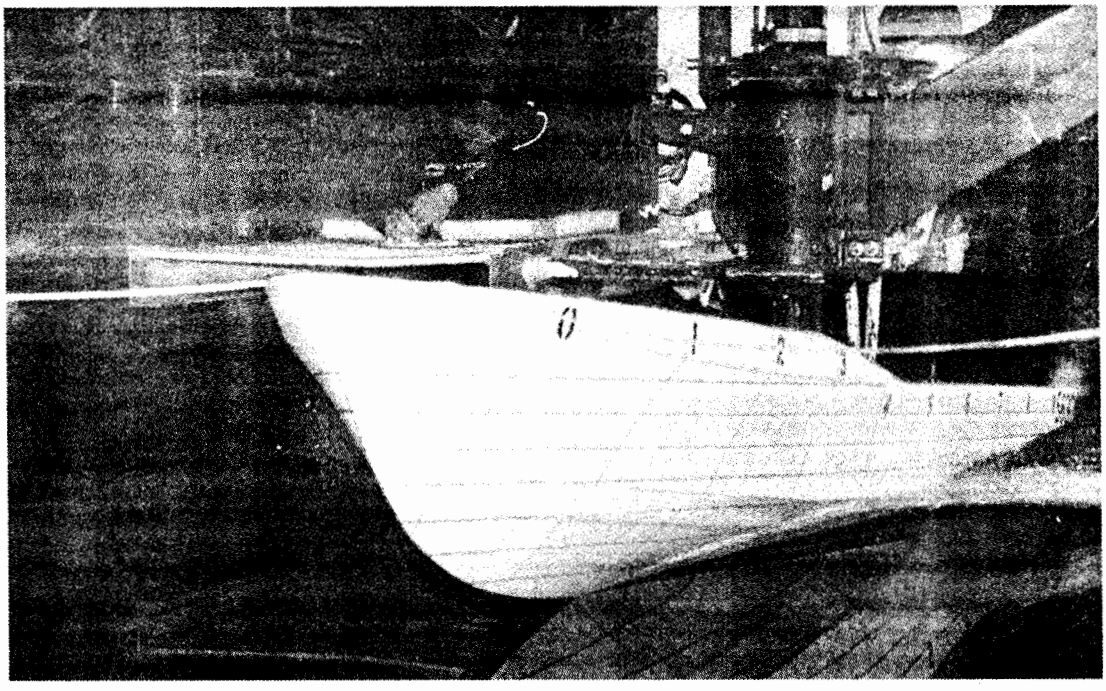

Figure C-2. Visual inspection of the wave profile on model 5630

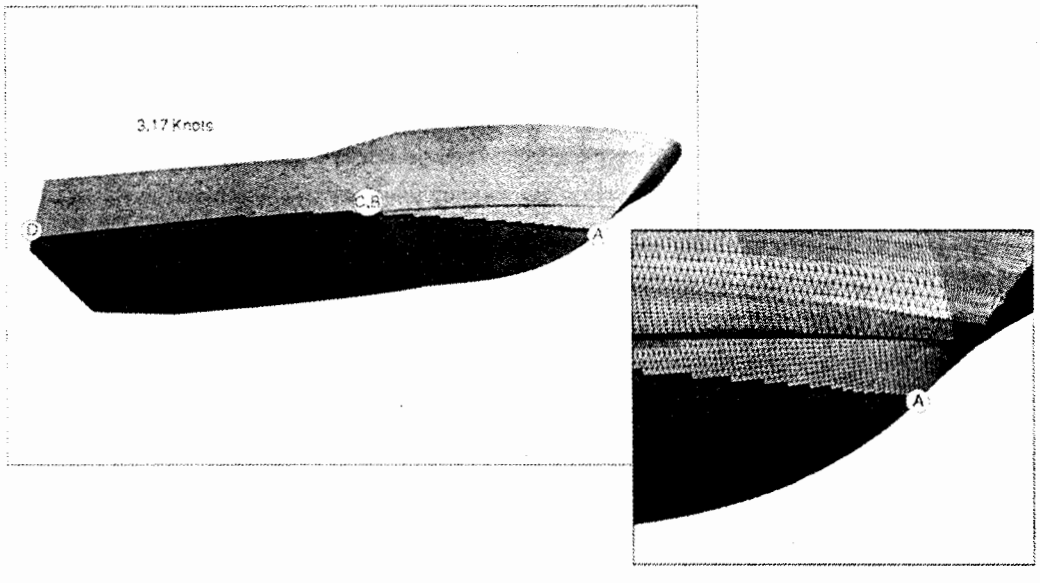

Figure C-3. Discretized Three-Dimensional Mesh utilized to Calculate Dynamic Wetted Area.

APPENDIX D: EXPANSION TO FULL SCALE METHOD AND EXAMPLE

The principal of testing models to predict full scale performance is that the total resistance can be broken into two parts, the residuary resistance that is related to shape and waves and the frictional resistance that is related to wetted surface. The assumption is that the residuary resistance coefficient is the same for the model as for the full scale boat or ship. The following takes the reader through the expansion to full scale of a planing boat.

This calculation is performed using model test data that includes the following information:

- Model total resistance per run, unit force(lbs), R_m
- Model wetted keel length per run, unit length(inches), Lk
- Model running wetted surface per run, unit area(in^2), S
- Model speed per run, length per second, V_m
- Model weight per condition, pounds
- Test water temperature and viscosity

- All measured data is placed in non-dimensional formats as follows, $C = R_m/½\rho V_m^2 S$

Then, solving the following equation gives the components of the resistance of the model.
CTm = CFm + CR ; where CFm is from the ITTC Friction Line.
CRship = CRmodel.

From the model test…

1. Calculate the wetted area to be used, S
2. Calculate the Reynolds Number of the model based on the wetted keel length to be used for the frictional portion of the total resistance. RN = VLk/ν
3. Calculate Frictional Resistance Coefficient, $CF= 0.075/(\log RN-2)^2$
4. Calculate the CTm, Total Resistance Coefficient, model $CTm = R_m/½\rho V_m^2 S$
5. Solve governing equation for CR. CR = CTm – CFm
6. Calculate CFs which is governed by the same equation used for the model calculation, substituting the full scale ship value for RN. The wetted keel length is scaled from the model observations linearly(Lship = Lmodel X scale ratio(λ))
7. Then calculate the ship resistance, CTs = CR + CFs + CA. The correlation allowance, CA,is assumed to be zero for the work reported herein.
8. There is one other calculation to be made to complete this translation and that is to properly scale the speed from the model to full scale. For planing boats this is done using the volume Froude number defined as; $F_\nabla = V/\sqrt{g\nabla^{1/3}}$
   The volume Froude numbers remain equal and the corresponding speeds are calculated, knowing g and ∇, the displaced volume.

   $F_{\nabla s} = F_{\nabla m}$

   $V_s = F_\nabla \sqrt{g\nabla^{1/3}}$

Discussion

Donald L. Blount, Member

It is a great pleasure to see experimental data for high-speed hard-chine hulls published in a format readily useable by naval architects. I send to the authors my congratulations and many thanks for this paper and trust that they have learned much about the trends of calm water resistance and trim from the variables studied. I do believe, however, that as USCG requirements become fixed, a wider range for loading values may be desired as an extension of test variables.

Upon reading this paper, two thoughts came to mind. The first is a request to the authors to provide some comments about seakeeping qualities of the parent hull and anticipated seakeeping qualities of new hulls developed that make up this four-model series. Were seakeeping comparisons (such as vertical accelerations, pitch and heave) made with several vessels of similar size and speed which influenced the selection of the 47-foot MLB as the parent hull form? May we expect seakeeping test results for this series of hulls to be available in the future?

The second area I wish to explore is in regard to the main theme of the calm water experimental data reported:

• Data were not reported for all tests at high speeds, for example, Model 5628/Test 7 and Model 5631/Test 17. Was there a technical reason for not towing models at these high speeds, i.e., porpoising, loll, bow dropping, etc.?

• Were test protocols from previous systematic series programs of hard chine hull forms reviewed when organizing this program?

• It would be most helpful for some added dimensions which are often reported for hard chine model particulars be added to Table 1 or A1. The following are requested: projected length of chine, L_P; A_P and centroid of A_P forward of transom; projected maximum chine beam, B_{PX}; and projected chine beam at the transom, B_{PT}.

• Do the authors have any comments with regard to the indications of saddle point/slope reverse seen in the speed-trim curves between volume Froude numbers 1 and 2 in Figures 11 and 13?

Finally, I offer the following to show an example of benefits of studying trends when systematic series data are available. These four figures show calm water resistance to displacement ratio for several volume Froude numbers as a comparison of hard chine hull results from Series 62 with the systematic series data reported in this paper.

These data represent hulls operating in calm, deep salt water at a displacement of 100,000 pounds for a correlation allowance of zero. The geometric and loading variables are slenderness and length-beam ratios. For constant volume Froude numbers (F_V) the following trends are indicated. Solid symbols in the figures are USCG series data; open symbols are for Series 62 with 12.5 degrees of deadrise. To highlight trends, lines connect data points for the parent hulls.

F_V	Hydrodynamics	Comments
1.5	Semi-displacement	R/W is essentially only a function of slenderness ratio. Low R/W is indicated for high values of slenderness ratio.
2.5	Semi-planing	Both L/B and slenderness ratio influence R/W. Low R/W is indicated for high values of L/B and slenderness ratios.
3.5	Planing	R/W is almost independent of L/B and slenderness ratio.
4.5	High Planing	Both L/B and slenderness ratio influences R/W. Low R/W is indicated for low values of both L/B and slenderness ratios.

This example of systematic series data analysis for hulls with dynamic lift shows changes of trends over a range of speeds.

Again, the authors' data will be an invaluable addition to resources in open literature. Many thanks.

Daniel Savitsky, Member

It has been many years since model tests have been conducted of a systematic series of planing hulls. The high-speed boat community is fortunate that the U. S. Coast Guard has developed and model tested a new hull series and above all that these data are now being made available to the naval architect. The authors are to be commended for having presented the raw model data for each test run. This is always a convenience to researchers who may be interested in conducting additional analysis of the test results.

I will confine my discussion of this paper to the authors' section on "Analysis and Expansion to Notional 80 Foot Patrol Boat"-- particularly to their comparisons of predicted full-scale total resistance and trim with their computed results using the methods of Savitsky (1964) and Blount et al. (1976) as listed at the end of this discussion.

Total Resistance

Unfortunately the authors' method of expansion of model resistance to full-scale is different from the expansion methods that have been used previously and that are imbedded in the resistance prediction methods of Savitsky (1964) and Blount et al. (1976). Specifically, the authors use the wetted keel length to calculate the bottom Reynolds number in contrast to the usual method of using the mean wetted length (average of wetted keel and chine lengths). In addition, the authors use the total wetted bottom area (wetted pressure area, side wetting, and whisker spray area) to calculate the viscous resistance in contrast to using only the wetted pressure area as defined in Savitsky (1964) and Blount et al. (1976).

Also when using the predictive method of Savitsky (1964) and Blount et al. (1976), the authors use the deadrise angle at the transom rather than the recommended deadrise angle at the LCG. Hence, the author's comparison of full-scale resistance extrapolated from model data with computed estimates of the resistance may not be suitable. To avoid any controversy concerning expansion techniques, the present discusser estimated the total model resistance for model 5631 and compared this with the measured model test data.

The calculation procedure used is described in a recent paper (Savitsky, 2006) presented to the NY Metropolitan Section of SNAME in March, 2006. This most recent method calculates separately the total drag in the pressure area (Rh); the aerodynamic drag of the hull model above the water line (Rair); and finally a newly quantified resistance component, which is referred to as "whisker-spray drag" (Rspray). Each of these resistance components has been calculated and is tabulated below, as a function of volume Froude number (Fvol) for the following U. S. Coast Guard test model:

Model 5631
_ = Displacement -- 298 lbs.
LCG -- 38% LBP forward of transom
Beam -- 2.24 ft.
Deadrise at LCG -- 23 deg.
Roughness allowance -- 0.00

The calculated resistance displacement ratio for each component of resistance and their total sum is tabulated below:

Vk	F_{vol}	Rh/□	Rair/□	Rspray/□	Rtotal/_
11kts	2.5	.141	.0025	.003	.146
12	2.8	.148	.0030	.004	.152
14	3.2	.161	.0040	.005	.170
16	3.7	.171	.0050	.007	.183
18	4.1	.185	.0070	.012	.204

The values of Rtotal/_ are compared with the model test data in Figure 1. There is good agreement between both sets of results thus verifying the computational method described in Savitsky (2006).

It is to be appreciated that computational methods are used to estimate the resistance of a given hull. These results are not to be compared with experimental results to judge the performance of a given hull configuration (such as the authors have done). Rather, such a comparison serves to evaluate the accuracy of the computational method.

Equilibrium Trim Angle

In Figure 13 the authors compare trim angle predictions with experimentally measured trim angle and conclude that the computed trim angles are approximately 1 degree larger than those measured. Unfortunately, their comparison is based on two different definitions of trim angle so that their conclusion is incorrect. The following discussion explains this difference.

Model Trim Angle

Although they do not specifically define the reference for the measured trim angle, it appears to be the angle of the keel relative to the level water surface.

Calculated Trim Angle

The analytical methods of Savitsky (1964), Blount et al. (1976), and Savitsky (2006) are based on prismatic hull geometries where all longitudinal buttock lines are parallel to each other and, of course, are also parallel to the keel. The calculated trim angle is referred to as the "hydrodynamic" trim angle and is measured relative to the level water surface. For a realistic warped hull (deadrise increasing forward of the transom), the buttock lines are at a positive angle relative to the keel and the "hydrodynamic" trim angle of the bottom surface must thus be larger than the angle of the keel relative to the level water. Thus, the computed trim angle should not be compared with the measured keel trim angle but rather with the trim angle of some mean buttock line. Based on very limited data for a bow dry warped hull, Savitsky (2006) suggests that the effective trim angle of the _ buttock line be taken at the forward edge of the mean wetted length. Unfortunately, for the present model, at volume Froude numbers less than approximately 2.5 the wetted keel length extends into the curved up bow area where the trim angle of the buttock lines increase rapidly as Station 0 is approached. Thus, it does not seem appropriate to use the guidance of Savitsky (2006) to define the effective trim angle of the _ buttock line.

For the present test model 5631, the trim angle of the _ buttock line at the LCG is taken to be

representative of the hydrodynamic trim angle of the bottom surface. This angle is approximately 0.97 deg measured upward relative to the keel. Hence, for a proper comparison with the measured model trim angles of the keel, the computed trim angles for model 5631 should be reduced by 0.97 deg. These calculations have been carried out, and the results presented on Figure 2 for volume Froude numbers □ 2.5. It is seen that the agreement between calculated and measured keel trim angles is reasonable, further justifying the use of the computational method of Savitsky (2006).

In conclusion, I would like to thank the authors for sharing their data with the high-speed marine design community and for providing this discusser with an opportunity to further expand upon the hydrodynamics of planing craft.

References

Savitsky, Daniel 1964 Hydrodynamic design of planing hulls, Marine Technology, SNAME, **1**, 1, October.

Blount, Donald L. and Fox, David L. 1976 Small-craft power prediction, Marine Technology, SNAME, **13**, 1, January.

Savitsky, Daniel, Delorme, Michael, F., and Datla, Raju 2006 Inclusion of whisker-spray drag in performance prediction method for planing hulls, Metropolitan Section, SNAME, New York, New York, March 14.

John Zseleczky, Member

It is great to see series model test data being published in our SNAME TRANSACTIONS and especially useful to have access to the raw data and experiment details so that readers can modify their analysis to suit their needs. The United States Coast Guard has been especially generous in sharing the fruits of its research budgets with the Society, and we should all be grateful to them.

As was noted in the paper, the original 47' MLB design program included model tests that were conducted at the U. S. Naval Academy Hydromechanics Lab (NAHL) back in 1988. Those test results were published in a technical report prepared for the Coast Guard but were not widely distributed. The paper notes that these tests used an 8 foot model, but actually the scale ratio was 8 and the model length overall was 5.91 feet. Towing tank establishments are always interested in comparing their results with those of other tanks so we were very interested in seeing this new data. Unfortunately, given the differences in the hull configurations (stern wedge and rounded transom) and loading conditions between the two test programs, a direct comparison is not possible. The effect of the stern wedge on the NAHL MLB model can be estimated using the method given by Savitsky and Brown (1976) but this approach produces effective displacements and LCG positions that also do not match up with any of these new series test conditions. The best we can do is to say that the results from the two test programs are in the same ballpark.

In comparing the data sets, a few questions arose concerning experimental details of the test program and it may be useful for other readers as well, if the authors expand on them in their closure. First is the definition of "trim" used in the plots and tables. Is "trim" the angle between the hull baseline and the still water surface? If so, it would be useful to include a table showing the zero-speed "trim" angle, which must be quite different with LCG located at the 38% and 42% positions. At NAHL we routinely re-zero instrumentation between test runs so the recorded variable is really "trim" minus the zero-speed trim angle, and we have to shift it back before plotting. This is a simple bookkeeping detail but can cause confusion if not formally declared.

The second question is in relation to the towing method. The Experimental Procedures section provides details on the location of the towing point but does not mention if any methods were used to simulate the upward component of propeller shaft thrust. The MLB has a propeller shaft angle of 12 degrees. When the boat runs with a trim angle of 4 degrees, the upward component of shaft thrust is TAN(12 + 4deg) = 0.29 of the towing force. This is typically accounted for at the time of testing by assuming a shaft angle and unloading the towing post, as in the MLB tests at NAHL, or by towing with an inclined towing link, as in the Series 62 planing boat series. If no upward force was present in the tests, and we were making predictions for an MLB-type hull with an inclined shaft, this difference in test technique would make the new series test results representative of heavier hulls. However, if the reader is contemplating waterjet propelled hulls, where the shaft line is near horizontal, this difference would have a reduced impact. Either way, readers would benefit from a more detailed description of the towing method. This sort of detail is extremely important, not only for tank people comparing data sets, but also for the people who use these data in developing prediction methods.

One last note involves the Reynolds number used to obtain friction coefficients. In Appendix C, the paper states that the Reynolds number was based on the wetted keel length. It should be noted that the MLB tests at NAHL used the mean of wetted keel and wetted chine length. This is the method used in Series 62 (Clement and Blount) and is the procedure

recommended by the 22nd ITTC specialists committee on Model Tests of High Speed Marine Vehicles.

Thanks again to the authors for their work and to the U. S. Coast Guard for sharing it with us.

References

Clement, E. P. and Blount, D. L. 1962 Resistance tests of a systematic series of planing hull forms, *Transactions*, SNAME.

Savitsky, D. and Brown, P. 1976 Procedures for hydrodynamic evaluation of planing hulls in smooth and rough water, Marine Technology, SNAME, October.

22nd ITTC Report and Recommendations, Model tests of high speed marine vehicles specialist committee, Section 4.2.3 Turbulence Stimulation.

Authors' Closure

First, the authors would like to thank Messrs Blount, Savitsky, and Zseleczky for taking the time to submit written discussions. We appreciate the efforts made in preparing your comments and will try to address each of your concerns.

Mr. Zseleczky has caught us in a typographical error that is embarrassing to admit. He is completely correct in pointing out that the 47' MLB model tests conducted at the Naval Academy's Hydrodynamics Lab (NAHL) were done with a model that had a scale ratio of 8.0 and a model length overall of 5.91 feet, and is not an 8.0 foot model as reported. This model sits on a shelf in the Boat Engineering work area at the USCG's Engineering Logistics Center and I, Dina, see it every day, or shall I say, I view it but do not really see it. Thank you, John.

Zseleczky also asks about shaft lines with regards to towing methods and corrections these moments. He notes that the 47' MLB has an inclined shaft angle of 12 degrees. For these tests where the top speed is 40 knots as opposed to the 47' MLB's top speed of 25 knots, the USCG assumed a waterjet propulsion method that eliminated the shaft angles. Our tow point height corresponds to the height of the thrust bearing of the 47' MLB, making the assumption that this would be close to the preliminary design arrangements for a new vessel. These arrangements eliminated the need for shifting weights while towing. From the resulting data it can be found that the maximum thrust-induced lift was 1.9% of the displacement. Therefore, the resulting data are found to represent very closely the hull resistance of the presented rather than heavier loading conditions.

Dr. Savitsky and Mr. Zseleczky both point out the fact that we did not use the mean wetted length for our Reynolds's number length, choosing instead to use the wetted keel length at each speed that was recorded through visual inspection during testing. This choice was driven by the methodology employed for calculating wetted surface for each run by combining the three-dimensional surface definition of the hull with the observed waterline of the model as presented in Appendix C of our paper. This wetted surface derived for each speed based on the observed waterlines gave us added confidence that we were capturing the exact shape of the wetted surface and describing it accurately. Furthermore, we have investigated the effect on C_f through use of the wetted keel length rather than mean wetted length in Reynolds number. It had a small effect, 3% on average. The maximum difference was 12% for the low-speed, light-displacement MLB model data and occurred when the wave profiles did not impact the chine. At these conditions the wetted keel should have been used. Dr. Savitsky's discussion reinforces this result by showing that his theoretical predictions are very close to our reported values.

We are greatful to Dr. Savitsky for pointing out our misinterpretations of the prediction methodology and for providing more information about his newest calculation procedures and those comparisons to our data. Dr. Savitsky's discussion demonstrated exactly our intent in publishing this model data. That is, for the hydrodynamic community to analyze and utilize the data for their individual purposes, whether it be verification and validation of prediction methodologies or performance estimation of similar high-speed planing hulls. Lastly, we are fully aware that prediction results are not a benchmark by which one can judge the actual performance of a given hull. The comment in the original publication simply stated the obvious: that the data was consistently less than the prediction and, not therefore, the hull is likely to perform well. This conclusion was drawn from the magnitude of the resistance to weight ratio rather than the comparison to a prediction method. It was convenient that our data could be made available to Dr. Savitsky to help verify his work on the prediction of frictional resistance of planing hulls for design.

Also, Dr. Savitsky and Mr. Zseleczky both requested a better definition of the presented trim. The tabular and graphically presented trim data are the *change* in trim from the calm, zero-speed, model condition. The trim angle of the baseline can be determined by adding to the presented trim values, the tabular zero-speed trim data in Table B1, Static Model Conditions.

Mr. Blount asks if we considered the seakeeping capabilities of the current series and that answer is yes, and the selection of the 47' MLB is directly related to the experience gained from operation of this vessel. However, the initial phase of this research only funded resistance testing and so nothing more has been done. We hope to pursue additional research funds to complete the analyses.

Mr. Blount asks for information on the dynamic stability characteristics of the models while towing and to that we answer that these model were completely stable at high speed and never exhibited any porpoising, loll, or bow dipping. The data at high speeds are available. The other geometric quantities requested can be computed from the electronically available lines plans, which we have made available through request.

Mr. Blount took the time to plot some of the data in the format of Series 62. This is greatly appreciated and is a good reminder of the value of series data. Our focus at the time of the testing and paper presentation was more specific in nature. This may be short-sighted, and we take the comments as constructive criticism.

Table 1 Model Particulars

Model No.	Parent 5628	Variant 1 5629	Variant 2 5630	Variant 3 5631
LBP ft(m)	10 (3.05)	10 (3.05)	10 (3.05)	10 (3.05)
Beam, B_{PX} ft(m)	3.09(0.94)	2.5(0.76)	2.24(0.68)	2.24(0.68)
Draft ft(m)	0.61(0.18)	0.49(0.15)	0.44(0.14)	0.51(0.16)
L/B	3.24	4.0	4.47	4.47
B/T	5.08	5.08	5.08	4.39
β, deg.	16.61	16.61	16.61	20.0
∇, $ft^3(m^3)$	8.05(0.23)	5.29(0.15)	4.24(0.12)	4.88(0.14)
A_P	25.88	20.97	18.76	18.76
l_{cp}				
B_{PT}, ft(m)	2.94(0.90)	2.4(0.73)	2.13(0.65)	2.13(0.65)
β, midships deg.	20.0	20.0	20.0	23.0

© Marine Technology, Vol. 45, No. 4, October 2008, pp. 30–32

Discussion

When the discussion by Donald L. Blount, Member, of the 2006 Annual Meeting paper, "A USCG Systematic Series of High Speed Planing Hulls," by Dina H. Kowalyshyn and Bryson Metcalf was published in the 2006 *Transactions* the figures were omitted. The complete discussion follows.

It is a great pleasure to see experimental data for high-speed hard-chine hulls published in a format readily useable by naval architects. I send to the authors my congratulations and many thanks for this paper and trust that they have learned much about the trends of calm water resistance and trim from the variables studied. I do believe, however, that as USCG requirements become fixed, a wider range for loading values may be desired as an extension of test variables.

Upon reading this paper, two thoughts came to mind. The first is a request to the authors to provide some comments about seakeeping qualities of the parent hull and anticipated seakeeping qualities of new hulls developed which make up this four model series. Were seakeeping comparisons (such as vertical accelerations, pitch, and heave) made with several vessels of similar size and speed which influenced the selection of the 47-foot MLB as the parent hull form? May we expect seakeeping test results for this series of hulls to be available in the future? The second area I wish to explore is in regard to the main theme of the calm water experimental data reported.

1. Data were not reported for all tests at high speeds. For example, Model 5628/Test 7 and Model 5631/Test 17. Was there a technical reason for not towing models at these high speeds, i.e., porpoising, loll, bow dropping, etc.?

2. Were test protocols from previous systematic series programs of hard chine hull forms reviewed when organizing this program?

3. It would be most helpful for some added dimensions which are often reported for hard chine model particulars be added to Table 1 or Al. The following are requested: projected length of chine, Lp; Ap and centroid of Ap forward of transom; projected maximum chine beam, Bpx; and projected chine beam at the transom, BPT.

4. Do the authors have any comments with regard to the indications of saddle point/slope reverse seen in the speed-trim curves between volume Froude numbers 1 and 2 in Figures 11 and 13?

Finally, I offer the following to show an example of benefits of studying trends when systematic series data are available. These four figures show calm water resistance to displacement ratio for several volume Froude numbers as a comparison of hard chine hull results from Series 62 with the systematic series data reported in this paper.

These data represent hulls operating in calm, deep salt water at a displacement of 100,000 pounds for a correlation allowance of zero. The geometric and loading variables are slenderness and length-beam ratios. For constant volume Froude numbers (Fv) the following trends are indicated. Solid symbols in the figures are USCG series data; open symbols are for Series 62 with 12.5 degrees of deadrise. To highlight trends, lines connect data points for the parent hulls.

This example of systematic series data analysis for hulls with dynamic lift shows changes of trends over a range of speeds.

Again, the authors' data will be an invaluable addition to resources in open literature.

Many thanks.

Fv	Hydrodynamics	Comments
1.5	Semi-displacement	R/W is essentially only a function of slenderness ratio. Low R/W is indicated for high values of slenderness ratio.
2.5	Semi-planing	Both L/B and slenderness ratio influence R/W. Low R/W is indicated for high values of L/B and slenderness ratios.
3.5	Planing	R/W is almost independent of L/B and slenderness ratio.
4.5	High Planing	Both L/B and slenderness ratio influences R/W. Low R/W is indicated for low values of both L/B and slenderness ratios.

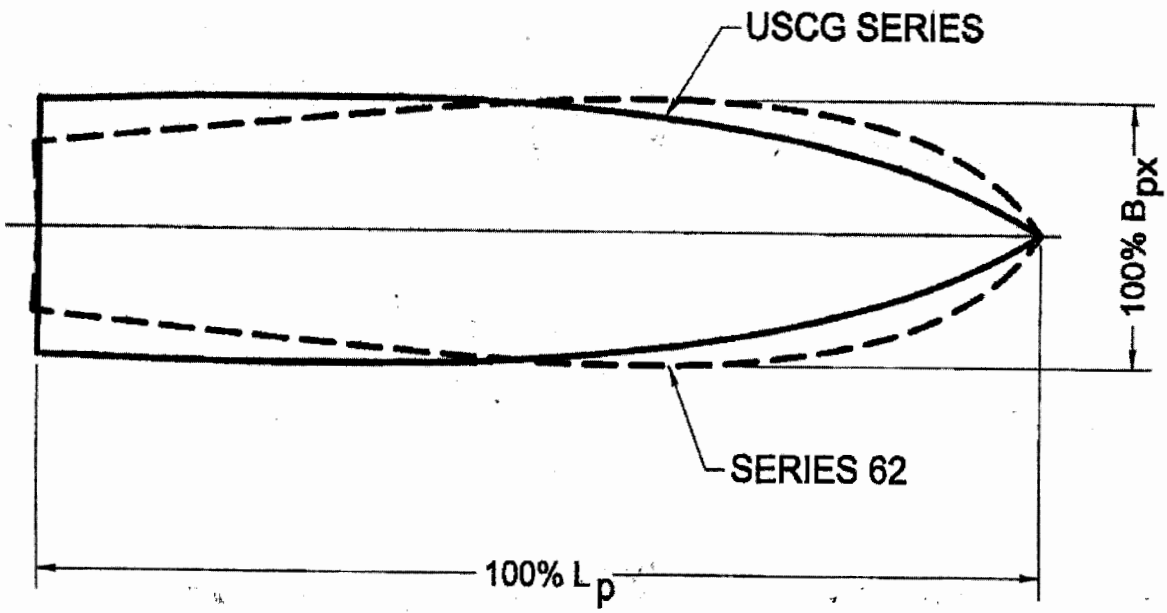

Length to Beam Ratio

USCG Series: Solid Symbols Series 62: Open Symbols

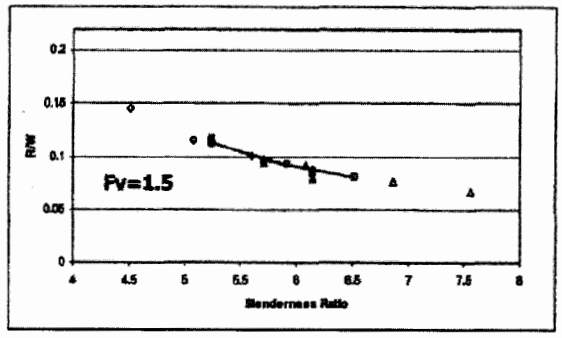

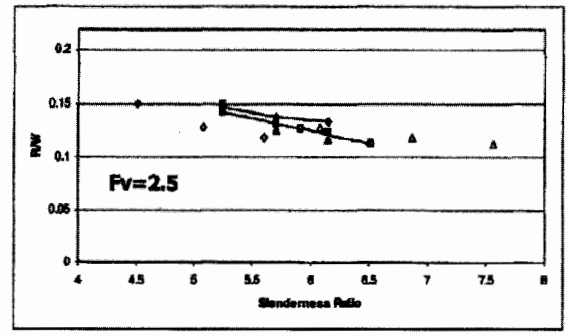

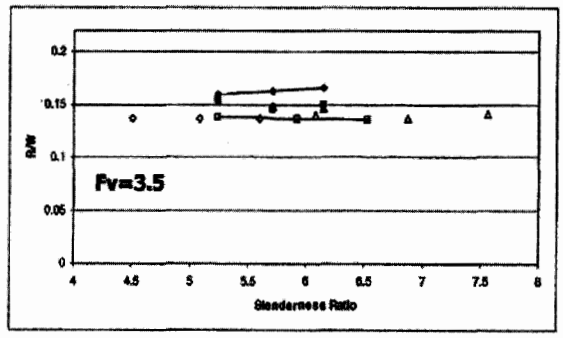

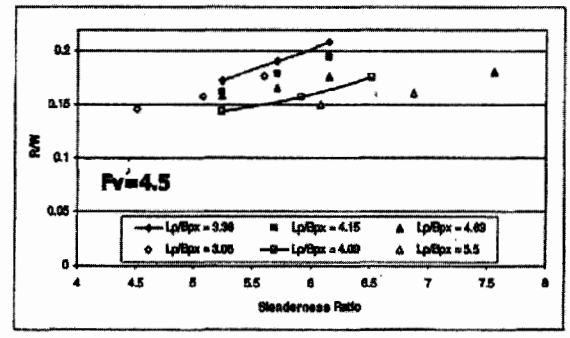

Carderock Division, Naval Surface Warfare Center

West Bethesda, Maryland 20817-5700

NSWCCD-50-TR-2005/063 December 2005
Hydromechanics Department Report

Resistance Tests of a Systematic Series of U.S. Coast Guard Planing Hulls

by
Bryson J. Metcalf
Lisa Faul
Elissa Bumiller
Jonathan Slutsky

REPORT DOCUMENTATION PAGE

Form Approved
OMB No. 0704-0188

1. AGENCY USE ONLY (Leave blank)	2. REPORT DATE	3. REPORT TYPE AND DATES COVERED
	December 2005	Final

4. TITLE AND SUBTITLE
RESISTANCE TESTS OF A SYSTEMATIC SERIES OF USCG PLANING HULLS

5. FUNDING NUMBERS
04-1-5200-158

6. AUTHOR(S)
Bryson J. Metcalf, Lisa Faul, Elissa Bumiller, Jonathan Slutsky

7. PERFORMING ORGANIZATION NAME(S) AND ADDRESS(ES)
NSWCCD Code 5200
9500 MacArthur Blvd.
West Bethesda, MD 20817-5700

8. PERFORMING ORGANIZATION REPORT NUMBER
NSWCCD-50-TR-2005/063

9. SPONSORING / MONITORING AGENCY NAME(S) AND ADDRESS(ES)
United States Coast Guard Engineering and Logistics Center
Propulsion Systems Acquisition Branch- Code 046, M/S 26, Bldg. 31
2401 Hawkins Point Road
Baltimore, MD 21226-5000

10. SPONSORING / MONITORING AGENCY REPORT NUMBER

11. SUPPLIMENTARY NOTES

12a. DISTRIBUTION / AVAILABILITY STATEMENT
Approved for Public Release; Distribution Unlimited.

12b. DISTRIBUTION CODE

13. ABSTRACT *(Maximum 200 words)*

Resistance experiments were performed on a systematic series of models based on the United States Coast Guard 47-foot Motor Lifeboat (MLB) hull form. The series includes three models with varying length-to-beam ratios and one model with transom dead-rise angle variation. Resistance tests were completed on each model for a range of conditions, with displacements varying from 298 lbs to 680 lbs and longitudinal center of gravity located at 38% and 42% of the length between perpendiculars (measured forward of the aft perpendicular). The results are presented as model scale values in the form of; R_T/Δ, S_{DYN}, C_R, LCG Heave, and Pitch angle. Additionally, EHP was calculated for the 47–foot MLB from 5628 model data and compared with EHP calculations from previous 47-foot MLB model test data.

14. SUBJECT TERMS
Calm water resistance, planing hull

15. NUMBER OF PAGES
59+vi

16. PRICE CODE

17. SECURITY CLASSIFICATION OF REPORT	18. SECURITY CLASSIFICATION OF THIS PAGE	19. SECURITY CLASSIFICATION OF ABSTRACT	20. LIMITATION OF ABSTRACT
Unclassified	Unclassified	Unclassified	Unclassified/Limited

Standard Form 298 (Rev. 2-89)

THIS PAGE IS INTENTIONALLY LEFT BLANK

CONTENTS

LIST OF TABLES

LIST OF FIGURES

NOTATION

STANDARD SYMBOLS (ABBREVIATED LIST)

V	Speed (Velocity)	Δ	Displacement
$F_{n\forall}$	Volumetric Froude Number $= \frac{V}{\sqrt{g\nabla^{1/3}}}$	R_n	Reynold's Number
R_T	Total Resistance	C_T	Total Resistance Coefficient
C_F	Frictional Resistance Coefficient	C_R	Residuary Resistance Coefficient
S	Wetted Surface	EHP	Effective Horsepower
λ	[Lambda] Model linear scale ratio	ρ	[Rho] Water Density ($lb*sec^2/ft^4$)
ν	[Nu] Kinematic Viscosity (ft^2/s)	S_{DYN}	Dynamic wetted surface area
LBP	Length between Perpendiculars	LWL	Waterline Length
LCG	Longitudinal center of gravity	ABL	Above Baseline
FP	Forward Perpendicular	AP	Aft Perpendicular
$A_P/\nabla^{2/3}$	Hull loading coefficient	∇	Volume
WP_{AREA}	Water-plane Area		
Ap	Projected area on the free surface from the hull, below and including the chine.		

INTERNATIONAL SYSTEM OF UNITS (SI) CONVERSION FACTORS

U.S. CUSTOMARY	METRIC EQUIVALENT
1 inch	25.4 millimeter (mm), 0.0254 meter (m)
1 foot	0.3048 meter (m)
1 pound of force	0.4536 kilograms (kg)
1 foot-pound (ft-lb)	0.1382 kilogram-meter (kg-m)
1 foot per second (ft/s)	0.3048 meter per second (m/s)
1 knot	0.5144 meter per second (m/s)
1 horsepower	0.7457 kilowatts (kW)
1 long ton	1.016 tonnes, 1.016 metric tons, or 1016.0 kilograms
1 inch water (60 F)	248.8 Pascals (Pa)

ABSTRACT

Resistance experiments were performed on a systematic series of models based on the United States Coast Guard 47-foot Motor Lifeboat (MLB) hull form. The series includes three models with varying length-to-beam ratios and one model with transom deadrise-angle variation. Resistance tests were completed on each model for a range of conditions, with displacements varying from 298 lbs to 680 lbs and longitudinal center of gravity located at 38% and 42% of the length between perpendiculars (measured forward of the aft perpendicular). The results are presented as model scale values in the form of; R_T/Δ, S_{DYN}, C_R, LCG Heave, and Pitch angle. Additionally, EHP was calculated for the 47-foot MLB from 5628 model data and compared with EHP calculations from previous 47-foot MLB model test data.

ADMINISTRATIVE INFORMATION

The test results presented in this report were performed by the Resistance and Powering Division (Code 5200) within the Hydromechanics Department of the Naval Surface Warfare Center, Carderock Division (NSWCCD) at the David Taylor Model Basin, herein referred to as DTMB. Dina Kowalyshyn at the Boat Engineering Branch (ELC-024) of the U.S. Coast Guard's Engineering and Logistics Center sponsored the work, under work unit No. 04-1-5200-158.

INTRODUCTION

This report presents the results of calm water resistance experiments that were conducted at DTMB on a systematic series of models based on the United States Coast Guard 47 foot Motor Life Boat (MLB). The 47 foot MLB is a self-righting planing-hull design utilized by the United States Coast Guard (USCG) for inshore search and rescue missions in all sea states. The 47-foot MLB has proven to be a very successful hull form in terms of both seakeeping and resistance. This experimental program was designed to explore the possibility of adapting this hull form to larger length-beam ratio, higher-displacement, and much higher speed vessels.

The objective was to identify the influence of; length-to-beam ratio, transom deadrise angle, longitudinal center of gravity (LCG), and displacement on the resistance and trim attitude of the planing hullforms within the systematic series. This was achieved by constructing a 1/4.3 scale model of the 47-foot MLB, with a slight transom modification, and three variations of that geometry. They were all tested at three displacements and two longitudinal centers of gravity. The range of test conditions simulated ships ranging from 55-100 feet in length and displacements from 23-221 LT.

DESCRIPTION OF MODELS

Four scale models were constructed and designated by DTMB model numbers: 5628, 5629, 5630, and 5631. All models were constructed to a twelve inch station spacing and a length between perpendiculars (LBP) of 120 inches, corresponding to a scale factor of λ=4.30 for the 43 foot full-scale LBP of the 47 foot MLB. The four scale models were developed from the 47 Foot MLB lines plan by removing the stern wedge and extending the buttocks and waterlines to create a flat transom located at the aft perpendicular (AP). Each of the models have the same projected chine length, L_p=124.8 inches and the projected planing-area centroid, A_{pcent}=52.8 inches forward of the aft perpendicular. Table 1 presents the particulars of all four models determined us-

ing the design waterline from the 47-foot MLB drawings. In Table 1 the beam is listed as the maximum width at the waterline, the deadrise angle is taken at the transom, the volume excludes the spray rails, and the projected planning area includes the surfaces below the outer chine (excluding the spray rail). The hullforms body plans and profiles appear in Figures 1 and 2.

Model 5628 is the parent model of this series, as shown in Figure 3. This model is substantially the same as the full scale 47 foot MLB hull with the following differences: model 5628 has a flat transom rather than the rounded transom of the full scale ship, and it does not have the stern wedge found on the actual 47 foot MLB hull. It has a length-to-beam ratio of 3.24 and a beam-to-draft ratio of 3.67.

Model 5629 is considered Variant #1 of the series, as shown in Figure 4. The model was designed to obtain a length-to-beam ratio of 4.0 by scaling the body plan with a constant (0.810), while maintaining the length between perpendiculars, this will be referred to as a yz-scaling in the remainder of the document.

Model 5630 is considered Variant #2 of the series, as shown in Figure 5. The model was also designed by a direct yz-scaling (0.725) of the parent hull. The scale factor was obtained by the minimum beam corresponding to the limit of intact stability of this geometry, resulting in a length-to-beam ratio of 4.47.

Model 5631 is considered Variant #3 of the series, as shown in Figure 6. The model is a variation of Variant #2 in which the hull below the chine was stretched in the z-direction to obtain a transom deadrise of 20 degrees while maintaining the Variant #2 hull shape above and including the chine. Each station line below the chine was scaled independently (1.1-1.22) to achieve a smooth hull form connecting the chine to the flat keel (lowered 0.07036').

Models 5628-5630 were constructed by MAPC from transverse sections of numerically cut (NC) low-density urethane foam. The sections were assembled on a flat table and covered with fiberglass cloth, painted and marked with stations and waterlines. Internal structural members were constructed from ¼ inch plywood.

Model 5631was constructed by Don Trumpy from model-scale station lines provided by MAPC. This model was strip planked and finished with fiberglass.

EXPERIMENTAL PROCEDURES

All the resistance experiments reported herein were conducted on Carriage 3 in the high-speed basin, which has a cross sectional area of 21 feet wide by 16 feet deep. During these experiments the models were free to pitch, heave, and roll, but were restrained in surge, sway and yaw. The test agenda and the static, at rest conditions of the models are presented in Table 2 and 3 respectively.

The longitudinal position of the tow point was set by experimental design at 38 and 42 percent of the LBP forward of the aft perpendicular. The models were attached to the light heave staff mounted to the east end of carriage III. Two two-inch block gauges were used to measure drag (calibrated to ± 200 lbf) and side force (calibrated to ± 20 lbf). Running trim was measured with string potentiometers at the LCG and the stern of each model. A "grasshopper" was mounted at approximately station 8 in each model to restrain the model in yaw and provide a yaw-zeroing adjustment capability, while two tethers extended from the bow forward and outward for safety purposes to prevent excessive yaw and/or break away from the carriage. The

tethers were ¼ inch nylon rope attached with enough slack such that they would not interfere with the model running trim or influence the drag measurements.

Due to the small size and the internal structure of the models, the existing instrument stack could not be mounted to the hull in its standard configuration. A new mount for the existing two-inch gimbal was designed and built to lower the tow points to the desired levels and allow for easy longitudinal adjustment, Figure 7. The tow point heights, listed in Table 4, were determined from the height (above the keel) of the shaft thrust bearing on the full scale MLB. This height was obtained from the 47-foot MLB lines plans supplied by ELC-024. For each variant hullform the height was scaled according to the appropriate yz-scale ratio.

The ballast conditions of the models were given by model displacement and LCG supplied by the ELC-024. To obtain the proper ballast conditions the longitudinal centers of gravity were first determined for the unballasted, rigged models. This was achieved by hanging each model from the 38% LCG such that it was free to pivot about this transverse axis. Trim weights were added to level the model in pitch, which allowed the model's longitudinal center of gravity to be calculated by a simple balancing of moments. Given each of the model's longitudinal centers of gravity, the desired displacement and center of gravity for each test configuration was obtained through the precise placement of ballast weights. The achieved ballast conditions are listed in Table 3.

The models were tested over a range of model speeds corresponding to ship speeds of 10 through 55 knots. Data were collected at 100 Hz in ten-second spots, with two or more spots taken per speed. The number of spots collected per pass varied with the number and magnitude of speeds being run. Additionally, at each speed, the wave profile was observed at 4 locations on the model and documented. This was documented to determine the dynamic (at speed) wetted surface area of the model. These locations pertained to the keel-water intersection, the foremost location of the intersection between the chine and the spray-sheet, the chine reattachment point (the location where the chine no longer sheds water from the hullform above the chine), and the height of the water on station 10 (side of the model at the transom). Figure 8 shows these measurements for Model 5631 at 10.87 knots and 375 lbs of displacement at the 38% LCG. The solid line represents a generalized wave profile from the four observed locations on the model. The surface of the model was discretized into thousands of triangular panels in order to determine the wetted surface areas. The three colors on figure 8 represent panels, which were fully, partially, and non-wetted. The dynamic wetted surface area is then the total of the fully and ½ the partially wetted panels.

The deep transoms of the models, especially at high displacements and speeds, generated large divergent wave systems. With the removal of the wave-dampening troughs in the high-speed basin, the only dampers in the basin were a single line of swimming lane markers. Under these conditions, coherent packets of waves could be seen moving up and down the basin as much as ten minutes after a run. To damp the waves in the basin more quickly, additional lane markers were placed at the east end of the basin and the large horizontal wave suppressor plate was mounted to the carriage. The plate was lowered to the water surface when backing up between runs. This significantly reduced the persistence of the wave systems resulting in calmer tank conditions at the start of each run.

EXPERIMENTAL RESULTS

All of the data presented in this report, shown in Tables 5-29 and Figures 11-56, are model scale values. Figures 9 and 10 are the 47-foot MLB extrapolation to full scale. The results of the resistance experiments' analysis are presented in the form of; R_T/Δ, S_{DYN}, C_R, LCG Heave, and Pitch angle. Additionally, EHP data were calculated for the 5628 model data to compare with EHP calculations from previous 47-foot MLB model test data published in [1] collected at the United States Naval Academy (USNA), Division of Engineering and Weapons.

The EHP comparison plots with [1] are presented in Figures 9 and 10. The EHP data were calculated identically using a correlation allowance of zero, the ITTC 1957 correlation line and assuming the full scale vessel is operating in smooth, deep salt water with a uniform standard temperature of 59° Fahrenheit (15° Celsius). The only differences between the current model geometry and that in [1] were the scale ratios and that Model 5628 had a flat transom and no stern wedge. The only appendages on both models as tested were simple spray rails. By visual inspection it is evident that the current data fits reasonably well with the USNA data, bearing in mind that the displacement conditions are not identical. This comparison gives good assurance that the current data are reasonable.

The influences of L/B and deadrise angle on R_T/Δ, are presented in Figures 11 through 16. The data is plotted for all of the models at a given displacement and LCG location. Through close inspection of the figures and data, four key points are worth noting. The resistance per pound of displacement is influenced approximately equally by the L/B ratio and LCG location and their influences are more substantial at higher speed. The resistance per pound of displacement is clearly ordered in terms of L/B ratio. At nearly all speeds, higher length-beam ratios result in reduced R_T/Δ. Shifting the LCG forward tends to flatten the curve causing the R_T/Δ to increase in the high-speed region and decrease in the low-speed region thus reducing the benefit of planning. The effect of an increased deadrise angle is noticeable however slight. It tends to reduce the benefit of a slender hull.

Figures 17 through 24 present the R_T/Δ for each model individually at a single LCG, revealing the impact of change in displacement. For a given L/B ratio, the displacement has a large impact on the R_T/Δ. The data exhibit an inflection point where the curves change from concave downward to concave upward for all of the hullforms. At approximately this speed all the curves cross over each other. The inflection point of the curves occurs between 11 and 14 knots model speed. At speeds below the inflection point the R_T/Δ is larger for heavy displacements. Above the inflection point the inverse is true. This means that at speeds higher than the inflection-point the hullforms, with regard to resistance, become more efficient as the displacement increases. Another trend exists in which, for increases in length-beam ratio the point of inflection moves slightly to the right, occurring at higher speed.

The dynamic wetted surface areas from the experimental measurements shown in Figures 25 through 32, exhibit a noticeable trend. Looking at each hullform individually it can be seen that the dynamic wetted surface area for all displacements converge to the same value at higher speeds. It is very clear that for a particular hullform and LCG location the dynamic wetted surface area reaches approximately a constant, once planing. For these hullforms the constant is achieved at approximately Fn_V=3.6. For greater displacements it can be seen that a larger reduction occurs in dynamic wetted surface area as a result of planing.

The residuary drag coefficients (C_R) presented in Figures 33 through 40 follow expected trends with regard to displacement. However, no coherent trends can be established with regard to L/B ratio. There does exist however, noticeable and expected effects due to the change in deadrise angle and the LCG location. The curves have the typical peak occurring at a volumetric Froude number slightly greater than 1.0 and arranged in ascending order according to increasing displacement. The forward LCG location results in a decreased C_R curve while the increased deadrise angle acts to increase the C_R curve.

The curves in Figures 41 through 48 represent the CG heave of the models. The curves are S shaped. The initial response as speed increases from very low speed is to sink slightly, before steadily increasing from low to medium speed, prior to leveling out once planing is achieved. They are in ascending order with regard to increasing displacement. At first thought this may seem incorrect, however the effect of planing is to elevate the hullform out of the water until the hullform above the chines is dry. Interestingly, in order to achieve the planing condition at the same speed noted previously (Fn_V =3.6), the rate of heave gets larger with increased displacement. This results in a greater amount of heave when planing for the heavier displacement condition. The figures also show that the amount of CG heave is relatively insensitive to the L/B ratio variation, although an increase in deadrise angle does indicate a higher amount of CG heave.

The pitch angle measurements are shown in Figures 49 through 56. Two humps appear in the curves, which occur very nearly the same speed as the two humps in the C_R curves, especially with the higher two L/B ratios. The curves of pitch angle are well ordered with regard to the displacements. The largest and smallest maximum-pitch angles occur for high and low displacements, respectively. The maximum-pitch angle can also be seen to occur shortly prior to the maximum CG heave, which becomes approximately constant when the hullform is on plane. The pitch angle is also responsive to the LCG location. A forward LCG location will minimally reduce the amount of pitch for a given displacement. Additionally, the maximum pitch angle occurs at a higher speed when the LCG is forward and also when the L/B ratio is larger.

CONCLUSIONS

Model experiments were performed on a systematic series of models based on the United States Coast Guard 47-foot Motor Lifeboat (MLB) hull form. The series includes four models with varying length-to-beam ratios and transom dead-rise angles. Resistance tests were completed on each model for a range of conditions, with displacements varying from 298 lbs to 680 lbs and longitudinal center of gravity located at 38% and 42% of the length between perpendiculars (measured forward of the aft perpendicular). The EHP data, which were calculated for the full-scale 47' MLB, compared well to existing EHP data from the previously collected USNA model data. However, the data presented herein, is collected from larger models and includes much higher speeds than the USNA model-test data.

The results are all presented as model scale values in the form of: R_T/Δ, S_{DYN}, C_R, LCG Heave, and Pitch angle. The experimental data were discussed in a manner to extract the effects of variation in displacement, L/B ratio, LCG location, and deadrise angle. There exist some strong, expected trends and some not-so-obvious, unanticipated trends with regard to the independently varied parameters. The trend most worth noting is that the resistance per pound of

displacement is more favorable for high displacement at high speed and low displacement at low speed. Likewise, the effect of LCG location on the resistance per pound of displacement also reveals a favorable result with aft LCG location at higher speeds and forward LCG location at lower speeds. There exists a common, small, speed range (11-14 V_{MK}) in which this inflection takes place for all independent variables. This speed is where the aft LCG location and heavier displacements become more favorable considering resistance per pound of displacement. Additionally, the dynamic wetted-surface-area data revealed an interesting trend with regard to high-speed and the variation of displacement. The dynamic wetted surface area of a particular hull-form and LCG location for all of the displacements, converge to the same value once the hull-form is planing. It can also be seen that, for the same hullform, a forward LCG location will increase the dynamic wetted-surface-area to which all the displacements converge.

The results in this report are presented as model scale values due to the conceptual nature of the program. It must be noted that the curves of resistance per pound of displacement will be affected when scaled to some notional full-scale vessel. However, the trends will not vary, but may become less obvious. The effect of expanding to full-scale will result in a flatter curve, where the low speed hump becomes less pronounced and less curvature exists at high speed.

ACKNOWLEDGEMENTS

The United States Coast Guard Technical Point of Contact was Dina Kowalyshyn. The author would like to extend a special thanks to the following NSWCCD employees for their contributions and support towards this project: Dennis Mullinix (5200) for calibration and installation of the Data Acquisition System (DAS) electronics and the staff of the Facilities Engineering Division, Code 5100 for reworking the exterior of all 4 models to provide a consistent surface finish with very short notice. Without all of your efforts the test could not have been successfully completed.

Table 1. Model Form Particulars.

Model	LBP [ft]	B [ft]	T [ft]	L/B	B/T	Deadrise [Deg]	Disp. [ft^3]	Ap [ft^2]
5628	10	3.08	0.608	3.24	5.08	16.61	8.05	25.88
5629	10	2.50	0.492	4.0	5.08	16.61	5.29	20.97
5630	10	2.24	0.441	4.47	5.08	16.61	4.24	18.76
5631	10	2.24	0.510	4.47	4.39	20.00	4.88	18.76

Table 2: Test Agenda for Series.

Model	LCG	Displ	$A_p/\nabla^{2/3}$
	%LWL fwd AP	Lbs	
5628	38%	298	9.13
		375	7.83
		483	6.61
		560	5.99
		680	5.27
	42%	298	9.13
		375	7.83
		483	6.61
5629	38%	298	9.13
		375	7.83
		483	6.61
	42%	298	9.13
		375	7.83
		483	6.61
5630	38%	298	9.13
		375	7.83
		483	6.61
	42%	298	9.13
		375	7.83
		483	6.61
5631	38%	298	9.13
		375	7.83
		483	6.61
	42%	298	9.13
		375	7.83
		483	6.61

Table 3. Experimentally Tested Ballast Conditions

Model	LCG	Displ	$A_P/\nabla^{2/3}$	T_{AP}	T_{FP}	TRIM	WP_{AREA}	S
	[%LWL fwd AP]	[Lbs]		[in]	[in]	[in]	[in^2]	[in^2]
5628	38.08%	297.76	9.13	5.406	5.710	-0.304	2950	3228
	37.97%	375.69	7.83	6.000	6.556	-0.556	3211	3558
	38.00%	483.68	6.62	7.000	7.312	-0.312	3391	3867
	38.00%	560.16	5.99	7.750	7.750	0.000	3475	4052
	37.90%	679.94	5.26	9.000	8.243	0.757	3565	4305
	42.12%	297.76	9.13	4.750	6.742	-1.992	2948	3251
	42.04%	375.69	7.83	5.350	7.553	-2.203	3280	3632
	42.01%	484.19	6.61	6.000	8.767	-2.767	3497	3979
5629	37.99%	298.28	7.40	5.593	5.557	0.035	2700	3022
	37.98%	375.85	6.35	6.400	6.274	0.126	2820	3296
	38.00%	484.18	5.36	7.650	7.301	0.349	2924	3583
	41.98%	298.24	7.40	4.905	6.577	-1.672	2777	3131
	42.03%	376.16	6.34	6.030	6.812	-0.782	2855	3334
	42.06%	484.18	5.36	7.030	7.883	-0.853	2969	3638
5630	38.03%	297.77	6.62	5.750	5.518	0.232	2515	2935
	38.01%	375.46	5.68	6.900	5.888	1.012	2590	3153
	38.01%	483.78	4.79	8.250	6.696	1.554	2682	3455
	42.00%	297.77	6.62	5.000	6.587	-1.587	2584	3010
	42.02%	375.46	5.68	5.750	7.489	-1.739	2674	3253
	42.00%	483.78	4.79	7.000	8.410	-1.410	2764	3556
5631	38.01%	298.92	6.62	6.438	5.478	0.960	2439	2870
	38.01%	375.34	5.68	7.500	6.011	1.489	2537	3108
	38.00%	483.59	4.79	8.750	7.006	1.744	2645	3427
	42.00%	298.88	6.62	5.519	6.831	-1.313	2526	2964
	42.00%	375.27	5.68	6.206	7.855	-1.649	2634	3222
	42.01%	483.59	4.79	8.000	8.069	-0.069	2692	3486

Table 4. Tow Point Heights

Model Number	**5628**	**5629**	**5630**	**5631**
Tow Point ABL [in]	6.06	4.91	4.39	5.05

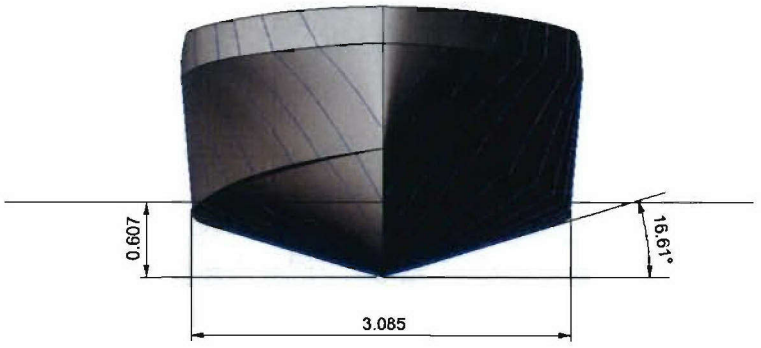

5628, 47' MLB Hull (L/B=3.24, B/T=5.08)

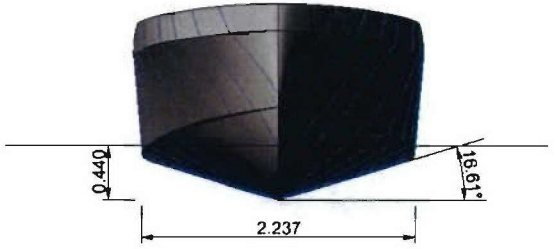

5630, Variant #2 (L/B=4.47, B/T=5.08)

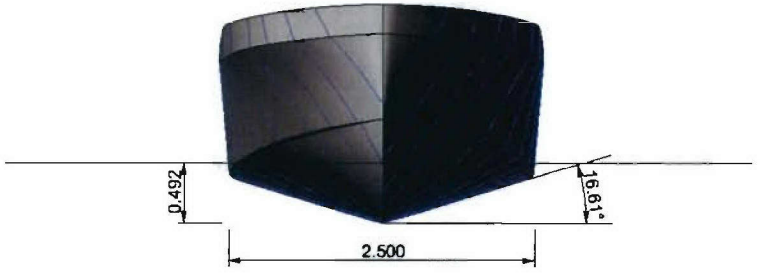

5629, Variant #1 (L/B=4.0, B/T=5.08)

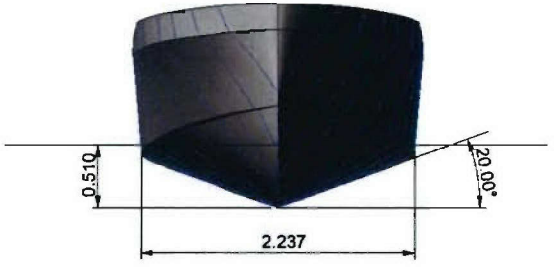

5631, Variant #3 (L/B=4.47, B/T=4.39)

Figure 1. Series Hullforms Body-Plan Views

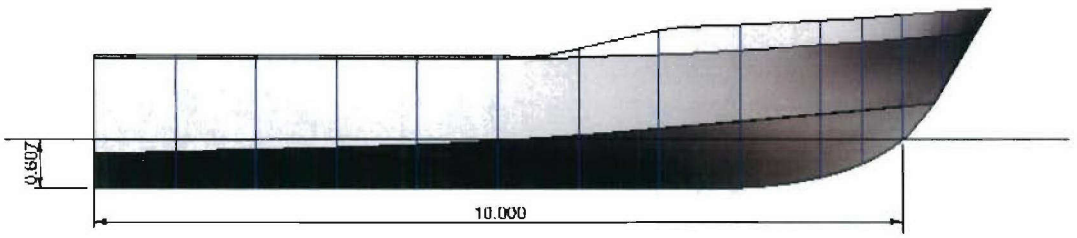

47' MLB Hull Profile

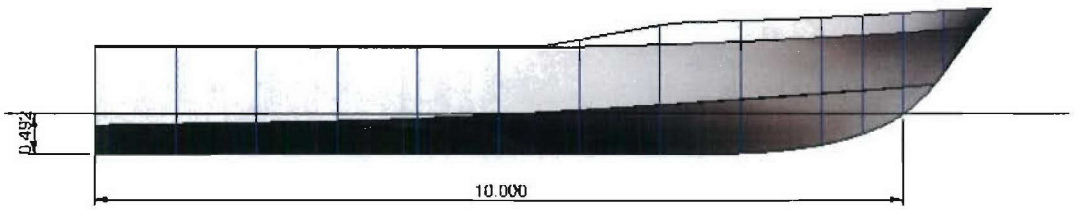

Variant #1 Hull Profile

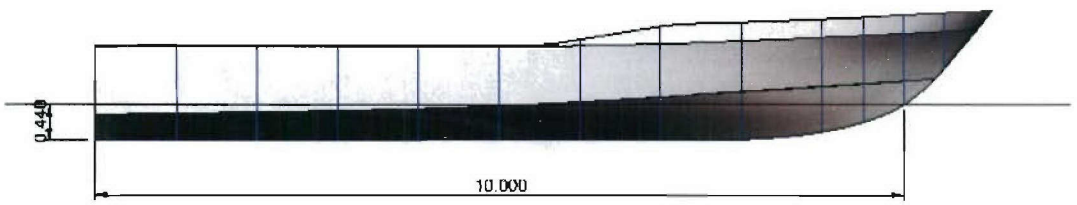

Variant #2 Hull Profile

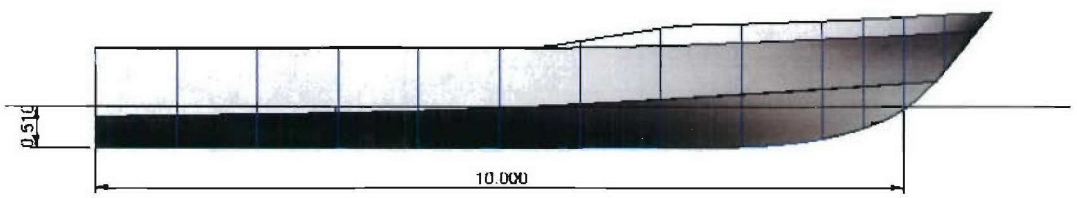

Variant #3 Hull Profile

Figure 2. Series Hullforms Profile-Views

Figure 3. Model 5628 Dry and at 298lbs, 43%, 25.47 Knots

Figure 5. Model 5630 Dry and at 298lbs, 43%, 25.47 Knots

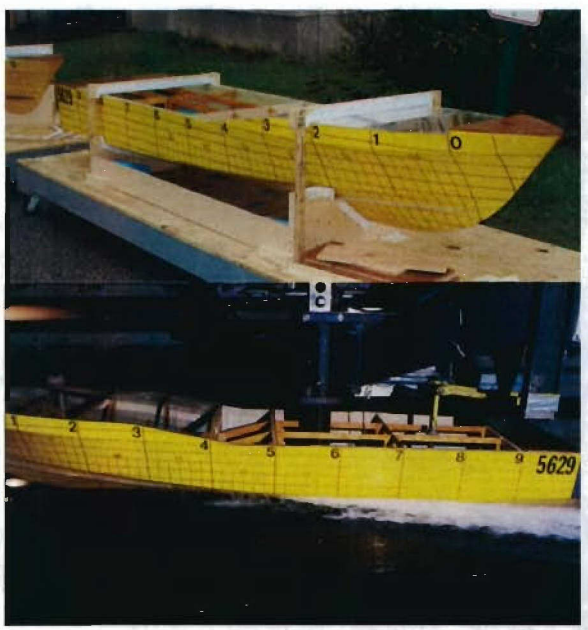

Figure 4. Model 5629 Dry and at 298lbs, 43%, 25.47 Knots

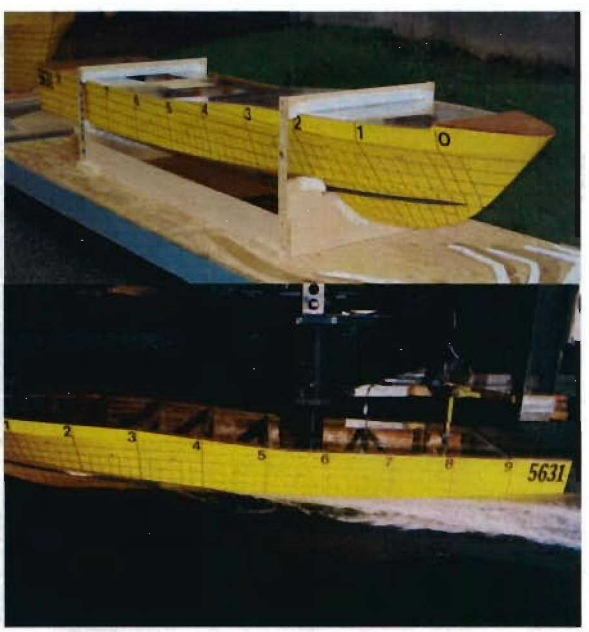

Figure 6. Model 5631 Dry and at 298lbs, 43%, 25.47 Knots

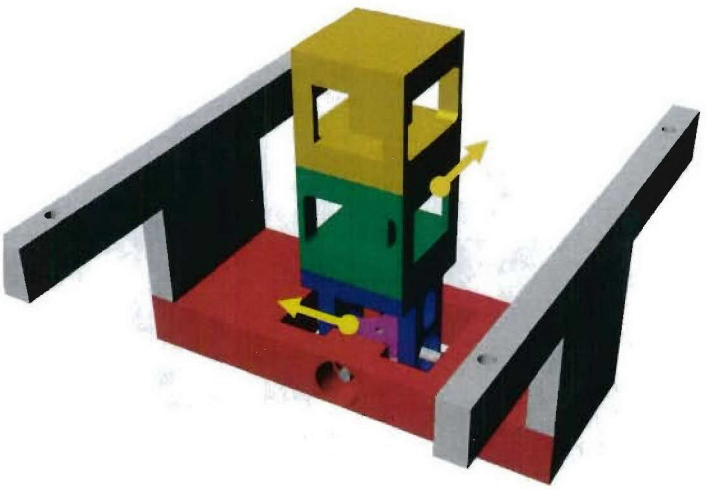

Figure 7. Block Gauge and Gymbal Assembly.

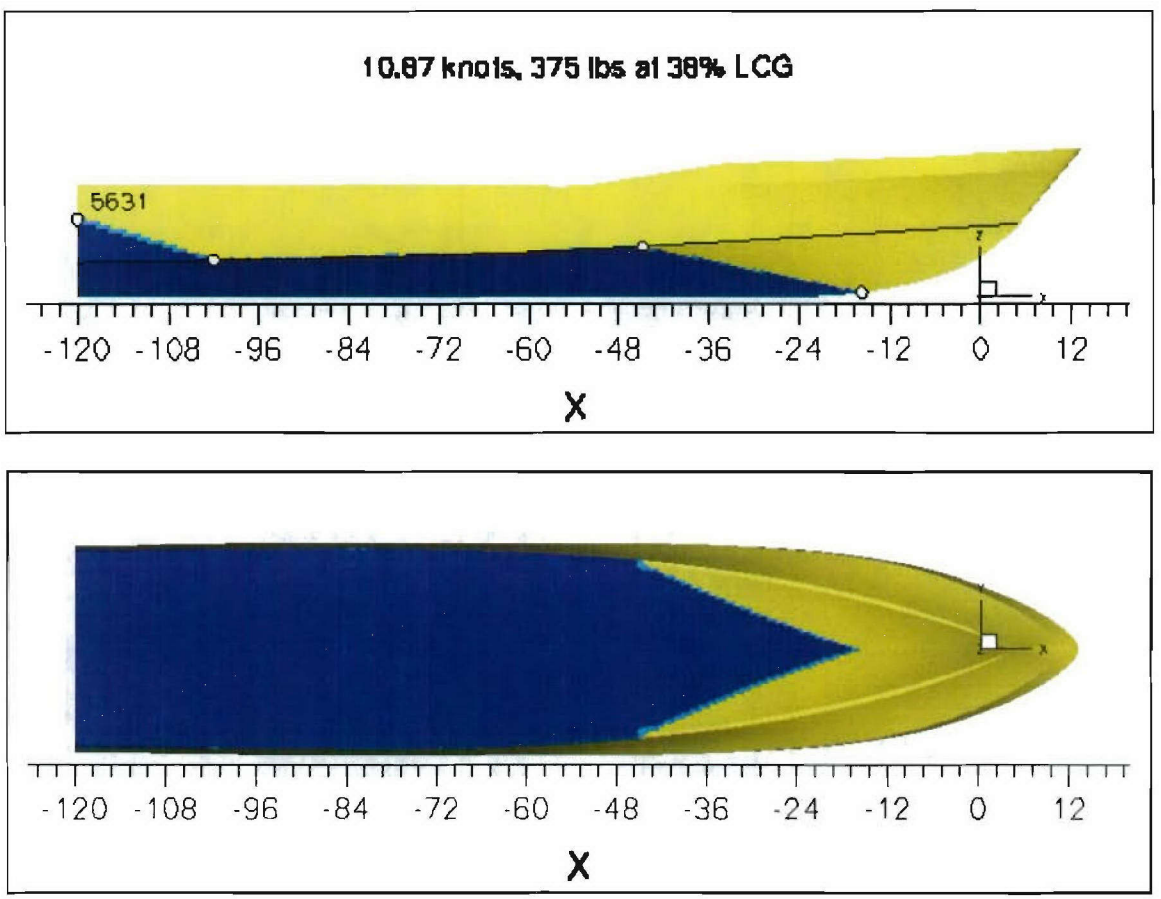

Figure 8. Dynamic Wetted Surface Area of Model 5631

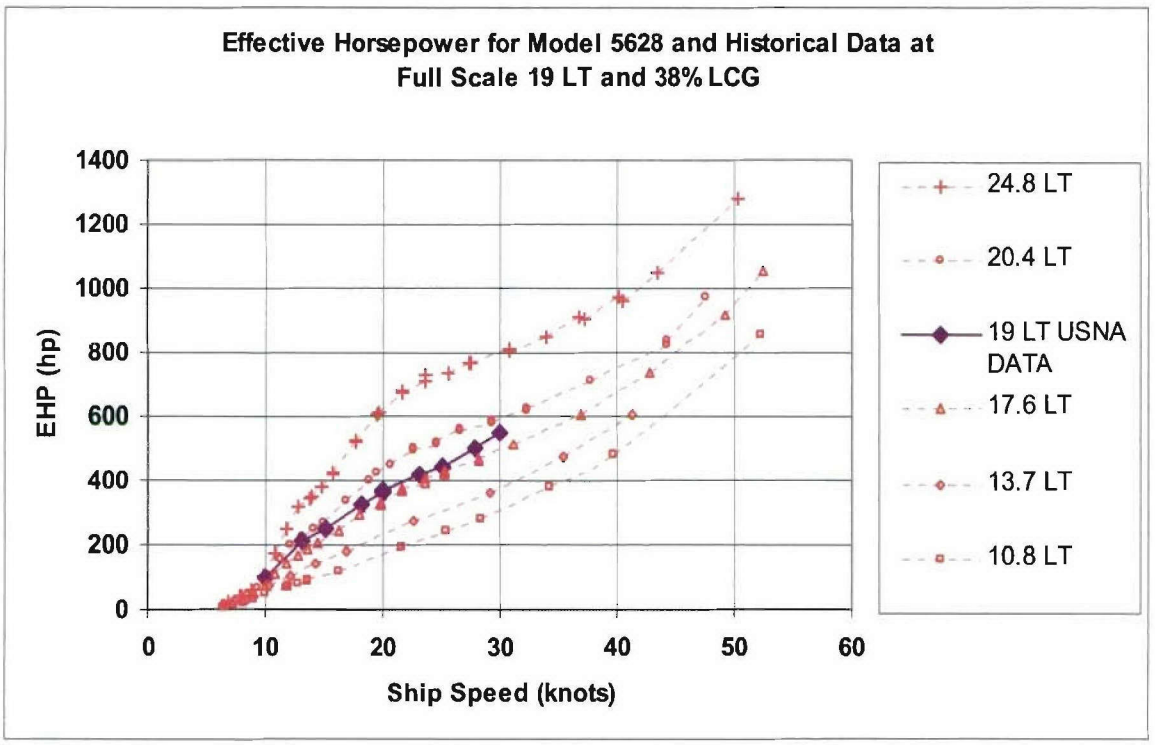

Figure 9. EHP for Full Scale 47 ft MLB at 38% LCG

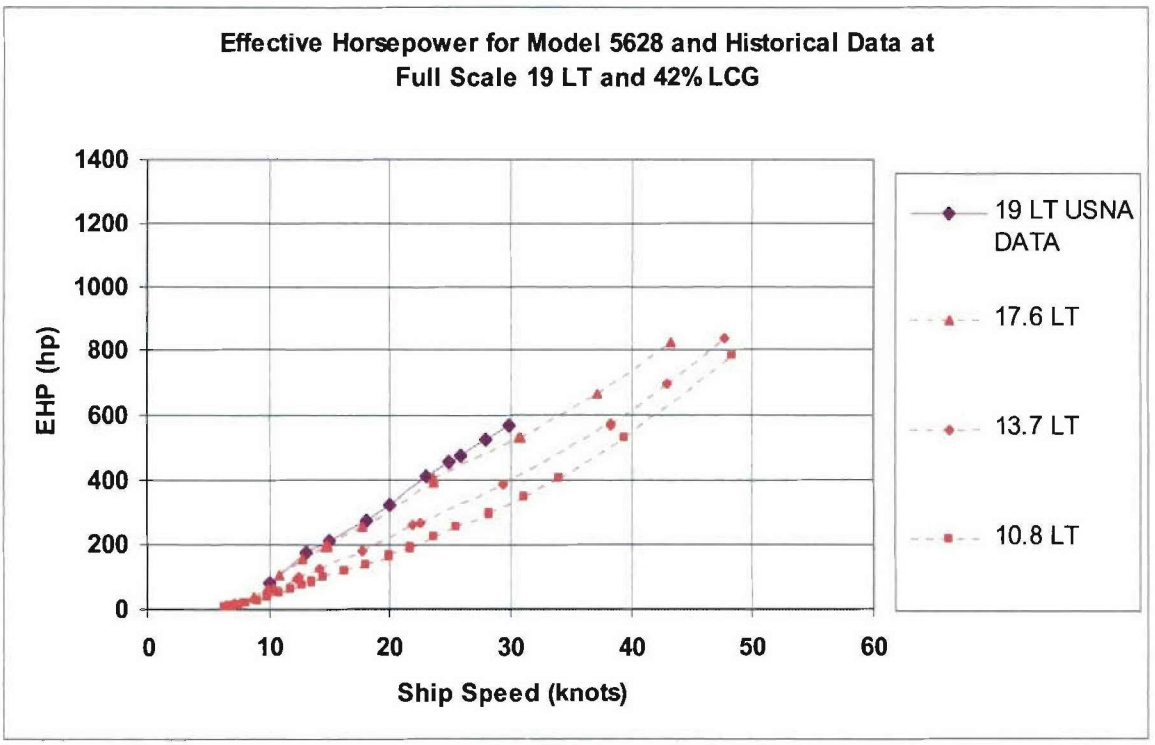

Figure 10. EHP for Full Scale 47 ft MLB at 42% LCG

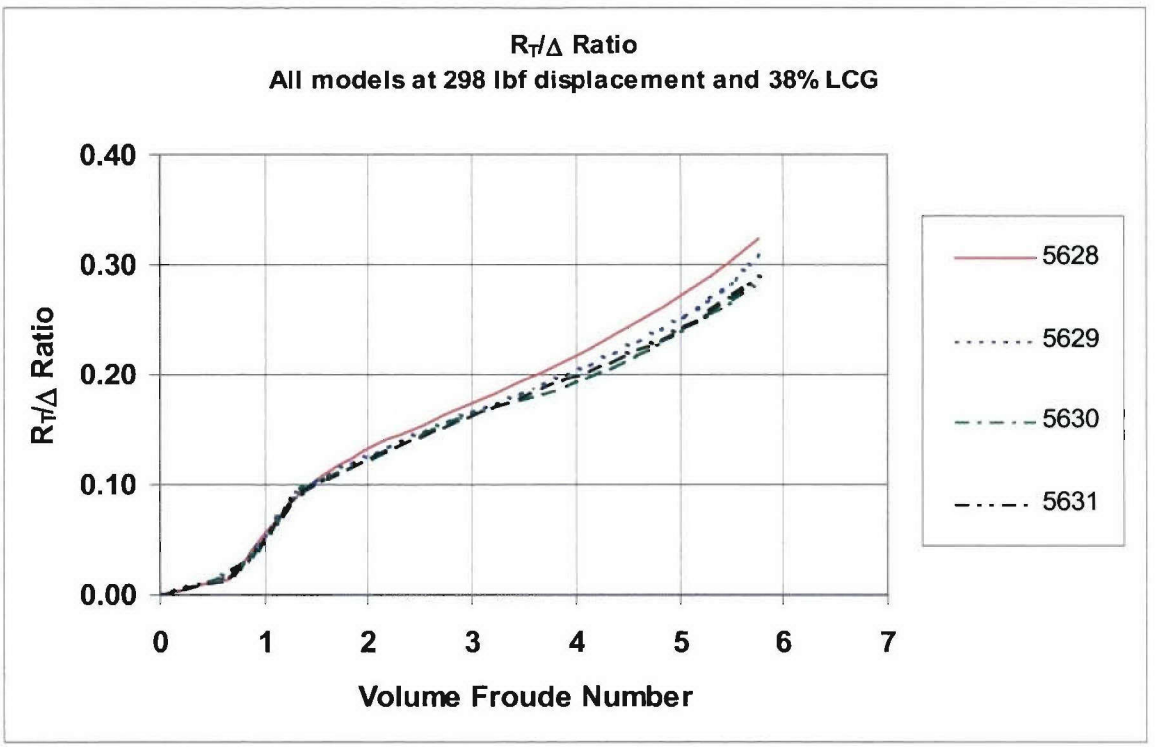

Figure 11. L/B & on Resistance for 298Lbs at 38% LCG

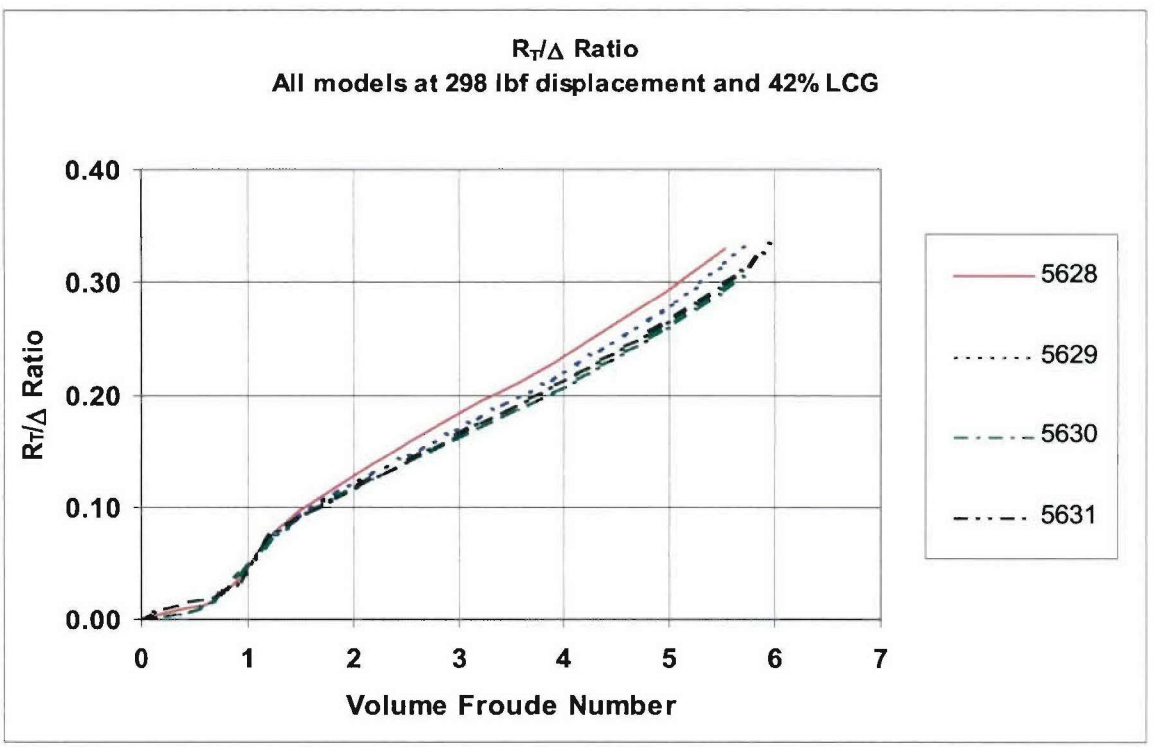

Figure 12. L/B & Deadrise Influence on Resistance for 298Lbs at 42% LCG

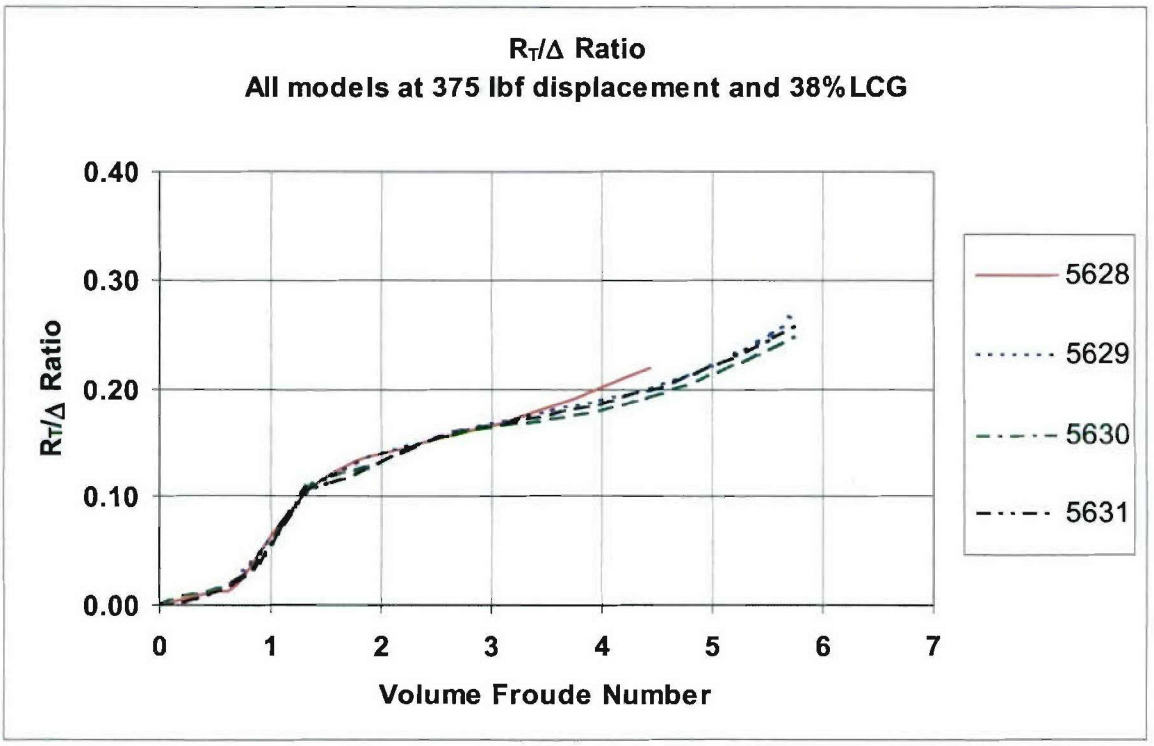

Figure 13. L/B & Deadrise Influence on Resistance for 375Lbs at 38% LCG

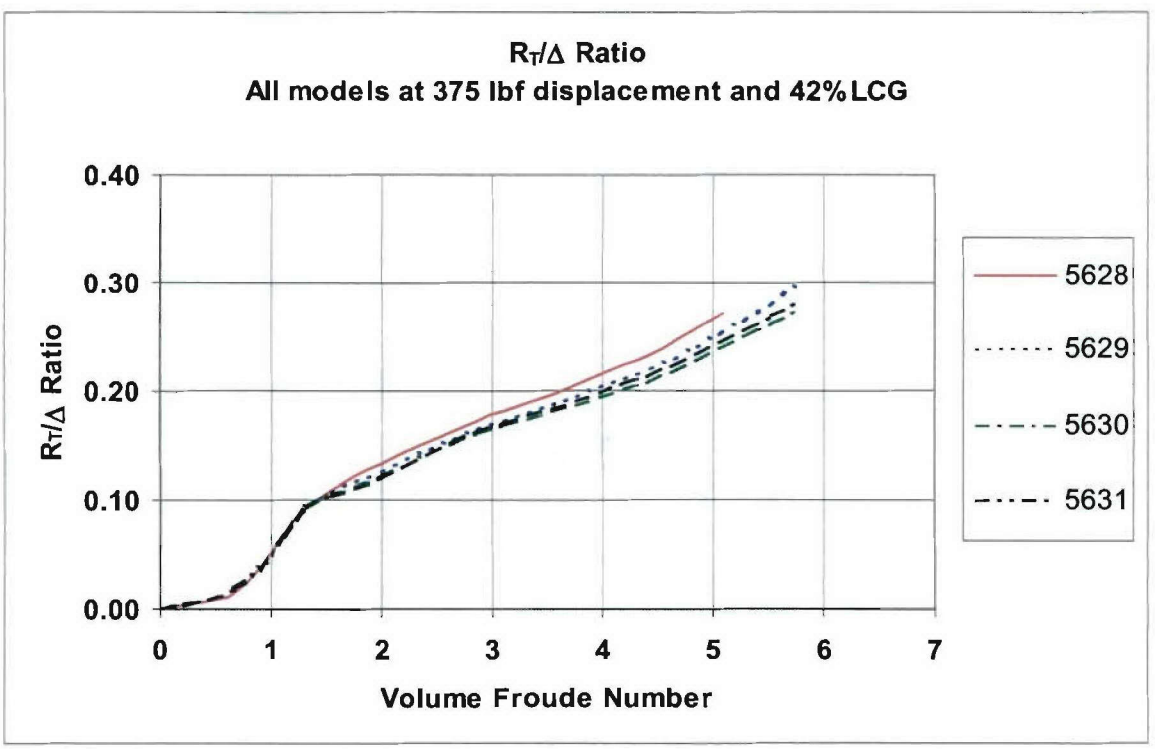

Figure 14. L/B & Deadrise Influence on Resistance for 375Lbs at 42% LCG

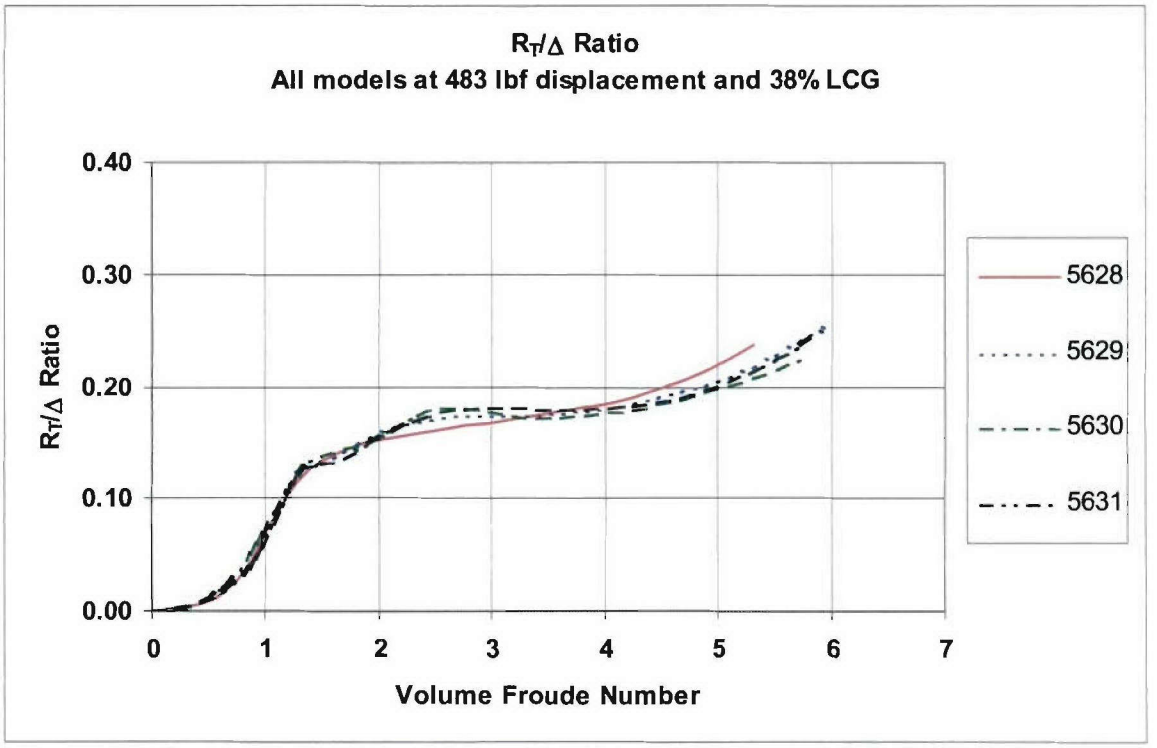

Figure 15. L/B & Deadrise Influence on Resistance for 483Lbs at 38% LCG

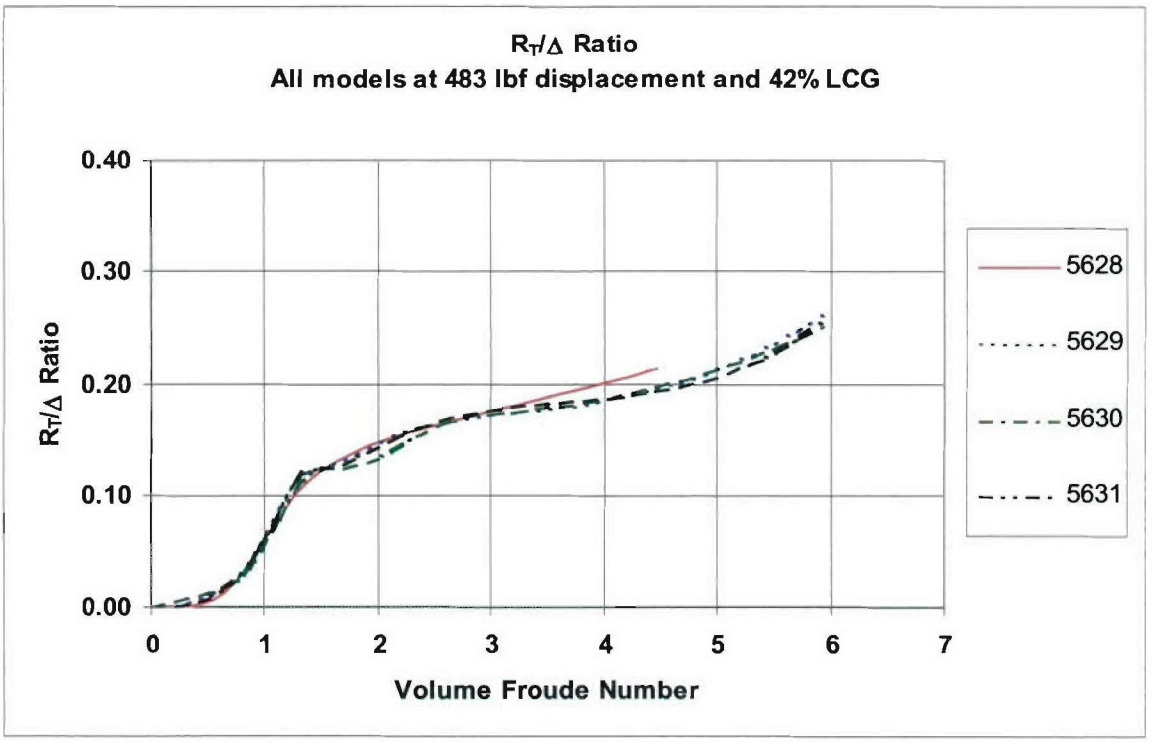

Figure 16. L/B & Deadrise Influence on Resistance for 483Lbs at 42% LCG

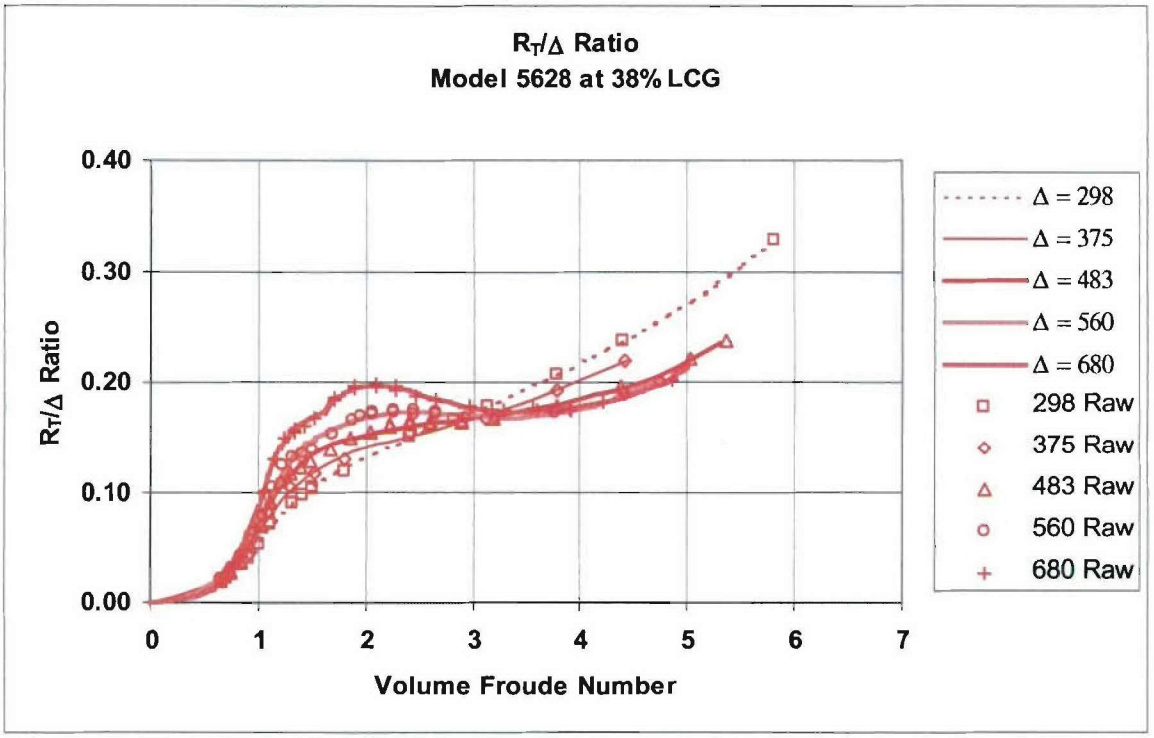

Figure 17. Model-Scale R_T/Displ for Model 5628 at 38% LCG

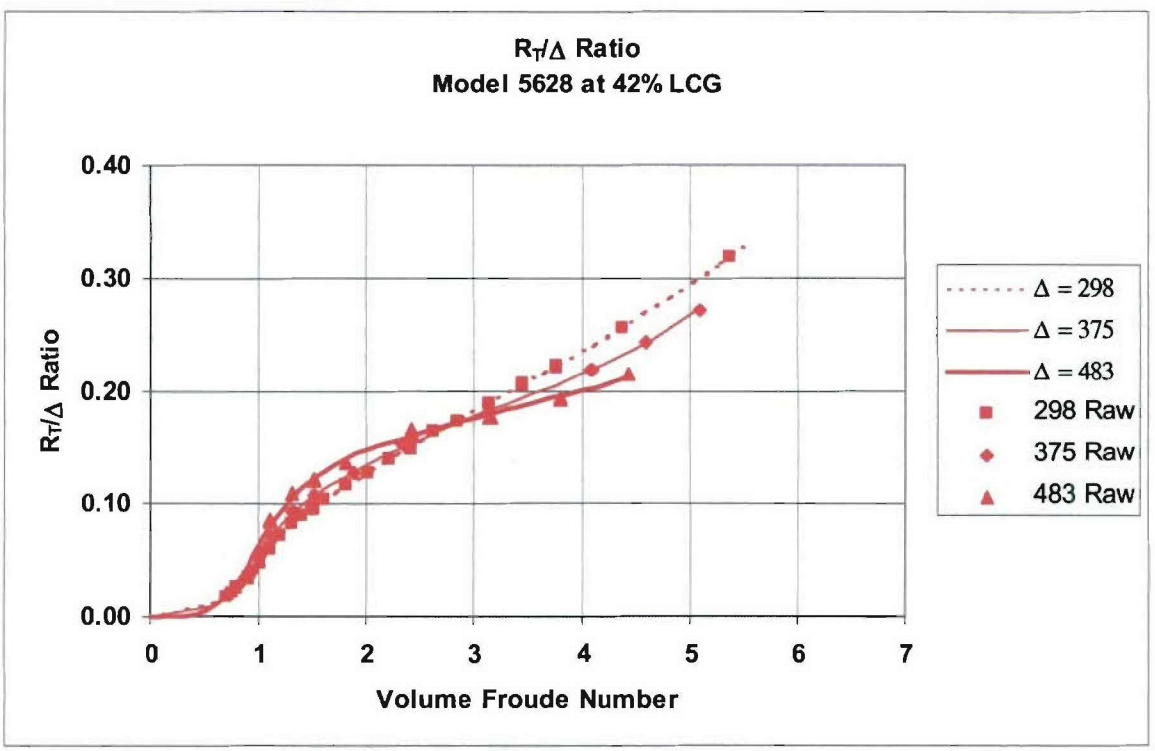

Figure 18. Model-Scale R_T/Displ for Model 5628 at 42% LCG

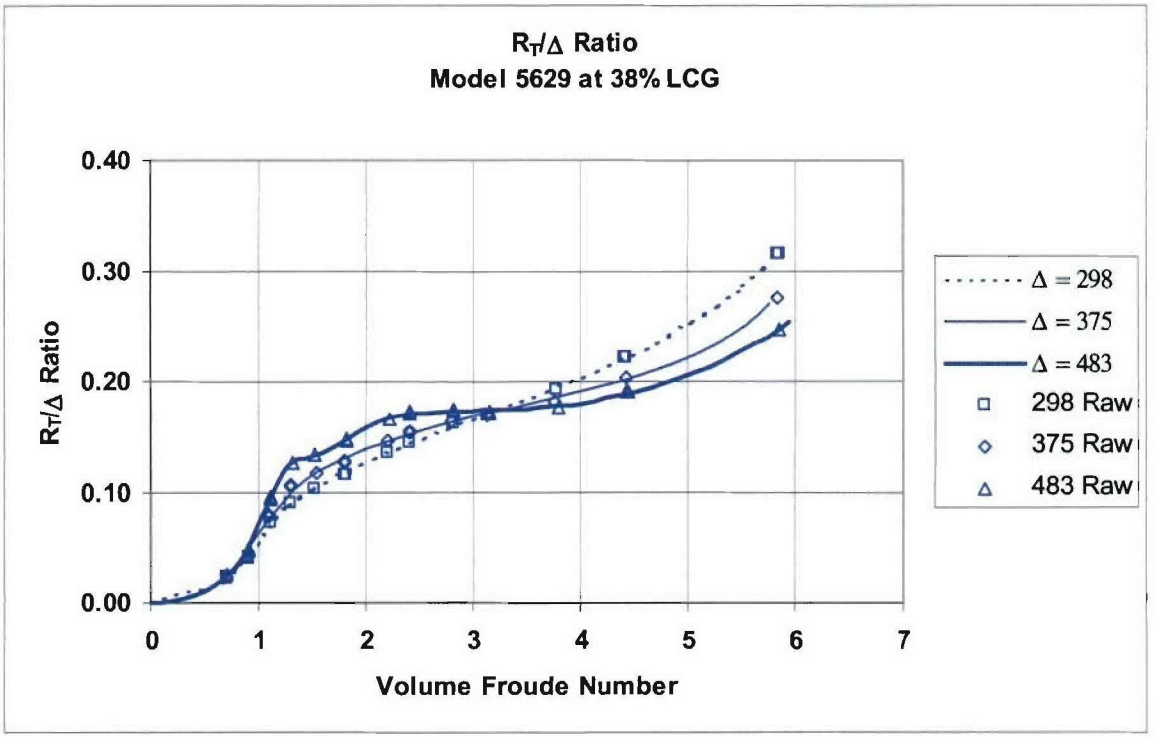

Figure 19. Model-Scale R_T/Displ for Model 5629 at 38% LCG

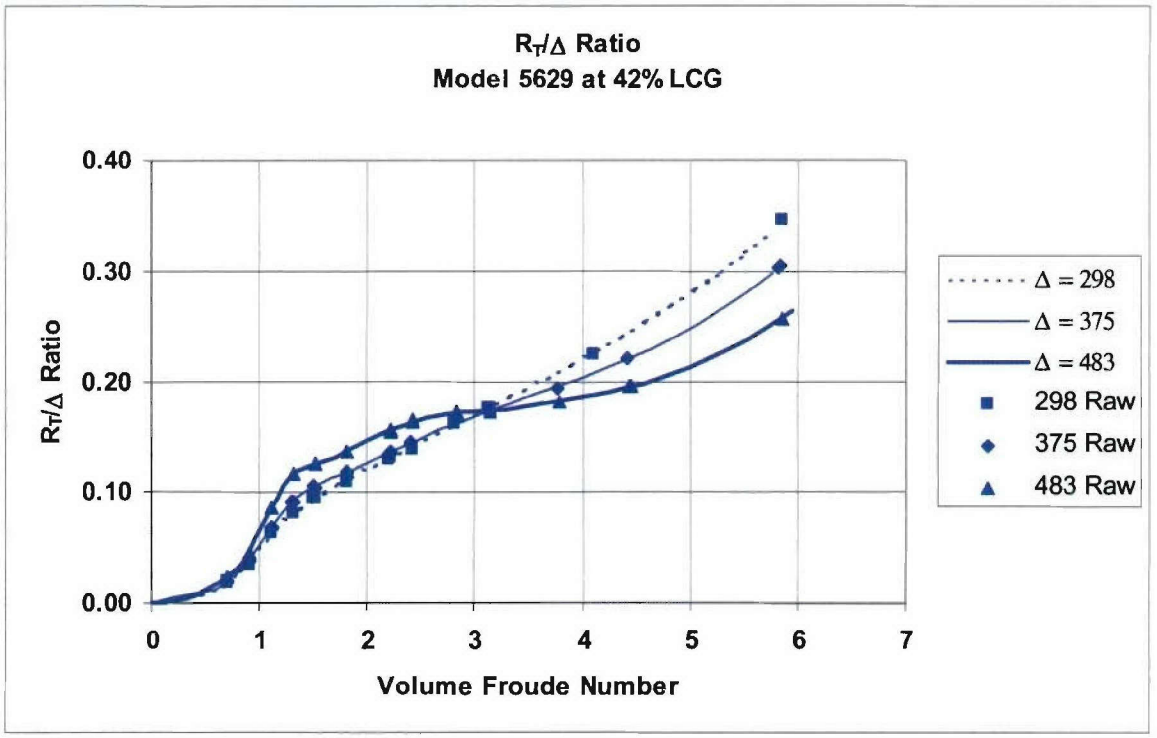

Figure 20. Model-Scale R_T/Displ for Model 5629 at 42% LCG

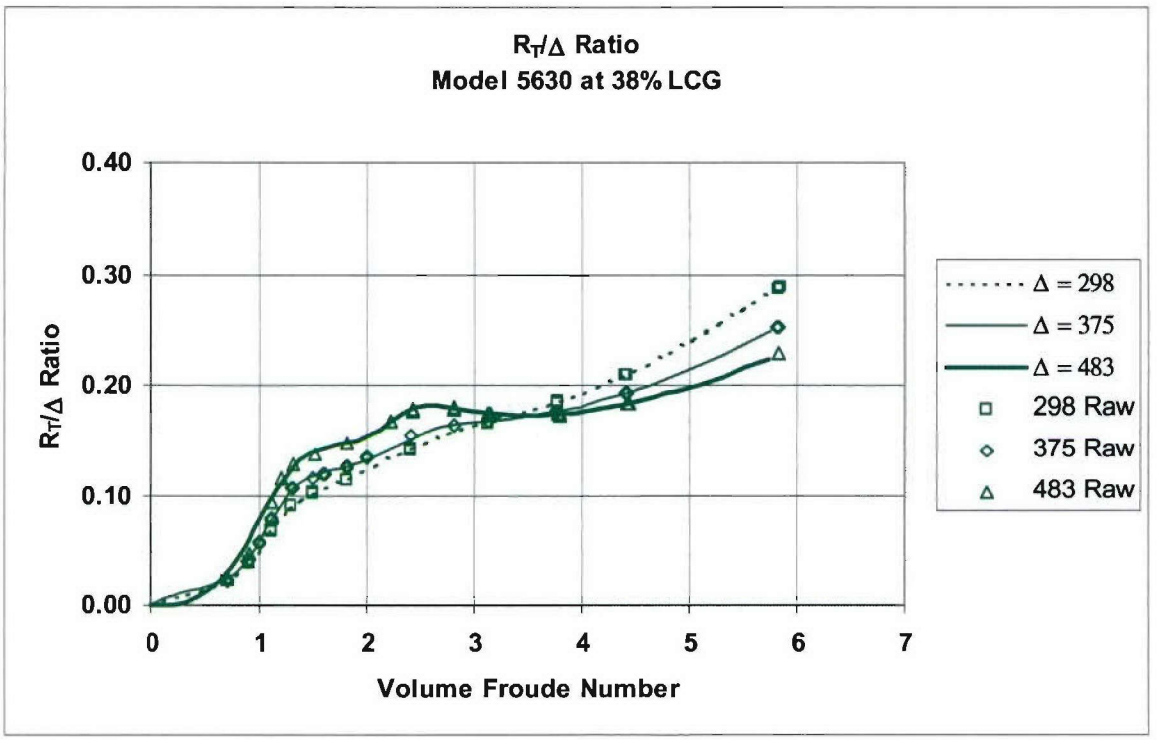

Figure 21. Model-Scale R_T/Displ for Model 5630 at 38% LCG

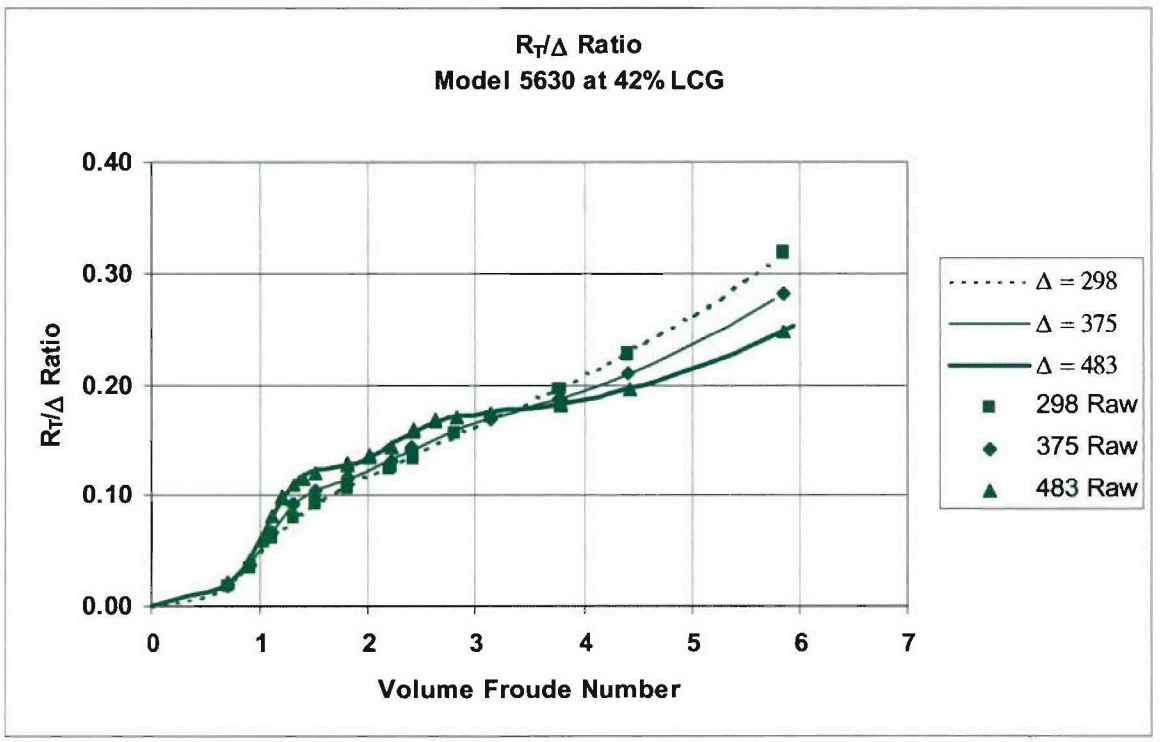

Figure 22. Model-Scale R_T/Displ for Model 5630 at 42% LCG

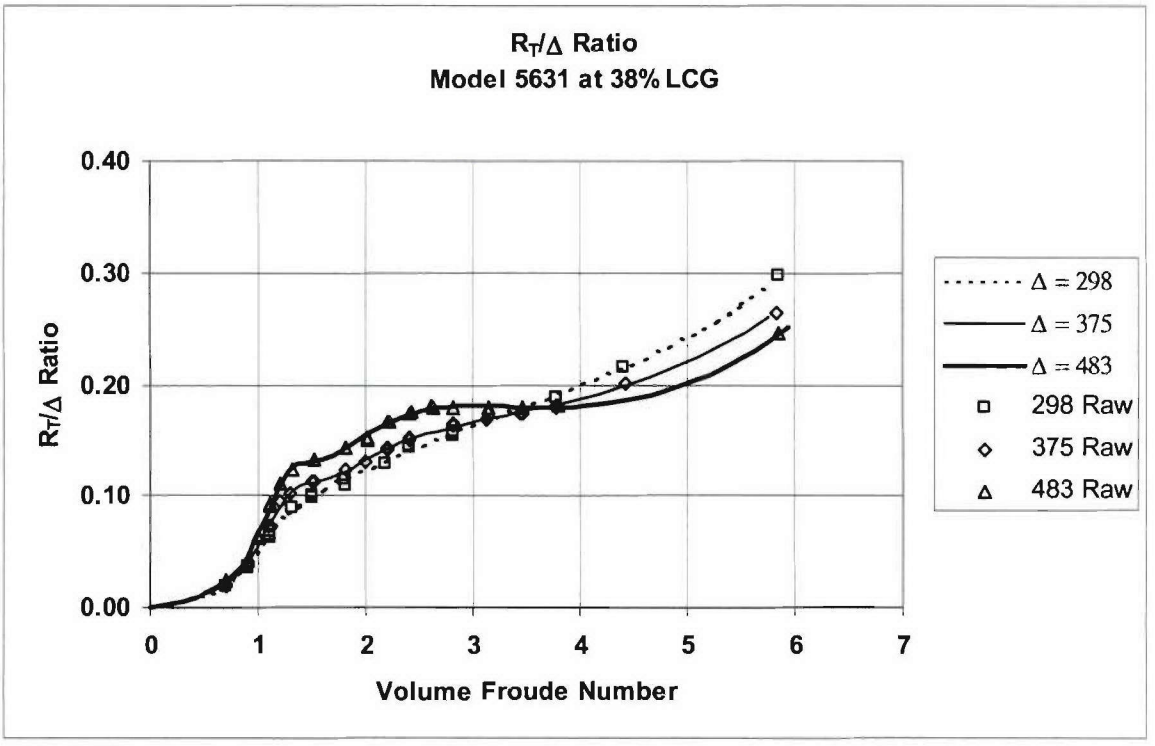

Figure 23. Model-Scale R_T/Displ for Model 5631 at 38% LCG

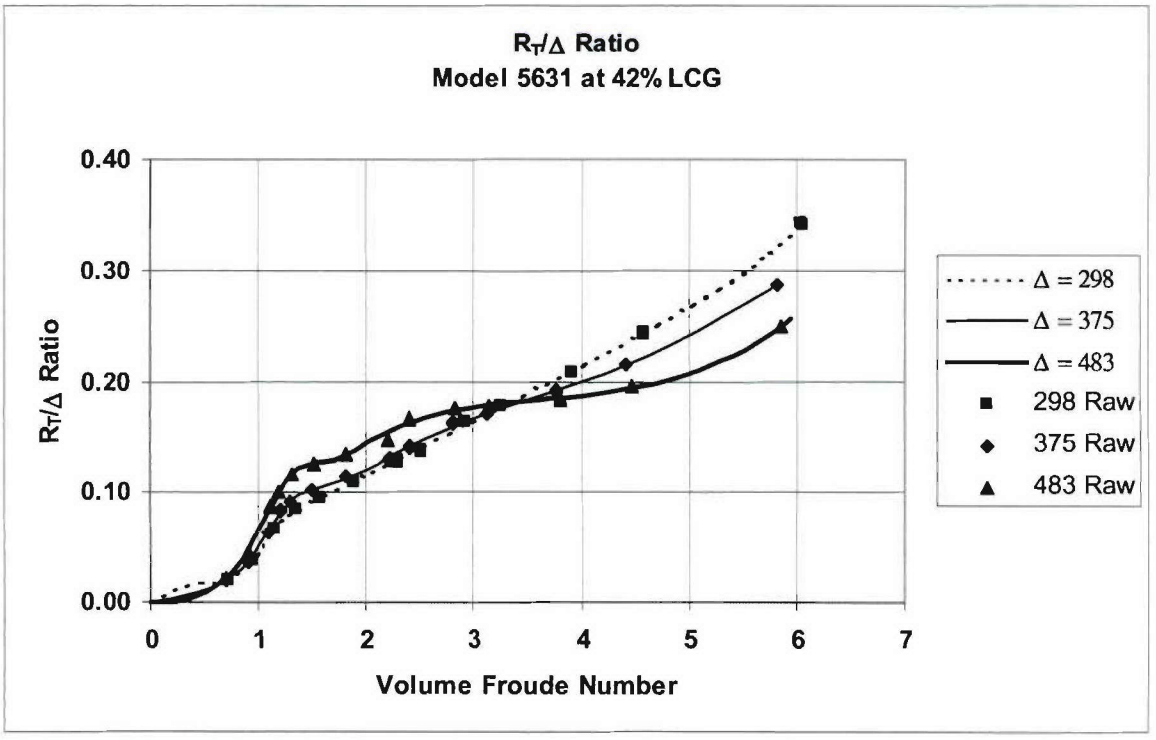

Figure 24. Model-Scale R_T/Displ for Model 5631 at 42% LCG

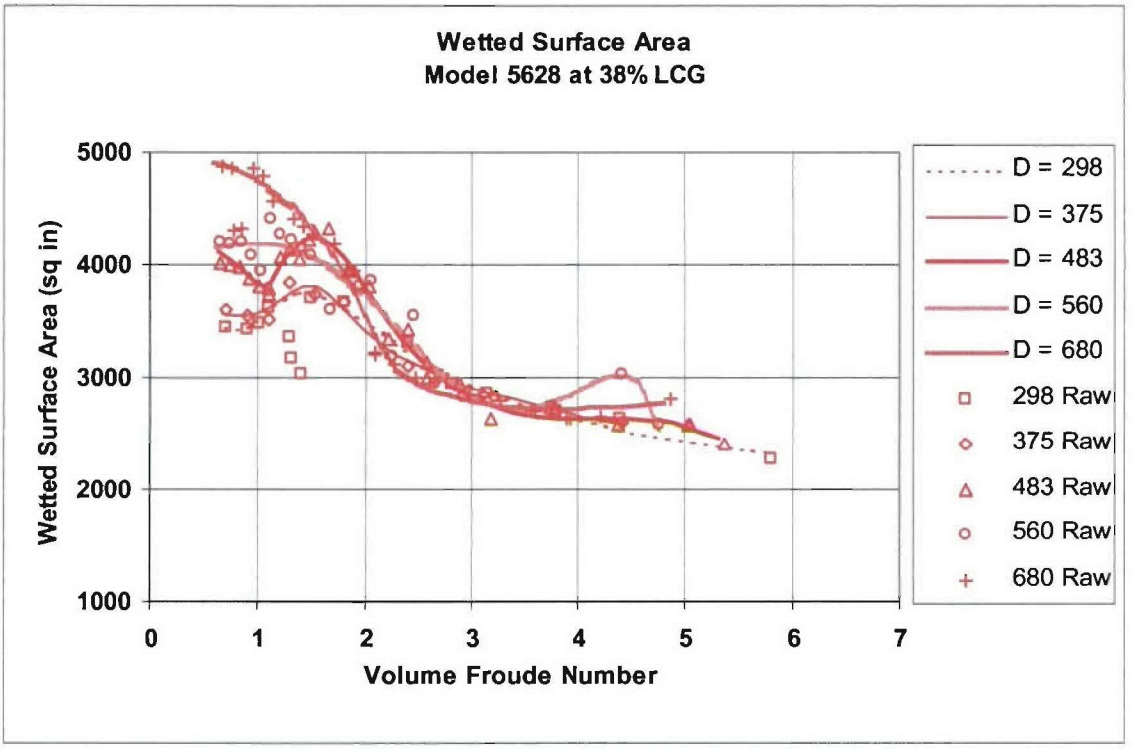

Figure 25. Model-Scale Dynamic Wetted Surface Area for Model 5628 at 38% LCG

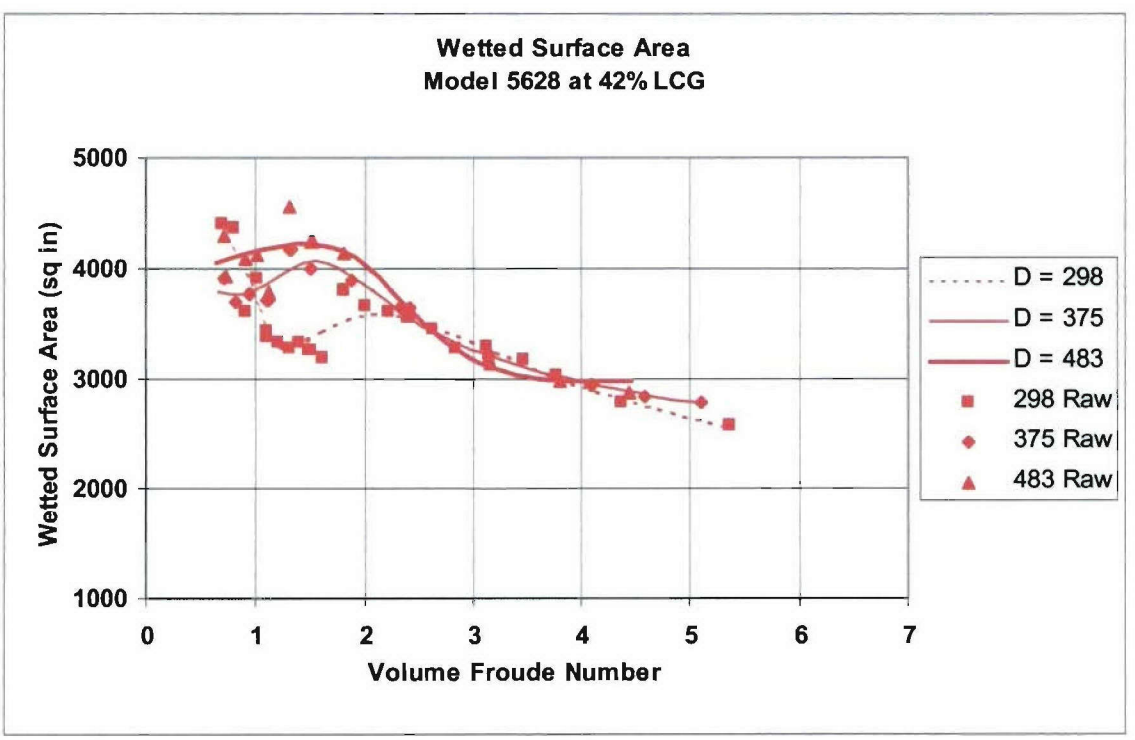

Figure 26. Model-Scale Dynamic Wetted Surface Area for Model 5628 at 42% LCG

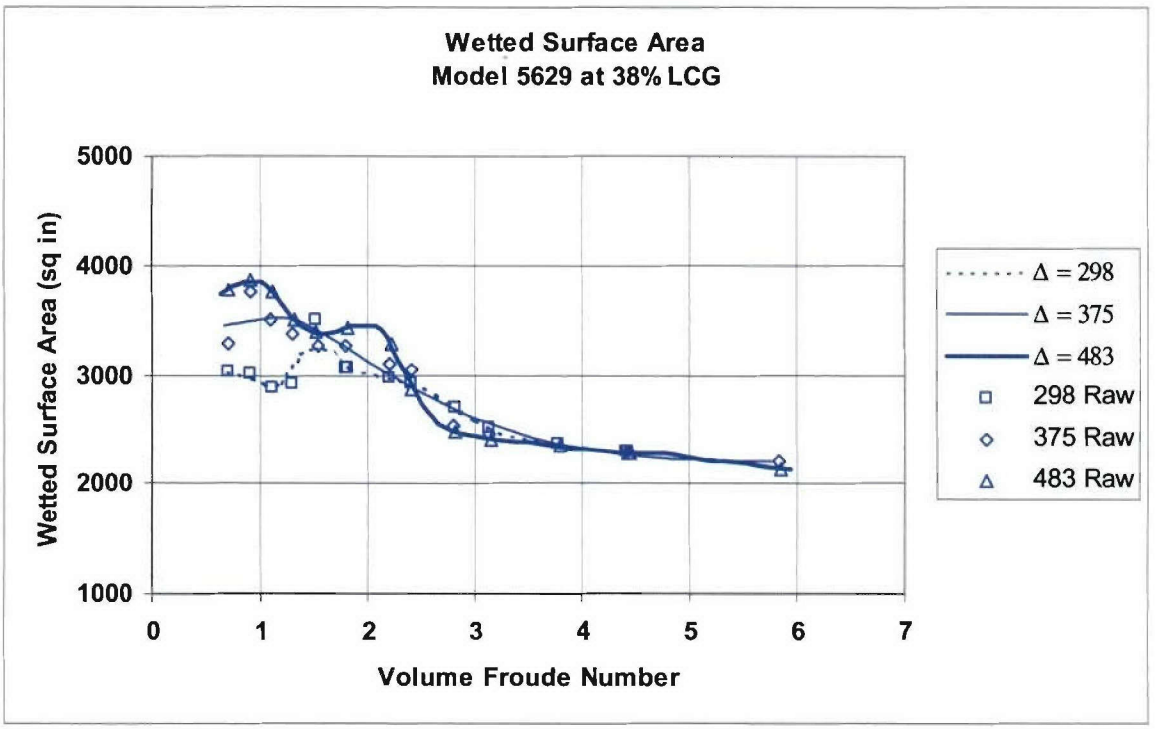

Figure 27. Model-Scale Dynamic Wetted Surface Area for Model 5629 at 38% LCG

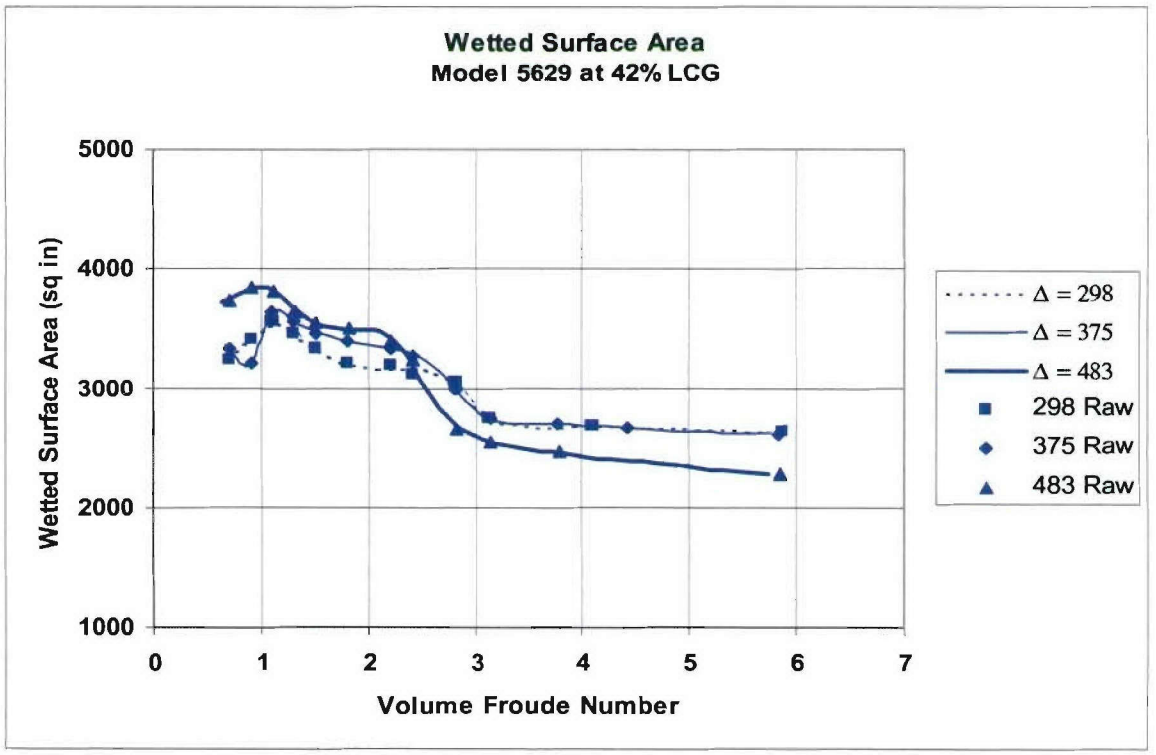

Figure 28. Model-Scale Dynamic Wetted Surface Area for Model 5629 at 42% LCG

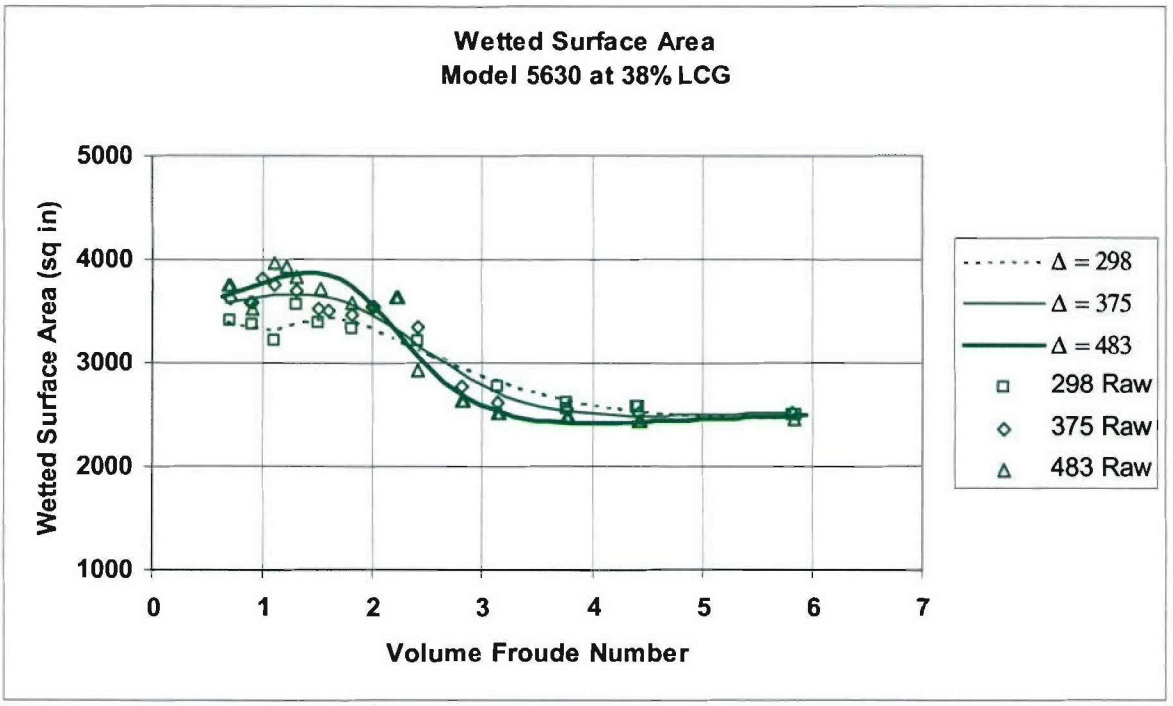

Figure 29. Model-Scale Dynamic Wetted Surface Area for Model 5630 at 38% LCG

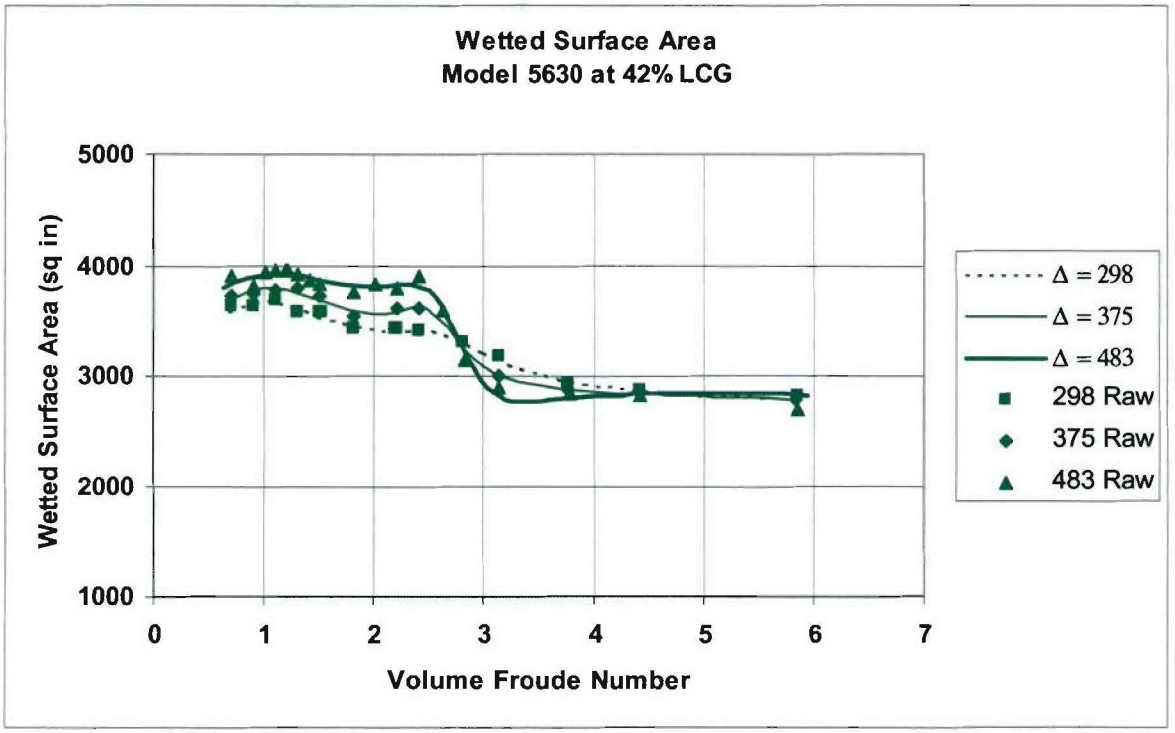

Figure 30. Model-Scale Dynamic Wetted Surface Area for Model 5630 at 42% LCG

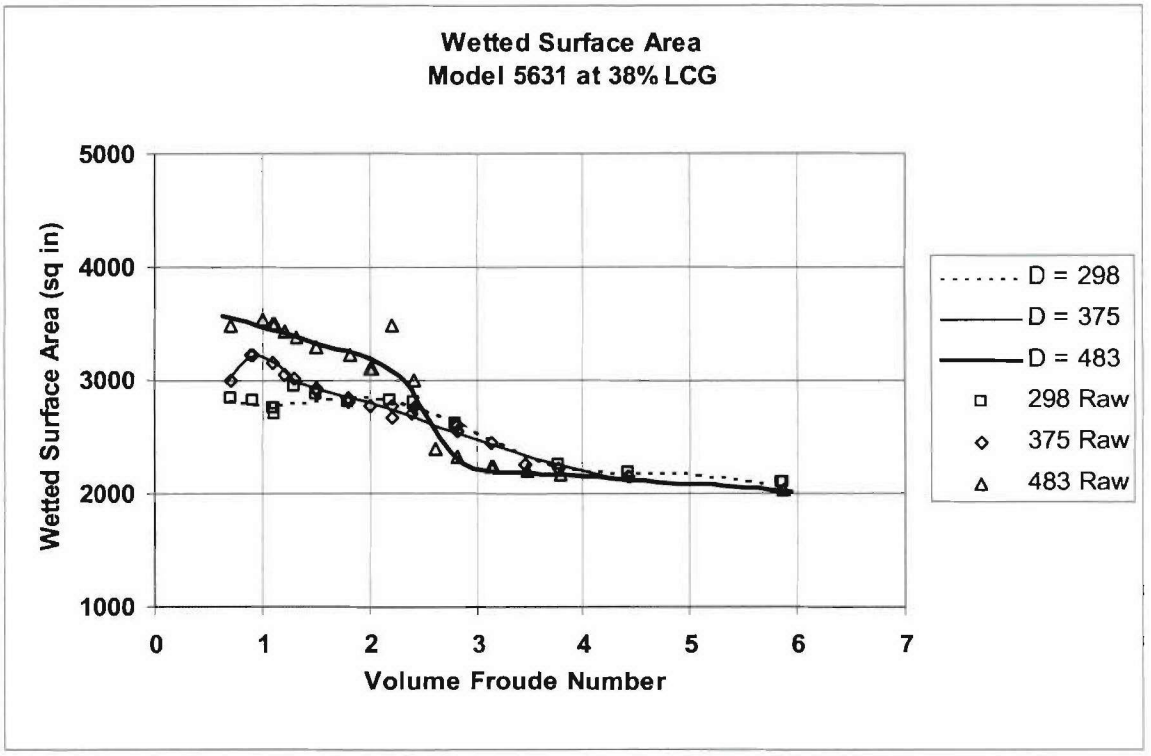

Figure 31. Model-Scale Dynamic Wetted Surface Area for Model 5631 at 38% LCG

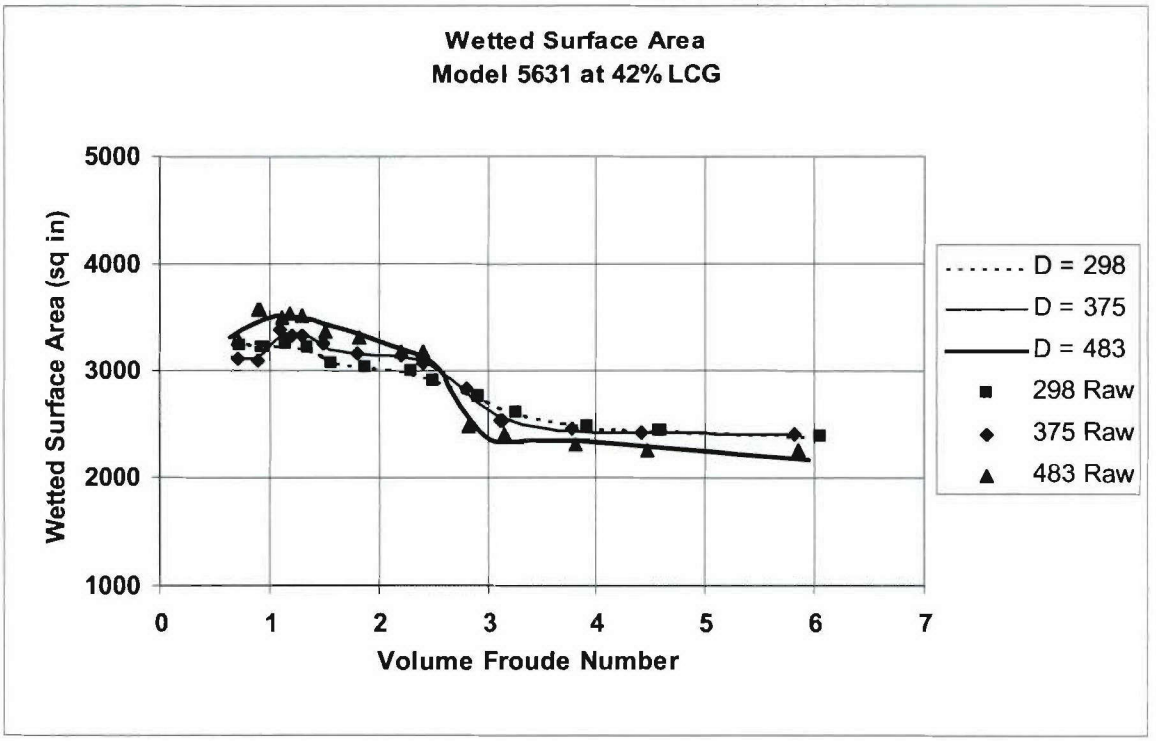

Figure 32. Model-Scale Dynamic Wetted Surface Area for Model 5631 at 42% LCG

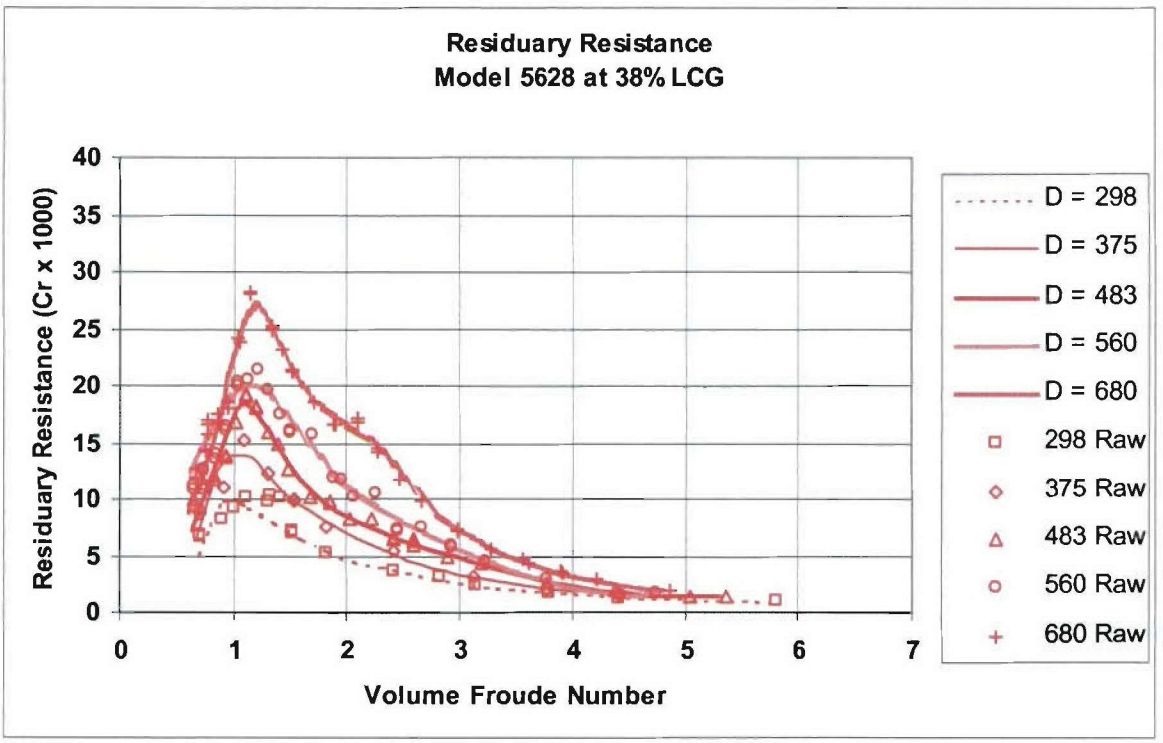

Figure 33. Residuary Resistance Coefficient for Model 5628 at 38% LCG

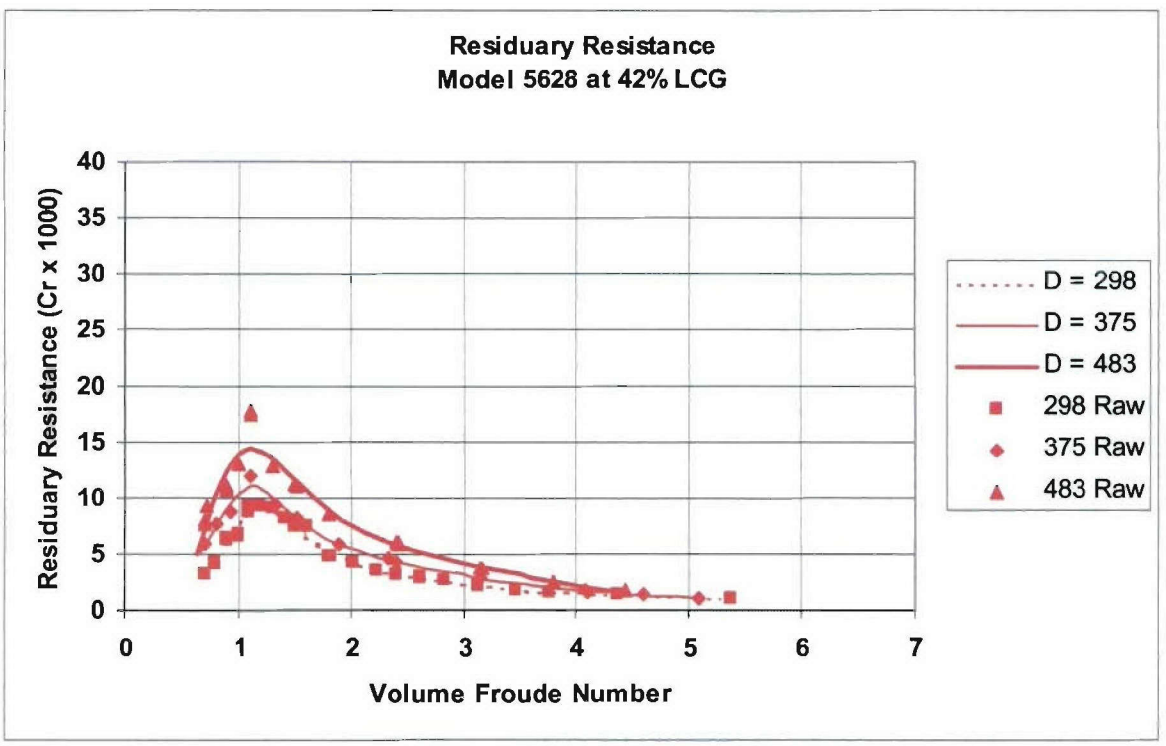

Figure 34. Residuary Resistance Coefficient for Model 5628 at 42% LCG

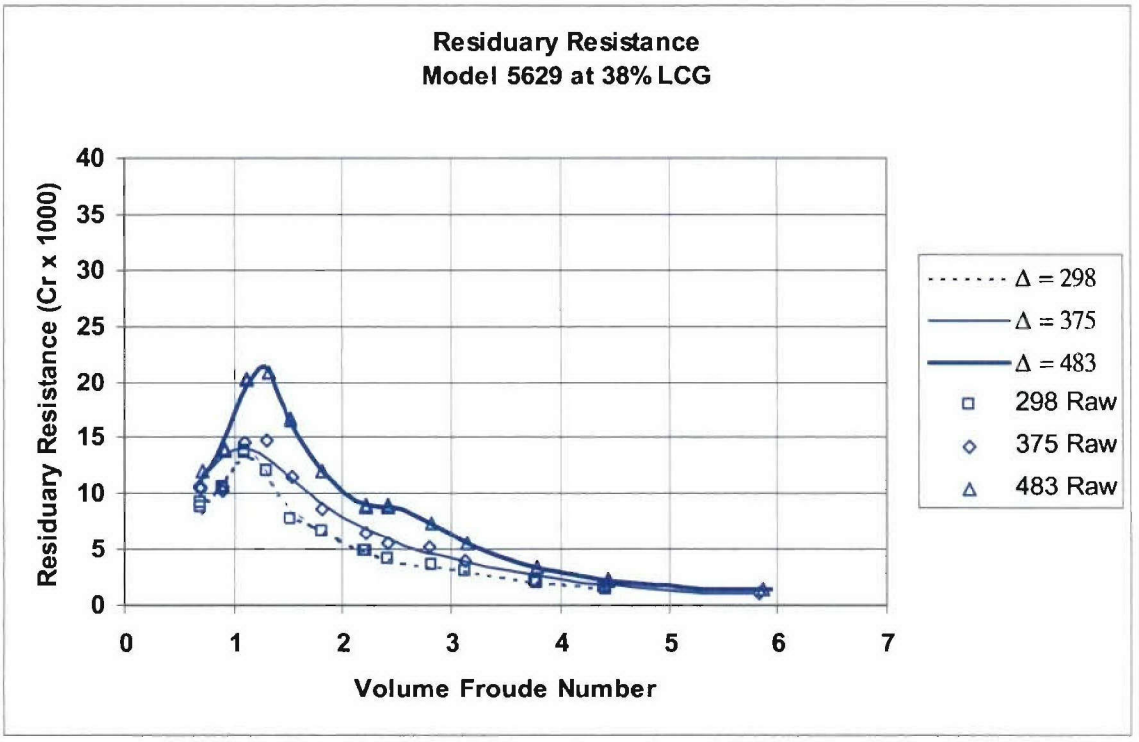

Figure 35. Residuary Resistance Coefficient for Model 5629 at 38% LCG

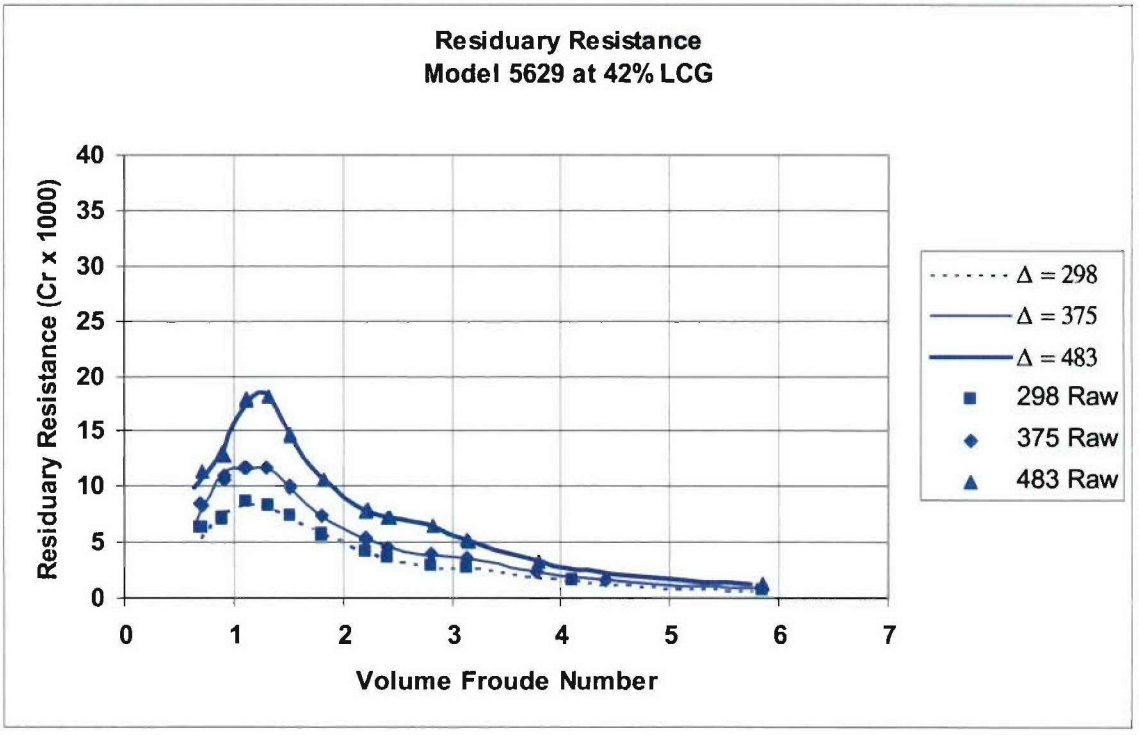

Figure 36. Residuary Resistance Coefficient for Model 5629 at 42% LCG

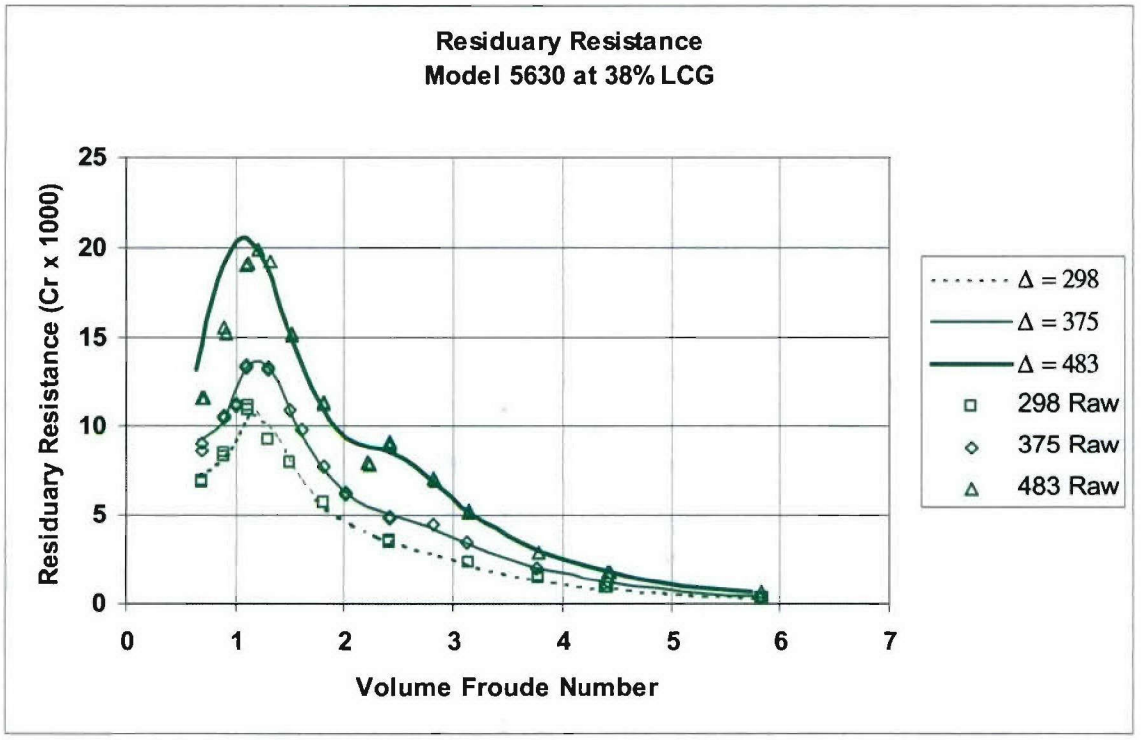

Figure 37. Residuary Resistance Coefficient for Model 5630 at 38% LCG

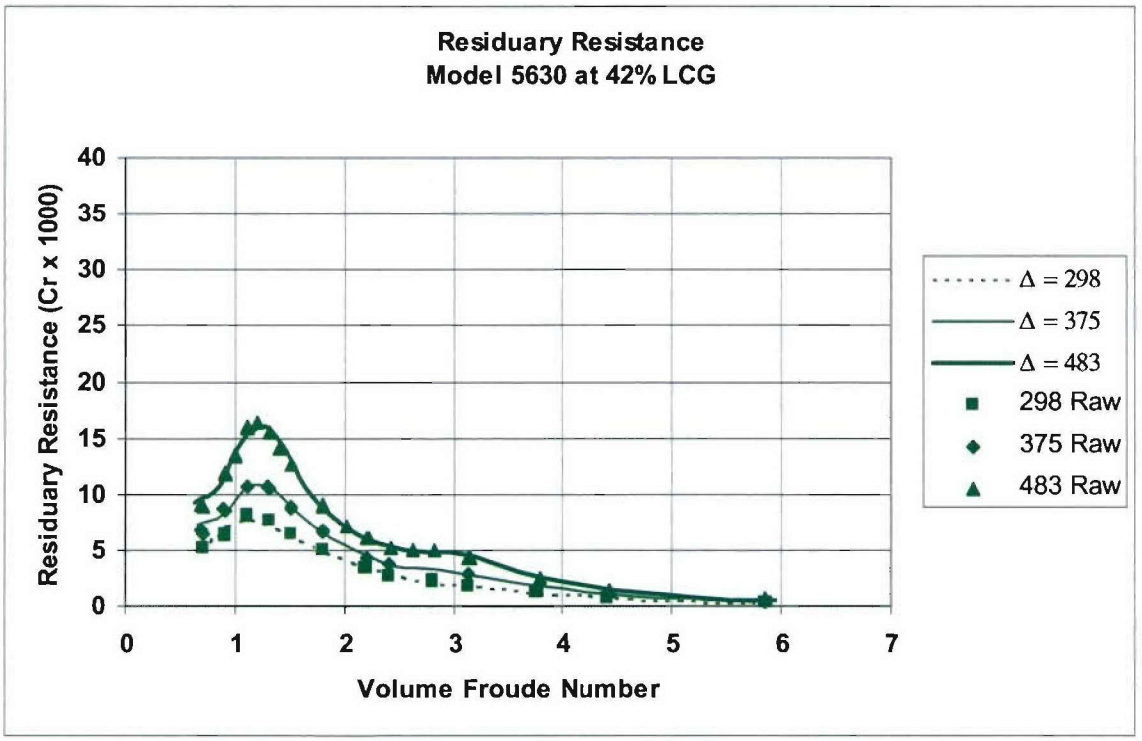

Figure 38. Residuary Resistance Coefficient for Model 5630 at 42% LCG

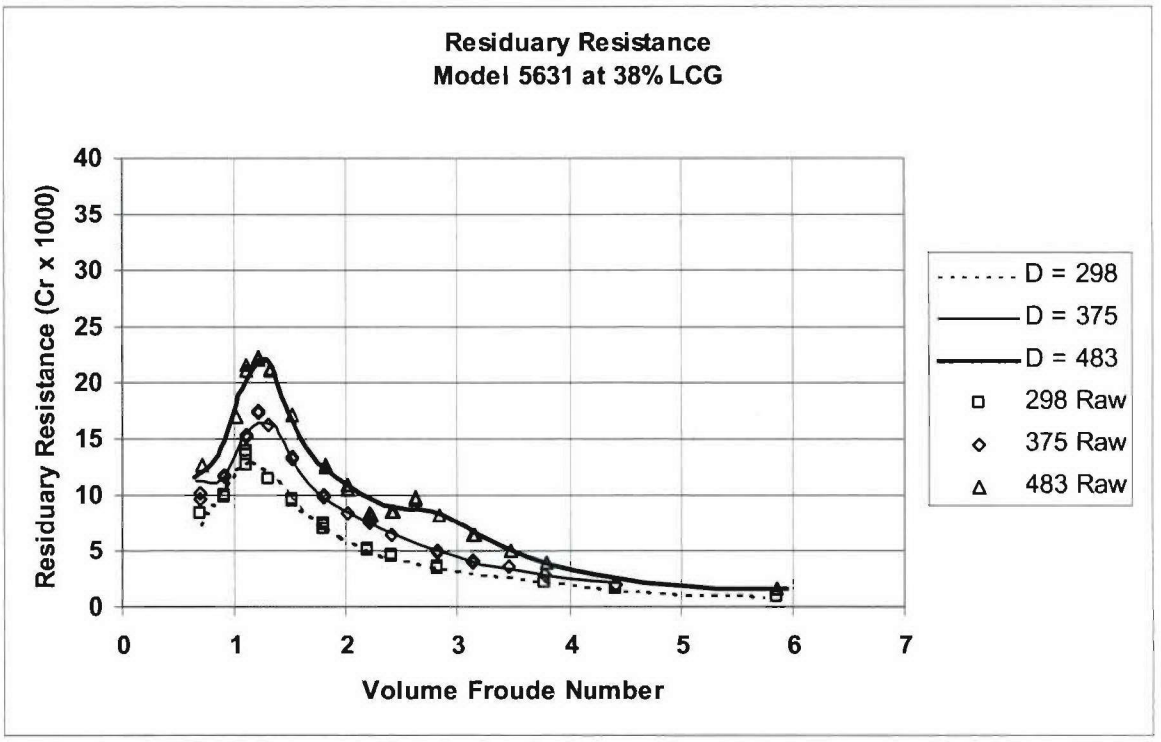

Figure 39. Residuary Resistance Coefficient for Model 5631 at 38% LCG

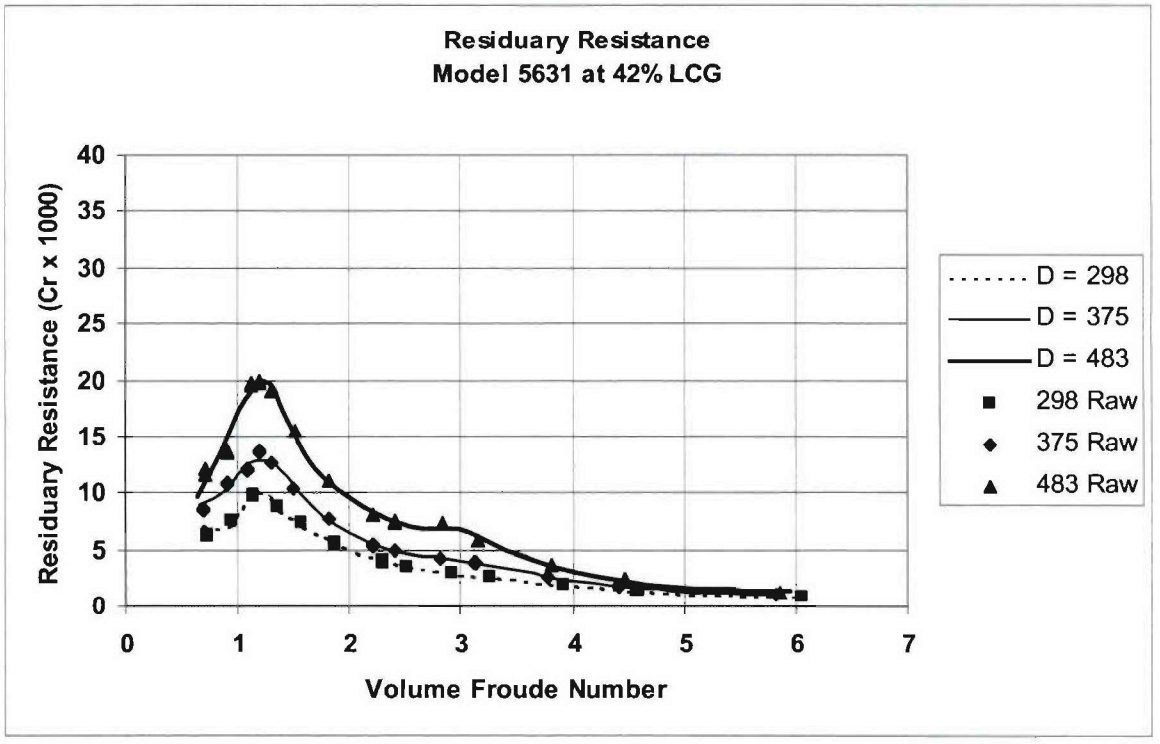

Figure 40. Residuary Resistance Coefficient for Model 5631 at 42% LCG

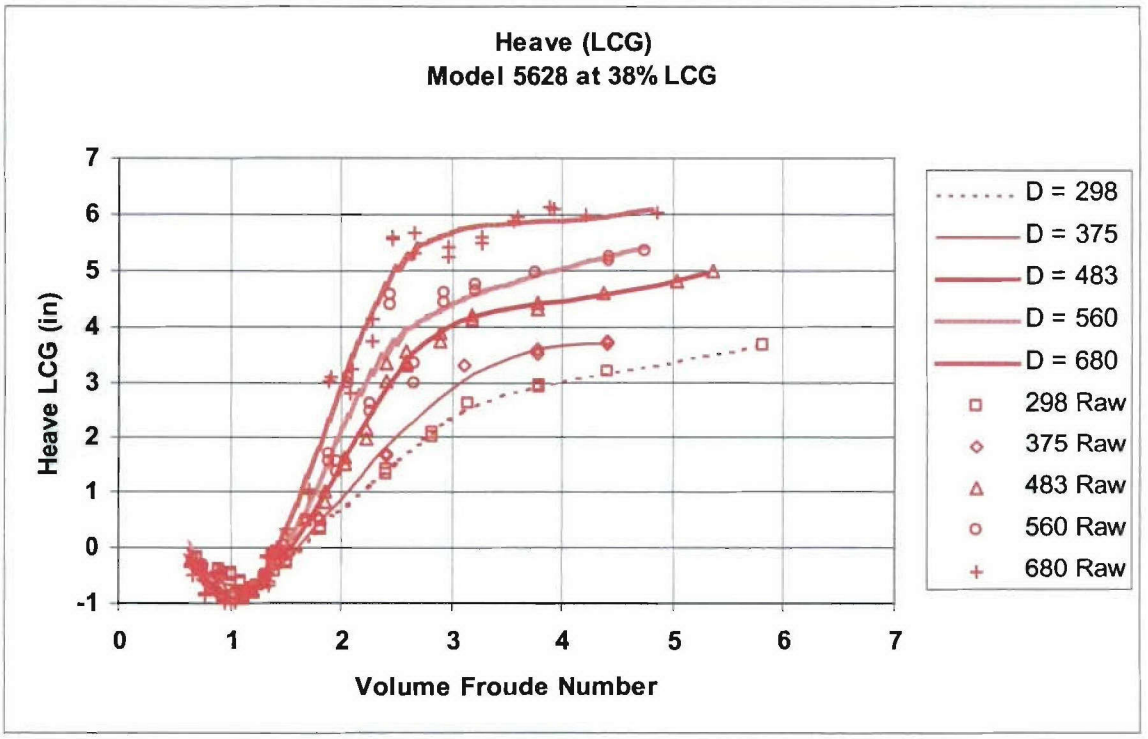

Figure 41. Model-Scale Center of Gravity Heave for Model 5628 at 38% LCG

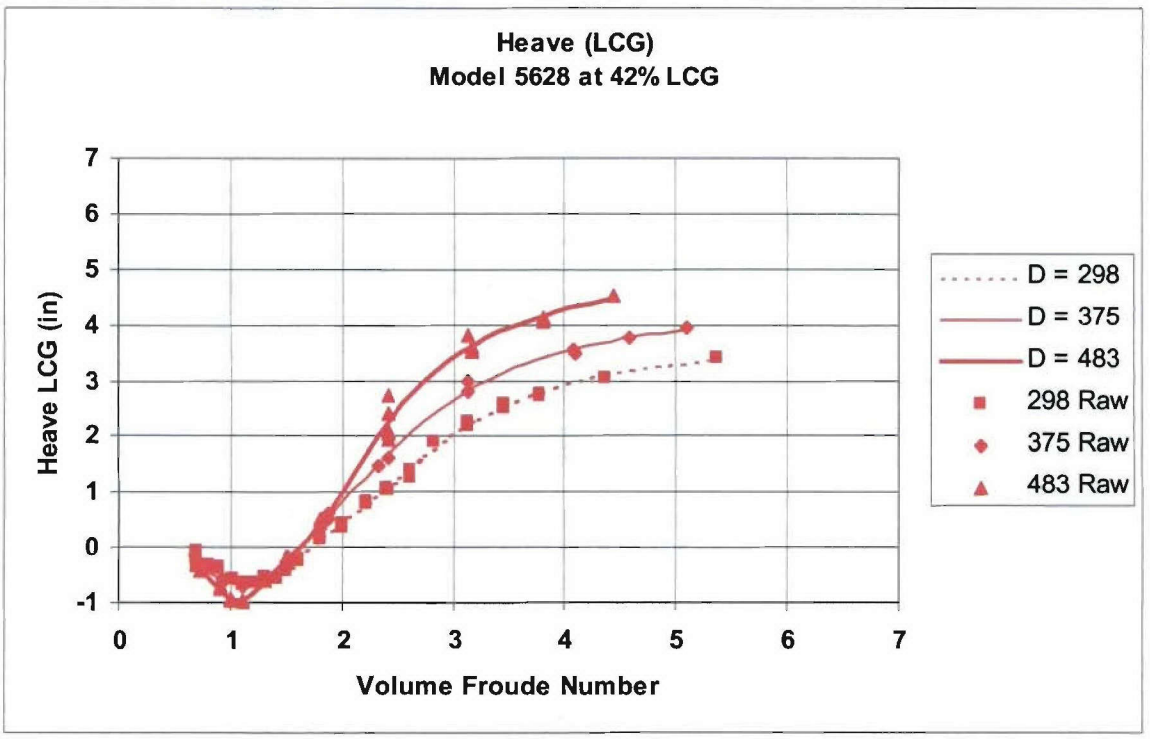

Figure 42. Model-Scale Center of Gravity Heave for Model 5628 at 42% LCG

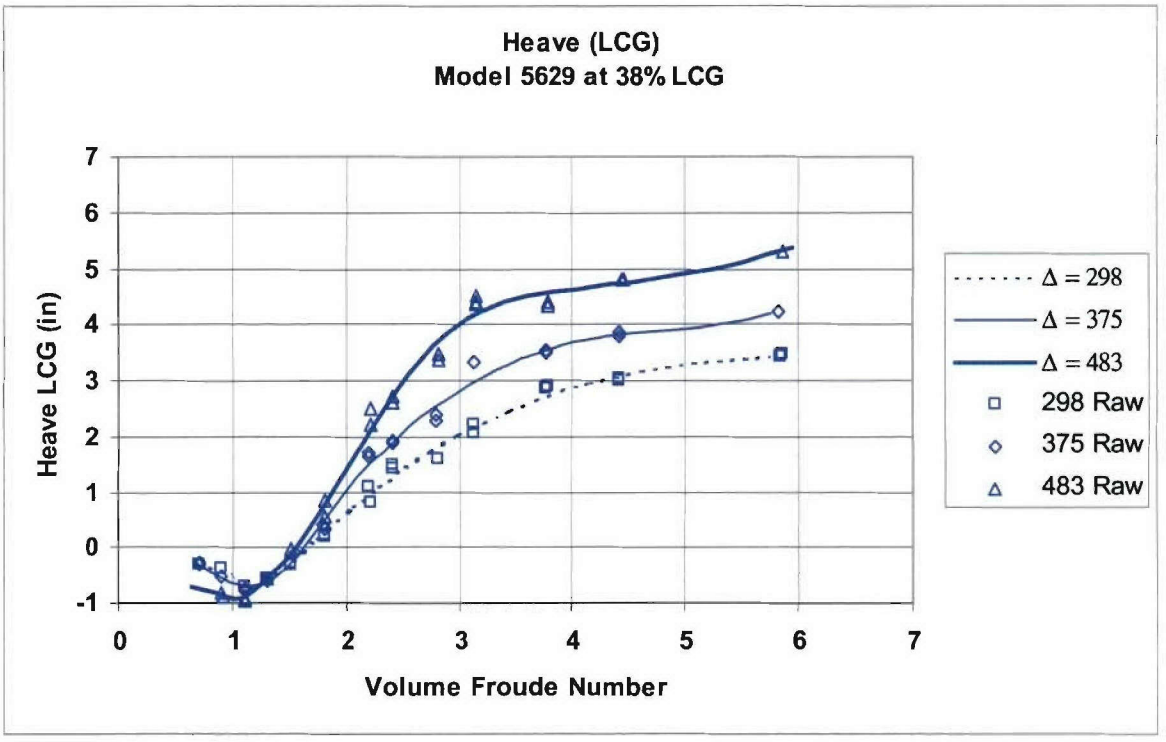

Figure 43. Model-Scale Center of Gravity Heave for Model 5629 at 38% LCG

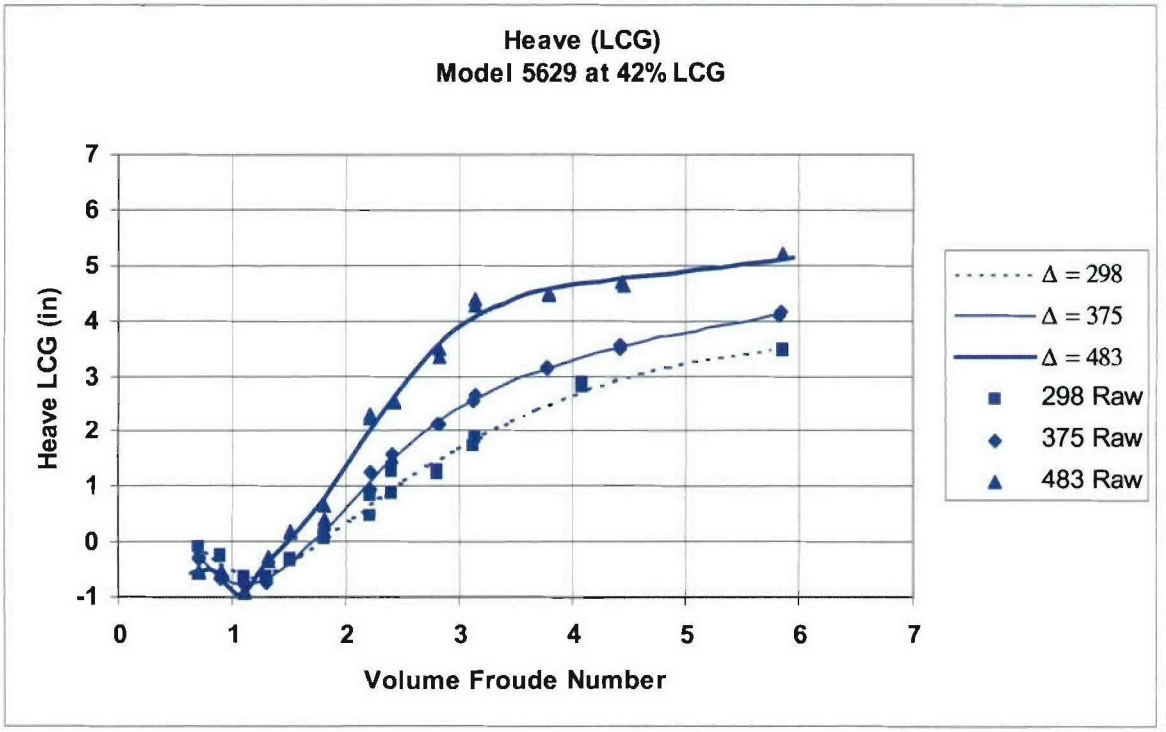

Figure 44. Model-Scale Center of Gravity Heave for Model 5629 at 42% LCG

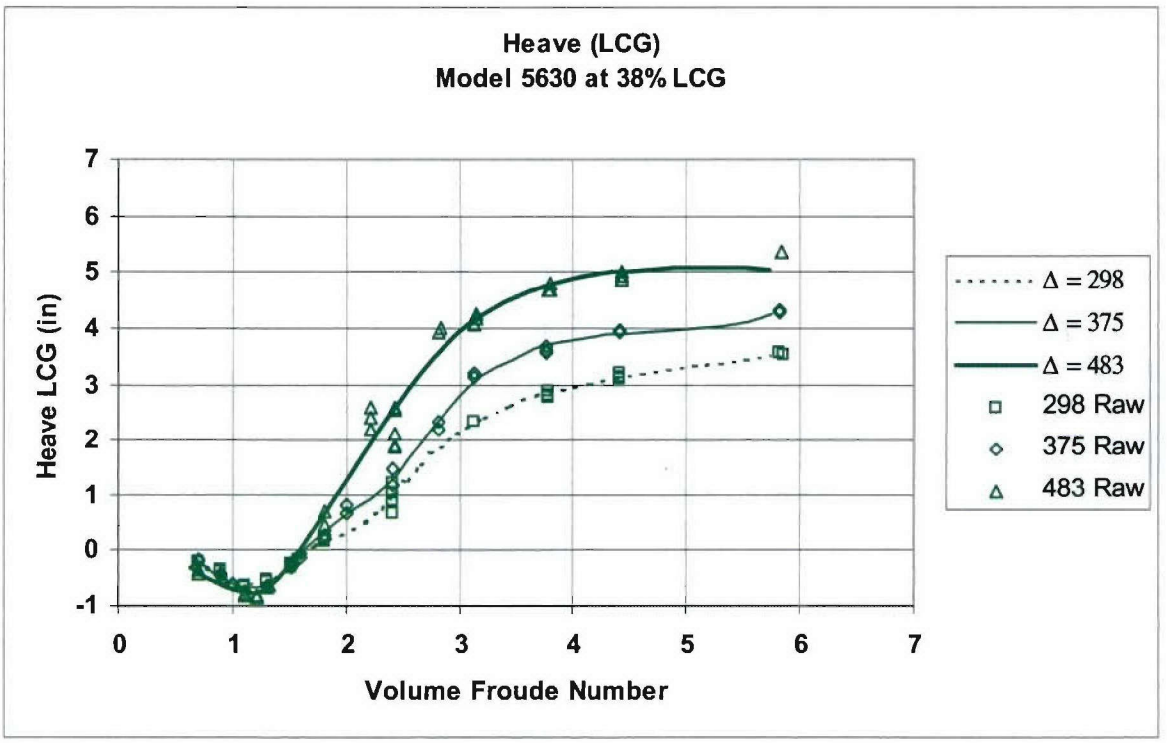

Figure 45. Model-Scale Center of Gravity Heave for Model 5630 at 38% LCG

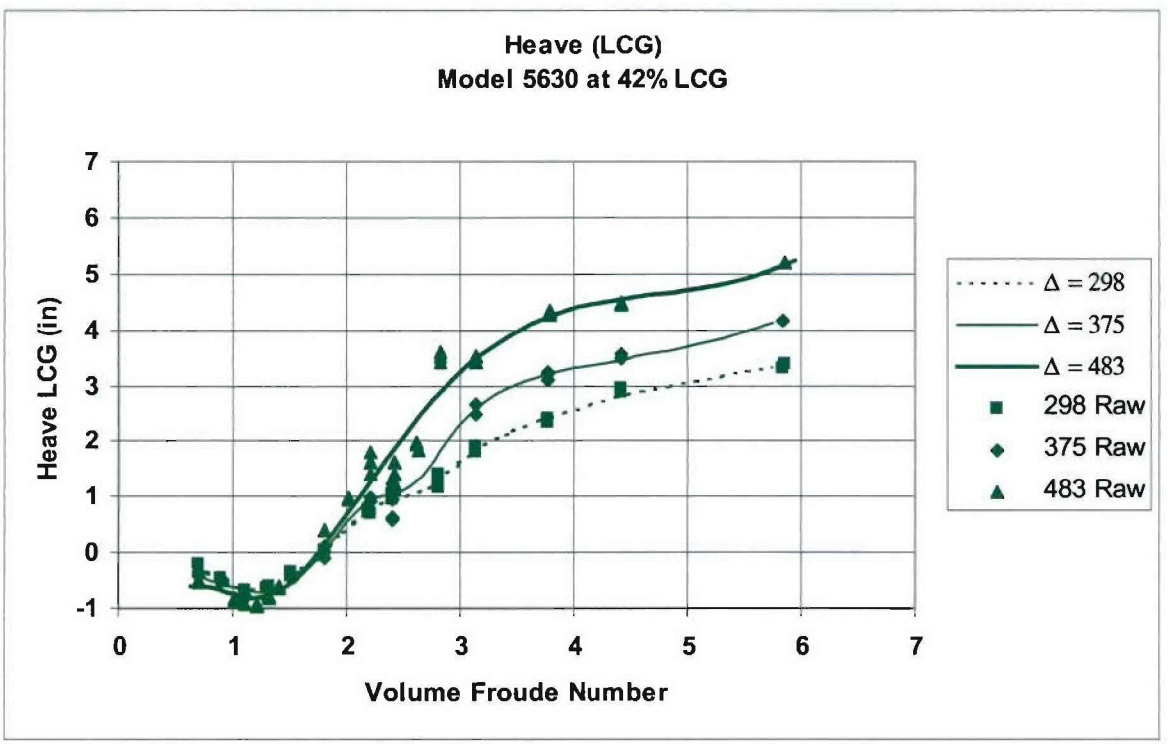

Figure 46. Model-Scale Center of Gravity Heave for Model 5630 at 42% LCG

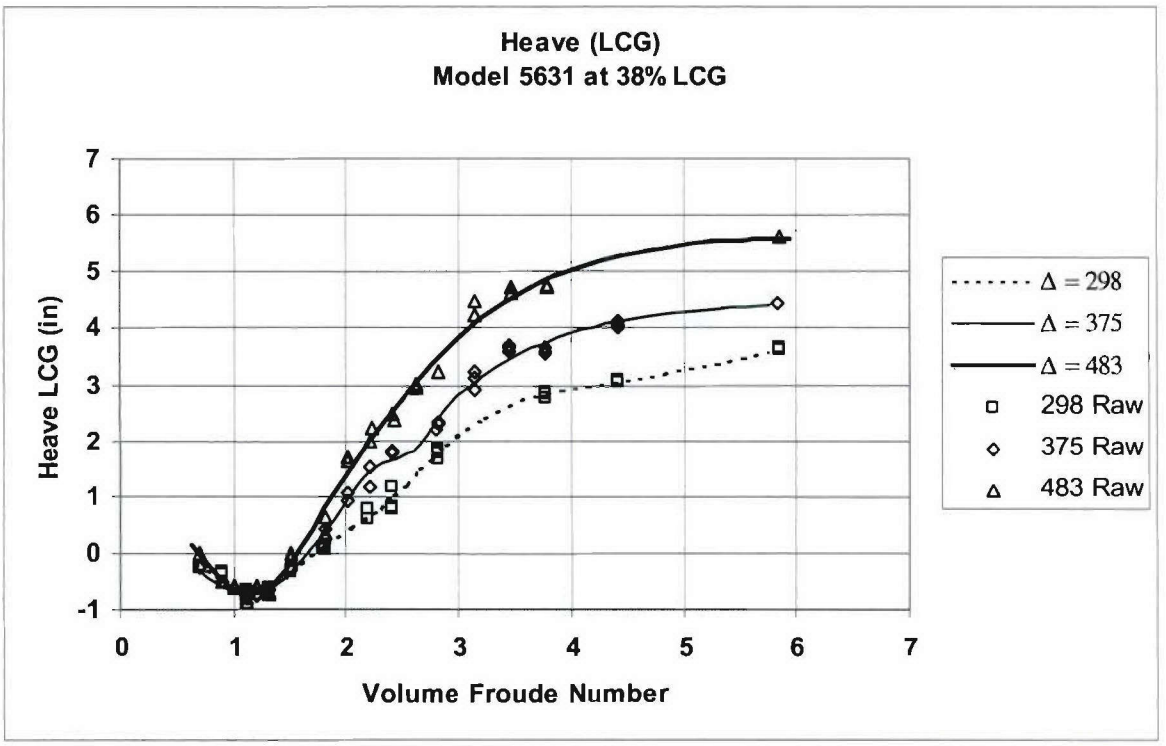

Figure 47. Model-Scale Center of Gravity Heave for Model 5631 at 38% LCG

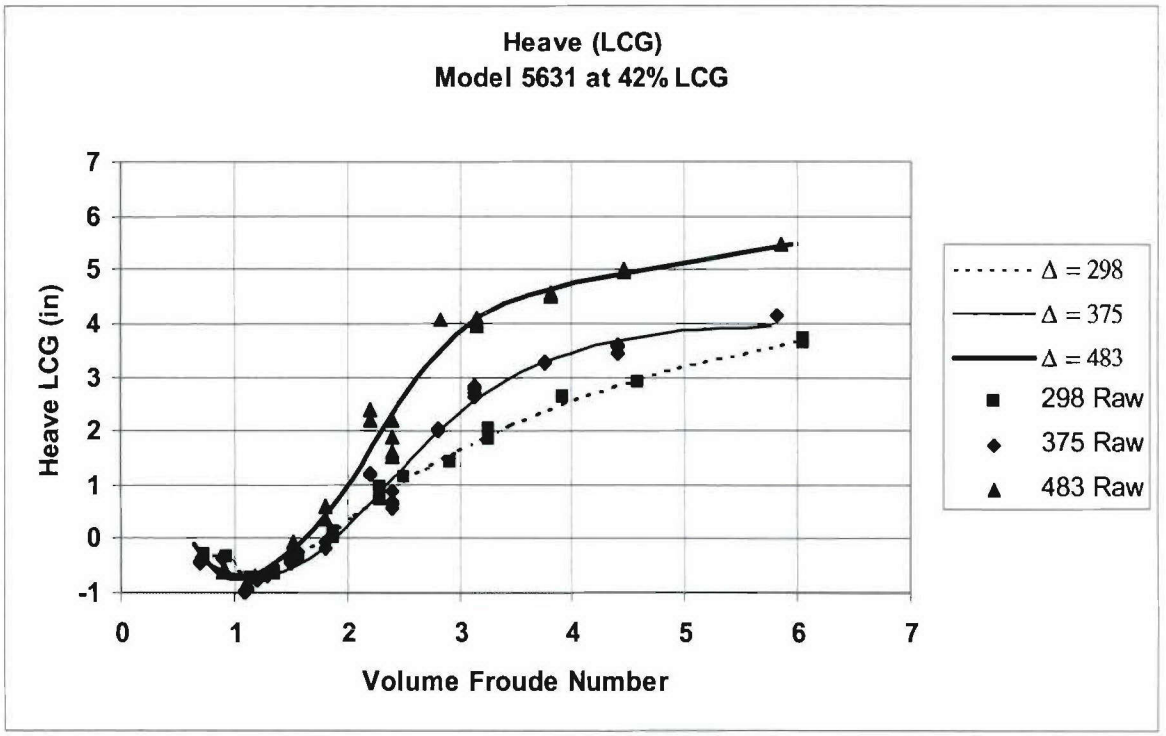

Figure 48. Model-Scale Center of Gravity Heave for Model 5631 at 42% LCG

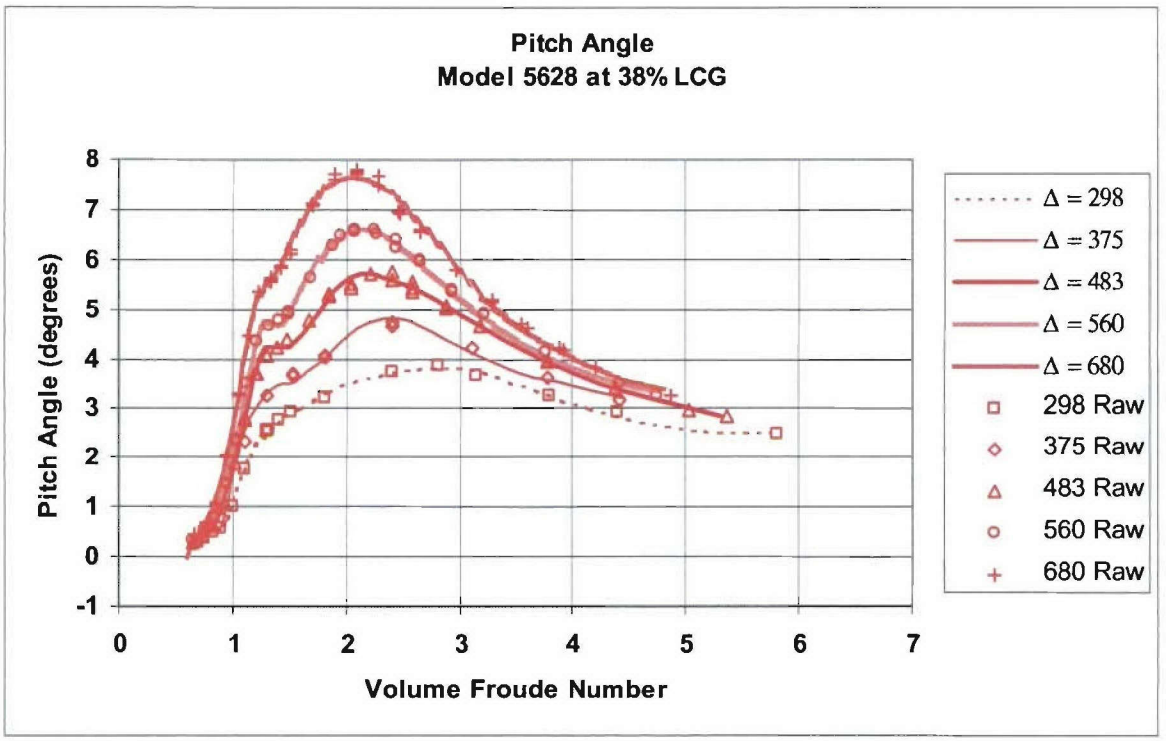

Figure 49. Pitch Angle for Model 5628 at 38% LCG

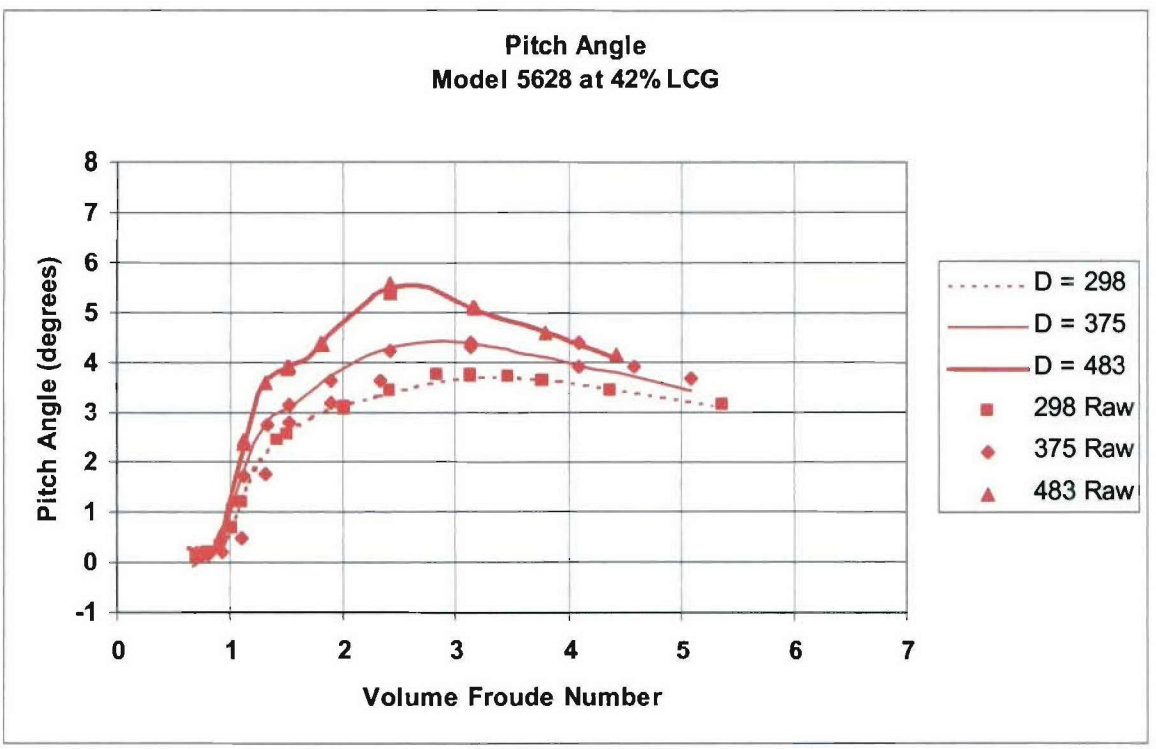

Figure 50. Pitch Angle for Model 5628 at 42% LCG

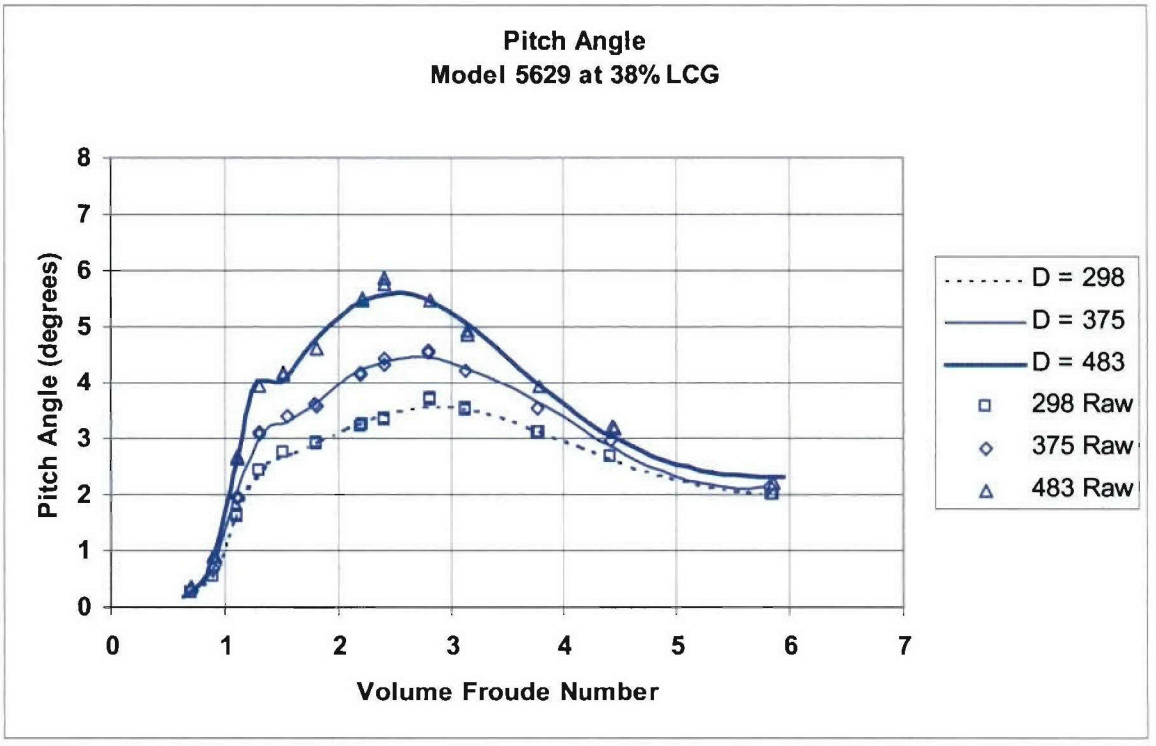

Figure 51. Pitch Angle for Model 5629 at 38% LCG

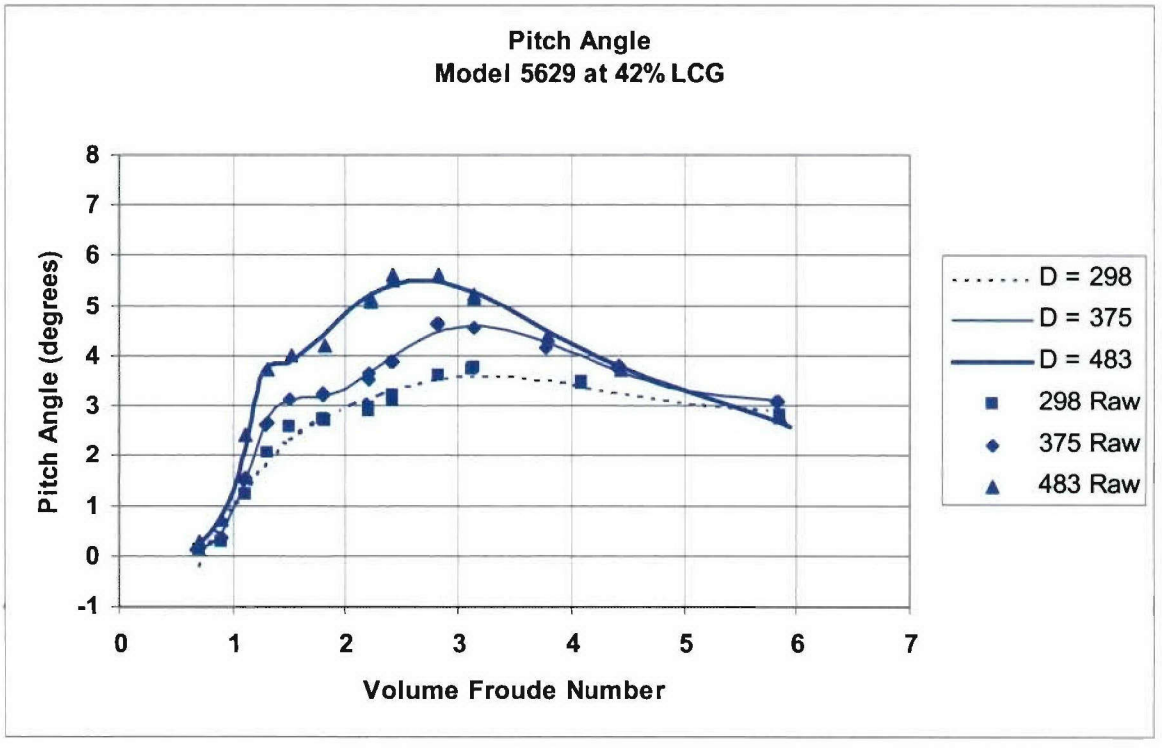

Figure 52. Pitch Angle for Model 5629 at 42% LCG

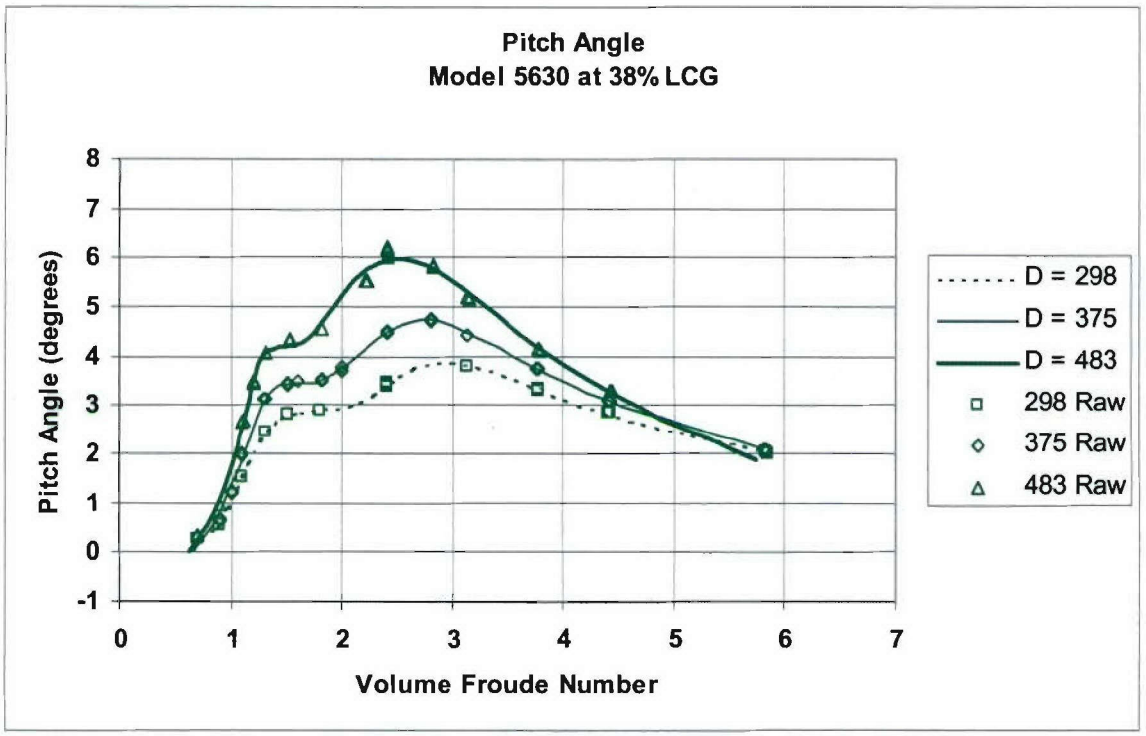

Figure 53. Pitch Angle for Model 5630 at 38% LCG

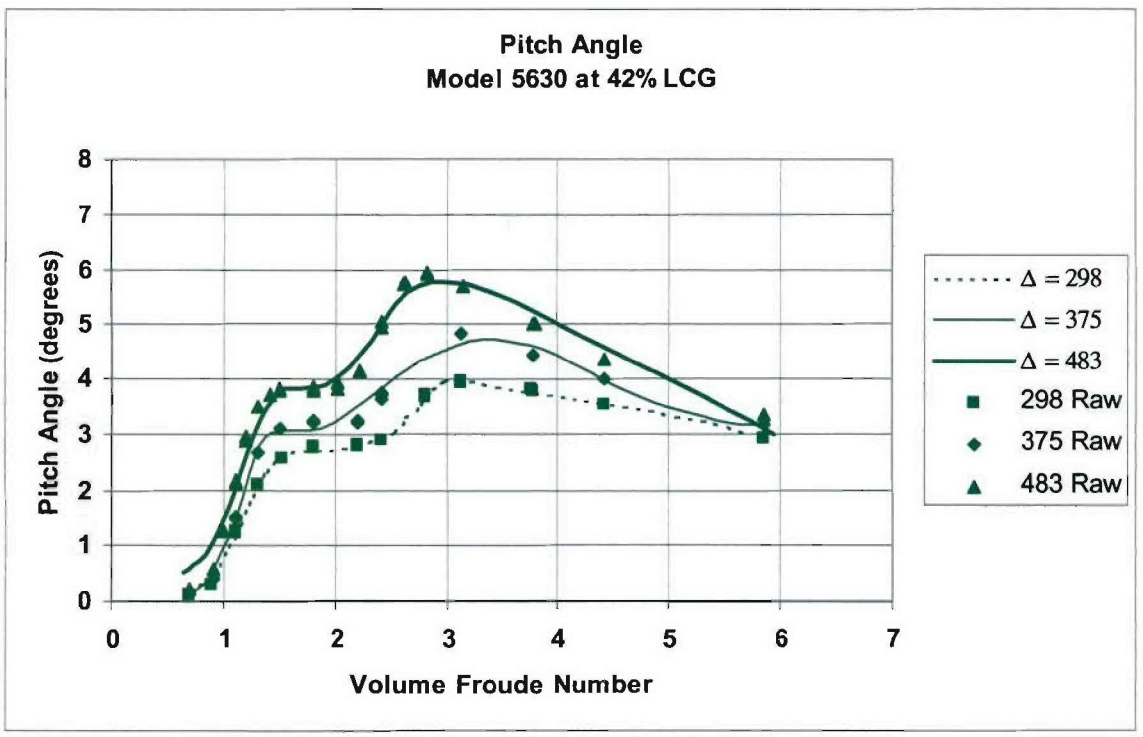

Figure 54. Pitch Angle for Model 5630 at 42% LCG

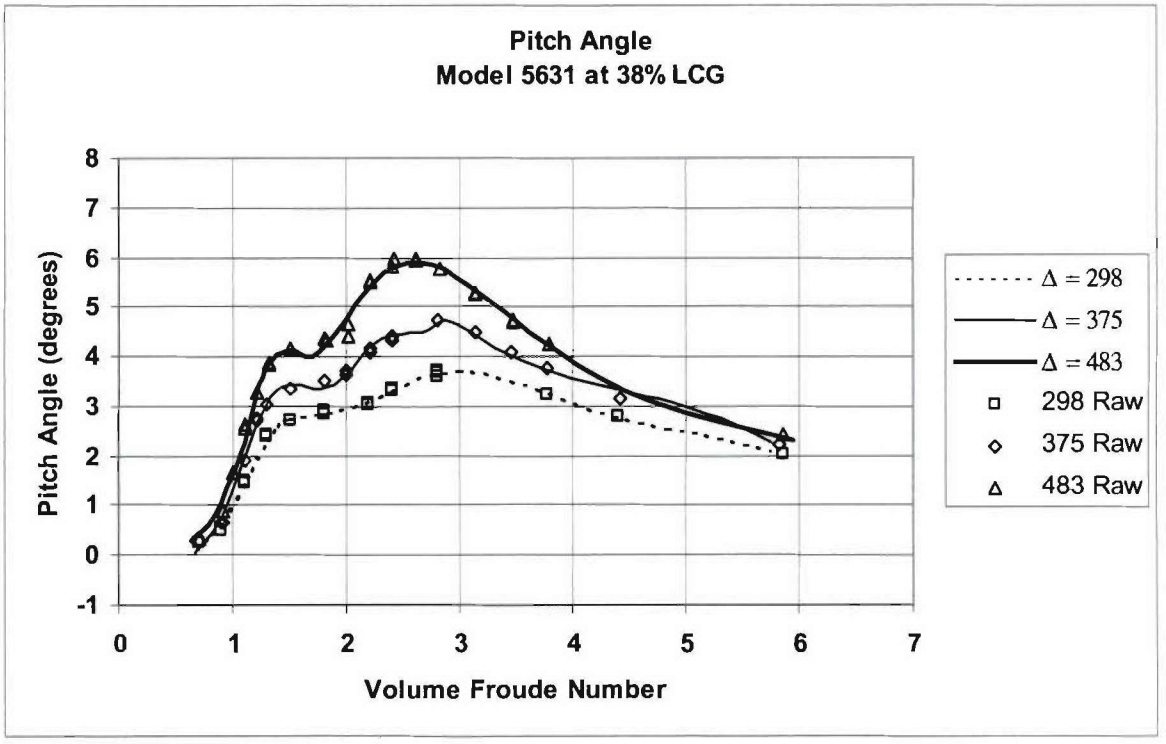

Figure 55. Pitch Angle for Model 5631 at 38% LCG

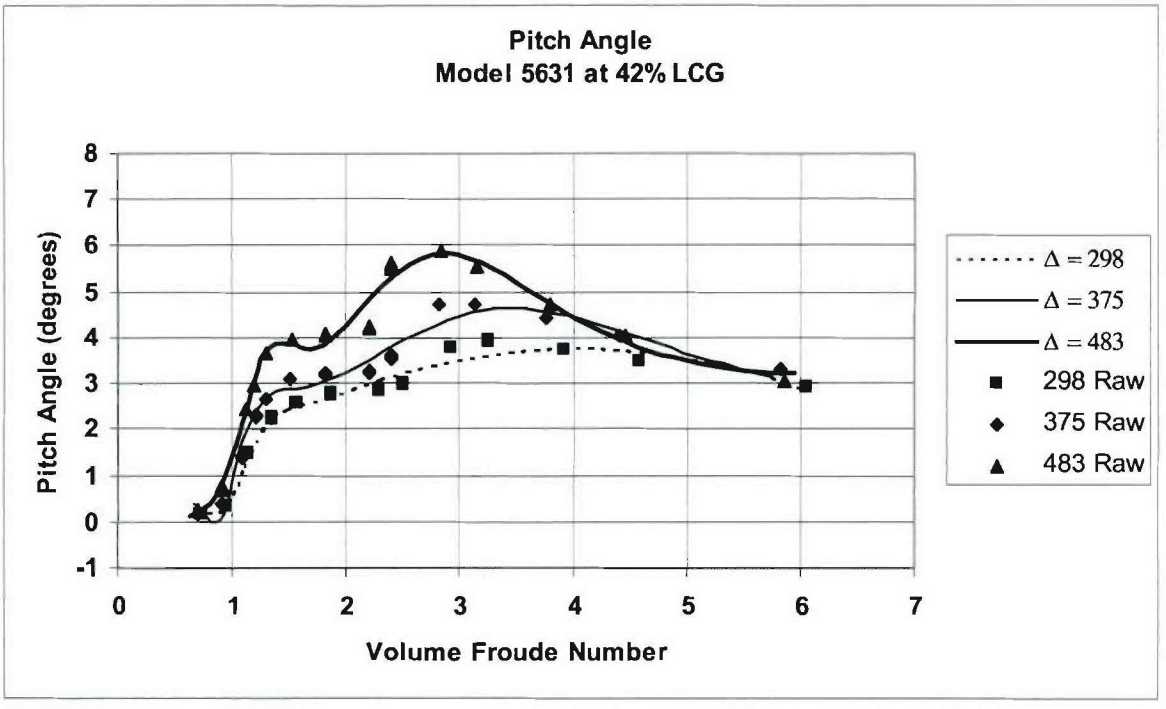

Figure 56. Pitch Angle for Model 5631 at 42% LCG

Table 5. Model-Scale RT/Displ at 298 Lbs of Displacement

Test #	8	5	22	25	10	13	16	19
Model #	**5628**	**5628**	**5629**	**5629**	**5630**	**5630**	**5631**	**5631**
Δ =	298	298	298	298	298	298	298	298
LCG	**38%**	**42%**	**38%**	**42%**	**38%**	**42%**	**38%**	**42%**

V_m (knots)	R_T/Δ Lbs/Lbs	R_T/Δ Lbs/Lbs	R_T/Δ Lbs/Lbs	R_T/Δ Lbs/Lbs	R_T/Δ Lbs/Lbs	R_T/Δ Lbs/Lbs	R_T/Δ Lbs/Lbs	R_T/Δ Lbs/Lbs
0	0.0000	0.0000	0.0000	0.0000	0.0000	0.0000	0.0000	0.0000
1	0.0039	0.0052	0.0066	0.0027	0.0063	0.0028	0.0054	0.0106
2	0.0099	0.0098	0.0123	0.0069	0.0127	0.0070	0.0102	0.0176
3	0.0169	0.0172	0.0205	0.0167	0.0210	0.0170	0.0176	0.0199
4	0.0461	0.0368	0.0446	0.0388	0.0394	0.0390	0.0405	0.0342
5	0.0727	0.0663	0.0763	0.0661	0.0735	0.0638	0.0721	0.0680
6	0.0945	0.0883	0.0959	0.0861	0.0957	0.0828	0.0922	0.0848
7	0.1111	0.1034	0.1087	0.1004	0.1063	0.0972	0.1053	0.0968
8	0.1240	0.1167	0.1194	0.1125	0.1155	0.1094	0.1162	0.1080
9	0.1349	0.1302	0.1292	0.1239	0.1257	0.1206	0.1262	0.1191
10	0.1447	0.1441	0.1387	0.1352	0.1366	0.1311	0.1358	0.1302
11	0.1542	0.1576	0.1478	0.1463	0.1473	0.1414	0.1450	0.1413
12	0.1635	0.1702	0.1567	0.1575	0.1569	0.1515	0.1539	0.1524
13	0.1729	0.1819	0.1654	0.1687	0.1647	0.1616	0.1625	0.1636
14	0.1824	0.1933	0.1740	0.1800	0.1708	0.1717	0.1708	0.1747
15	0.1921	0.2048	0.1825	0.1915	0.1762	0.1820	0.1791	0.1860
16	0.2022	0.2166	0.1912	0.2033	0.1820	0.1924	0.1873	0.1972
17	0.2127	0.2290	0.2000	0.2153	0.1890	0.2032	0.1956	0.2086
18	0.2237	0.2418	0.2093	0.2278	0.1974	0.2142	0.2041	0.2201
19	0.2353	0.2553	0.2190	0.2408	0.2071	0.2258	0.2131	0.2318
20	0.2476	0.2692	0.2296	0.2544	0.2179	0.2378	0.2226	0.2438
21	0.2607	0.2837	0.2412	0.2687	0.2296	0.2505	0.2329	0.2562
22	0.2747	0.2986	0.2541	0.2838	0.2420	0.2639	0.2444	0.2691
23	0.2898	0.3142	0.2688	0.3000	0.2550	0.2781	0.2573	0.2829
24	0.3062	0.3302	0.2860	0.3174	0.2684	0.2934	0.2721	0.2979
25	0.3239		0.3064	0.3362	0.2822	0.3097	0.2894	0.3149
26								0.3353
27								
28								

Table 6. Model-Scale RT/Displ at 375 Lbs of Displacement

Test #	9	6	23	26	11	14	17	20
Model #	**5628**	**5628**	**5629**	**5629**	**5630**	**5630**	**5631**	**5631**
Δ =	375	375	375	375	375	375	375	375
LCG	**38%**	**42%**	**38%**	**42%**	**38%**	**42%**	**38%**	**42%**

V_m (knots)	R_T/Δ Lbs/Lbs	R_T/Δ Lbs/Lbs	R_T/Δ Lbs/Lbs	R_T/Δ Lbs/Lbs	R_T/Δ Lbs/Lbs	R_T/Δ Lbs/Lbs	R_T/Δ Lbs/Lbs	R_T/Δ Lbs/Lbs
0	0.0000	0.0000	0.0000	0.0000	0.0000	0.0000	0.0000	0.0000
1	0.0054	0.0029	0.0025	0.0061	0.0094	0.0048	0.0043	0.0044
2	0.0119	0.0065	0.0087	0.0091	0.0138	0.0100	0.0104	0.0097
3	0.0159	0.0149	0.0222	0.0159	0.0208	0.0179	0.0200	0.0177
4	0.0467	0.0367	0.0464	0.0375	0.0396	0.0352	0.0383	0.0346
5	0.0785	0.0693	0.0768	0.0680	0.0769	0.0667	0.0751	0.0676
6	0.1038	0.0943	0.1023	0.0945	0.1079	0.0931	0.1061	0.0948
7	0.1209	0.1101	0.1192	0.1074	0.1195	0.1056	0.1127	0.1045
8	0.1320	0.1224	0.1305	0.1168	0.1247	0.1136	0.1210	0.1117
9	0.1397	0.1335	0.1391	0.1264	0.1315	0.1221	0.1322	0.1211
10	0.1459	0.1441	0.1466	0.1363	0.1416	0.1319	0.1430	0.1319
11	0.1517	0.1541	0.1533	0.1460	0.1530	0.1424	0.1518	0.1430
12	0.1574	0.1635	0.1595	0.1553	0.1618	0.1527	0.1587	0.1531
13	0.1635	0.1723	0.1652	0.1641	0.1662	0.1616	0.1639	0.1621
14	0.1700	0.1806	0.1705	0.1723	0.1682	0.1688	0.1684	0.1700
15	0.1769	0.1888	0.1756	0.1801	0.1699	0.1748	0.1725	0.1772
16	0.1844	0.1969	0.1805	0.1877	0.1725	0.1806	0.1768	0.1842
17	0.1924	0.2053	0.1854	0.1953	0.1762	0.1867	0.1815	0.1913
18	0.2010	0.2141	0.1905	0.2030	0.1810	0.1936	0.1867	0.1988
19	0.2101	0.2237	0.1959	0.2113	0.1867	0.2013	0.1926	0.2069
20	0.2197	0.2342	0.2018	0.2202	0.1934	0.2098	0.1993	0.2155
21		0.2457	0.2085	0.2301	0.2008	0.2192	0.2069	0.2249
22		0.2584	0.2163	0.2410	0.2091	0.2293	0.2153	0.2350
23		0.2724	0.2255	0.2532	0.2180	0.2400	0.2247	0.2460
24			0.2369	0.2667	0.2277	0.2515	0.2351	0.2577
25			0.2511	0.2817	0.2382	0.2636	0.2466	0.2703
26			0.2694	0.2982	0.2494	0.2763	0.2593	0.2838
27								
28								

Table 7. Model-Scale RT/Displ at 483 Lbs of Displacement

Test #	2	7	24	27	12	15	18	21
Model #	**5628**	**5628**	**5629**	**5629**	**5630**	**5630**	**5631**	**5631**
Δ =	483	483	483	483	483	483	483	483
LCG	**38%**	**42%**	**38%**	**42%**	**38%**	**42%**	**38%**	**42%**

V_m (knots)	R_T/Δ Lbs/Lbs	R_T/Δ Lbs/Lbs	R_T/Δ Lbs/Lbs	R_T/Δ Lbs/Lbs	R_T/Δ Lbs/Lbs	R_T/Δ Lbs/Lbs	R_T/Δ Lbs/Lbs	R_T/Δ Lbs/Lbs
0	0.0000	0.0000	0.0000	0.0000	0.0000	0.0000	0.0000	0.0000
1	0.0022	0.0000	0.0023	0.0022	0.0009	0.0062	0.0039	0.0006
2	0.0060	0.0010	0.0076	0.0072	0.0064	0.0099	0.0096	0.0048
3	0.0156	0.0121	0.0186	0.0176	0.0214	0.0170	0.0191	0.0155
4	0.0408	0.0376	0.0405	0.0381	0.0505	0.0344	0.0375	0.0372
5	0.0808	0.0714	0.0820	0.0756	0.0887	0.0691	0.0775	0.0744
6	0.1142	0.1005	0.1235	0.1134	0.1208	0.1065	0.1216	0.1139
7	0.1332	0.1205	0.1317	0.1240	0.1381	0.1223	0.1308	0.1251
8	0.1435	0.1340	0.1410	0.1313	0.1452	0.1250	0.1372	0.1288
9	0.1499	0.1437	0.1535	0.1421	0.1504	0.1291	0.1487	0.1385
10	0.1545	0.1512	0.1633	0.1525	0.1603	0.1394	0.1610	0.1501
11	0.1581	0.1575	0.1692	0.1605	0.1742	0.1527	0.1710	0.1600
12	0.1613	0.1633	0.1720	0.1660	0.1816	0.1636	0.1773	0.1674
13	0.1643	0.1687	0.1732	0.1696	0.1804	0.1699	0.1803	0.1726
14	0.1672	0.1739	0.1736	0.1722	0.1768	0.1730	0.1810	0.1762
15	0.1702	0.1791	0.1740	0.1744	0.1741	0.1750	0.1806	0.1788
16	0.1734	0.1843	0.1748	0.1767	0.1729	0.1770	0.1799	0.1808
17	0.1770	0.1896	0.1761	0.1792	0.1731	0.1795	0.1795	0.1828
18	0.1810	0.1952	0.1782	0.1822	0.1745	0.1827	0.1798	0.1848
19	0.1855	0.2009	0.1810	0.1858	0.1769	0.1866	0.1809	0.1872
20	0.1908	0.2068	0.1847	0.1902	0.1802	0.1912	0.1831	0.1900
21	0.1970	0.2131	0.1893	0.1953	0.1843	0.1966	0.1865	0.1936
22	0.2042		0.1948	0.2013	0.1891	0.2025	0.1910	0.1980
23	0.2129		0.2013	0.2083	0.1947	0.2092	0.1969	0.2034
24	0.2234		0.2090	0.2164	0.2009	0.2165	0.2042	0.2100
25	0.2362		0.2178	0.2257	0.2078	0.2244	0.2131	0.2182
26			0.2281	0.2364	0.2154	0.2331	0.2238	0.2284
27			0.2400	0.2487	0.2238	0.2424	0.2365	0.2411
28			0.2538	0.2628		0.2525	0.2517	0.2572

Table 8. Model-Scale RT/Displ at 560 Lbs of Displacement

Test #	3
Model #	**5628**
Δ =	560
LCG	**38%**

V_m (knots)	R_T/Δ Lbs/Lbs
0	0.0000
1	0.0014
2	0.0068
3	0.0200
4	0.0452
5	0.0812
6	0.1171
7	0.1418
8	0.1555
9	0.1639
10	0.1697
11	0.1728
12	0.1733
13	0.1721
14	0.1703
15	0.1689
16	0.1684
17	0.1691
18	0.1710
19	0.1743
20	0.1791
21	0.1856
22	0.1939
23	0.2045
24	
25	
26	
27	
28	

Table 9. Model-Scale RT/Displ at 680 Lbs of Displacement

Test #	4
Model #	**5628**
Δ =	680
LCG	**38%**

V_m (knots)	R_T/Δ Lbs/Lbs
0	0.0000
1	0.0011
2	0.0050
3	0.0151
4	0.0388
5	0.0861
6	0.1404
7	0.1617
8	0.1739
9	0.1884
10	0.1964
11	0.1964
12	0.1919
13	0.1863
14	0.1813
15	0.1774
16	0.1750
17	0.1738
18	0.1740
19	0.1754
20	0.1780
21	0.1816
22	0.1865
23	0.1924
24	0.1997
25	
26	
27	
28	

Table 10. Model-Scale Dynamic Wetted Surface Area at 298 Lbs of Displacement

Test #	8	5	22	25	10	13	16	19
Model #	**5628**	**5628**	**5629**	**5629**	**5630**	**5630**	**5631**	**5631**
Δ =	298	298	298	298	298	298	298	298
LCG	**38%**	**42%**	**38%**	**42%**	**38%**	**42%**	**38%**	**42%**

V_m (knots)	S_{DYN} in^2	S_{DYN} in^2	S_{DYN} in^2	S_{DYN} in^2	S_{DYN} in^2	S_{DYN} in^2	S_{DYN} in^2	S_{DYN} in^2
0								
1								
2								
3	3454.1	4370.4	3026.5	3240.0	3410.4	3575.3	2834.3	3257.3
4	3441.2	3926.3	2968.3	3423.3	3338.7	3666.5	2791.5	3234.7
5	3644.1	3333.5	2900.1	3558.4	3318.2	3658.3	2791.5	3235.3
6	3763.9	3309.6	3199.4	3418.5	3403.1	3589.8	2815.7	3208.2
7	3724.3	3432.1	3242.4	3269.0	3441.4	3508.1	2844.5	3065.7
8	3605.2	3538.7	3062.2	3193.5	3400.2	3444.1	2860.5	3037.9
9	3459.7	3590.6	3002.0	3164.2	3309.7	3413.4	2851.3	3015.9
10	3313.8	3583.7	2956.1	3161.2	3198.4	3415.3	2811.1	2975.4
11	3179.0	3530.2	2874.0	3159.1	3084.5	3412.3	2741.0	2908.9
12	3059.0	3447.3	2731.3	3077.0	2977.5	3342.2	2648.1	2818.5
13	2953.7	3350.3	2584.3	2859.1	2881.9	3221.2	2543.6	2719.2
14	2862.0	3249.5	2484.3	2712.2	2798.9	3110.9	2439.9	2630.7
15	2782.0	3151.1	2423.2	2675.1	2728.5	3030.3	2348.6	2563.4
16	2712.0	3058.2	2381.5	2671.9	2669.8	2973.4	2277.4	2517.2
17	2650.6	2972.1	2348.3	2673.9	2621.4	2932.2	2229.7	2486.5
18	2596.2	2893.0	2318.7	2674.5	2582.3	2901.0	2203.6	2465.6
19	2547.9	2820.6	2290.9	2672.7	2551.3	2876.7	2193.0	2450.7
20	2504.8	2754.4		2669.0	2527.3	2857.0	2189.6	2439.2
21	2465.9	2693.8		2663.7	2509.5	2840.8	2184.9	2429.4
22	2430.9	2638.2		2657.3	2497.2	2827.1	2172.9	2420.6
23	2399.0	2587.1		2649.9	2489.5	2815.3	2152.2	2412.4
24	2369.9			2641.8	2486.2	2805.1	2127.0	2404.3
25	2343.3			2633.2	2486.6	2796.2	2107.2	2396.4
26								2388.5
27								
28								

Table 11. Model-Scale Dynamic Wetted Surface Area at 375 Lbs of Displacement

Test #	9	6	23	26	11	14	17	20
Model #	**5628**	**5628**	**5629**	**5629**	**5630**	**5630**	**5631**	**5631**
Δ =	375	375	375	375	375	375	375	375
LCG	**38%**	**42%**	**38%**	**42%**	**38%**	**42%**	**38%**	**42%**

V_m (knots)	S_{DYN} in^2	S_{DYN} in^2	S_{DYN} in^2	S_{DYN} in^2	S_{DYN} in^2	S_{DYN} in^2	S_{DYN} in^2	S_{DYN} in^2
0								
1								
2								
3	3566.1	3794.4	3447.4	3361.8	3568.5	3663.2	2977.2	3131.3
4	3556.7	3775.8	3481.2	3192.5	3613.6	3769.8	3198.7	3123.3
5	3617.2	3858.0	3526.1	3644.2	3644.5	3796.8	3149.6	3333.0
6	3752.7	3995.7	3495.6	3542.1	3653.6	3747.5	2982.3	3328.9
7	3807.3	4065.2	3397.6	3458.5	3631.8	3664.2	2909.9	3212.8
8	3645.7	4000.3	3266.6	3403.0	3570.4	3591.2	2858.1	3162.4
9	3430.1	3854.8	3127.2	3363.0	3466.3	3559.1	2801.9	3146.0
10	3259.8	3694.8	2992.0	3329.6	3325.3	3585.1	2736.9	3131.2
11	3133.1	3549.6	2866.5	3280.3	3163.1	3622.3	2665.5	3071.7
12	3034.8	3425.2	2753.1	3153.0	3000.0	3455.6	2591.1	2924.6
13	2954.2	3320.0	2652.4	2918.0	2853.6	3172.7	2517.0	2731.0
14	2885.2	3230.5	2564.4	2750.5	2733.9	3013.9	2445.3	2582.0
15	2824.4	3153.6	2488.6	2701.8	2643.3	2940.3	2377.4	2499.7
16	2769.5	3086.8	2424.3	2693.0	2579.0	2901.3	2313.8	2460.2
17	2719.2	3028.0	2370.6	2689.1	2536.2	2877.1	2254.8	2441.8
18	2672.7	2975.8	2326.7	2682.8	2509.8	2859.9	2200.2	2432.6
19	2629.2	2929.1	2291.6	2674.0	2495.3	2846.6	2149.8	2427.5
20	2588.3	2886.9	2264.4	2663.5	2489.4	2835.6	2103.3	2423.9
21		2848.6	2243.9	2652.5	2489.4	2826.3		2421.0
22		2813.7	2229.3	2641.6	2493.4	2818.1		2418.1
23		2781.6	2219.5	2631.5	2500.1	2810.8		2415.1
24			2213.6	2622.8	2508.5	2804.1		2412.0
25			2210.6	2616.0	2517.9	2797.9		2408.8
26			2209.9	2611.5	2527.9	2792.2		2405.4
27								
28								

Table 12. Model-Scale Dynamic Wetted Surface Area at 483 Lbs of Displacement

Test #	2	7	24	27	12	15	18	21
Model #	**5628**	**5628**	**5629**	**5629**	**5630**	**5630**	**5631**	**5631**
Δ =	483	483	483	483	483	483	483	483
LCG	**38%**	**42%**	**38%**	**42%**	**38%**	**42%**	**38%**	**42%**

V_m (knots)	S_{DYN} in^2	S_{DYN} in^2	S_{DYN} in^2	S_{DYN} in^2	S_{DYN} in^2	S_{DYN} in^2	S_{DYN} in^2	S_{DYN} in^2
0								
1								
2								
3	4118.5	4057.0	3742.2	3725.4	3625.5	3790.6	3566.1	3323.0
4	3964.7	4116.6	3852.7	3810.6	3708.8	3877.5	3513.0	3452.9
5	3812.1	4172.9	3819.5	3847.9	3789.2	3926.7	3453.2	3516.4
6	4065.8	4216.4	3539.4	3687.6	3851.5	3918.8	3391.0	3504.6
7	4248.5	4231.7	3397.2	3553.1	3870.1	3873.3	3330.6	3450.2
8	4178.5	4198.4	3394.6	3499.6	3812.7	3827.3	3274.1	3381.1
9	3937.5	4098.9	3448.1	3497.4	3658.1	3805.0	3218.4	3311.9
10	3642.0	3931.9	3405.2	3480.1	3421.0	3811.9	3142.8	3246.1
11	3365.5	3721.9	3037.0	3306.7	3153.6	3822.9	2983.6	3168.6
12	3138.4	3509.4	2656.4	2978.4	2912.0	3727.7	2672.4	3011.0
13	2964.9	3327.8	2495.5	2725.6	2726.1	3360.0	2364.1	2669.8
14	2838.7	3191.4	2437.2	2596.7	2597.9	2955.4	2229.3	2386.3
15	2751.0	3098.2	2408.5	2532.3	2516.2	2792.5	2194.8	2334.0
16	2693.7	3039.2	2386.4	2494.2	2467.4	2766.3	2185.7	2344.7
17	2660.2	3004.8	2364.0	2466.8	2440.7	2778.3	2178.1	2351.5
18	2644.4	2986.9	2339.1	2443.9	2428.2	2796.0	2167.7	2347.8
19	2640.3	2979.9	2311.4	2423.0	2424.6	2811.1	2154.7	2336.5
20	2641.0	2979.9	2289.0	2403.2	2426.6	2822.5	2140.0	2320.6
21	2639.1	2984.1	2286.4	2384.0	2432.0	2830.2	2124.4	2302.1
22	2626.7		2275.6	2365.3	2439.3	2835.0	2108.7	2282.4
23	2596.5		2253.8	2347.1	2447.7	2837.5	2093.1	2262.1
24	2542.8		2229.3	2329.2	2456.6	2838.2	2078.0	2241.8
25	2462.4		2204.4	2311.7	2465.7	2837.3	2063.4	2221.7
26			2179.7	2294.6	2474.7	2835.3	2049.6	2202.1
27			2155.3	2277.8	2483.5	2832.4	2036.5	2183.0
28			2131.3	2261.5	2491.9	2828.7	2024.2	2164.6

Table 13. Model-Scale Dynamic Wetted Surface Area at 560 Lbs of Displacement

Test #	3
Model #	**5628**
Δ =	560
LCG	**38%**

V_m (knots)	S_{DYN} in^2
0	
1	
2	
3	4161.0
4	4187.3
5	4195.0
6	4171.2
7	4106.5
8	3996.9
9	3844.9
10	3659.6
11	3455.6
12	3250.6
13	3062.9
14	2908.6
15	2799.0
16	2739.8
17	2731.3
18	2769.7
19	2846.7
20	2944.9
21	3020.9
22	2966.1
23	2528.1
24	
25	
26	
27	
28	

Table 14. Model-Scale Dynamic Wetted Surface Area at 680 Lbs of Displacement

Test #	4
Model #	**5628**
Δ =	680
LCG	**38%**

V_m (knots)	S_{DYN} in^2
0	
1	
2	
3	4912.8
4	4854.4
5	4754.4
6	4610.5
7	4424.8
8	4199.7
9	3923.0
10	3556.7
11	3184.2
12	2992.7
13	2904.3
14	2843.3
15	2796.5
16	2762.8
17	2741.0
18	2729.3
19	2725.8
20	2728.6
21	2736.0
22	2746.7
23	2759.8
24	2774.4
25	
26	
27	
28	

Table 15. Residuary Resistance Coefficient at 280 Lbs of Displacement

Test #	8	5	22	25	10	13	16	19
Model #	**5628**	**5628**	**5629**	**5629**	**5630**	**5630**	**5631**	**5631**
Δ =	298	298	298	298	298	298	298	298
LCG	**38%**	**42%**	**38%**	**42%**	**38%**	**42%**	**38%**	**42%**

V_m (knots)	C_R x1000	C_R x1000	C_R x1000	C_R x1000	C_R x1000	C_R x1000	C_R x1000	C_R x1000
0								
1								
2								
3	5.044	3.396	8.313	5.470	7.214	4.818	7.306	7.138
4	9.783	5.880	11.374	7.794	8.256	7.109	10.874	7.056
5	9.297	9.270	13.255	8.457	10.659	7.756	12.968	9.973
6	7.826	8.518	9.930	7.874	9.124	6.963	11.120	8.405
7	6.517	6.621	7.690	6.811	6.849	5.866	8.794	7.087
8	5.464	5.127	6.578	5.686	5.363	4.849	6.977	5.770
9	4.634	4.125	5.420	4.697	4.447	3.962	5.661	4.765
10	3.967	3.457	4.491	3.872	3.835	3.201	4.717	4.029
11	3.443	2.979	3.841	3.216	3.364	2.592	4.034	3.502
12	3.014	2.604	3.458	2.824	2.944	2.189	3.535	3.130
13	2.656	2.299	3.179	2.753	2.535	1.936	3.160	2.852
14	2.354	2.050	2.872	2.611	2.140	1.726	2.864	2.613
15	2.096	1.848	2.547	2.314	1.783	1.522	2.606	2.381
16	1.876	1.683	2.241	2.011	1.483	1.326	2.359	2.151
17	1.686	1.548	1.971	1.748	1.244	1.144	2.109	1.928
18	1.524	1.435	1.741	1.527	1.056	0.982	1.860	1.720
19	1.385	1.340	1.548	1.341	0.906	0.837	1.622	1.530
20	1.267	1.260		1.187	0.783	0.712	1.410	1.360
21	1.168	1.191		1.058	0.677	0.603	1.237	1.210
22	1.086	1.131		0.951	0.583	0.510	1.110	1.080
23	1.020	1.079		0.865	0.497	0.432	1.028	0.970
24	0.970			0.797	0.417	0.367	0.984	0.884
25	0.935			0.745	0.343	0.316	0.964	0.825
26								0.804
27								
28								

Table 16. Residuary Resistance Coefficient at 375 Lbs of Displacement

Test #	9	6	23	26	11	14	17	20
Model #	**5628**	**5628**	**5629**	**5629**	**5630**	**5630**	**5631**	**5631**
Δ =	375	375	375	375	375	375	375	375
LCG	**38%**	**42%**	**38%**	**42%**	**38%**	**42%**	**38%**	**42%**

V_m (knots)	C_R x1000	C_R x1000	C_R x1000	C_R x1000	C_R x1000	C_R x1000	C_R x1000	C_R x1000
0								
1								
2								
3	6.258	5.134	10.618	6.865	9.256	7.227	11.244	8.902
4	12.829	8.658	13.065	11.134	10.176	8.193	11.411	10.306
5	13.873	10.950	13.944	11.503	13.402	10.656	15.554	12.772
6	12.007	9.815	12.899	11.498	13.044	10.511	16.320	12.476
7	9.719	7.880	11.067	9.470	10.197	8.576	12.521	10.060
8	8.163	6.472	9.327	7.621	7.794	6.802	10.055	7.931
9	6.979	5.533	7.909	6.260	6.321	5.468	8.557	6.481
10	5.932	4.837	6.780	5.231	5.520	4.421	7.419	5.478
11	5.023	4.261	5.866	4.456	5.038	3.617	6.433	4.792
12	4.268	3.756	5.111	3.983	4.565	3.291	5.562	4.406
13	3.655	3.307	4.473	3.827	4.001	3.209	4.807	4.189
14	3.160	2.908	3.926	3.596	3.418	2.929	4.167	3.914
15	2.757	2.557	3.450	3.164	2.889	2.534	3.631	3.531
16	2.424	2.253	3.032	2.718	2.436	2.143	3.187	3.112
17	2.151	1.991	2.663	2.333	2.054	1.802	2.822	2.716
18	1.929	1.769	2.337	2.013	1.731	1.517	2.522	2.368
19	1.741	1.583	2.050	1.750	1.458	1.282	2.277	2.071
20	1.575	1.430	1.799	1.534	1.226	1.089	2.077	1.822
21		1.306	1.583	1.359	1.027	0.929		1.613
22		1.208	1.403	1.217	0.858	0.795		1.439
23		1.134	1.258	1.103	0.712	0.683		1.294
24			1.152	1.014	0.588	0.588		1.174
25			1.089	0.944	0.482	0.506		1.074
26			1.079	0.890	0.391	0.436		0.992
27								
28								

Table 17. Residuary Resistance Coefficient at 483 Lbs of Displacement

Test #	2	7	24	27	12	15	18	21
Model #	**5628**	**5628**	**5629**	**5629**	**5630**	**5630**	**5631**	**5631**
Δ =	483	483	483	483	483	483	483	483
LCG	**38%**	**42%**	**38%**	**42%**	**38%**	**42%**	**38%**	**42%**

V_m (knots)	C_R x1000	C_R x1000	C_R x1000	C_R x1000	C_R x1000	C_R x1000	C_R x1000	C_R x1000
0								
1								
2								
3	7.223	4.974	10.502	9.805	13.162	9.179	11.570	9.690
4	12.980	11.184	13.336	12.548	18.216	10.743	13.600	13.746
5	18.263	14.166	18.553	16.723	20.510	14.650	19.518	18.252
6	16.648	13.681	21.407	18.522	18.943	16.028	22.093	19.749
7	13.176	11.721	16.989	15.025	15.419	13.324	17.255	15.727
8	10.642	9.695	13.476	11.895	12.118	10.004	13.614	12.129
9	8.993	8.074	11.018	9.810	9.946	7.749	11.537	10.197
10	7.850	6.894	9.277	8.251	8.986	6.449	10.105	8.877
11	6.971	6.050	8.804	7.344	8.701	5.596	9.139	7.764
12	6.207	5.403	8.551	7.010	8.123	4.963	8.831	6.993
13	5.501	4.845	7.588	6.558	7.094	4.831	8.617	6.926
14	4.839	4.321	6.426	5.829	5.997	4.854	7.712	6.802
15	4.222	3.818	5.389	5.040	5.020	4.377	6.512	5.912
16	3.655	3.340	4.536	4.323	4.195	3.682	5.421	4.949
17	3.143	2.898	3.851	3.709	3.508	3.041	4.526	4.159
18	2.687	2.497	3.306	3.198	2.940	2.510	3.812	3.528
19	2.291	2.140	2.875	2.775	2.467	2.081	3.244	3.021
20	1.957	1.825	2.515	2.428	2.074	1.734	2.794	2.611
21	1.689	1.548	2.183	2.145	1.745	1.450	2.437	2.277
22	1.490		1.927	1.914	1.470	1.217	2.157	2.007
23	1.365		1.741	1.728	1.239	1.024	1.940	1.791
24	1.318		1.602	1.581	1.047	0.864	1.775	1.624
25	1.358		1.501	1.468	0.887	0.729	1.656	1.501
26			1.432	1.387	0.755	0.617	1.579	1.421
27			1.394	1.334	0.646	0.523	1.539	1.385
28			1.385			0.445	1.535	1.399

Table 18. Residuary Resistance Coefficient at 560 Lbs of Displacement

Test #	3
Model #	**5628**
Δ =	560
LCG	**38%**

V_m (knots)	C_R x1000
0	
1	
2	
3	12.226
4	16.478
5	19.544
6	19.782
7	17.630
8	14.864
9	12.506
10	10.685
11	9.238
12	8.009
13	6.934
14	5.981
15	5.118
16	4.325
17	3.593
18	2.927
19	2.339
20	1.848
21	1.496
22	1.392
23	1.933
24	
25	
26	
27	
28	

Table 19. Residuary Resistance Coefficient at 680 Lbs of Displacement

Test #	4
Model #	**5628**
Δ =	680
LCG	**38%**

V_m (knots)	C_R x1000
0	
1	
2	
3	8.689
4	14.498
5	22.607
6	27.013
7	23.515
8	20.046
9	18.159
10	16.729
11	15.236
12	12.979
13	10.676
14	8.779
15	7.270
16	6.064
17	5.091
18	4.305
19	3.671
20	3.163
21	2.758
22	2.432
23	2.166
24	1.949
25	
26	
27	
28	

Table 20. Model-Scale Center of Gravity Heave at 298 Lbs of Displacement

Test #	8	5	22	25	10	13	16	19
Model #	**5628**	**5628**	**5629**	**5629**	**5630**	**5630**	**5631**	**5631**
Δ =	298	298	298	298	298	298	298	298
LCG	**38%**	**42%**	**38%**	**42%**	**38%**	**42%**	**38%**	**42%**

V_m (knots)	CG Heave In	CG Heave in	CG Heave in	CG Heave in	CG Heave in	CG Heave in	CG Heave in	CG Heave in
0								
1								
2								
3	-0.152	-0.113	-0.326	-0.062	-0.164	-0.217	-0.189	-0.284
4	-0.444	-0.475	-0.428	-0.382	-0.444	-0.502	-0.435	-0.356
5	-0.599	-0.647	-0.715	-0.642	-0.616	-0.647	-0.702	-0.746
6	-0.460	-0.553	-0.504	-0.530	-0.484	-0.579	-0.541	-0.583
7	-0.054	-0.203	-0.102	-0.232	-0.073	-0.299	-0.131	-0.274
8	0.410	0.193	0.322	0.101	0.195	0.110	0.180	0.079
9	0.809	0.530	0.727	0.442	0.360	0.536	0.454	0.437
10	1.182	0.888	1.102	0.779	0.732	0.874	0.785	0.780
11	1.586	1.275	1.441	1.102	1.249	1.018	1.204	1.099
12	1.991	1.654	1.746	1.406	1.736	1.192	1.667	1.392
13	2.330	1.996	2.017	1.689	2.121	1.608	2.090	1.660
14	2.581	2.289	2.256	1.948	2.409	1.944	2.416	1.903
15	2.759	2.533	2.467	2.185	2.623	2.188	2.640	2.125
16	2.890	2.732	2.650	2.398	2.786	2.377	2.790	2.327
17	2.992	2.892	2.810	2.589	2.914	2.534	2.896	2.512
18	3.079	3.021	2.947	2.759	3.020	2.668	2.980	2.682
19	3.158	3.123	3.064	2.909	3.110	2.787	3.056	2.839
20	3.234	3.205	3.163	3.042	3.189	2.895	3.131	2.984
21	3.310	3.271	3.246	3.158	3.262	2.995	3.209	3.118
22	3.389	3.323	3.314	3.259	3.331	3.089	3.294	3.243
23	3.471	3.364	3.369	3.346	3.397	3.178	3.385	3.359
24	3.558		3.411	3.422	3.461	3.265	3.485	3.467
25	3.650		3.443	3.488	3.524	3.349	3.592	3.569
26								3.664
27								
28								

Table 21. Model-Scale Center of Gravity Heave at 375 Lbs of Displacement

Test #	9	6	23	26	11	14	17	20
Model #	**5628**	**5628**	**5629**	**5629**	**5630**	**5630**	**5631**	**5631**
Δ =	375	375	375	375	375	375	375	375
LCG	**38%**	**42%**	**38%**	**42%**	**38%**	**42%**	**38%**	**42%**

V_m (knots)	CG Heave in	CG Heave in	CG Heave In	CG Heave in	CG Heave in	CG Heave in	CG Heave in	CG Heave in
0								
1								
2								
3	-0.2269	-0.3269	-0.2681	-0.1931	-0.1408	-0.4034	-0.2356	-0.3513
4	-0.6080	-0.5233	-0.5357	-0.6445	-0.4828	-0.5556	-0.5644	-0.5895
5	-0.6718	-0.7009	-0.6954	-0.7775	-0.6887	-0.6831	-0.7074	-0.6978
6	-0.4849	-0.5253	-0.6005	-0.6390	-0.6075	-0.7161	-0.6035	-0.6730
7	-0.1220	-0.1691	-0.1985	-0.3125	-0.2119	-0.5381	-0.2508	-0.5079
8	0.3467	0.2865	0.3898	0.1268	0.2728	-0.0657	0.2853	-0.2083
9	0.8623	0.7819	0.9945	0.6137	0.6250	0.5444	0.9011	0.2013
10	1.3802	1.2720	1.5249	1.0965	0.9156	0.9240	1.4664	0.6803
11	1.8693	1.7268	1.9675	1.5416	1.3435	1.0516	1.6762	1.1829
12	2.3100	2.1308	2.3387	1.9325	1.9252	1.3850	1.9018	1.6689
13	2.6914	2.4786	2.6573	2.2657	2.5089	1.9815	2.5481	2.1107
14	3.0089	2.7719	2.9354	2.5454	2.9791	2.5068	2.9952	2.4940
15	3.2622	3.0159	3.1774	2.7792	3.3142	2.8506	3.3147	2.8154
16	3.4534	3.2171	3.3824	2.9756	3.5397	3.0611	3.5565	3.0784
17	3.5864	3.3821	3.5479	3.1422	3.6882	3.1967	3.7450	3.2896
18	3.6656	3.5170	3.6730	3.2859	3.7858	3.2949	3.8942	3.4572
19	3.6959	3.6272	3.7613	3.4122	3.8513	3.3775	4.0137	3.5886
20	3.6821	3.7171	3.8210	3.5257	3.8973	3.4565	4.1100	3.6909
21		3.7905	3.8632	3.6298	3.9329	3.5392	4.1881	3.7699
22		3.8504	3.9001	3.7273	3.9653	3.6301	4.2515	3.8302
23		3.8992	3.9427	3.8206	4.0011	3.7326	4.3027	3.8759
24			3.9998	3.9113	4.0487	3.8492	4.3434	3.9098
25			4.0786	4.0010	4.1219	3.9826	4.3742	3.9346
26			4.1847	4.0908	4.2515	4.1355	4.3939	3.9520
27								
28								

Table 22. Model-Scale Center of Gravity Heave at 483 Lbs of Displacement

Test #	2	7	24	27	12	15	18	21
Model #	**5628**	**5628**	**5629**	**5629**	**5630**	**5630**	**5631**	**5631**
Δ =	483	483	483	483	483	483	483	483
LCG	**38%**	**42%**	**38%**	**42%**	**38%**	**42%**	**38%**	**42%**

V_m (knots)	CG Heave in	CG Heave in	CG Heave in	CG Heave in	CG Heave in	CG Heave in	CG Heave In	CG Heave in
0								
1								
2								
3	-0.0141	-0.1313	-0.7234	-0.5565	-0.2987	-0.6165	0.1524	-0.1100
4	-0.6623	-0.6412	-0.8234	-0.5498	-0.5521	-0.6234	-0.3620	-0.6272
5	-0.8253	-0.9808	-0.9201	-0.9629	-0.7524	-0.7915	-0.6994	-0.7186
6	-0.5815	-0.7214	-0.6344	-0.4365	-0.7353	-0.7891	-0.6476	-0.5759
7	-0.1351	-0.2481	-0.1560	0.0057	-0.2900	-0.5545	-0.2101	-0.2696
8	0.4501	0.1549	0.4433	0.5069	0.3306	-0.1283	0.4135	0.1731
9	1.1588	0.7355	1.1197	1.0991	0.9820	0.4192	1.0804	0.7357
10	1.9347	1.3973	1.8267	1.7447	1.6560	1.0215	1.7312	1.3912
11	2.6721	2.0281	2.5096	2.3841	2.3173	1.6271	2.3398	2.0899
12	3.2750	2.5716	3.1153	2.9626	2.9228	2.1997	2.8916	2.7636
13	3.7075	3.0152	3.6071	3.4466	3.4440	2.7168	3.3789	3.3483
14	3.9902	3.3676	3.9739	3.8273	3.8709	3.1660	3.7996	3.8087
15	4.1659	3.6452	4.2279	4.1133	4.2078	3.5432	4.1561	4.1447
16	4.2754	3.8641	4.3943	4.3219	4.4660	3.8494	4.4536	4.3797
17	4.3489	4.0383	4.5011	4.4717	4.6594	4.0901	4.6990	4.5436
18	4.4060	4.1787	4.5725	4.5794	4.8012	4.2731	4.8993	4.6632
19	4.4591	4.2937	4.6270	4.6588	4.9030	4.4080	5.0613	4.7578
20	4.5156	4.3898	4.6767	4.7200	4.9741	4.5054	5.1915	4.8400
21	4.5802	4.4717	4.7297	4.7706	5.0219	4.5765	5.2951	4.9173
22	4.6558		4.7904	4.8162	5.0520	4.6325	5.3769	4.9940
23	4.7446		4.8611	4.8607	5.0690	4.6845	5.4409	5.0720
24	4.8484		4.9428	4.9069	5.0760	4.7434	5.4902	5.1524
25	4.9688		5.0358	4.9570	5.0756	4.8195	5.5275	5.2351
26			5.1397	5.0126	5.0697	4.9229	5.5551	5.3201
27			5.2541	5.0750	5.0598	5.0629	5.5747	5.4070
28			5.3783	5.1450	5.0469	5.2484	5.5879	5.4954

Table 23. Model-Scale Center of Gravity Heave at 560 Lbs of Displacement

Test #	3
Model #	**5628**
Δ =	560
LCG	**38%**

V_m (knots)	CG Heave in
0	
1	
2	
3	0.0481
4	-0.6728
5	-0.8129
6	-0.5965
7	-0.1555
8	0.5362
9	1.4568
10	2.4057
11	3.1686
12	3.6958
13	4.0465
14	4.2901
15	4.4736
16	4.6238
17	4.7553
18	4.8756
19	4.9889
20	5.0974
21	5.2023
22	5.3042
23	5.4036
24	
25	
26	
27	
28	

Table 24. Model-Scale Center of Gravity Heave at 680 Lbs of Displacement

Test #	4
Model #	**5628**
Δ =	680
LCG	**38%**

V_m (knots)	CG Heave in
0	
1	
2	
3	-0.2114
4	-0.7297
5	-0.9862
6	-0.7827
7	-0.1301
8	0.7602
9	1.7649
10	2.8746
11	3.9367
12	4.7381
13	5.2412
14	5.5287
15	5.6873
16	5.7746
17	5.8243
18	5.8558
19	5.8803
20	5.9052
21	5.9359
22	5.9770
23	6.0337
24	6.1126
25	
26	
27	
28	

Table 25. Pitch Angle at 298 Lbs of Displacement

Test #	8	5	22	25	10	13	16	19
Model #	**5628**	**5628**	**5629**	**5629**	**5630**	**5630**	**5631**	**5631**
Δ =	298	298	298	298	298	298	298	298
LCG	**38%**	**42%**	**38%**	**42%**	**38%**	**42%**	**38%**	**42%**

V_m (knots)	Trim Deg	Trim Deg	Trim Deg	Trim Deg	Trim Deg	Trim Deg	Trim Deg	Trim Deg
0								
1								
2								
3	0.316	0.139	0.212	-0.189	0.207	0.208	0.115	0.294
4	0.590	0.300	0.620	0.648	0.609	0.467	0.642	0.234
5	2.012	1.594	1.901	1.412	1.785	1.355	1.703	1.511
6	2.710	2.414	2.585	2.067	2.627	2.319	2.587	2.313
7	3.036	2.772	2.756	2.503	2.856	2.674	2.793	2.535
8	3.351	3.059	2.950	2.799	2.950	2.707	2.862	2.708
9	3.548	3.216	3.165	3.044	2.980	2.746	3.002	2.896
10	3.659	3.350	3.355	3.250	3.234	2.847	3.211	3.083
11	3.762	3.490	3.492	3.411	3.584	3.032	3.447	3.256
12	3.838	3.609	3.563	3.523	3.814	3.538	3.642	3.406
13	3.829	3.689	3.563	3.587	3.863	3.964	3.726	3.530
14	3.725	3.726	3.499	3.606	3.774	3.958	3.677	3.627
15	3.559	3.725	3.381	3.585	3.606	3.860	3.532	3.697
16	3.370	3.692	3.223	3.534	3.407	3.771	3.341	3.742
17	3.183	3.637	3.041	3.461	3.205	3.696	3.146	3.763
18	3.013	3.566	2.853	3.375	3.017	3.627	2.966	3.760
19	2.868	3.487	2.672	3.284	2.847	3.558	2.809	3.735
20	2.749	3.401	2.507	3.196	2.696	3.486	2.675	3.687
21	2.656	3.314	2.365	3.116	2.562	3.408	2.558	3.617
22	2.589	3.227	2.248	3.048	2.439	3.322	2.451	3.526
23	2.547	3.141	2.155	2.994	2.324	3.226	2.347	3.413
24	2.527		2.086	2.955	2.208	3.118	2.236	3.278
25	2.529		2.035	2.929	2.085	2.997	2.103	3.121
26								2.939
27								
28								

Table 26. Pitch Angle at 375 Lbs of Displacement

Test #	9	6	23	26	11	14	17	20
Model #	**5628**	**5628**	**5629**	**5629**	**5630**	**5630**	**5631**	**5631**
Δ =	375	375	375	375	375	375	375	375
LCG	**38%**	**42%**	**38%**	**42%**	**38%**	**42%**	**38%**	**42%**

V_m (knots)	Trim Deg	Trim Deg	Trim Deg	Trim Deg	Trim Deg	Trim Deg	Trim Deg	Trim Deg
0								
1								
2								
3	0.444	-0.087	0.230	0.096	0.007	0.082	0.064	0.366
4	0.475	0.322	0.615	0.370	0.693	0.426	0.723	0.026
5	2.559	1.705	2.066	1.512	1.958	1.479	1.996	1.848
6	3.387	2.844	3.125	2.797	3.204	2.827	3.186	2.742
7	3.529	3.150	3.290	3.132	3.465	3.064	3.450	2.870
8	3.954	3.504	3.564	3.144	3.476	3.058	3.368	2.988
9	4.425	3.861	3.932	3.334	3.758	3.224	3.626	3.214
10	4.741	4.142	4.234	3.662	4.152	3.516	4.190	3.518
11	4.811	4.322	4.409	4.013	4.513	3.854	4.444	3.846
12	4.663	4.408	4.461	4.305	4.719	4.177	4.508	4.145
13	4.400	4.421	4.412	4.498	4.709	4.444	4.727	4.383
14	4.125	4.381	4.287	4.577	4.529	4.627	4.502	4.543
15	3.893	4.309	4.107	4.550	4.268	4.713	4.180	4.621
16	3.715	4.216	3.889	4.438	3.989	4.699	3.912	4.623
17	3.578	4.113	3.644	4.270	3.725	4.596	3.715	4.562
18	3.462	4.004	3.382	4.072	3.486	4.423	3.564	4.451
19	3.350	3.895	3.116	3.871	3.273	4.209	3.439	4.304
20	3.230	3.785	2.858	3.682	3.083	3.981	3.323	4.133
21		3.676	2.623	3.517	2.910	3.763	3.204	3.950
22		3.565	2.422	3.380	2.751	3.572	3.073	3.765
23		3.447	2.268	3.273	2.599	3.417	2.922	3.584
24			2.165	3.196	2.449	3.299	2.744	3.415
25			2.121	3.146	2.296	3.215	2.527	3.262
26			2.136	3.121	2.137	3.161	2.258	3.126
27								
28								

Table 27. Pitch Angle at 483 Lbs of Displacement

Test #	2	7	24	27	12	15	18	21
Model #	**5628**	**5628**	**5629**	**5629**	**5630**	**5630**	**5631**	**5631**
Δ =	483	483	483	483	483	483	483	483
LCG	**38%**	**42%**	**38%**	**42%**	**38%**	**42%**	**38%**	**42%**

V_m (knots)	Trim Deg	Trim Deg	Trim Deg	Trim Deg	Trim Deg	Trim Deg	Trim Deg	Trim Deg
0								
1								
2								
3	0.327	0.286	0.187	0.110	0.010	0.498	0.309	0.141
4	0.593	0.282	0.566	0.566	0.781	0.839	0.833	0.537
5	2.323	1.838	2.138	1.638	2.168	1.742	2.055	1.937
6	4.125	3.500	3.978	3.678	3.992	3.008	3.755	3.650
7	4.209	3.870	4.006	3.827	4.196	3.752	4.130	3.862
8	4.775	4.138	4.531	4.197	4.365	3.805	4.011	3.718
9	5.439	4.637	5.011	4.644	4.973	3.888	4.503	4.051
10	5.700	5.041	5.349	5.048	5.553	4.210	5.179	4.608
11	5.648	5.458	5.541	5.340	5.899	4.674	5.690	5.161
12	5.461	5.553	5.590	5.491	5.976	5.358	5.915	5.576
13	5.214	5.504	5.500	5.502	5.833	5.689	5.869	5.788
14	4.939	5.265	5.289	5.396	5.550	5.772	5.625	5.793
15	4.657	5.041	4.986	5.207	5.196	5.712	5.274	5.630
16	4.384	4.868	4.630	4.968	4.820	5.573	4.884	5.360
17	4.131	4.745	4.257	4.708	4.452	5.391	4.502	5.039
18	3.902	4.601	3.892	4.445	4.105	5.188	4.151	4.712
19	3.697	4.411	3.556	4.193	3.784	4.976	3.839	4.404
20	3.516	4.239	3.257	3.958	3.490	4.760	3.567	4.130
21	3.356	4.027	3.002	3.745	3.221	4.544	3.331	3.897
22	3.213		2.791	3.553	2.973	4.328	3.128	3.703
23	3.085		2.623	3.382	2.741	4.113	2.951	3.548
24	2.970		2.496	3.227	2.521	3.897	2.797	3.427
25	2.865		2.406	3.085	2.307	3.680	2.661	3.335
26			2.350	2.944	2.091	3.460	2.542	3.271
27			2.325	2.786	1.865	3.237	2.436	3.228
28			2.328	2.563		3.009	2.329	3.204

Table 28. Pitch Angle at 560 Lbs of Displacement

Test #	3
Model #	**5628**
Δ =	560
LCG	**38%**

V_m (knots)	Trim Deg
0	0.000
1	0.000
2	0.000
3	0.195
4	0.762
5	2.464
6	4.643
7	4.695
8	5.624
9	6.279
10	6.590
11	6.561
12	6.278
13	5.874
14	5.445
15	5.043
16	4.686
17	4.378
18	4.118
19	3.898
20	3.713
21	3.558
22	3.428
23	3.320
24	
25	
26	
27	
28	

Table 29. Pitch Angle at 680 Lbs of Displacement

Test #	4
Model #	**5628**
Δ =	680
LCG	**38%**

V_m (knots)	Trim Deg
0	
1	
2	
3	-0.011
4	0.833
5	2.586
6	5.077
7	5.774
8	6.702
9	7.397
10	7.648
11	7.605
12	7.298
13	6.810
14	6.262
15	5.738
16	5.271
17	4.871
18	4.532
19	4.247
20	4.008
21	3.808
22	3.639
23	3.496
24	3.373
25	
26	
27	
28	

REFERENCES

[1] Zseleczky, John, "Effective Horsepower Model Tests of the U.S. Coast Guard 47' Motor Lifeboat (MLB)", United States Naval Academy, Division of Engineering and Weapons, Annapolis, 1988.

THIS PAGE IS INTENTIONALLY LEFT BLANK

DISTRIBUTION

Number of Copies	Office	Individual	Total Copies
5	United States Coast Guard Engineering and Logistics Center Code 046		5
1	DTIC		6
1	3442 (Library) 5010 (w/o enclosure)		7
4	5060	Walden	11
2	5200	5200 Office Files	13
3	5200	Metcalf, Day, Karafiath	16

Flow Research Report No. 449

MODEL TESTS TO COMPARE CAPSIZE RESISTANCE OF THE USCG 44' MLB AND PROPOSED 47' MLB IN BREAKING WAVES

John J. Zseleczky
Louise A. Wallendorf
Jim H. Duncan

December 1987

APPROVED FOR PUBLIC RELEASE
DISTRIBUTION UNLIMITED

FLOW RESEARCH, INC.
21414 - 68th Avenue South
Kent, Washington 98032
(206) 872-8500

UNCLASSIFIED

SECURITY CLASSIFICATION OF THIS PAGE (When Data Entered)

REPORT DOCUMENTATION PAGE	READ INSTRUCTIONS BEFORE COMPLETING FORM
1. REPORT NUMBER	2. GOVT ACCESSION NO. AD-A197420 / 3. RECIPIENT'S CATALOG NUMBER
4. TITLE (and Subtitle) Model Tests to Compare Capsize Resistance of the USCG 44' MLB and Proposed 47' MLB in Breaking Waves	5. TYPE OF REPORT & PERIOD COVERED Final 6. PERFORMING ORG. REPORT NUMBER Flow Res. Report No. 449
7. AUTHOR(s) John J. Zseleczky, Louise A. Wallendorf, James H. Duncan	8. CONTRACT OR GRANT NUMBER(s) N00014-84-C0698
9. PERFORMING ORGANIZATION NAME AND ADDRESS Flow Research, Inc. 21414-68th Avenue South Kent, WA 98032	10. PROGRAM ELEMENT, PROJECT, TASK AREA & WORK UNIT NUMBERS
11. CONTROLLING OFFICE NAME AND ADDRESS	12. REPORT DATE December 1987 13. NUMBER OF PAGES 33
14. MONITORING AGENCY NAME & ADDRESS(if different from Controlling Office)	15. SECURITY CLASS. (of this report) UNCLASSIFIED 15a. DECLASSIFICATION/DOWNGRADING SCHEDULE
16. DISTRIBUTION STATEMENT (of this Report) Unlimited	
17. DISTRIBUTION STATEMENT (of the abstract entered in Block 20, if different from Report)	
18. SUPPLEMENTARY NOTES Also published by U.S. Naval Academy as Report No. EW-14-87.	
19. KEY WORDS (Continue on reverse side if necessary and identify by block number)	
20. ABSTRACT (Continue on reverse side if necessary and identify by block number) The U.S. Coast Guard has designed a new 47' Motor Lifeboat which has twice the design speed of the existing 44' Motor Lifeboats. Because of the difference in design speeds, the hulls are considerably different. This report documents model tests and techniques used to compare the capsize resistance of the two boats in beam-sea breaking waves. The new 47' Motor Lifeboat was found to be less prone to capsize than the older 44' Motor Lifeboat.	

DD FORM 1 JAN 73 1473 EDITION OF 1 NOV 65 IS OBSOLETE

S/N 0102-LF-014-6601

UNCLASSIFIED

SECURITY CLASSIFICATION OF THIS PAGE (When Data Entered)

TABLE OF CONTENTS

LIST OF TABLES

LIST OF FIGURES

Nomenclature

B	Maximum beam of boat	(ft)
C_W	Wave celerity	(ft/sec)
Disp	Hull Displacement (weight)	(lb)
f	Wave frequency	(hz)
GM_T	Transverse metacentric height of hull	(ft)
g	Acceleration caused by gravity	(ft/sec^2)
H	Wave height	(ft)
H_0	Deep water wave height	(ft)
KG	Height of hull center of gravity above keel	(ft)
k_{xx}	Hull radius of gyration in roll	(ft)
L	Length of wave; also length of boat (LBP)	(ft)
L_0	Deep water wave length	(ft)
LBP	Length between perpendiculars	(ft)
LCG	Longitudinal center of gravity; measured forward of aft perpendicular	(ft)
MLB	Motor Lifeboat	
s_C'	Crest front steepness *	
T	Period of wave; also roll period of boat	(sec)
V	Velocity	(ft/sec)
μ_H	Horizontal asymmetry *	
μ_V	Vertical asymmetry *	
ν	Kinematic viscosity of water	(ft^2/sec)
ρ	Mass density of water	($lb\text{-}sec^2/ft^4$)
σ	Surface tension of water	(lb/ft)

* See Figure 3.

1.0 Introduction

Coast Guard rescue boats frequently operate in surf zones near beaches, areas of strong currents with waves at the mouths of rivers, and in rough seas caused by high winds. During these operations they are subjected to the risk of capsizing due to encounters with breaking waves. At the present time, there is no established method for designing capsize resistant boats. Theoretical efforts to attack this problem are hindered by the complexity of capsize events. The first major difficulty is the flow field. The approach of the wave to the breaking event is a highly nonlinear, unsteady, free surface flow. In the process of breaking itself the flow also becomes turbulent and entrains air. Potential flow numerical techniques have been used to follow the flow field up to breaking, but little or no work has been done to describe the ensuing turbulent flow. The next major difficulty is the description of the response of the boat to the flow field. Its motion is highly dependent on the position of the boat relative to the breaking event. The resulting motion is, of course, not describable by linear theory.

In view of the complexity of the phenomenon, the most fruitful approach to determining the capsize resistance of an existing vessel is to develop a laboratory testing capability. The first step in the development of this capability is choosing the waves. Waves break in nature due to shoaling, interaction with a current field (at an inlet or the mouth of a river), or wave-wave interactions in the open ocean. In the present study we have generated breaking waves by a wave-wave interaction technique in which a train of waves of varying frequency is used. Due to the dispersive characteristics of the waves, the wave train converges as it moves along the tank, eventually forming a breaker. Work of this type was begun at the United States Naval Academy in 1982 [1,2]. This technique was later modified so that a given breaker type, ranging from a spilling to a plunging breaker, could be produced at various wave frequencies [3]. Having chosen the waves, one must next choose the method of testing the model with the waves. Of particular importance is the position and orientation of the model relative to the breaking wave. Boats are probably most vulnerable to breakers in a beam sea orientation resulting from loss of power or broaching in following seas. With this in mind, both the earlier work [1,2] and the present work have used the beam sea orientation. During the earlier tests, a single breaking wave was produced and used to capsize the model. The position of the model relative to the breaker and a number of dynamic and geometric characteristics of the model were varied in an attempt to change its capsizing resistance. The study showed that

position and roll moment of inertia had significant effects on whether a boat would capsize when struck by a breaking wave.

In the present experiments we have recognized that, for a given model, there will always be breaking waves large enough to cause capsizing and waves small enough so that the model will resist capsizing. Increasing the capsize resistance of a design will mean increasing the maximum wave size for which it remains upright. With this fact in mind, two wave forms, one a strong plunging breaker and one a spilling breaker, were scaled to a number of wave heights and lengths. Two 1/16th scale models - one of the existing 44' Motor Lifeboat (44 MLB) and the other of the proposed 47' Motor Lifeboat (47 MLB) - were tested for capsize resistance with the waves.

The remainder of the report is divided into four sections. In section 2 the experimental apparatus and techniques are discussed. In section 3, the results of the capsizing tests are presented and discussed. The results include maximum roll angle versus position for each wave and model, and a qualitative description of the motion of the model relative to the wave during the encounter. The relationship of the test data to full scale performance is discussed in section 4 and estimates of the relative probability of capsize for the two designs are given. Finally, the conclusions of the study are presented in section 5.

2.0 Experimental Details

2.1 Tanks

The model tests were carried out in two wave tanks at the United States Naval Academy Hydromechanics Laboratory. Most of the tests were run in the smaller of the two tanks, which is 120 feet long, 8 feet wide and 5 feet deep. A wavemaker is located at one end of the tank and consists of two horizontally hinged flaps which are sealed at the tank walls (see Figure 1 for details). A hydraulic actuator is used to drive the lower board with respect to the tank foundation; a second actuator drives the upper wave board with respect to the lower wave board. Tests with a larger wave were conducted in the Laboratory's 380 foot long tank. This tank is 26 feet wide and 16 feet deep as shown in Figure 2. The wavemaker is a larger version of the system used in the 120 foot long tank.

2.2 Waves

A series of geometrically scaled breaking waves were developed using the Hydromechanics Laboratory's computer program which drives the wavemaker to produce a series of waves of increasing amplitude and period which converge to form a breaking wave at a repeatable location in the wave tank [3,4]. The plunging and spilling breakers previously developed and described in [3] were not severe enough to capsize either the 44 MLB or the 47 MLB, so a large plunging breaker was developed which would capsize both vessels. This plunging breaker was scaled down to four smaller plunging breakers; five spilling breakers were created from the plunging breaker drive signals by adjusting the peak signal phase and overall signal amplitude. The wavemaker drive signal parameters for these waves are summarized in Table I. A detailed description of the drive signal is described in [3].

The breaking wave profiles were measured near the breakpoint and characterized by single probe measurements. The probe location was set according to the criteria established in [3], at the point where the height of the crest reached a maximum value; this point was close to the point where the wave visually appeared to break. Water surface profile measurements were taken with MTS variable resistance wave probes at a sampling frequency of 500 hertz, using a Hewlett Packard engineering workstation with a 12 bit analog to digital converter. The wave signal was filtered with a 20 hertz Ithaco analog low pass filter. The wave signal was truncated to include the preceding trough, crest and following trough of the breakers shown in

Figure 3. Wave asymmetry parameters, crest front steepness (s_c'), asymmetry about a horizontal axis (μ_H), and asymmetry about a vertical axis (μ_V) were calculated from the water surface profile at the breakpoint. A thorough discussion of the evolution of these wave asymmetry parameters during the breaking process is described in [3]. The average values of the asymmetry parameters at the breakpoint for the spilling and plunging breakers in the present experiments are given in Table II.

In the discussion of test results the different plunging and spilling breakers are referred to in terms of their breaking wave periods rather than wave heights. Figure 3 shows how breaking wave period (T_d) is defined using a fixed wave probe time history of wave height. The wave periods of the plunging breakers used in the test program ranged from 3.3 seconds to 7.2 seconds (full scale). The spilling breaker wave periods ranged from 4.8 seconds to 7.6 seconds. Two different measures of breaking wave height are included in Table I for each wave: crest height measured above mean still water, and crest-to-trough height. As can be seen in the table, crest height always increases with increasing wave period, but crest-to-trough height does not always increase. Therefore, the wave with the longest period and largest crest height does not necessarily have the largest crest-to-trough height. When observing the waves in the laboratory, the waves with longer periods were clearly more powerful than the shorter period waves. Therefore, each wave is referred to in terms of wave period rather than wave height throughout this report.

2.3 Models

One-sixteenth scale models of the 44 MLB and the proposed 47 MLB were used in the test program. The 44 MLB model was built from a commercially available fiberglass shell which was modified at the Naval Academy to conform with the lines shown in Coast Guard Drawing 44MLB(S)0500-2 RE10. The 47 MLB model was built out of high density, closed cell foam and fiberglass. The 47 MLB model hull conforms to an unnumbered Coast Guard lines drawing dated 29 May 86, by D. Ghosh. The superstructure was modeled according to Coast Guard Drawing 47MLB 802-7,8 and 11, Rev. A.

Since projected side area and realistic 360 degree roll righting characteristics were considered to be essential in these experiments, the key elements of each hull's superstructure were built into the models as listed:

44 MLB

1) Forward deckhouse with raised console
2) Wrap around windshield
3) Aft deckhouse
4) Cockpit well
5) Radar

47 MLB

1) Deckhouse with flying bridge and side bulkheads
2) Side hull cut outs
3) Aft lazarette
4) Flying bridge seat lockers
5) Radar enclosure

Figures 4 and 5 show outboard profiles and body plans for the two boats.

Each model was ballasted with the center of gravity located as specified by the Coast Guard; Table III shows the values used for longitudinal center of gravity (LCG) and vertical center of gravity (KG). Roll inertia for the full scale hulls was an unknown, so estimates were made based on the limited information available. Reference [6] suggests the following relationship between roll inertia and beam for surface ships:

$$1.108k_{xx} = 0.44B \quad , \text{ or}$$

$$k_{xx}/B = 0.397 \quad ,$$

where:

k_{xx} = roll radius of gyration

B = beam of ship

There were problems in ballasting the models with both the specified centers of gravity and the estimated roll inertia. In order to obtain the low center of gravity specified for the 47 MLB model, all of the moveable ballast was placed as low as possible. The resulting k_{xx}/B was 3 percent below the suggested value of 0.397. The 44 MLB model was easily ballasted to the specified center of gravity, but the highest obtainable k_{xx}/B was 12 percent below the suggested value. Table III shows the final values used. It was suspected that the relatively tall superstructure of the 47 MLB was responsible for the model's higher k_{xx}/B. If that were the case, the difference in k_{xx}/B for the two models may be more representative of the boats in full scale than if the models were arbitrarily set up with equal values of k_{xx}/B. No attempt was made to model

pitch gyradius. The test program involved the beam sea condition in which roll angles were typically ten times greater than pitch angles, so the effect of pitch gyradius should not be significant.

The hydrostatic righting characteristics of the two models were physically measured in the tank at heel angles of zero through 180 degrees. The measurements have been expanded to full scale and are presented in Figure 6. Details and discussion of the model righting arm experiments are documented in [7].

2.4 Procedures

Although little work has been done to investigate the effects of model scale ratios on capsize testing in breaking waves, three well established physical relationships are generally thought to be of importance:

Froude Number	$[C_w/(gL)^{0.5}]\text{model} = [C_w/(gL)^{0.5}]\text{ship}$
Reynolds Number	$[C_w L/\nu]\text{model} = [C_w L/\nu]\text{ship}$
Weber Number	$[\sigma/(g\rho L^2)]\text{model} = [\sigma/(g\rho L^2)]\text{ship}$

Since the forward speed of the boat in these tests is zero, boat speed cannot be used to determine Froude or Reynolds Numbers. Instead, wave speed and wave length are used. It is impossible to model all three Numbers at once so a compromise must be made, keeping in mind the implications of the compromise when analyzing the test results. Since capsizing is clearly dominated by wave action, there is little doubt that Froude Number - the parameter which determines proper scaling of waves, gravity and inertia effects - is the most important relationship to scale. If the correct Froude Number is used, the Reynolds Number for the model is too low and the Weber Number is too high. The low Reynolds Number may slightly increase the model damping due to skin friction relative to full scale. The high model Weber Number may alter the characteristics of the the wave jet that strikes the hull. Since these scale effects have not been quantified we cannot say how accurately Froude scaled capsize tests simulate full scale events. We should however be able to reduce the risk of making poor full scale predictions if we limit ourselves to comparing the two models in terms of relative capsize resistance rather than absolute capsize resistance.

The overall test plan was to compare the motion of the two models in a family of breaking waves at different positions with respect to the oncoming breaker. The worst case scenario was assumed to be with the boat at zero speed,

broadside to a breaking wave; this was the only condition studied. Ideally the two hulls would have been tested simultaneously, at the same position in the same wave, but this was not practical because of physical limitations. Instead, a repetitive test sequence was set up in which one model was tested immediately after the other. A timed interval of 3 minutes between tests was chosen to ensure that background disturbances from previous tests had dissipated.

Repeatable model positions were made possible using the model release mechanism shown in Figure 7, which was based on a method described in [8]. Each model was outfitted with eyelets made of 1/8 inch diameter wire, located at the bow and stern, at the height of the center of gravity (near the nominal roll axis). Rods 1/2 inch in diameter were lowered through the eyelets from a beam mounted on the model towing carriage. The rods were simultaneously raised out of the eyebolts when the mechanism was triggered by a signal from the wavemaking computer. With this system both models were "launched" identically, several wave periods before the breaking event. Tests were run with the model released at several locations before and after the breakpoint of the wave. The release location was varied by moving the model towing carriage to different locations along the length of the tank.

For an estimation of relative behavior in breaking waves, the peak roll angle caused by the wave impact was measured for each condition. This roll angle will be referred to as the "impact roll angle" throughout the discussion. In some cases this was not the maximum roll angle, as will be explained later, but it provided a consistent reference point. The harsh realities of ballasting these small models with realistic mass distributions eliminated the possibility of on board sensors and telemetry gear. Instead, a simple method was used for measuring roll angle with a video camera, stop-action recorder, and protractor on the monitor screen. Checks were made to quantify camera parallax error by statically restraining the models at various known angles and displacements with respect to the camera. The maximum parallax error (which occured only under extreme conditions) was found to be +/-5 degrees. Impact roll angles measured by a given observer were found to be repeatable within +/-10 degrees. Different observers typically measured angles on the high or low side. A brief analysis of measurements made by different observers showed that 75 percent of measurements were within 11 degrees and 90 percent were within 17 degrees. The considerable difference between measurements of different observers was caused by the haziness of the model's television image as it moved sideways under the spray of the wave. Although each observer interpreted the image somewhat differently, there

was reasonable repeatability for a given observer. In order to minimize the scatter in the recorded results, the measurements of one observer were used exclusively, except in cases where the differences between observers was extreme. For these cases, the video's were carefully reviewed and discussed to find the reason for the discrepancy. Then the impact roll angles were re-measured by the original observer.

3.0 Results and Discussion

Before discussing details of the test results, some terminology will be established. Consider a stationary boat model floating in the tank with its longitudinal axis perpendicular to the longitudinal axis of the tank. The following terms will be used to describe the motions of that boat in beam sea breaking waves:

Upstream	- Toward the wavemaker
Downstream	- Away from the wavemaker
Upstream roll	- Roll in which deckhouse moves toward the wavemaker more than keel
Downstream roll	- Roll in which deckhouse moves away from the wavemaker more than keel
Impact roll angle	- Peak downstream roll angle caused by wave crest striking hull
Wave Breakpoint	- Longitudinal position in tank where breaking wave crest curls over and touches preceding trough

In a typical test run, the model started to roll with the slope of the waves preceding the breaker. Upon impact, the model rolled violently downstream under the force of the jet of water in the breaking wave crest. In certain positions with respect to the wave breakpoint, the wave jet landed on the upstream deck in such a way that the jet impulse opposed the roll motion induced by the waveslope. Here, the maximum roll angle was not the impact roll angle measured immediately after wave impact, but instead, the angle induced by the waveslope before or after the breaker. For these cases, the angle recorded was the smaller angle - the impact roll angle.

Figure 8 shows the impact roll angle for each boat at various positions upstream and downstream of the wave breakpoint, for the five plunging breakers used in the test program. The response of the 44 MLB is on top, in Figure 8a and the response of the 47 MLB is below. The distance between the position in which the model was released and the breakpoint is represented on the horizontal axis of the plots. This position has been nondimensionalized by the average beam of the two boats which is 13 feet in full scale. In the plots, a "Distance from Breakpoint / Beam" of +2.0 represents a test where the model was released two beams downstream of the point where the wave broke. Negative positions, on the far left of the plots represent cases where the models were released well upstream of the wave breakpoint. At these positions the models rode over the rising, but not yet breaking wave crest. Positive positions, at the far right represent cases where the models were released downstream of the breaker and were only mildly

tossed around in the turbulent aftermath of the breaker. The two models were knocked down or capsized only when they were within a zone of about plus or minus four beams from the breakpoint. In this zone, the 44 MLB capsized in the three longer period waves of the five plunging waves tested, whereas the 47 MLB capsized in only one - the longest period wave.

Although the 47 MLB capsized far less often than the 44 MLB, there were several cases in the shorter period breakers where the 47 MLB rolled to higher angles for a given wave and position. These results were cross-plotted to allow a comparison of the two boats in waves of different periods. In Figure 9, the ranges of position down the tank for which each hull rolled to a given angle are plotted as a function of wave period. Range of position is nondimensionalized by beam and the wave period is plotted in the dimensionless form: $[(g*T^2)/B]^{0.5}$. The plots show that the 47 MLB rolled more than the 44 MLB in the less powerful, short period waves while the 44 MLB rolled more in the stronger, long period waves. Also, the 44 MLB capsized over a much wider range of positions than the 47 MLB.

Some specific observations from the video tapes of the plunging wave tests help explain the humps and hollows in the maximum roll angle data shown in Figure 8. The dramatic decrease in roll angle, which consistently occurred when the model was released around the breakpoint, was found to be caused by the force of the wavejet when it crashed down on the upstream deck. This situation only occurred over a narrow range of positions. When the models were released upstream of this zone, the wavejet struck the exposed freeboard and augmented the waveslope induced roll. The 47 MLB model had more freeboard and therefore more lateral area exposed to the wave jet in this zone. It is important to realize however, that the wave jet never impacted broadside on the large 47 MLB superstructure; the hull always rose up with the soon-to-be-breaking wave crest and took the blow on the side of the hull. When the model was released downstream of the breakpoint, the wavejet freely crashed into the preceding wave trough, causing what resembled an underwater explosion. The upwelling of water from the impact pushed up against the bottom of the hull. The boat's upstream side was closer to the impact so it experienced higher pressures than the downstream side, resulting in a rolling moment in the same direction as the roll induced by the wave slope. Again, the 47 MLB had more exposed bottom area than the 44 MLB so it rolled more at this position.

Careful observations were made of the videotapes for cases where the 44 MLB capsized and the 47 MLB resisted. At the instant of wave impact, both hulls were rolled away from the wave, at approximately the same angle. Within 0.5

seconds, model scale (2 seconds full scale), both hulls were rolled past 90 degrees. The 47 MLB hesitated and resisted rolling past about 100 degrees while the 44 MLB kept on rolling. The hydrostatic curves of Figure 6 show that the 47 MLB has significantly greater righting moment past 90 degrees than the 44 MLB. Other factors such as inertia and center of gravity may contribute to the difference in capsize resistance, but the 47 MLB's hesitation around 100 degrees appears to be directly attributable to the hull's greater righting moment.

Neither boat capsized in the spilling breakers made in the 120 foot tank (Figure 10) or in the extreme spiller made in the 380 foot tank (Figure 11). The test results were plotted in the same manner used for the plunging breakers, but an expanded roll angle scale was used. The 44 MLB roll angles are shown at the top of Figure 10 and the 47 MLB data are below. The maximum roll angle of the 44 MLB was consistently greater than for the 47 MLB at all positions with respect to the breakpoint. As each model was released farther downwind, the maximum roll angle of both boats decreased. Apparently, the energy that dissipated as the wave spilled reduced the impact experienced by the models.

The models were also tested in regular, sinusoidal waves of constant height and varying frequency to find the period of roll resonance. Figure 12 shows the results from these tests. In 2.7 foot high beam sea waves, the 44 MLB rolled 35 degrees at its resonant point and the 47 MLB rolled 25 degrees at its resonant point. The wave periods where roll resonance occured were around 3.7 seconds for the 44 MLB and around 3.0 seconds for the 47 MLB (full scale). The formula used to predict still water roll period is: $\text{Period} = 1.108k_{xx} / (GM_T^{0.5})$ [6]. This is based on simple harmonic motion for small roll angles, with no damping. The formula predicts natural roll periods of 3.7 seconds for the 44 MLB and 2.7 seconds for the 47 MLB. It is interesting to see that the zero-damping formula closely predicts the true roll period of the 44 MLB but under-predicts the period of the 47 MLB. The hard chines of the 47 MLB presumably provide more roll damping than the round bottom of the 44 MLB. This would give the hull a longer roll period than the "no-damping" formula predicts.

The wave periods of the plunging breakers used in the test program were between 3.3 and 7.2 seconds (full scale), with the 7.2 second wave being the most powerful plunger. From the breaking wave tests it was found that both boats capsized in the 7.2 second breaker and neither capsized in the 3.3 second breaker. This shows that the resonant roll period in regular waves should not be used to predict the breaking wave period that will capsize a boat. The main reason for this is that as breaking wave period increases, wave height, wave speed and the amount of energy carried in

the wave increase. Ignoring the absolute differences, the regular wave resonant period may be useful for predicting relative performance in breaking waves. The test results show that the 47 MLB rolled more than the 44 MLB in the short period waves and less than the 44 MLB in the long period waves; this would have been predicted by looking at the regular wave data alone.

4.0 Relationship of Laboratory Results to Field Conditions

In this section, we attempt to use the laboratory data comparing the roll angles of the two models in the presence of deepwater breaking waves to make an estimate of the relative roll and capsize resistance of the two designs in the field. Rather than a detailed prediction of full scale performance at a given test site, the following is a rough estimate using our limited laboratory data, first order methods to predict the breaker characteristics in the field, and simple methods to scale the laboratory waves to those found in the field. At this point in the development of the testing technique, more detailed predictions of full-scale performance are not warranted.

The most practical cases of boats capsizing in breaking waves for the U.S. Coast Guard probably occur as waves propagate into shallow water. These areas include the shorelines, inlets, and the mouths of rivers. As a deepwater wave propagates into shallow water the period of the wavetrain (T), remains constant while the wavelength (L), height (H), and steepness (H/L) of the wavetrain first decrease slightly and then increase dramatically [9]. In deep water, the wavetrain is close to sinusoidal in shape; however, as it moves into shallow water the crests become narrow and high and the troughs become wide and shallow. At this point, the profile is close to that of a solitary wave. For these waves, the wavelength is effectively infinite and the wave is completely described by its crest to trough height, H. The shoaling wave eventually breaks, and the breaker type, ranging from a spilling to a plunging breaker, is determined by the steepness of the wave in deep water, H_0/L_0. If the deep water steepness is close to its limiting value, the wave will break as soon as it steepens slightly due to shoaling. These waves form spilling breakers. If the deep water wave steepness is very small, it forms a solitary wave and becomes a plunging breaker. In practice, waves with deep water steepness greater than 0.01 form spilling breakers while those with less steepness form plunging breakers (see Reference 9).

Making shoaling breakers for the laboratory tests was impractical because of excessive tank length requirements. In the present laboratory tests, the breakers were produced in deep water by interaction of wave components in a wave train. As it approaches breaking, the wave form steepens, its period decreases and it eventually forms a spilling or a plunging breaker. These waves never evolve into shapes like solitary waves, however breaking waves in deep and shallow water have gross similarities. In order to estimate the behavior of our models in shoaling waves, we compare the deepwater and shoaling breaking waves based on the height from the mean water level to the crest.

As a test site for comparison of the breaker heights and types in the field to those used in the laboratory experiments, we chose the area near the mouth of the Columbia River. This site has the advantage of being the training ground for the USCG Motor Lifeboat School, and of having a NOAA wave data buoy located near by at 46.2 degrees north latitude and 124.2 degrees west longitude. Table IV gives the distribution of wave height and period from this data buoy. Consider first the shoaling of the waves. For a wave shoaling on a shallow sloped beach independent of shoreline shape and currents, we can use standard wave forecasting techniques to predict the height and type of breaking waves. Using the deep water wave data in Table IV and the wave shoaling theory [9] we find the distribution of shoaling wave heights (mean water level to breaking wave crest) to be:

Crest Height Range (feet)	Percent of Wave Heights Within Range	Percent of Wave Heights Exceeding Range
0 - 3.75	17.6	82.4
3.75 - 7.50	39.3	43.1
7.50 - 11.3	32.2	10.9
11.3 - 15.0	5.4	5.5

The breaker heights from the experiments can be expanded to full scale by multiplying the laboratory wave height data in Table I by 16, the prototype to model scale ratio. Using Froude scaling, $T/(gL)^{0.5}$ is held constant, so the full scale wave periods are calculated by multiplying the laboratory data by 4 (the square root of the scale ratio). The following table shows the full scale characteristics of the laboratory waves:

Plunging Breakers		Spilling Breakers	
Period (sec)	Height * (ft)	Period (sec)	Height * (ft)
3.28	8.27	4.80	9.32
5.88	10.0	5.60	7.20
6.40	10.8	7.64	21.30
6.80	12.3		
7.20	12.5		

* Heights measured from mean still water to breaking crest

Comparison of the full scale height of the laboratory waves and the height of waves in the field indicates that there is some overlap. The range of laboratory waves was

chosen so that the smaller amplitude plunging breakers (shorter period) did not capsize the models while the larger amplitude (longer period) waves did. Waves with still larger amplitudes would be even more likely to capsize the models. For the spilling breakers, the laboratory data indicates that the 47 MLB rolls less than the 44 MLB and since waves of these scaled heights occur in the field it appears that this conclusion will be valid at the test site. For the plunging breakers, the range of distances over which either boat capsizes can be combined with the frequency of occurrence of those wave heights in the field to obtain a single plot. Such a plot appears in Figure 13. It shows that waves capable of capsizing either boat exist at the test sight (according to this very rough calculation), but that a smaller percentage of waves are capable of capsizing the 47 MLB.

5.0 Conclusions

With breaking waves on the beam and with zero forward speed, the proposed 47 MLB will be less likely to capsize than the 44 MLB. This appears to be mainly attributable to the reserve buoyancy of the 47 MLB when rolled past 90 degrees. No assessments were made in this test program about either boat's ability to avoid the vulnerable beam sea condition. This is an important point that should be addressed elsewhere. In smaller, shorter period plunging breakers, the 47 MLB will roll to higher maximum angles than the 44 MLB. This has been attributed to the higher beam and corresponding higher GM of the 47 MLB. In longer period plunging and spilling breakers, the 47 MLB will roll less than the 44 MLB.

When exposed to non-breaking beam seas with a dominant period near the boat's natural roll period, the 47 MLB will roll less than the 44 MLB for a given wave height.

References

1. Kirkman, K.l., Nagle, T.J. and Salsich, J.O.; "Sailing Yacht Capsizing", SNAME 6th CSYS, Annapolis, MD, 1983.

2. Salsich, J.O. and Zseleczky, J.J.; "Experimental Studies of Capsizing in Breaking Waves", AIAA/SNAME 13th Ancient Interface Symposium, Vol. 29, San Diego, CA, 1983.

3. Duncan, J.H., Wallendorf, L.A. and Johnson, B.; "An Experimental Investigation of the Kinematics of Breaking Waves", Proceedings IAHR Symposium on Wave Generation in Laboratory Basins, Laussanne, Switzerland, 1987.

4. Salsich, J.O., Johnson, B. and Holton, C.; "A Transient Wave Generation Technique", Proceedings 20th ATTC, Hoboken, NJ, 1983.

5. Myrhaug, D. and Kjeldsen, P.; "Parametric Modelling of Joint Probability Density Distributions for Steepness and Asymmetry in Deep Water Waves", J. Coastal Engineering, Amsterdam, 1983.

6. "Principles of Naval Architecture", SNAME, New York, NY, 1967.

7. Hudgens, J.A.; "Hydrostatic Righting Arm Measurements for Models of the U.S. Coast Guard 44' and 47' Motor Lifeboats", U.S. Naval Academy Hydromechanics Laboratory Technical Note: 87-1, Annapolis, MD, 1987.

8. Claughton, A. and Handley, P.; "An Investigation into the Stability of Sailing Yachts in Large Breaking Waves", Wolfson Unit, University of Southampton, UK, 1984.

9. H.O. Publication No. 234; "Breakers and Surf, Principles of Forcasting", U.S. Naval Oceanographic Office, Washington, D.C., Reprinted 1969.

	Plunging					Spilling		
Wave File	11	17a	18	12	13	21	16	EX
Period (sec)	1.80	1.70	1.60	1.47	0.82	1.4	1.2	1.91
Wavelength (ft)	16.6	14.8	13.1	4.9	3.4	10.0	7.38	18.5
Crest Height (ft)	0.781	0.769	0.675	0.625	0.517	0.450	0.583	1.33
Crest-Trough Height (ft)	0.950	0.967	0.975	0.808	0.750			
f(start) (hz)	1.05	1.10	1.15	1.20	1.37	1.15	1.20	0.795
f(peak) (hz)	0.613	0.641	0.669	0.700	0.800	0.664	0.700	0.464
f(stop) (hz)	0.525	0.550	0.574	0.600	0.686	0.574	0.600	0.397
Theor. Break Pt. (ft)	111	101	92.8	85.0	65.0	92.8	85.0	194
Delay Time (sec)	2.095	1.954	1.739	0.833	1.423	1.608	1.541	
Span Settings								
(Upper)	4.60	4.00	3.70	4.10	2.90	2.60	2.46	1.96
(Lower)	6.90	6.00	5.55	6.15	4.44	3.90	3.70	1.96

Table I - Model Scale Characteristics of Laboratory Waves and Wavemaker Drive Signal Parameters

	Average Asymmetry Parameter		
	$s_{C'}$	μ_H	μ_V
Type of Breaking Wave			
Plunging	0.60	0.79	2.0
Spilling	0.37	0.71	1.7

Table II - Breaking Wave Asymmetry Parameters

	44 MLB		47 MLB	
	Model	Ship	Model	Ship
Length Overall (ft)	2.76	44.1	2.96	47.3
Length Between Perp. (ft)	2.50	40.0	2.69	43.0
Beam, Max. (ft)	0.744*	11.9*	0.875	14.0
Draft, w/o skeg (ft)	0.19	3.0	0.19	3.0
Displacement (lbs)	9.43	38,300	10.1	42,600
LCG, fwd. of AP (ft)	1.26	20.1	1.08	17.2
KG (ft)	0.262	4.19	0.303	4.85
GM_T (ft)	0.100	1.60	0.313	5.00
k_{xx}, roll gyradius (ft)	0.263	4.20	0.338	5.41
LBP/B	3.36		3.07	
$(Disp/2240)/(LBP/100)^3$	267		239	
LCG/LBP	0.503		0.400	
k_{xx}/B	0.354		0.386	

* 44 MLB beam does not include rub rails.

Table III - Hull Characteristics As Tested

PERCENT FREQUENCY OF WAVE HEIGHT (METERS) VS WAVE PERIOD (SECONDS)

WBOUC
DECEMBER, JANUARY, FEBRUARY — LATITUDE 46.2N LONGITUDE 124.2W

WAVE PERIOD (SEC)	DIR	WAVE HEIGHT(METERS) 0.5-1.0	1.5-2.0	2.5-3.0	3.5-4.0	4.5-5.0	5.5-6.0	6.5-7.0	7.5-8.0	8.5-9.0	9.5-10.0	>10	TOT %	TOT N
>15.5	**	.0	.1	.2	1.3	1.1	.7	.4	.1	*	*	.0	4.0	408
11.6-15.5	**	3.2	6.1	14.3	9.2	4.2	2.0	.7	.2	.1	*	.0	42.0	4315
7.6-11.5	**	5.2	17.9	19.5	9.6	3.2	1.0	.3	.1	*	*	.0	56.1	5691
6-7.5	**	.2	1.1	1.0	.2	.1	.0	.0	.0	.0	.0	.0	2.6	263
<6	**	2.0	.6	*	.0	.0	.0	.0	.0	.0	.0	.0	2.7	275
TOT %		10.7	25.7	35.0	19.1	8.3	3.7	1.4	.4	.2	.1	.0	100.0	
TOT N		1087	2605	3543	1939	844	376	142	44	20	7	0		10172

WBOUC
MARCH, APRIL, MAY — LATITUDE 46.2N LONGITUDE 124.2W

WAVE PERIOD (SEC)	DIR	WAVE HEIGHT(METERS) 0.5-1.0	1.5-2.0	2.5-3.0	3.5-4.0	4.5-5.0	5.5-6.0	6.5-7.0	7.5-8.0	8.5-9.0	9.5-10.0	>10	TOT %	TOT N
>15.5	**	.3	.7	1.8	1.4	.2	.2	*	.0	.0	.0	.0	4.6	250
11.6-15.5	**	1.7	6.5	14.6	9.2	2.2	.5	.1	.1	*	*	.0	35.9	1938
7.6-11.5	**	3.9	25.1	15.0	5.9	1.5	.3	.1	*	.0	.0	.0	56.1	3211
6-7.5	**	.0	1.1	.9	.2	.0	.0	.0	.0	.0	.0	.0	4.9	278
<6	**	.5	.2	*	.0	.0	.0	.0	.0	.0	.0	.0	.7	42
TOT %		6.4	33.6	32.3	15.3	3.8	1.0	.2	.1	*	*	.0	100.0	
TOT N		366	1919	1844	731	219	59	17	6	1	1	0		5719

WBOUC
JUNE, JULY, AUG — LATITUDE 46.2N LONGITUDE 124.2W

WAVE PERIOD (SEC)	DIR	WAVE HEIGHT(METERS) 0.5-1.0	1.5-2.0	2.5-3.0	3.5-4.0	4.5-5.0	5.5-6.0	6.5-7.0	7.5-8.0	8.5-9.0	9.5-10.0	>10	TOT %	TOT N
>15.5	**	.0	.0	.0	.0	.0	.0	.0	.0	.0	.0	.0	.0	0
11.6-15.5	**	.1	.4	1.6	.6	.4	.3	.0	.0	.0	.0	.0	3.4	141
7.6-11.5	**	25.0	39.1	5.7	.4	.1	.0	.0	.0	.0	.0	.0	71.4	2916
6-7.5	**	16.9	4.9	.5	*	.0	.0	.0	.0	.0	.0	.0	21.3	870
<6	**	3.1	.7	.0	.0	.0	.0	.0	.0	.0	.0	.0	3.9	159
TOT %	**	44.0	45.0	7.8	.5	.0	.0	.0	.0	.0	.0	.0	100.0	
TOT N	**	1810	1844	319	19	2	0	0	0	0	0	0		4112

WBOUC
SEPTEMBER, OCTOBER, NOVEMBER — LATITUDE 46.2N LONGITUDE 124.2W

WAVE PERIOD (SEC)	DIR	WAVE HEIGHT(METERS) 0.5-1.0	1.5-2.0	2.5-3.0	3.5-4.0	4.5-5.0	5.5-6.0	6.5-7.0	7.5-8.0	8.5-9.0	9.5-10.0	>10	TOT %	TOT N
>15.5	**	.2	.4	.3	.7	.5	.4	.2	.1	*	.0	.0	3.1	318
11.6-15.5	**	2.6	7.4	4.6	6.3	2.2	1.2	.5	.2	.1	*	.0	25.1	2550
7.6-11.5	*	16.2	27.4	12.1	5.4	1.9	.6	.1	.0	.0	.0	.0	63.8	6481
6-7.5	**	2.1	2.9	.4	.2	.0	.0	.0	.0	.0	.0	.0	5.8	593
<6	**	1.6	.4	.0	.0	.0	.0	.0	.0	.0	.0	.0	2.1	217
TOT %	*	21.7	38.4	20.4	12.6	4.7	2.2	.8	.3	.1	*	.0	100.0	
TOT N	1	2207	3736	2116	1277	476	226	79	30	10	1	0		10159

WBOUC
ANN AL — LATITUDE 46.2N LONGITUDE 124.2W

WAVE PERIOD (SEC)	DIR	WAVE HEIGHT(METERS) 0.5-1.0	1.5-2.0	2.5-3.0	3.5-4.0	4.5-5.0	5.5-6.0	6.5-7.0	7.5-8.0	8.5-9.0	9.5-10.0	>10	TOT %	TOT N
>15.5	**	.1	.7	.9	.9	.6	.4	.2	.1	*	*	.0	3.9	1176
11.6-15.5	**	1.9	6.9	10.4	6.2	2.5	1.2	.4	.1	.1	*	.0	29.7	8944
7.6-11.5	*	12.2	27.0	12.6	5.8	2.0	.6	.2	*	*	*	.0	57.4	17319
6-7.5	*	3.0	3.7	.8	.2	.0	.0	.0	.0	.0	.0	.0	6.7	2030
<6	**	1.7	.7	*	.0	.0	.0	.0	.0	.0	.0	.0	2.3	693
TOT %	*	19.0	39.0	24.8	13.0	5.1	2.2	.8	.3	.1	*	.0	100.0	
TOT N	1	5736	13944	7434	3936	1539	661	238	80	31	*	0		30162

Table IV - Columbia River Wave Buoy Data
From: NOAA NDBC Publication April 1986

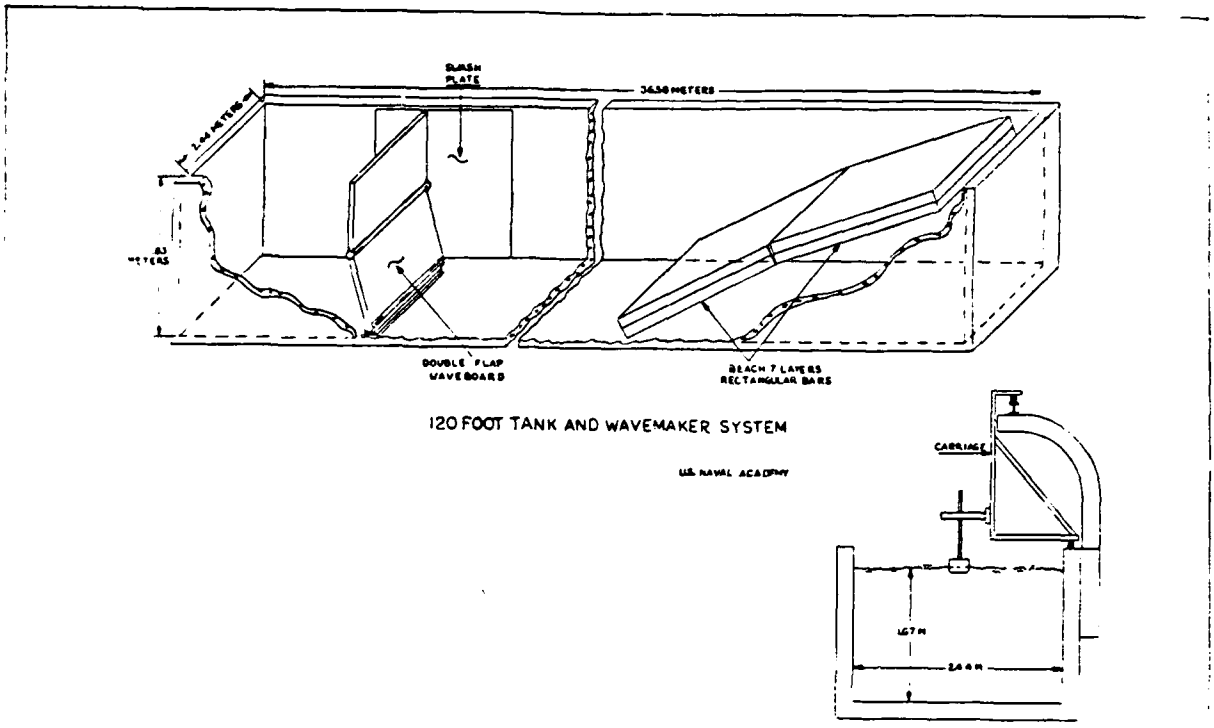

Figure 1 - U.S. Naval Academy 120 Foot Tank

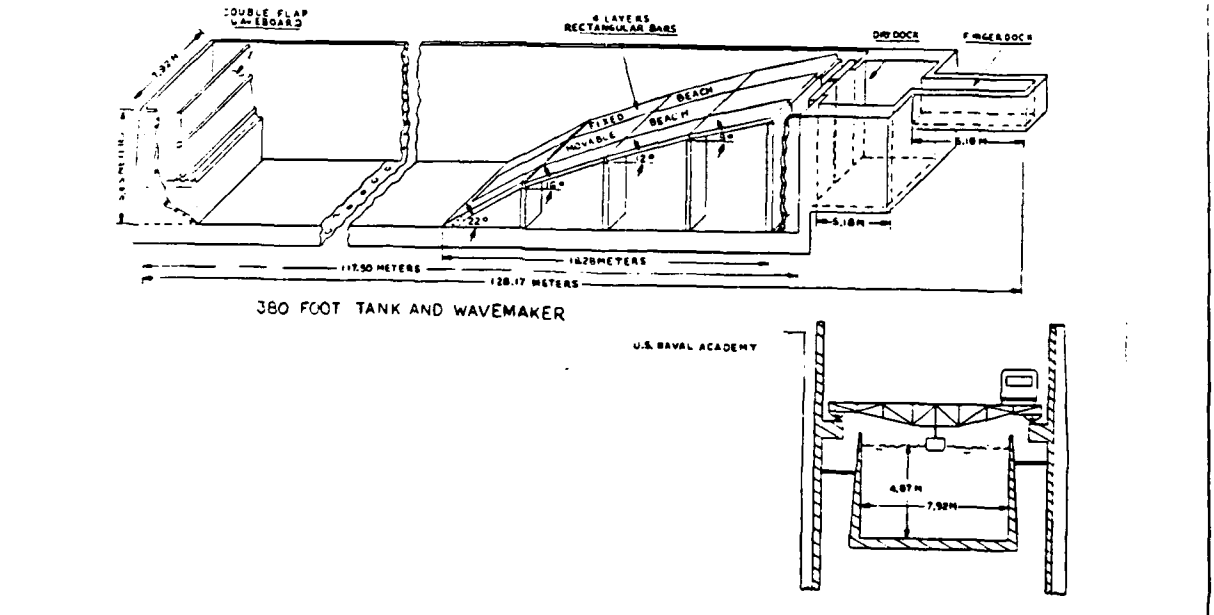

Figure 2 - U.S. Naval Academy 380 Foot Tank

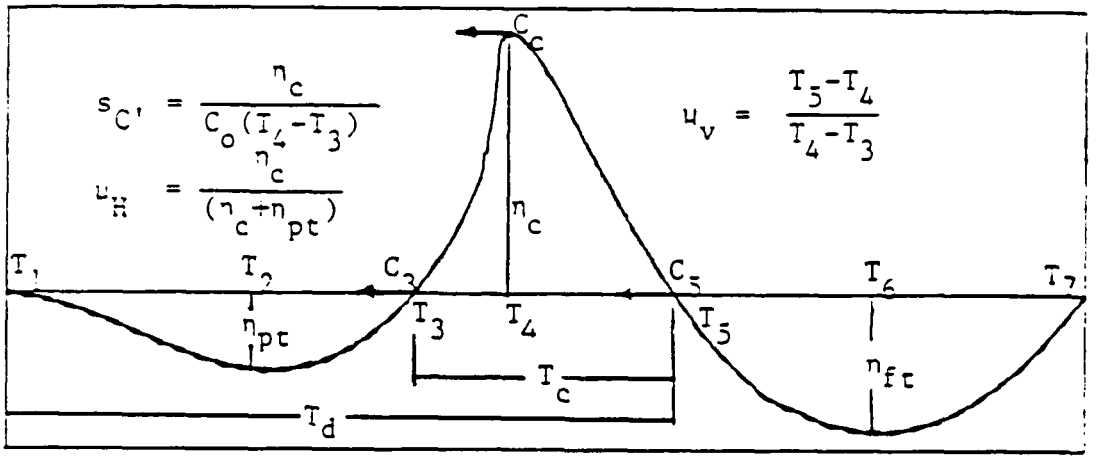

Time history of breaking wave height (from Reference 3)

C	Celerity
C_c	Crest celerity
C_o	Celerity from linear theory, $\frac{gT_d}{2\pi}$
$s_{C'}$	Crest front steepness
T	Time of probe reading
T_c	Crest period
T_d	Breaking wave period
η_c	Breaking crest amplitude
η_{ft}	Trough amplitude following breaking crest
η_{pt}	Trough amplitude preceding breaking crest
μ_H	Asymmetry about horizontal axis
μ_V	Asymmetry about vertical axis

Figure 3 - Definition of Breaking Wave Parameters from Fixed Wave Probe Time History

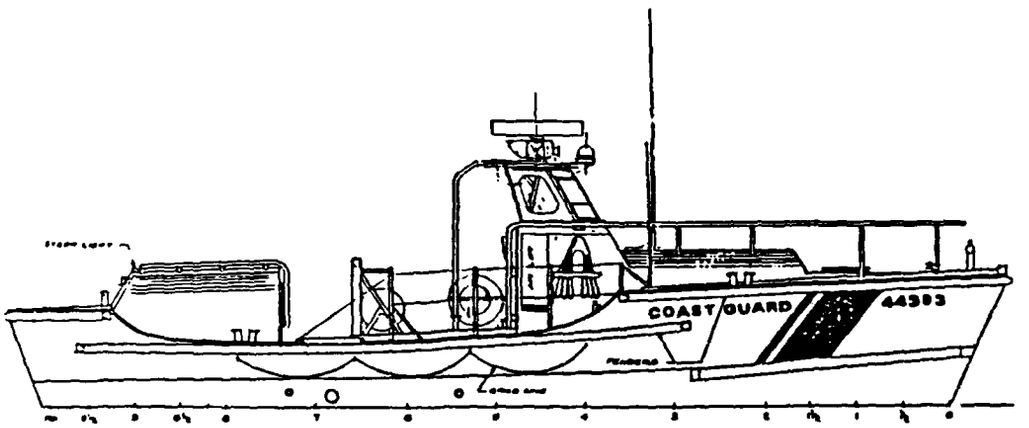

44ft MOTOR LIFEBOAT
OUTBOARD PROFILE

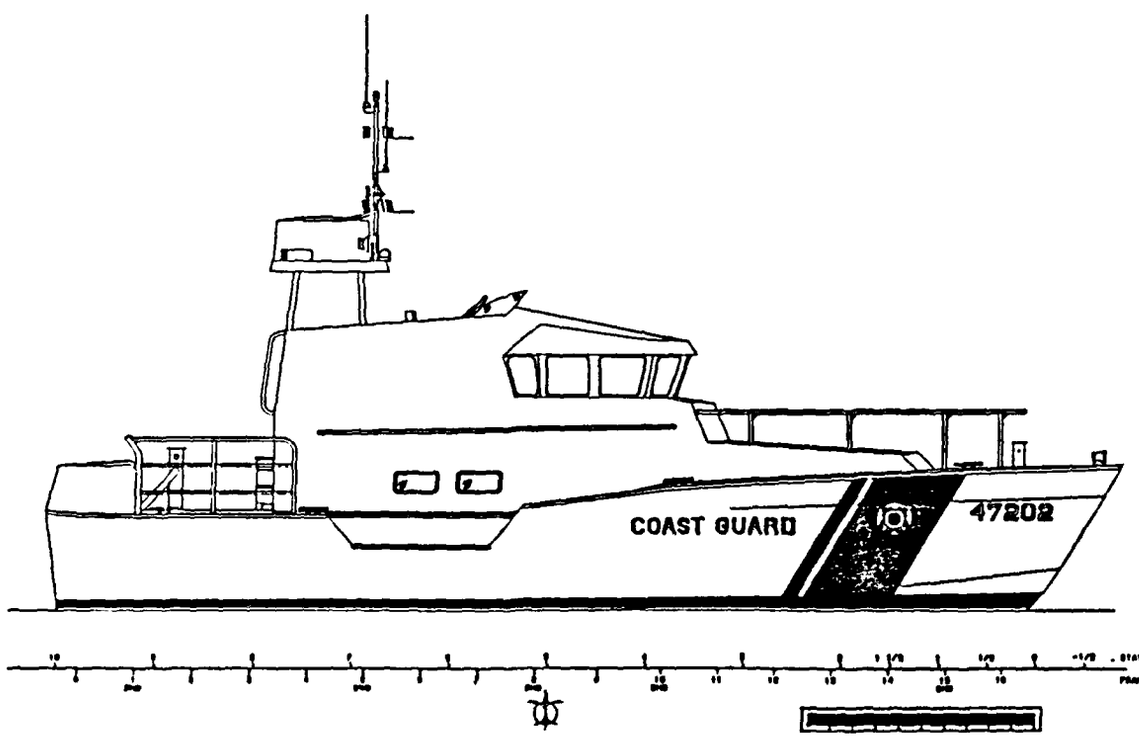

47ft CONCEPT DESIGN
OUTBOARD PROFILE

Figure 4 - Outboard Profiles of 44' and 47' Motor Lifeboats

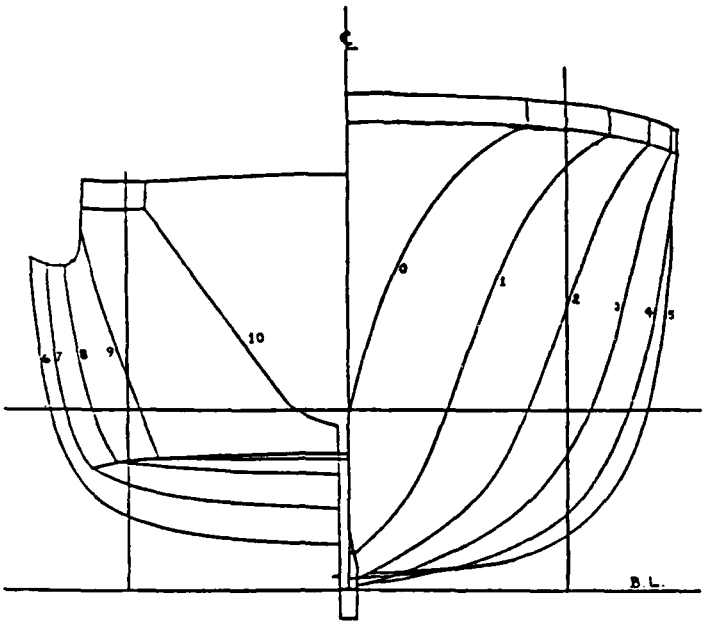

44ft MOTOR LIFEBOAT

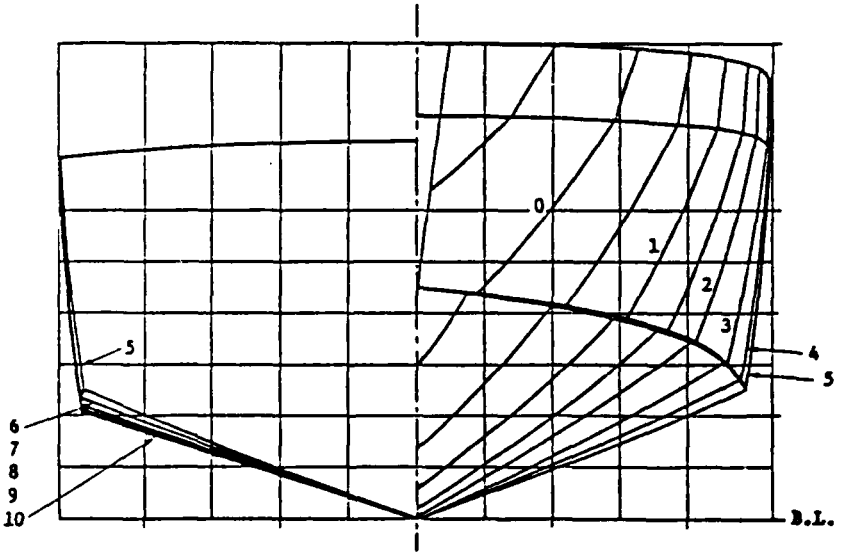

47ft CONCEPT DESIGN

Figure 5 - Body Plans of 44' and 47' Motor Lifeboats

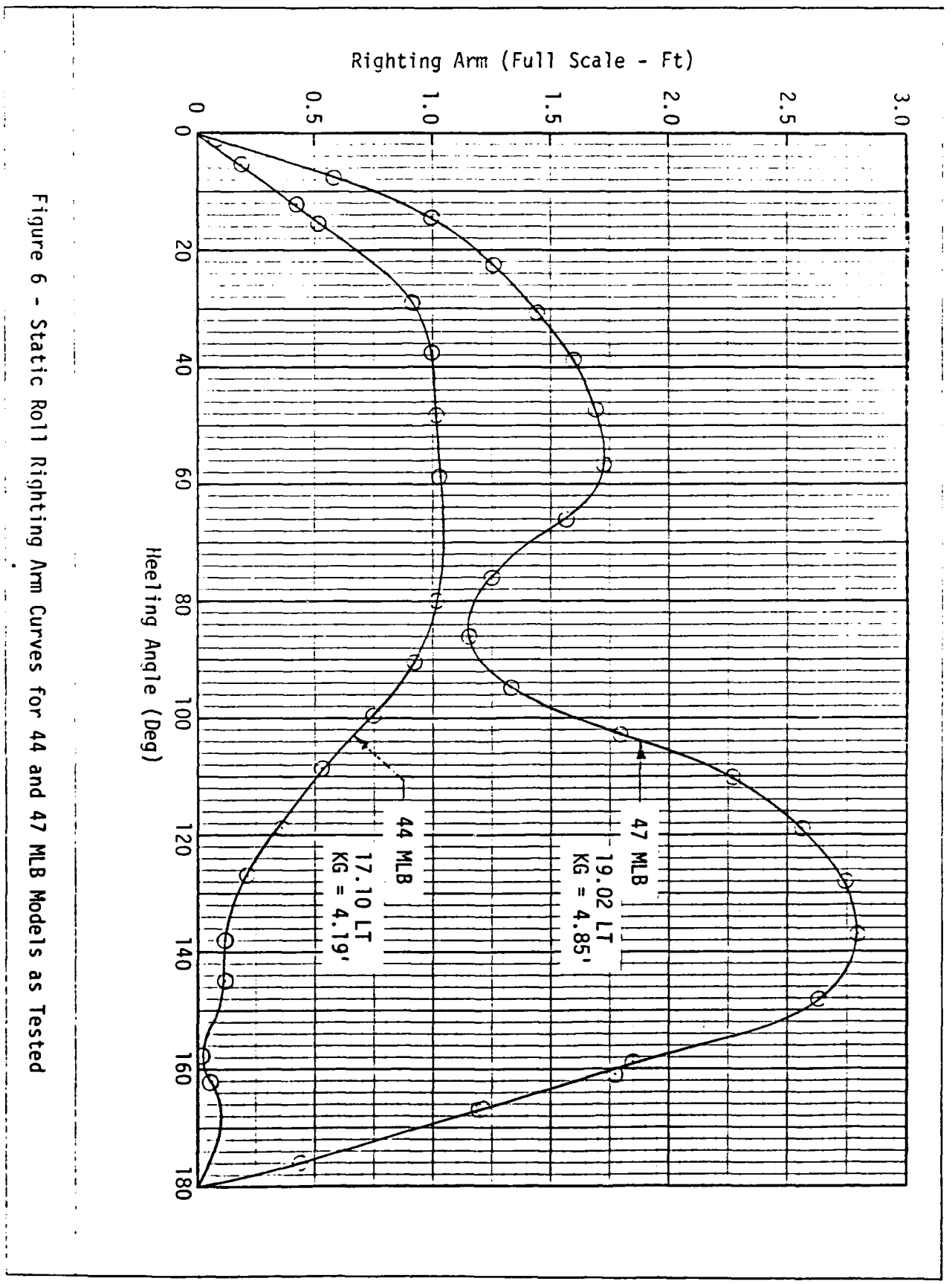

Figure 6 - Static Roll Righting Arm Curves for 44 and 47 MLB Models as Tested

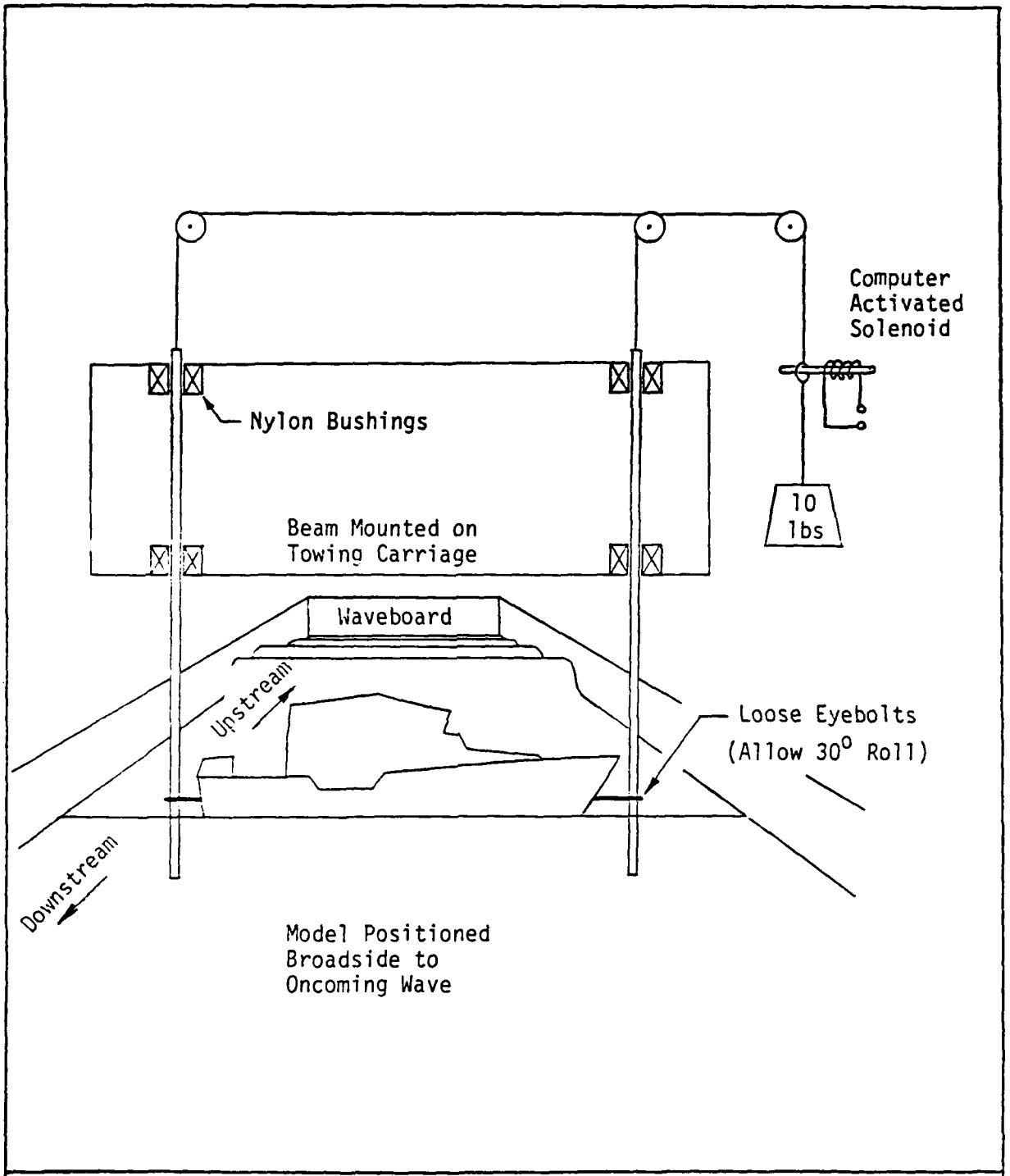

Figure 7 - Model Release Mechanism

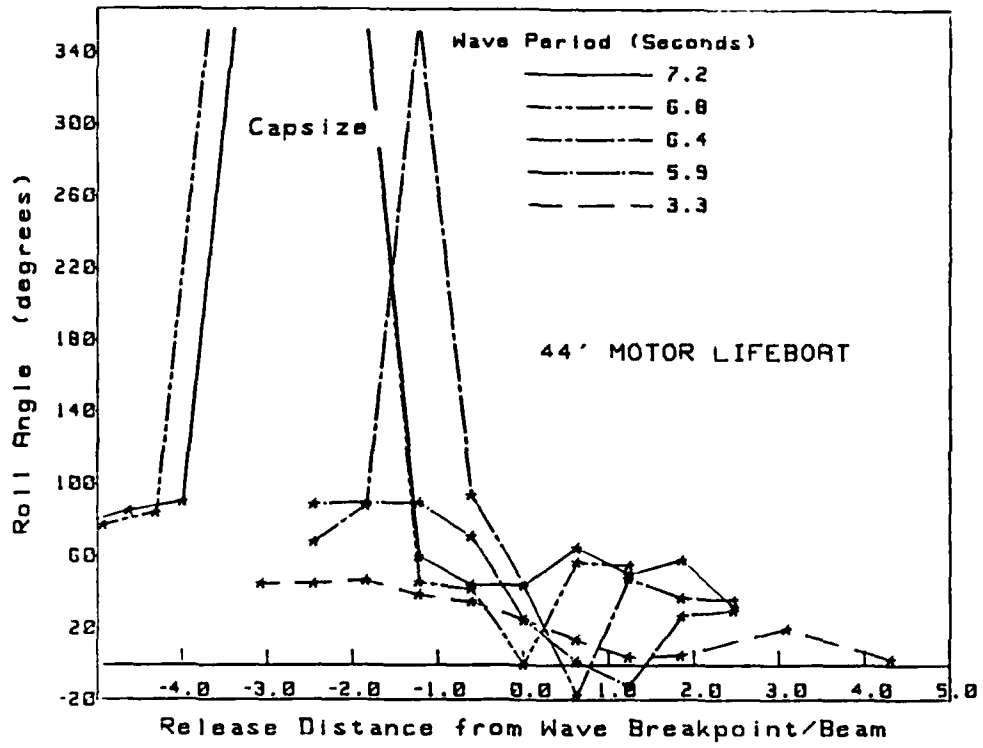

FIGURE 8a - Roll Angle vs. Nominal Breakpoint/Beam
44' MLB - Plunging Breakers

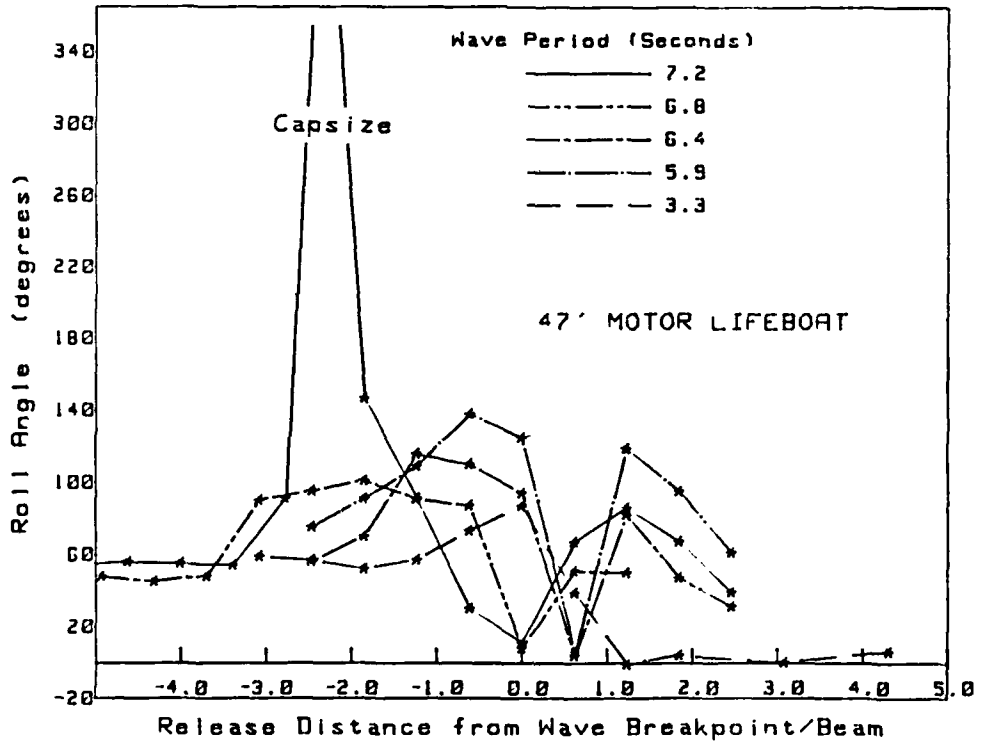

FIGURE 8b - Roll Angle vs. Nominal Breakpoint/Beam
47' MLB - Plunging Breakers

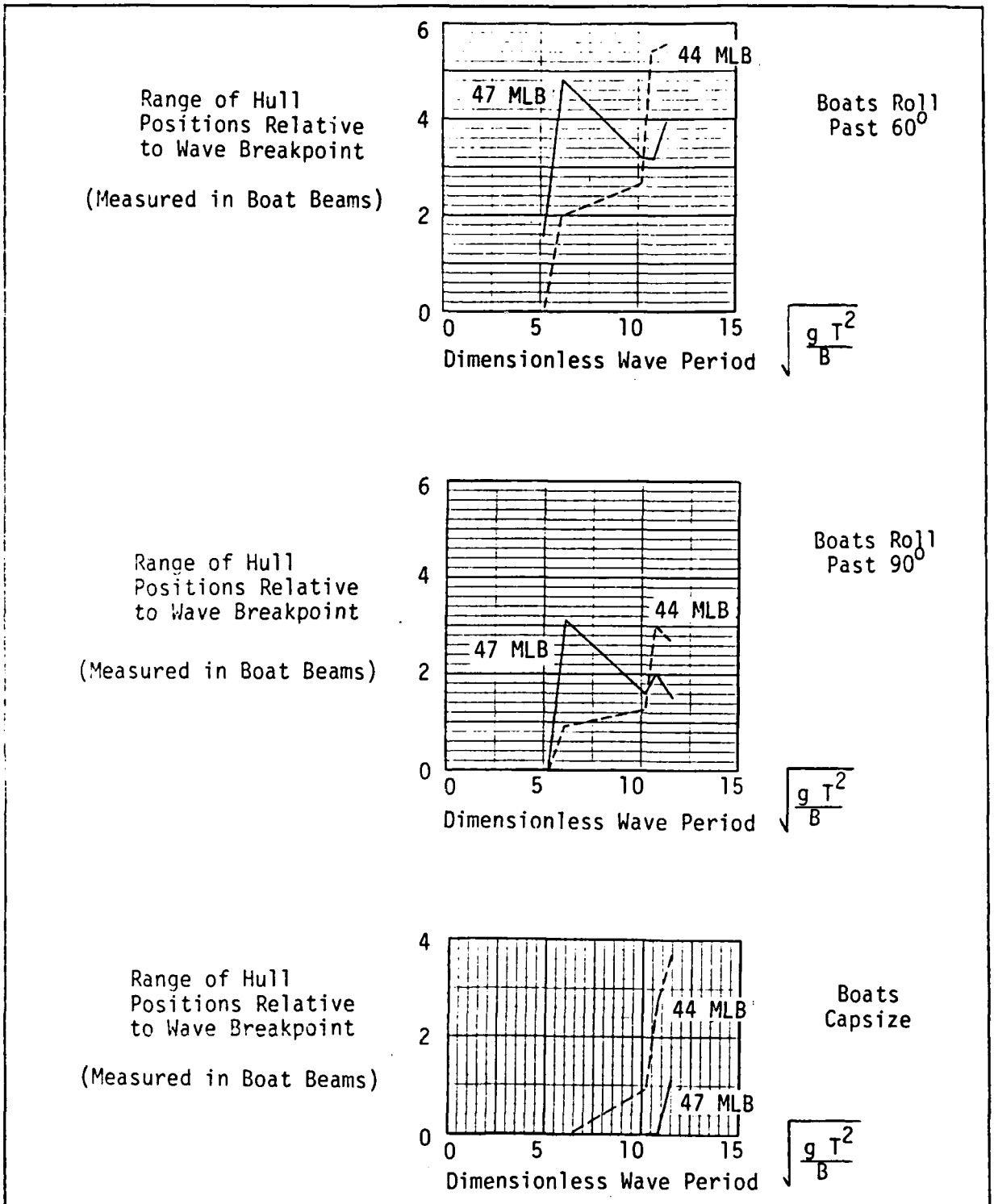

Figure 9 - Range of Hull Positions Relative to Wave Breakpoint Where Boats Roll Past Specific Angles

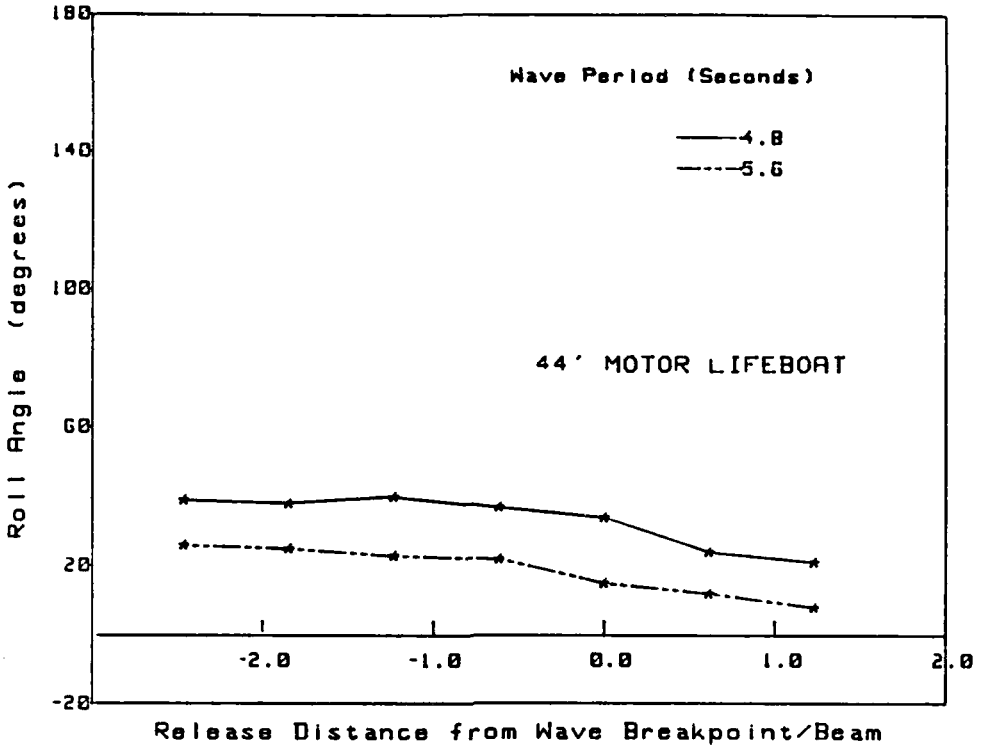

FIGURE 10a Roll Angle vs. Nominal Breakpoint/Beam
44' MLB - Spilling Breakers

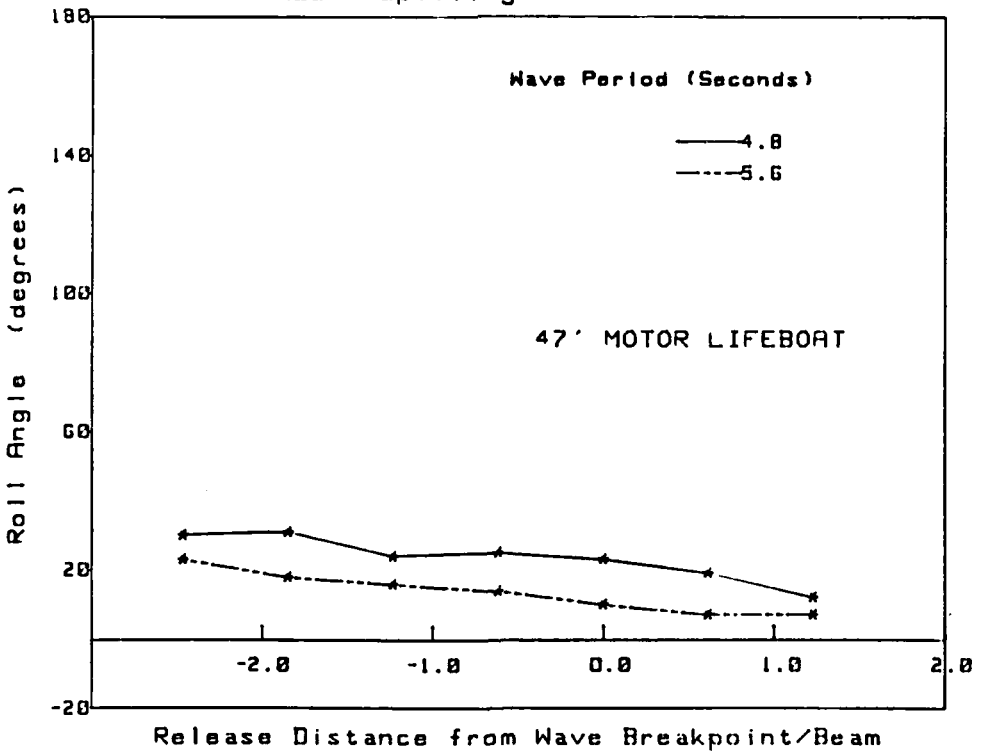

FIGURE 10b Roll Angle vs. Nominal Breakpoint/Beam
47' MLB - Spilling Breakers

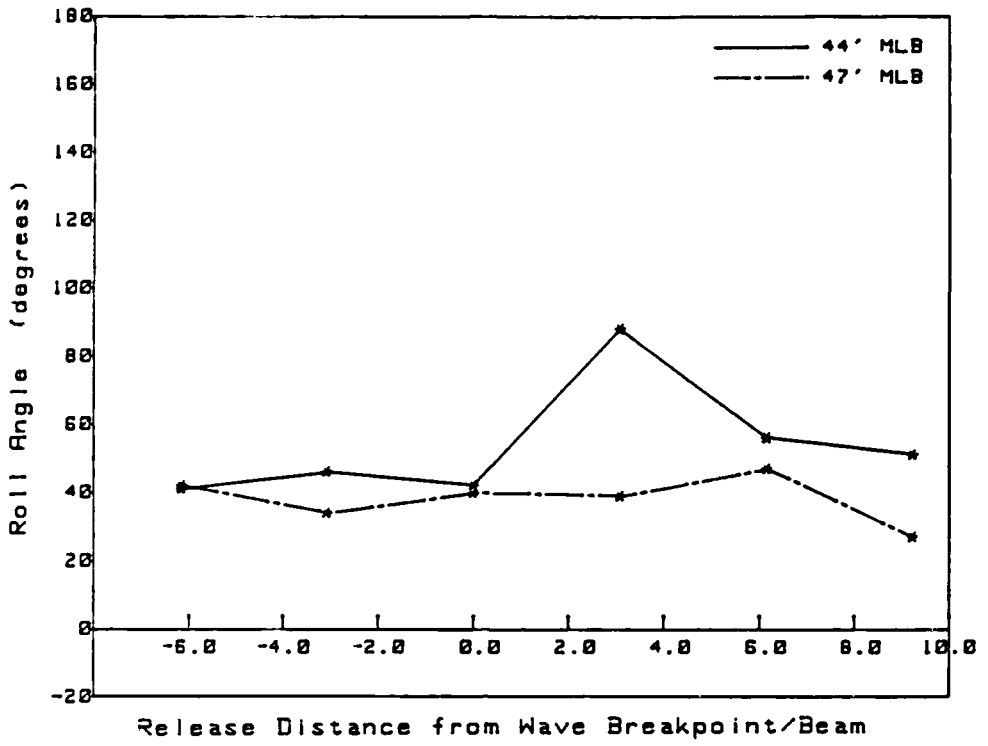

FIGURE 11 Roll Angle vs. Nominal Breakpoint/Beam
Extreme Spilling Breaker

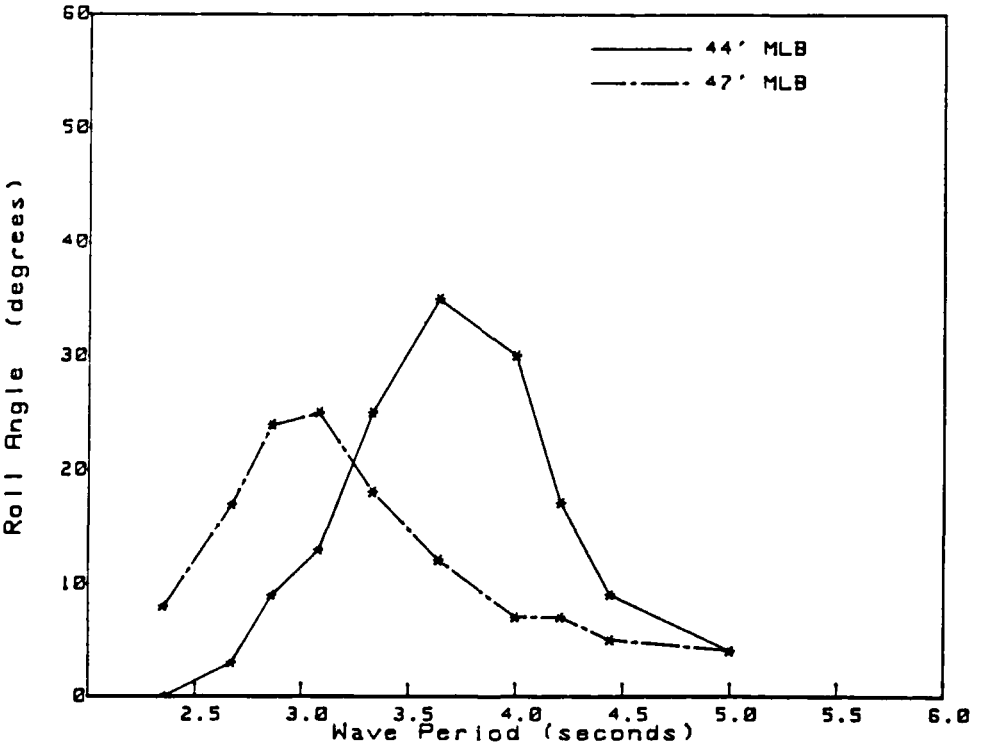

FIGURE 12 Maximum Roll Angle vs. Period of Regular Wave, H=2.7'

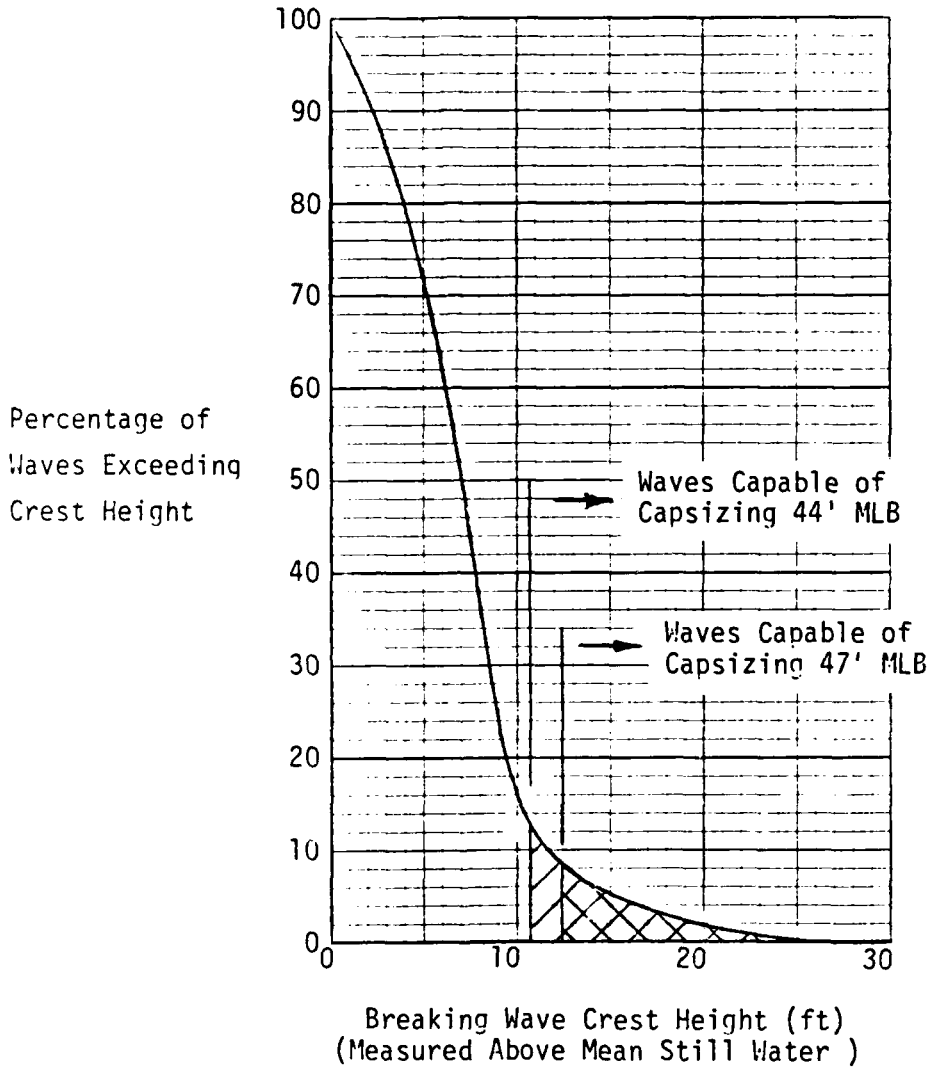

Figure 13 - Estimated Percentage of Waves at Columbia River Buoy Capable of Capsizing Motor Lifeboats